PHOSPHATE BASED DIELECTRIC CERAMICS AND COMPOSITES FOR MICROWAVE APPLICATIONS

THESIS SUBMITTED TO

THE UNIVERSITY OF KERALA

FOR THE AWARD OF THE DEGREE OF

DOCTOR OF PHILOSOPHY

IN PHYSICS

UNDER THE FACULTY OF SCIENCE

BY

DHANESH THOMAS

MATERIALS SCIENCE AND TECHNOLOGY DIVISION
NATIONAL INSTITUTE FOR INTERDISCIPLINARY
SCIENCE & TECHNOLOGY (CSIR)
THIRUVANANTHAPURAM- 695 019
KERALA, INDIA.

2012

Dedicated to……

My family and friends

DECLARATION

I hereby declare that the Ph. D. thesis entitled **"PHOSPHATE BASED DIELECTRIC CERAMICS AND COMPOSITES FOR MICROWAVE APPLICATIONS"** is an independent work carried out by me at the Materials Science and Technology Division, National Institute for Interdisciplinary Science and Technology (CSIR), Thiruvananthapuram, under the supervision of Dr. M. T. Sebastian and it has not been submitted any where else for any other degree, diploma or title.

Thiruvananthapuram — Dhanesh Thomas

December 2012

National Institute for Interdisciplinary Science and Technology (NIIST)
Council of Scientific & Industrial Research (CSIR)
(Department of Scientific and Industrial Research, Ministry of Science and Technology, Govt. of India)
Industrial Estate P.O., Trivandrum-695 019
Kerala, India

M.T. Sebastian, Ph.D., F.I.I. Cer.
Deputy Director & Chief Scientist
Head, Materials Science & Technology Division

Tel : 91- 471-2515294
Fax :+91 - 471- 249 17 12
E-mail : mailadils@yahoo.com
mtsebastian@niist.res.in
http :// www.niist.res.in

CERTIFICATE

This is to certify that the work embodied in the thesis entitled **"PHOSPHATE BASED DIELECTRIC CERAMICS AND COMPOSITES FOR MICROWAVE APPLICATIONS"** has been carried out by **Mr. Dhanesh Thomas** under my supervision and guidance at the Materials Science and Technology Division of National Institute for Interdisciplinary Science and Technology, Thiruvananthapuram.

Thiruvananthapuram
December 2012

Dr. M. T. Sebastian

Acknowledgments

I present this thesis, in the name of God, the Almighty, who showers his unperturbed blessings undeservingly upon me throughout my life.

I wish to express my deepest gratitude to my thesis supervisor, Dr. M. T. Sebastian (Head, Materials Science and Technology Division, NIIST, Thiruvananthapuram) for suggesting an interesting problem. I am grateful to him for his intellectual support, encouragement and enthusiasm expressed throughout the course of this research work.

I am highly thankful to Dr. Suresh Das, Director, NIIST, Trivandrum; Prof. T. K. Chandrashekar and Dr. B. C. Pai (former Directors of NIIST), for providing all the research facilities for my Ph. D. work.

I wish to express my sincere thanks to Dr. Jose James, Dr. Manoj Raama Varma and Dr. K. P Surendran (Scientists, NIIST) for fruitful scientific discussions and advices during my work.

I am deeply indebted to Dr. K. G. K. Warrier (former Head, Materials Science and Technology Division, NIIST), Dr. U. Syamaprasad, Dr. P. Prabhakar Rao (Scientists, NIIST) and Dr. Peter Koshy for their help rendered during the course of this work. The support provided by other scientists of NIIST is also thankfully acknowledged.

The creative suggestions, valuable advices and helps given by my seniors in the lab, Dr. P. S. Anjana (Assistant Professor, All Saints College, Thiruvananthapuram), Dr. G. Subodh (Kyoto University, Japan), Dr. Sumesh George (Assistant Professor, St. George's College, Aruvithura), Dr. Sherin Thomas (Assistant Professor, Assumption College, Changanacherry), Dr. Tony Joseph (Assistant Professor, Govt. Victoria College, Palakkad) and Dr. T. S. Sasikala are greatly acknowledged.

I thank my fellow lab mates in Fine Ceramics Lab: Mrs. K. S. Deepa, Mr. K. M. Manu, Mrs. J. Chameswary, Mrs. P. Neenu Lekshmi, Mr. Jobin Varghese, Ms. Nina Joseph, Mrs. G. R. Raji, Mr. P. Abhilash, Mrs. L. K. Namitha, Ms. Ann Rose Sunny, Ms. T. H. Gayathri, Mr. B. Arun, Mr. K. S. Dijith, Ms. R. Aiswarya, Mrs. Y. Jasna, Mrs. Sreejitha, Ms. U. Bhagya and Ms. S. Chinthu for their support and

stimulating discussions. I am also thankful to my former colleagues in fine ceramics, Mr. M. A. Sanoj, Mr. K. Jithesh, Mrs. P. Nisha, Mrs. C. P. Reshmi, Mrs. Anlin Lazar K, Ms. K. T. Rethika, Ms. Varsha V., Mrs. Savitha Pillai, Ms. M. Betsy, Mrs. Nisha, Mr. James, Mrs. Mridula, Ms. Shani, Mr. V. K Sajith, Ms. B. Sayoojyam, Ms. T. Raseena, Mrs. Sreelakshmi, Mrs. Sreena, Mr. G. Sumesh, Mrs. Sachna, Ms. Gopika and Mrs. Sumy Mathew for their love and support.

I am indebted to Mr. M. R. Chandran, Mr. P. Gurusamy and Mr. M. Brahmakumar (NIIST) for extending the SEM, XRD and tensile measurement facilities for my research work. I am thankful to all the office and library staff at NIIST for all their help and cooperation.

I cherish the companionship of Mr. Alex Andrews, Mr. Jinish Antony M., Mr. M. Shantil, Mr. Deepak D Prabhu, Mr. A. Aravind, Mr. M. Bejoy, Mr. Biju Francis, Mr. K. Ratheesh, Mr. M. V. Vinayak, Mr. C. R. Sinu and Mr. Tony George Thomas who made my days at NIIST and Thiruvananthapuram a memorable one.

I would like to extend my sincere gratitude to Dr. R. Ratheesh (Scientist, C-MET, Thrissur) and Dr. H. Sreemoolanadhan (Scientist, VSSC) for dielectric measurements as well as the valuable suggestions during my research.

The financial assistance from Council of Scientific and Industrial Research (CSIR), New Delhi is gratefully acknowledged.

Finally, I need to express my appreciation to all those who have helped and inspired me during my doctoral study.

Dhanesh Thomas

Contents

List of Tables

List of Figures

Abbreviations

AFM	Atomic Force Microscope
BET	Brunauer-Emmett-Teller
BR	Butyl rubber
CLSP	$Ca_4La_6(SiO_4)_4(PO_4)_2O_2$
CTE	Coefficient of thermal expansion
DR	Dielectric resonator
DRA	Dielectric resonator antenna
E-field	Electric field
EM	Electromagnetic
EMT	Effective Medium Theory
GPS	Global Positioning Systems
HDPE	High density polyethylene
HTCC	High Temperature Co-fired Ceramic
IC	Integrated circuit
ITS	Intelligent Transport Systems
JCPDS	Joint Committee on Powder Diffraction Standards
LMDS	Local Multipoint Distribution Service
LMP	$LiMgPO_4$
LRR	Long range radar
LTCC	Low Temperature Co-fired Ceramic
MCM	Multi Chip Module
MLC	Multilayer ceramic
PDMS	Polydimethylsiloxane
phr	Parts per hundred parts of rubber
PS	Polystyrene
PTFE	Polytetrafluoroethylene
PVA	Poly vinyl alcohol
Q-factor	Quality factor

RE	Rare earth
RFID	Radio-frequency identification
SEM	Scanning electron microscope
SPDR	Split Post Dielectric Resonator
SRR	Short range radar
TC	Thermal conductivity
TE	Transverse Electric
TGA	Thermo gravimetric analysis
TM	Transverse Magnetic
WLAN	Wireless Local Area Network
Wi-Fi	Wireless Fidelity
WSN	Wireless Sensor Network

Preface

In recent years, wireless communication using microwaves has been emerged as the prominent way of information exchange. Dielectric materials have played a pivotal role in universalizing the microwave communication systems by making them more efficient, miniaturized and cheaper. The continuing developments in wireless technology demand low cost materials with good microwave dielectric properties. In microwave modules, low loss dielectric materials function as oscillators, filters, antennas and substrates. The relative permittivity (ε_r) and loss factor determines the function of a dielectric in microwave electronics. Microwave dielectric resonators should have high ε_r for miniaturization. For substrate applications, on the other hand low ε_r is essential to decrease the signal propagation delay. New high performance electronic systems for wireless communication, automotive, industrial, medical, military and space applications insist on higher circuit densities. This challenge mandates the use of unique packaging techniques such as multi-chip modules (MCMs) that must not only provide the increased circuit density but also the reliability, thermal, mechanical and electrical performance. Low temperature co-fired ceramic (LTCC) technology is competent to address the requirements. The incredible growth of consumer electronics market stimulated the manufacturers to seek out ways to make their products cheaper. Consequently, except in high performance applications ceramic substrates have been largely replaced with cheaper polymer based substrates having reasonably good performance. Polymer-ceramic composites are capable to deliver balanced mechanical, thermal and dielectric properties at very low cost. The present thesis is divided into 6 chapters based on the various applications of dielectric materials.

The first chapter gives a general introduction about the dielectric materials for microwave applications. The chapter also describes the important characteristics of dielectric materials required for various applications. A detailed description of various preparation and characterization techniques employed is given in Chapter 2.

Third chapter discusses the preparation and characterization of a series of rare earth based apatites $Ca_{2+x}RE_{8-x}(SiO_4)_{6-x}(PO_4)_xO_2$ [RE= La, Pr, Nd, Sm, Eu, Gd

and Tb] (x= 0, 2, 4 and 6). The structure, microstructure and microwave dielectric properties of the different compositions have been studied. Among the various compositions synthesized, $Ca_4La_6(SiO_4)_4(PO_4)_2O_2$ shows the best microwave dielectric properties. Effect of various isovalent substitutions on the microwave dielectric properties of $Ca_4La_6(SiO_4)_4(PO_4)_2O_2$ has also investigated. The partial substitution of Pr^{3+} for La^{3+} is found to be effective in improving the temperature coefficient of resonant frequency (τ_f).

Chapter 4 describes the development of some low loss, glass free phosphate ceramics for LTCC applications. Detailed investigation on the microwave dielectric properties of the series $LiMg_{(1-x)}Zn_xPO_4$ has been carried out. The ceramics show low ε_r and high quality factor. The τ_f of the ceramics has been tuned to a practically acceptable range by TiO_2 addition. The excellent microwave dielectric properties and the glass-free nature make compositions competitive with the commercially available LTCC substrates. The tape casting of one of the developed composition, $LiMgPO_4$ has been accomplished which is one of the critical technological issues in practical applications.

Fifth chapter deals with the preparation and characterization of polymer matrix composites for microwave applications. Low loss ceramic $Ca_4La_6(SiO_4)_4(PO_4)_2O_2$ (CLSP) developed as part of the present study has been used as filler. High Density Polyethylene (HDPE) with low loss and good processability has been chosen as one of the polymer matrix. Preparation and characterization of mechanically flexible composites for microwave applications with butyl rubber (BR) as matrix and CLSP as filler has also been carried out. The results of present investigation are summarized in Chapter 6. This chapter also proposes the scope for some future work.

Chapter 1

Microwave dielectrics

This chapter discusses the role of dielectrics in microwave electronics. A general introduction about the dielectric ceramics for microwave applications is given. The fundamental physical aspects, working principle and some of the practical applications of dielectric resonators are briefly discussed. The various scientific and technological features of ceramic as well as polymer-ceramic composites for electronic packaging applications are also discussed. The chapter also cites the important characteristics of Low Temperature Co-fired Ceramics (LTCCs) and mechanically flexible substrates for microwave applications.

1.1 Introduction

Communication by any means is imperative in the development of a society. From radio and television broadcasting to cellular telephone, wireless communication has reformed the world. Wireless communication has become an omnipresent part of the modern civilization. Among the various wireless systems, cellular phone systems have shown an explosive growth over the last decade. The number of mobile cellular subscriptions worldwide has reached almost 6 billion with around 900 million in India. Wireless technology finds a wide range of applications which includes radio and television broadcasting, cellular telephone systems, Satellite communication, Wireless Local Area Networks (WLANs), Global Positioning Systems (GPS), Radio Frequency Identification (RFID) systems, Intelligent Transport Systems (ITS), Wireless Sensor Networks (WSNs) etc. (Schwartz, 2005).

The evolution of present wireless communication systems has its roots in the theoretical prediction by J. C. Maxwell about the existence of Electromagnetic Waves and its experimental verification by H. Hertz (Pozar, 2008). Marconi's demonstration of wireless transmission of radio signals became a real breakthrough in the development of modern wireless communication (Goldsmith, 2005). The advent of using microwaves for wireless connectivity drastically improved the information exchange capabilities. Past two decades have witnessed remarkable developments in wireless technology. The development of Wireless Fidelity (Wi-Fi) enabled fast and easy networking of computers and other devices. Bluetooth technology facilitated efficient short range communication between electronic devices (Khichar *et al.*, 2010). Wireless sensor networks are found to be extremely useful in many industrial and consumer applications like industrial process control, personal health monitoring etc. (Khichar *et al.*, 2010).

Today, most of the wireless systems operate at microwave frequencies. The spectrum crowding and the requirement of higher data rates were the driving forces behind the migration towards the microwave frequencies for wireless communication. Microwaves span from 0.3 GHz to 300 GHz of the electromagnetic spectrum with the wavelengths ranging from 100 cm to 1 mm. Microwaves having frequencies greater than 30 GHz are more specifically referred to as millimeter

waves. The microwave region is divided into different bands as per the recommendations of Institute of Electrical and Electronics Engineers (IEEE) and the band designations are listed in Table 1.1 (Sisodia *et al.*, 2001).

Table 1.1 Microwave frequency bands (Sisodia *et al.*, 2001)

Frequency range (GHz)	Designation
0.3 – 1	UHF
1 – 2	L band
2 – 4	S band
4 – 8	C band
8 – 12	S band
12 – 18	Ku band
18 – 26	K band
26 – 40	Ka band
40 – 300	Millimeter

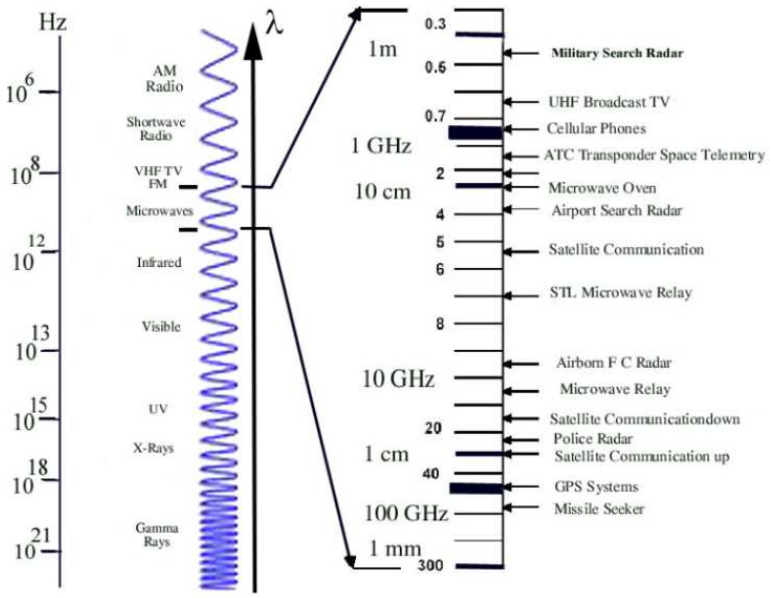

Figure 1.1 The electromagnetic spectrum and various microwave applications.

Major applications of microwaves are summarized in Fig. 1.1. The use of microwaves for wireless communication has several advantages. Primarily, microwaves offer higher bandwidth (information carrying capacity). For faster data

transmission greater bandwidth is needed. Microwave signals travel by line of sight which allows effective frequency reuse. Since the microwave signals are not refracted off the ionosphere, like many low frequency signals do, they are more suitable for satellite communication (Pozar, 2008). Wireless connectivity using microwaves offer high speed voice, video and data access anywhere at any time.

1.2 Dielectrics

Ideally, dielectrics are materials that can store, but not conduct electrical energy. When a dielectric is introduced between two charges, the force between them will be reduced compared to its value in vacuum. This effect is allowed for in calculations by introducing a property of the dielectric called permittivity (ε) or equivalently relative permittivity which is the ratio of permittivity of the material to the permittivity of free space ($\varepsilon_r = \varepsilon/\varepsilon_o$). When a dielectric is placed in an external electric field, the atoms or molecules within it will get polarized resulting in a net dipole moment of the material. In an ideal dielectric, there will be no electrical energy loss under the action of an alternating field, since the energy absorbed in moving the bound charges during one half cycle will be recovered in the subsequent reverse half cycle. Thus in an ideal dielectric, current and voltage will be 90^o out of phase with each other. However, in actual dielectrics, losses occur. Losses are of two kinds, (a) ohmic losses: resistivity of the dielectric is finite, although high and hence there will be a net current in phase with the voltage and (b) absorptive losses: due to the friction associated with the motion of electric charges in applied electric field (Waye, 1967). In real dielectrics, the phase angle (ϕ) between total current (I) and voltage (V) will be 90-δ, where δ is called loss angle (Fig. 1.2).

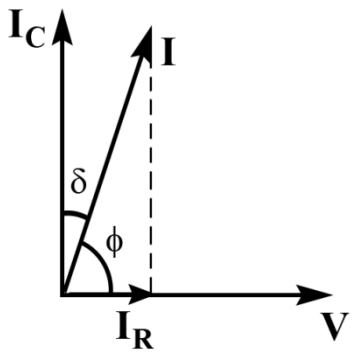

Figure 1.2 Vector diagram of charging, loss and total currents in a dielectric

$$\text{Dissipation factor} = \frac{\text{Power dissipated as heat}}{\text{Total power}} \tag{1.1}$$

$$= \frac{V.I_R}{V.I} = \cos\phi = \sin\delta$$

$$\approx \tan\delta \qquad \text{since } \delta \text{ is very small}$$

Alternately the real dielectric possessing energy storage and loss processes can be represented using the complex permittivity,

$$\varepsilon^* = \varepsilon' - j\varepsilon'' \tag{1.2}$$

or using complex relative permittivity

$$\varepsilon_r^* = \varepsilon_r' - j\varepsilon_r'' \tag{1.3}$$

If an alternating voltage $V = V_o e^{j\omega t}$ is applied to a capacitor containing the dielectric, the charge stored

$$q = CV = \varepsilon_r^* C_o V \tag{1.4}$$

Where C and C_o are the capacitances of the capacitor containing dielectric and vacuum respectively.

Total current,

$$I = \frac{dq}{dt}$$

$$= j\omega\varepsilon_r' C_o V + \omega\varepsilon_r'' C_o V \tag{1.5}$$

The first term on the right hand side of equation (1.5) represents the electrical energy storage and the second term the energy dissipation. ε_r' is called the relative permittivity and ε_r'' is called relative loss factor (Hench *et al.*, 1990).

Then the dissipation factor or loss tangent is given by

$$\tan\delta = \frac{\varepsilon_r''}{\varepsilon_r'} \tag{1.6}$$

The inverse of loss tangent is called quality factor ($Q = 1/ \tan \delta$) and is used as a figure of merit in high frequency applications. Generally for dielectric ceramics, tan δ increases with frequency. However, the product of quality factor and frequency ($Q \times f$) remains almost a constant. Hence it is customary to report the quality factor as $Q \times f$ (Sebastian, 2008).

1.2.1 Different polarization mechanisms

There are four different polarization mechanisms which contribute towards the relative permittivity of a dielectric: (1) interfacial (or space charge) polarization, (2) orientation (or dipolar) polarization, (3) ionic polarization and (4) electronic polarization. In a dielectric subjected to an alternating electric field, with each direction reversal of the field the dipoles try to reorient with the field direction. For each type of polarization, there exists a minimum reorientation time. The reciprocal of this reorientation time gives a relaxation frequency. If the frequency of applied electric field exceeds the relaxation frequency of a particular polarization mechanism, that mechanism will no more contribute towards the relative permittivity. The loss tangent will show a peak at this frequency due to the anharmonicity in the interaction between the dipole and electric field. At low frequencies, all the four mechanisms will be active and as the frequency increases, they weaken one by one as shown in Fig.1.3.

(1) Interfacial polarization: This kind of polarization occurs due to the charge accumulation at the interfaces or grain boundaries. It is also known as Maxwell-Wagner polarization. At higher frequencies, interfacial polarization cannot follow the field variations and hence disappears. The interfacial polarization will be active up to around 10^3 Hz.

(2) Dipolar polarization: It involves the rotation of dipoles under the action of an electric field. When an electric field is applied to a polar substance, the permanent dipoles within the materials will tend to align in the direction of applied field developing a net dipole moment in the material. The relaxation frequency of this mechanism is ~ 10^{11} Hz. In linear dielectrics, dipolar polarization occurs due to the motion of ions between interstitial positions in the

lattice. In such cases, the dipolar contribution relaxes out at around 10^6 Hz. Thermal disorder opposes dipolar polarization.

(3) Ionic polarization: The relative displacement of positive and negative ions in the material under the influence of an electric field is called ionic polarization. This mechanism contributes to the relative permittivity up to ~ 10^{13} Hz.

(4) Electronic polarization: It arises from the displacement of the charge centre of electron cloud relative to the nucleus. Electronic polarization follows the variation of electric field almost instantaneously due to the lighter mass of electrons. Above 10^{13} Hz electronic polarization solely defines the dielectric properties (Hench *et al.*, 1990).

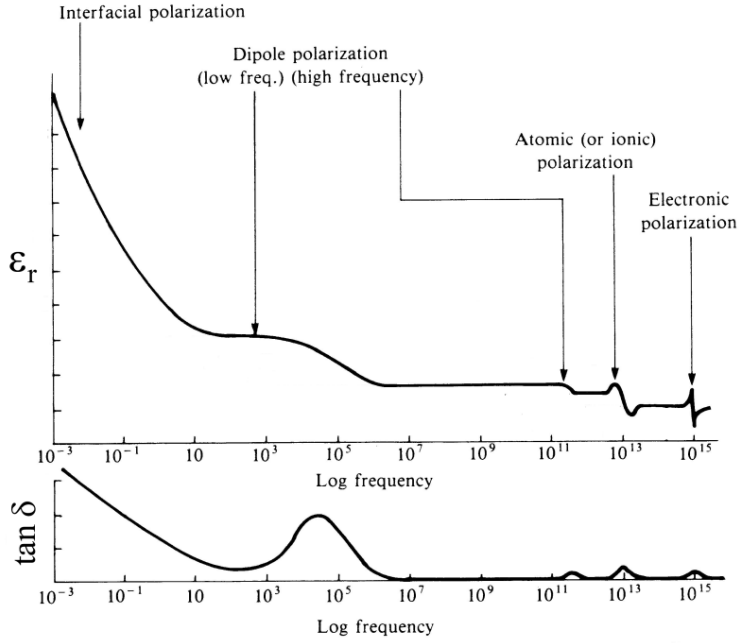

Figure 1.3 Frequency dependence of ε_r and tan δ (Hench *et al.*, 1990)

Both the ionic and electronic polarizations are subject to a counter-active restoring force and show resonance absorption at a characteristic frequency (Fig. 1.3) (Maexa *et al.*, 2003). At microwave frequencies ionic and electronic polarization are the mechanisms responsible for dielectric properties of the material.

1.2.2 Resonance absorption and relaxation absorption

There are two different types of mechanisms which give rise to frequency dependent behavior of dielectrics: resonance absorption and dipole relaxation.

(a) Resonance absorption

An induced dipole can be imagined to consist of a positive and a negative charge bound together by elastic restoring forces. The dipole will have a natural frequency of oscillation ω_o. It can follow the variation of an applied alternating electric field of frequency ω only if $\omega < \omega_o$. The system is equivalent to mechanical problem of forced harmonic oscillator (Rosenberg, 1988). If x is the relative separation of the charges of the dipole, then

$$\frac{d^2x}{dt^2} + \frac{\gamma}{m}\frac{dx}{dt} + \omega_o^2 x = -\frac{eE_o}{m}e^{j\omega t} \tag{1.7}$$

where γ is the damping coefficient, m is the mass, e the charge and E_o the amplitude of electric field.

The steady state solution of this equation is

$$x = \frac{-eE_o/m}{[(\omega_o^2-\omega^2)+j(\gamma\omega/m)]} \tag{1.8}$$

Now the induced dipole moment,

$$\mu_e = \text{Real}\left[\frac{(e^2/m)E_o e^{j\omega t}}{(\omega_o^2-\omega^2)+j(\gamma\omega/m)}\right] \tag{1.9}$$

The coefficient of the electric field is the polarizability and is given by

$$\alpha_e^* = \frac{(e^2/m)}{(\omega_o^2-\omega^2)+j(\gamma\omega/m)} \tag{1.10}$$

The complex relative permittivty,

$$\varepsilon_r^* = 1 + \frac{N\alpha_e^*}{\varepsilon_o}$$

$$= 1 + \frac{N(e^2/m)}{\varepsilon_o[(\omega_o^2-\omega^2)+j(\gamma\omega/m)]} \tag{1.11}$$

where N is the number of atoms per unit volume (Pillai, 2001). Comparing eqn. (1.11) and (1.3),

$$\varepsilon_r' = 1 + \frac{Ne^2}{m\varepsilon_o}\left[\frac{\omega_o^2-\omega^2}{(\omega_o^2-\omega^2)^2+(\gamma\omega/m)^2}\right] \quad (1.12)$$

and

$$\varepsilon_r'' = \frac{Ne^2}{m\varepsilon_o}\left[\frac{(\gamma\omega/m)}{(\omega_o^2-\omega^2)^2+(\gamma\omega/m)^2}\right] \quad (1.13)$$

The variation of ε_r' and ε_r'' near to ω_o is shown in Fig. 1.4.

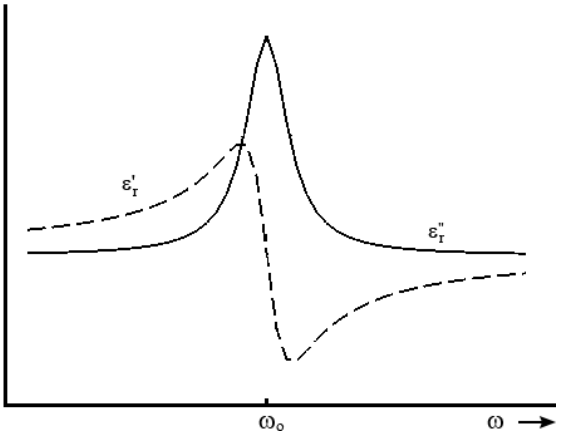

Figure 1.4 Resonance absorption

(b) Dielectric relaxation

If a permanent dipole is oriented in an electric field and is then displaced, it will vibrate about the field direction and eventually relax back into its original position. According to Debye, this orientational polarization is time dependent, approaching its final value in an exponential manner:

$$P(t) = P_o(1 - e^{-t/\tau}) \quad (1.14)$$

where τ is the relaxation time. The solution of eqn. (1.14) gives the Debye equations:

$$\varepsilon_r' = \varepsilon_{r\infty}' + \frac{\varepsilon_{rs}'-\varepsilon_{r\infty}'}{1+\omega^2\tau^2} \quad (1.15)$$

$$\varepsilon_r^{''} = \frac{(\varepsilon'_{rs} - \varepsilon'_{r\infty})\omega\tau}{1+\omega^2\tau^2} \tag{1.16}$$

where ε'_{rs} and $\varepsilon'_{r\infty}$ are the low frequency (static) and very high frequency values of relative permittivity (Buchanan, 2004). The relaxation behavior representing these parameters is shown in Fig. 1.5.

The transition from high to low ε'_r occurs at $\omega_o = \tau^{-1}$ and it tends to be broader than that for resonance absorption. It is also noteworthy that, unlike resonance absorption ε'_r has no maximum and minimum on either side of the drop at ω_o (Rosenberg, 1988).

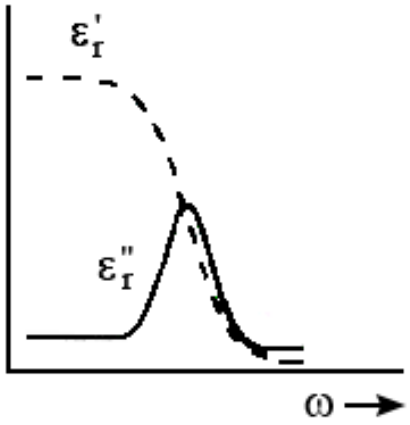

Figure 1.5 Relaxation absorption

1.2.3 Estimation of relative permittivity

The relative permittivity of a dielectric is related to the polarizability of the atoms comprising it. The value of ε_r can be calculated theoretically using Clausius–Mossotti equation for cubic or isotropic materials (Frohlics, 1950)

$$\frac{\varepsilon_r - 1}{\varepsilon_r + 2} = \left(\frac{4\pi}{3}\right)\left(\frac{\alpha_D}{V_m}\right) \tag{1.17}$$

Rearranging

$$\varepsilon_r = \frac{3V_m + 8\pi\alpha_D}{3V_m - 4\pi\alpha_D} \tag{1.18}$$

where V_m is the molar volume and α_D is the sum of the dielectric polarizability of individual ions. The value of ε_r depends on the dielectric polarizability of the constituent ions and the crystal structure. According to the additivity rule of molecular polarizability, α_D of a complex material can be broken up into the molecular polarizabilities of simpler substances (Shannon, 1993). For example

$$\alpha_D(A_2BO_4) = 2\ \alpha_D(AO) + \alpha_D(BO_2) \tag{1.19}$$

where A and B are the cations. It is also possible to break up the molecular polarizability of complex substance into the sum of ion polarizabilities as

$$\alpha(A_2BO_4) = 2\ \alpha(A^{2+}) + \alpha(A^{4+}) + 4\ \alpha(O^{2-}) \tag{1.20}$$

The dielectric polarizability of several ions has been reported by Shannon (Shannon, 1993). The calculated ε_r usually agrees well with porosity-corrected experimental values for well-behaved ceramics. It may be noted that deviations from calculated values can occur due to deviations from cubic symmetry, presence of ionic or electronic conductivity, H_2O or CO_2 in channels, rattling of ions, porosity, presence of dipolar impurities or ferroelectric behavior and also the fact that the sample is ceramic and not a single crystal (Shannon, 1993). The deviations in the reported values of dielectric polarizability and even a small error in determining the cell volume can significantly affect the calculated value of the relative permittivity (Sebastian, 2008).

1.2.4 Factors affecting dielectric properties

The dielectric properties rely on several parameters associated with the material like impurities, processing conditions, phase transitions, defects, porosity etc (Alford *et al.*, 1996; Alford *et al.*, 2001). The dielectric loss can be classified as intrinsic and extrinsic. The intrinsic loss results from the interaction of alternating electric field with the phonons (Gurevich *et al.*, 1991). The external field alters the equilibrium of the phonon system and the subsequent relaxation brings about energy dissipation (Penn *et al.*, 1997). Extrinsic losses occur due to the imperfections like dislocations, grain boundaries, inclusions and second phases (Wersing, 1996). The intrinsic losses set the lower limit of losses in pure defect free crystals. In sintered

ceramics, extrinsic factors dominate in determining the loss. There is no existing theory to predict the microwave loss in dielectric ceramics. Hence the approach to find out new dielectric ceramics for microwave applications is by trial and error method involving preparing and testing a large number of samples (Sebastian, 2008).

1.2.4.1 Effect of porosity

Usually it is very difficult to prepare sintered ceramic with 100% densification and pores will be present in the sample. The presence of porosity may decrease the relative permittivity since air has ε_r = 1. Penn *et al*. obtained the following equation for the porosity correction of relative permittivity of the ceramics by considering the ceramic as a composite of two phases (ceramic and porosity) with different values of ε_r (Penn *et al.*, 1997)

$$\varepsilon_m = \varepsilon_c \left[1 - \frac{3P(\varepsilon_c - 1)}{2\varepsilon_c + 1}\right] \tag{1.21}$$

where ε_m and ε_c are the measured and corrected ε_r. P is the fractional porosity. Similarly the correction for dielectric loss tangent has been obtained as

$$\tan\delta = (1 - P)\tan\delta_o + A'P\left(\frac{P}{1-P}\right)^{2/3} \tag{1.22}$$

where tan δ is the measured value of dielectric loss, tan δ_o is the loss tangent of fully dense material and A' a constant (Penn *et al.*, 1997).

1.2.4.2 Effect of moisture

The moisture captured within the pores will increase the dielectric loss of sintered ceramics. The ions tightly bound in dry condition may become free to move in the presence of moisture and produce an additional loss at low frequencies. The dissociation of water into proton and hydroxyl ion may also produce free charge carriers (Molla *et al.*, 1999). The dipole relaxation of water will result in increased loss at microwave frequencies also (Xiang *et al.*, 2006).

1.3 Dielectric ceramics

Ceramics are inorganic, non-metallic materials generally molded through high temperature sintering. The word ceramic is derived from the Greek word keramos, which translates to “potter’s clay”. Ceramic materials are in general thermally insulating, have high hardness and may have very low thermal expansion coefficients. Their shape is extremely stable due to the absence of capacity of plastic deformation and high modulus of elasticity. However, they are brittle due to the inability of plastic deformation. Ceramics are corrosion and wear resistant (Murray *et al.*, 2008). They show diverse electrical behavior. There are ceramic insulators, dielectrics, semiconductors, conductors, superconductors, varistors, thermistors, ferroelectrics, piezoelectrics etc. (Richerson, 2006).

1.4 Microwave applications of dielectric ceramics

The use of ceramics in electronic equipments is growing rapidly as a result of their superior physical properties. Dielectric ceramics play a vital role in microwave communication. Microwave dielectrics are used as (a) dielectric resonators in filters, oscillators and antennas, (b) microwave substrates and (c) Low Temperature Co-fired Ceramic (LTCC) for multilayer modules. The relative permittivity determines the suitability of a low loss ceramic for each of these applications. High relative permittivity ($\varepsilon_r > 20$) ceramics are required for microwave resonators in order to facilitate miniaturization. On the other hand a low relative permittivity ($\varepsilon_r < 15$) is required for microwave substrates and LTCC applications. Remarkable changes are underway in the computer, telecommunication, automotive and consumer electronics industries. The challenging requirements in all these electronics are: (1) lower cost, (2) light weight and portable, (3) high performance and (4) diverse functionality (Tummala *et al.*, 1999).

1.4.1 Dielectric Resonator

In 1939 Richtmeyer introduced the concept Dielectric Resonator (DR). Dielectric Resonator is a component that can store electromagnetic energy at certain discrete frequencies. DRs are usually made up of ceramics having high ε_r and low dielectric loss. DRs are smaller in size, weight and cost compared to the traditional

wave guide cavity resonators. They can be easily incorporated to Microwave Integrated Circuits (MICs). DRs offer temperature stability of resonant frequency. Due to these unique features, DRs have become key elements in microwave filters and oscillators (Pozar, 2008).

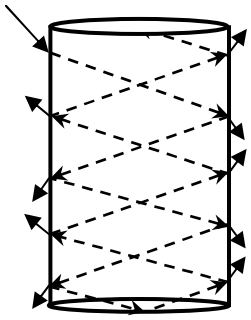

Figure 1.6 Sketch of multiple total internal reflections in DR

The energy confinement in DRs takes place through total internal reflection of electromagnetic (EM) waves at the high permittivity dielectric/air boundary (Fig. 1.6). If the transverse dimensions of the dielectric are comparable to the wavelength of the EM wave, then certain field distributions or modes will satisfy the boundary conditions for Maxwell's equations. As the relative permittivity of the dielectric increases, the impedance offered by the boundary also increases which allows better confinement of EM energy within the dielectric. The reflection coefficient approaches unity when the relative permittivity approaches infinity. The trapped electromagnetic waves will form standing waves to generate resonance. For resonance to occur, dimensions of the dielectric sample must be in the same order of wavelength EM wave (λ_d) inside the dielectric. Since, λ_d is related to the free space wavelength (λ_o) as

$$\lambda_d = \frac{\lambda_o}{\sqrt{\varepsilon_r}} \tag{1.23}$$

an increase in ε_r will decrease the value of λ_d and hence facilitate miniaturization. For microwaves, λ_o is in centimeters and hence λ_d inside the dielectric having ε_r in the range 20-100 will be in millimeters. Still larger values of ε_r give higher

confinement of energy and better miniaturization. However, higher ε_r will also result in higher dielectric losses because of inherent material properties (Sebastian, 2008).

The efficiency of a DR in confining EM energy can be estimated using the quantity called Quality factor (Q) defined as

$$Q = 2\pi \frac{\text{Total energy stored per cycle}}{\text{Average energy dissipated per cycle}} \tag{1.24}$$

Practically, the Q – factor is determined from the resonance peak, when the DR is connected in the transmission mode. If f_o is the resonant frequency and Δf is the -3 dB band width of the resonant peak,

$$Q = \frac{f_o}{\Delta f} \tag{1.25}$$

Q factor is a measure of the power loss of a microwave system. The Q-factor of a DR loaded in a circuit is termed as loaded quality factor (Q_l) given as

$$\frac{1}{Q_l} = \frac{1}{Q_u} + \frac{1}{Q_e} \tag{1.26}$$

where Q_u is the unloaded quality factor of the system and Q_e is external quality factor. In practice, external losses ($1/Q_e$) arise due to coupling. If the coupling is low then the unloaded Q-factor is approximately equal to the loaded Q-factor.

The unloaded quality factor is given by

$$\frac{1}{Q_u} = \frac{1}{Q_d} + \frac{1}{Q_c} + \frac{1}{Q_r} \tag{1.27}$$

where $1/Q_d$ is the dielectric loss ($\tan\delta$), $1/Q_c$ is the conductor loss, and $1/Q_r$ is the radiation loss.

If all conduction, radiation and external losses are negligible, then the loaded Q-factor depends only on the dielectric losses in the resonant structure

i.e. $$Q_l = \frac{1}{\tan \delta} \quad (1.28)$$

However, the reciprocal of Q_l or even Q_u will not be exactly equal to the loss tangent. This is due to the fact that total electric energy in the resonant structure is stored partly in the dielectric and partly in air (Sebastian, 2008).

The temperature coefficient of resonant frequency (τ_f) of the DR determines the frequency stability.

$$\tau_f = \frac{1}{f_o}\frac{\Delta f}{\Delta T} \quad (1.29)$$

where Δf is the difference in resonant frequency corresponding to a temperature difference of ΔT. The temperature coefficient of resonant frequency is related to the temperature coefficient of relative permittivity (τ_ε) through the relation

$$\tau_f = -\frac{\tau_\varepsilon}{2} - \alpha_l \quad (1.30)$$

where α_l is the coefficient of linear thermal expansion. The value of τ_f should be near to zero for practical applications. However, a value in the range -10 to + 10 ppm/^oC is preferred to compensate for the slight changes in the circuit design and device construction materials. The microwave dielectric properties of some important DRs are given in Table 1.2.

Table 1.2 Important microwave ceramics for DR applications (Wersing, 1996).

Ceramic	**ε_r**	**τ_f (ppm/^{o}C)**	**Quality factor (Q_u)**	
			At 2 GHz	**At 20 GHz**
$Ba_2Ti_9O_{20}$	40	2	15000	2000
$Zr_{0.8}TiSn_{0.2}O_4$	38	0	15000	3000
$BaTi_u[(Ni_xZn_{1-x})_{1/3}Ta_{2/3}]_{1-u}O_3$	30	-3 to +3	26000	5000
$Ba[Sn_x(Mg_{1/3}Ta_{2/3})_{1-x}]O_3$	25	0	> 40000	10000
Nd_2O_3-BaO-TiO_2-B_2O_3	~90	0	3000	--
$BiNbO_4$	~40	30	4000	--

1.4.1.1 Modes in DR

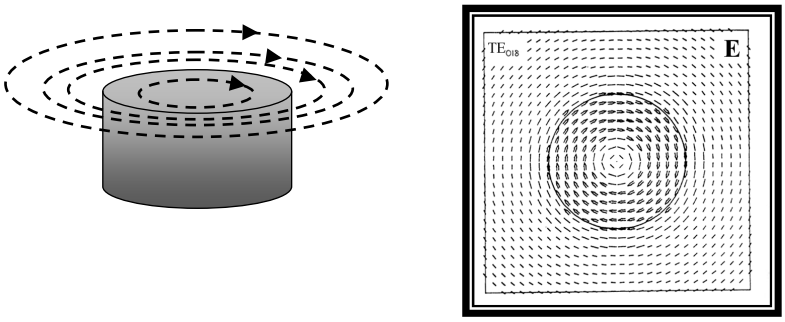

Figure 1.7 Electric field distribution of $TE_{01\delta}$ mode in equatorial plane (Kajfez *et al.*, 1998)

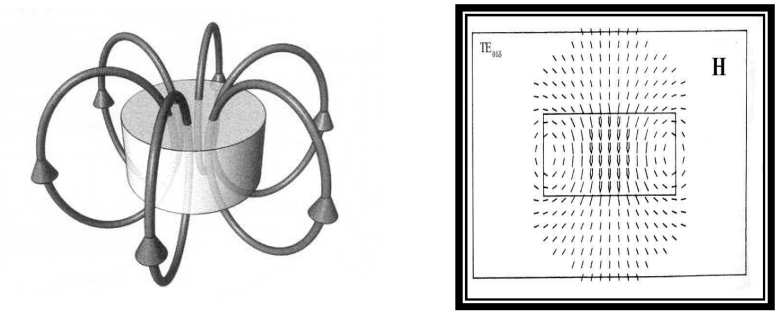

Figure 1.8 Magnetic field distribution of $TE_{01\delta}$ in the meridian plane (Kajfez *et al.*, 1998)

A microwave resonator possesses an infinite number of resonant modes. Each mode has a particular resonant frequency at which the stored electric energy is equal to the magnetic one. The possible resonant modes can be classified into three: Transverse Electric (TE) having only magnetic field component (H_z) along z-direction, Transverse Magnetic (TM) having only electric field component (E_z) along z-direction and Hybrid having non zero values for both H_z and E_z. The fields for TE and TM modes are axisymmetric whereas hybrid modes are azimuthally dependent. Hybrid modes are designated as HE or EH based on the relative contributions of E_z and H_z. The TE, TM, HE and EH modes are classified as

$TE_{nmp+\delta}$, $TM_{nmp+\delta}$, $HE_{nmp+\delta}$, and $EH_{nmp+\delta}$, respectively. The first index denotes the number of field variations in azimuthal direction, the index m (m = 1, 2, 3 …..) denotes the order of the field variations along the radial direction and the index p+δ (p = 0, 1, 2……) that of the field variation along the z-direction (Snitzer, 1961; Kobayashi *et al.*, 1980). Practically a part of the field in the z-direction will decay exponentially outwards the surface of the DR and is termed as evanescent field. Hence it is customary to denote the fraction of the half cycle variation in the z-direction with δ (Chen *et al.*, 2004; Pozar, 2008).

The resonant mode most often used in shielded microwave circuits is $TE_{01\delta}$. It is a transverse electrical mode having azimuthal symmetry. For a dielectric resonator with high ε_r, $TE_{01\delta}$ will be the lowest order mode, provided thickness (L) of the DR less than the diameter (D) (Krupka *et al.*, 1998). Typical field distributions of $TE_{01\delta}$ mode in a cylindrical dielectric resonator are shown in Figs. 1.7 and 1.8 respectively (Kajfez *et al.*, 1998). For practical applications the design of the resonators is done in such a way that there is maximum separation of modes. The DR aspect ratio (D/L) of around 2 is required to avoid the interference of spurious modes (Sebastian, 2008).

1.4.1.2 Applications of DR

Dielectric Resonators have become indispensable components in microwave communication systems due to their unique features. DRs are widely used in oscillators, filters and antennas. Oscillators provide signal sources for frequency conversion and carrier generation. Dielectric Resonator Oscillators (DROs) are typically employed in microwave communication systems, radar systems, navigation systems and other signal receiving or transmitting systems. Microwave filter is used to control the frequency response by enabling the transmission within the pass-band of the filter and attenuating the signal in the stop-band. Dielectric Resonator Filters are a class of stable microwave filters that are frequently used in radar and communication systems. Dielectric resonator antennas (DRAs) are miniaturized antennas of ceramics for microwave frequencies. DRAs are attractive as alternative to microstrip antennas in microwave communication.

1.4.2 Microwave Dielectric Substrate

Microwave substrates provide mechanical support and a guided medium for signal transmission. The dielectric properties of the substrate material have large impact on the performance of the microwave module. The signal propagation delay through the substrate is given by

$$t_d = \frac{l\sqrt{\varepsilon_r}}{c} \tag{1.31}$$

where l is the line length, ε_r is the relative permittivity of the substrate and c is the speed of light. Thus substrates with low relative permittivity are required to increase the speed of the signal (Sebastian, 2008). The signal cross talk between the conductors can also be reduced by decreasing the value of ε_r. The substrate should have low dielectric loss (or high quality factor) to minimize the signal attenuation and power loss. A microwave module experiences a range of steady-state temperatures, temperature gradients, and thermal shocks through manufacturing, storage and operation. The substrate material should have low temperature coefficient of resonant frequency ($-10 < \tau_f < +10$ ppm/^oC) to ensure the stability performance while operation. Several semiconductor components will be attached to the substrate and a large mismatch in their thermal expansion characteristics may lead to the de-lamination of the components. Commonly used semiconductors in microwave devices are Si and GaAs which have coefficients of thermal expansions (CTE) of 3.5 ppm/^{o}C and 6.6 ppm/^{o}C respectively (Lorenzen *et al.*, 2002; Watanabe *et al.*, 2004). Hence the ceramic substrates for microwave applications should have low CTE. High thermal conductivity for the substrate is also desirable for the proper dissipation of excess heat generated in the module. Dielectric substrate materials are classified into hard substrates and soft substrates.

1.4.2.1 Hard substrates

Hard substrates include ceramics and are desirable for applications where bare die (chips) are used such as in a hybrid module. Ceramics are preferred due to their dimension stability and inertness at typical thick-film firing temperatures.

Ceramics offer very high electrical resistivities in the order of 10^{13} Ω-cm. The physical properties of some of the commonly used substrate materials are given in Table 1.3.

Table 1.3 Physical properties of selected substrate materials (Herbert, 1985)

Property	**Al_2O_3**	**BeO**	**AlN**	**Borosilicate**
CTE (ppm/^oC)	6.6	7.5	2.7	3.2
Thermal conductivity ($Wm^{-1}K^{-1}$)	37	250	155	1.3
ε_r	9.9	6.9	10	4.1
tan δ	1×10^{-4}	2×10^{-4}	2×10^{-3}	6×10^{-4}

Alumina is the most commonly used ceramic substrate due to its electrical, mechanical and economical advantages. One disadvantage of alumina is its higher sintering temperature. Alumina substrates have to be sintered at high temperatures (> 1600 ^oC) in order to achieve adequate density (Buchanan, 2004). Berrylia (BeO) has high thermal conductivity and high strength which gives it good thermal shock resistant. It is used for applications in which rapid heat transfer through the substrate is required. Its main disadvantages are higher cost and toxicity. Aluminium nitride (AlN) is another possible candidate that can be utilized for substrate applications. AlN has high thermal conductivity and low coefficient of thermal expansion. However preparation of substrates requires the sintering of AlN powders in nitrogen atmosphere at high temperature. In the past two decades several low permittivity materials like Forsterite (Mg_2SiO_4), Cordierite ($Mg_2Al_4Si_5O_{18}$), Mullite (Al_2SiO_5), Wollastonite ($CaSiO_3$), Willemite (Zn_2SiO_4) and Spinel aluminates ($MgAl_2O_4$ and $ZnAl_2O_4$) have also been developed for microwave substrate application (Sebastian, 2008).

The increased performance requirements and limited space availability has led to the development of multilayer ceramic (MLC) packaging. In MLC technology the circuit patterns are fabricated on more than one layer of ceramic tape, the tapes are then stacked and co-fired to form a single module with three dimensional wiring. The origin of MLC technology lies in the developments at Radio Corporation of

America (RCA) in the late 1950s. In 1965 RCA patented a method of making multilayer circuits. Thereafter remarkable progress was made in this technology. Alumina was the ceramic used as substrate. Since the sintering temperature of alumina is very high, metals having high melting point like Mo and W were used for metallization. This multilayer technology is specifically referred to as High Temperature Co-fired Ceramic (HTCC) technology. In 1980 IBM commercialized HTCC circuit boards (Imanaka, 2005). Some of the commonly used metals for HTCC technology and their resistivity values are given in Table 1.4.

Table 1.4 Elements used as conductors in HTCC (Buchanan, 2004)

Element	Resistivity (μΩ-cm)	Melting point (^{o}C)
Pt	10.5	1769
Pd	10.8	1552
Mo	5.2	2610
W	5.6	3410

Efforts were continued to improve the performance and reduce the size of the electronic modules. The solution was to use finer wiring and thereby increase the circuit density. However if the line width decreases, electrical resistance of the wiring increases resulting in signal attenuation. In this context it was essential to use metals with low electrical resistivity like Au, Ag or Cu. Since these metals have low melting point (~ 1000 ^{o}C) they cannot be co-fired with alumina which necessitated the replacement of alumina with some other materials with low sintering temperature. There came the new technology called Low Temperature Co-fired Ceramic (LTCC) technology. The process steps involved in LTCC technology are similar to the HTCC technology except the materials used. In 1990s commercial use of LTCC technology was started for the development of multilayer electronic modules. The excellent microwave performance together with the possible integration of passives has led to increasing application of this technology in wireless communication systems (Buchanan, 2004; Imanaka, 2005).

1.4.2.2 Soft substrates

Traditionally the packaging of integrated circuits (ICs) has been made using ceramic substrates. However, the increase in the integration level of IC chips and the decrease in semiconductor prices forced the industry to replace ceramic packages with cheaper plastic packages or the so-called soft substrates. Except in the cases requiring high heat conduction and distribution, extremely high stability and operation at very high frequencies, soft substrates are common in use (Buchanan, 2004).

Table 1.5 Properties of some low loss polymers (Gwaily *et al.*, 1995; Koulouridis *et al.*, 2006; Zhou *et al.*, 2007; Thomas *et al.*, 2009; Anjana *et al.*, 2010; Thomas *et al.*, 2011; Joseph *et al.*, 2012)

Polymer	**ε_r**	**Tan δ**	**CTE (ppm/^{0}C)**	**TC ($Wm^{-1}K^{-1}$)**
Polytetrafluoroethylene (PTFE)	2.0	~ 10^{-4}	99	0.26
High Density Polyethylene (HDPE)	2.3	~ 10^{-4}	250	0.45
Polystyrene	2.1	~ 10^{-4}	100	0.08
Epoxy	3.0	~ 10^{-2}	90	0.12
Butyl rubber	2.4	~ 10^{-3}	191	0.8
Silicone rubber	3.5	~ 10^{-2}	285	0.2

Generally, the polymers or polymer based composites are used as soft substrates. Polymers like polytetrafluroethylene (PTFE), polyethylene, polystyrene, poly-ether-ether-ketone and epoxy shows good dielectric properties (Bur, 1985). However, their low thermal conductivity and high thermal expansion limits their application as substrate in electronic modules. The formation of polymer-ceramic composites by loading particles of hard ceramics in a polymer matrix is an effective method in reducing the thermal expansion and improving the thermal conductivity. For some applications, electronic circuits are to be conformally wrapped around curved surfaces. In such cases, either hard substrates or the conventional soft substrates based on plastics cannot be used. However, mechanically flexible soft substrates based on some elastomer may fulfill these requirements. The properties of some of the commonly used polymers for electronic applications are given in Table 1.5.

1.5 Low Temperature Co-fired Ceramics

The tremendous growth of electronic industry has placed new and even more stringent requirements for improved materials and processes. New electronic systems for wireless communication, automotive, industrial, medical, military and space applications have and will continue to demand increased performance requirements and higher densities at low cost. This challenge mandates the use of unique packaging techniques such as Multi Chip Modules (MCMs) that must not only provide the increased circuit density but also the reliability, thermal, mechanical and electrical performance. Low temperature co-fired ceramic (LTCC) technology is competent to address the requirements. In LTCC modules the passive components like resistors, capacitors and inductors are integrated into a monolithic package thereby making the valuable circuit surface area free to incorporate more active components.

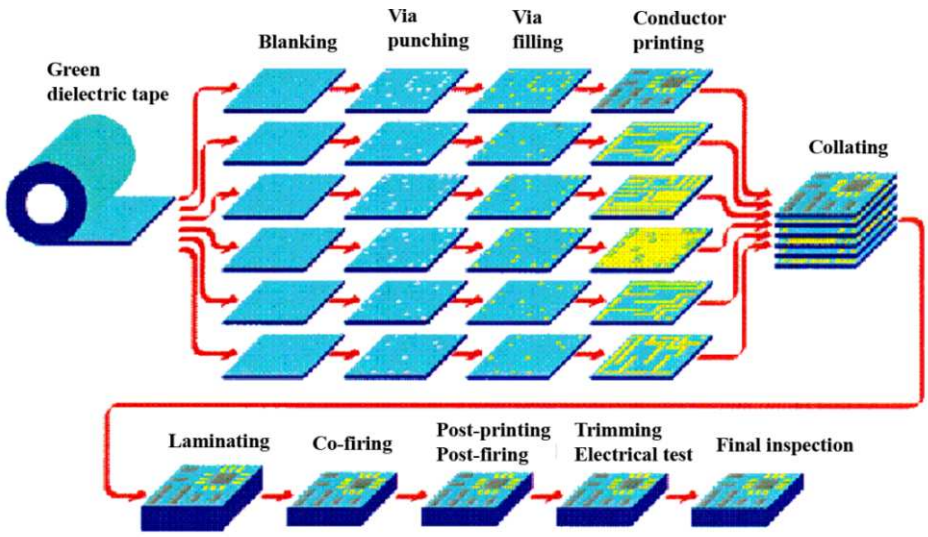

Figure 1.9 Schematic representation of LTCC tape casting process (www.esiee.fr/~vasseurc/images/techno-LTCC.gif)

The process steps of LTCC technology starts with the tape casting of the substrate ceramic into thin sheets. The wiring patterns are then screen printed on the green tapes. Vias for interlayer connection are punched on the tape and are filled with the metal paste. The patterned tapes are stacked and laminated by applying

pressure and heat. The laminate is then fired at suitable temperature to form a monolithic structure (Imanaka, 2005). The overall processes are shown in Fig. 1.9.

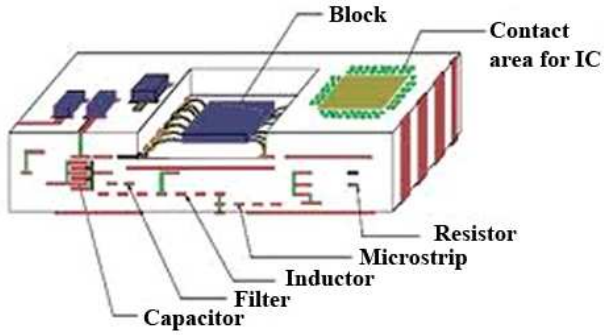

Figure 1.10 A schematic representation of an LTCC multilayer module (courtesy: www.mshak.am)

The LTCC technology offers significant benefits over the other packaging technologies in the development of MCMs. The specific advantages include low processing temperature, single firing step, high print resolution of conductors, good dielectric thickness control and unlimited layer count (Gongora-Rubio *et al.*, 2001). The low line losses and competitive manufacturing costs make the LTCC technology attractive for microwave and even millimeter wave applications (Barnwell *et al.*, 1997; Wolff, 2009). Figure 1.10 shows the schematic of a typical LTCC multilayer module.

1.5.1 Materials selection and requirements

1.5.1.1 Metal powder and paste for LTCC

The general requirements for the electrodes are low electrical resistivity and good adhesion to the substrate. Table 1.6 gives the melting point and the resistivity values of the commonly used metals for wiring in LTCC modules. Among the possible candidates, Ag is the best choice due to its low resistivity and cost effectiveness. The metallization paste is composed of metal powder, glass frit or metal oxide binder and an organic vehicle. The binder is necessary for adhesion to the substrate. In LTCC modules Ag may be used to form all the inner conductors and via fills. However, it will not be used as such for surface conductors due to its

poor leach resistance and poor migration resistance across the surface of the substrate in the presence of an electric field and humid atmosphere. The poor leach resistance Ag (it dissolves rapidly in molten solder) can be improved by making alloys with platinum (Pt) or palladium (Pd) with minimal effect on conductivity. The silver migration can be circumvented by eliminating the possibility of large voltage differences between adjacent conductors in circuit design or by encapsulating the conductor with some glass encapsulant. In the case of Cu metallurgy, Cu based pastes can be used for all the electrical connections. Since Cu can be easily oxidized, deoxidizing firing atmosphere is necessary for copper. While using Au metallurgy, all the inner and outer conductors can be formed using Au as it has good migration resistance. However, due to the poor solder leach resistance of gold, conductors based on Pt/Au or Pt/Pd/Au is used for solderable outer conductors (Buchanan, 2004; Imanaka, 2005).

Table 1.6 Elements used as conductors in LTCC (Buchanan, 2004)

Element	Resistivity (μΩ-cm)	Melting point (^{o}C)
Cu	1.7	1083
Au	2.3	1063
Ag	1.6	961

1.5.1.2 Substrate materials

LTCC technology is evolved from HTCC technology with the purpose of achieving high performance and hence the properties of ceramic substrate should be so adjusted to fulfill the objective. Several factors ranging from the densification temperature to production cost are to be taken into account in the selection of ceramic substrate for LTCC applications.

1.5.1.2.1 Densification temperature

In LTCC technology, the metal electrodes are to be co-fired with the ceramic substrate and hence the sintering temperature of the ceramic should be less than the melting point of the electrode material. In the previous section we have seen that Ag

is the commonly used metal for the wiring in LTCC module. The melting point of Ag is 961 ^{o}C and hence the ceramic should densify at a temperature lower than this value. It is also noteworthy that the densification of the ceramic below 800 ^{o}C is undesirable. If the densification occurs at such a low temperature, it may prevent complete evaporation of organics used during LTCC processing resulting in the traces of residual carbon in the module. The residual carbon left, if any, will degrade the dielectric properties (Tummala, 1991).

1.5.1.2.2 Chemical compatibility with electrode material

The ceramic substrate used should not react with the electrode material. Fine strip-line circuitry screen-printed on ceramic green sheets, must maintain its structure, even after co-firing. Any reaction that occurs between the electrode and the ceramic can destroy the functionality of the module. In order to achieve high strength at the interface between conductor and green sheet, it is essential to consider the compatibility of the resinous constituents used in the conductor and those in the green sheet (Imanaka, 2005). The main difficulties in the development of new LTCC materials are not related to their dielectric properties; instead, they are related to their sintering behavior, thermo-mechanical properties, and especially their chemical compatibility (Valant *et al.*, 2000).

1.5.1.2.3 Dielectric properties

(i) Relative permittivity

The dielectric materials used in LTCC must have a range of values for relative permittivity to permit packaging and integration of embedded passive components. Generally low relative permittivity (ε_r = 4-12) materials are used as substrates in LTCC modules in order to reduce the signal propagation delay. High permittivity materials are used as capacitor layers or to form resonator structures

(ii) Dielectric loss

At low frequencies, conductor loss is more dominant than dielectric loss as far as signal attenuation is concerned. However, above 1 GHz, the impact of dielectric loss becomes significant with the increase in frequency (Imanaka, 2005).

The dielectric loss value of LTCC materials are generally expressed as the product of Q_u value (1/tan δ) and the measurement frequency in GHz (ie. as $Q_u \times f$). The value of $Q_u \times f$ should be high (> 1000 GHz) for the dielectric substrate materials used in LTCC (Sebastian *et al.*, 2008).

(iii) Temperature stability of dielectric properties

The temperature stability of resonant frequency is essential for good circuit performance. A temperature coefficient of resonant frequency value of 10 ppm/^oC causes a 0.11 % shift of the resonant frequency within the temperature range from -30 to +80 ^oC, a common operation temperature range for mobile terminals. Such a shift in resonant frequency brings about a similar change in relative permittivty since both are proportional to each other (eqn. 1.30). Large τ_f values are unfavorable, because temperature compensation requires additional mechanical structures or electrical circuits. The value of τ_f close to zero is greatly appreciable for LTCC applications (Sebastian, 2008).

1.5.1.2.4 Thermal properties

The substrates undergo repeated cycles of thermal stress during assembly processes, reliability tests and device operation. Thus in addition to the dielectric properties, the thermal properties of the LTCC materials must also be considered. The important thermal properties under consideration are thermal conductivity and coefficient of thermal expansion.

(a) Thermal expansion

The thermal expansion characteristics of a material can be expresses in terms of its coefficient of thermal expansion (CTE). CTE gives the characteristic change in dimension of the material for each degree change in temperature, as the material is uniformly heated or cooled. Thus, linear CTE can be written as:

$$\alpha_l = \frac{\Delta L}{L\,\Delta T} \tag{1.32}$$

where ΔL represents the change in length over a temperature span ΔT and L the initial length. For most of the ceramics a near linear variation in length can be observed in the temperature range 25 ^{o}C-500 ^{o}C. Several semiconductor components will be attached to the substrate and a large mismatch in their thermal expansion characteristics may lead to the de-lamination of the components. Hence the LTCC substrates for microwave applications should have low CTE matching with these values.

(b) Thermal conductivity

The semiconductor chips will get heated during their operation. The removal of heat from the chip is very important in order to maintain the chip temperature below 100 ^{o}C for its efficient operation. In recent years considerable attention has been devoted to the heat removal because of the ever growing need to fabricate high density and high power devices that can operate at high speed. There are methods to remove the heat from the back of the chip directly to a heat sink without going through the ceramic (Schwartz, 1984; Tummala, 1991). However it is desirable that the ceramic substrate has high thermal conductivity so that the heat generated can be easily dissipated especially in high power LTCC modules. Special thermal conduction paths called thermal vias are often formed in the LTCC for the efficient heat dissipation. In this case, high thermal conductivity metals with excellent heat transference are required as conductive materials.

1.5.2 Development of LTCC substrate

Most of the conventional ceramics with good microwave dielectric properties have very high sintering temperature which is unsuitable for LTCC applications. In general, there are three methods to develop low temperature fireable ceramics such as (a) using glass-ceramic compositions (b) starting with fine powders prepared through chemical processing as precursors and (c) using ceramics with inherently low sintering temperature (glass free LTCC).

(a) Glass-ceramic compositions

There are three ways to prepare glass-ceramic compositions suitable for LTCC applications. The first approach called the glass-ceramic route starts with fine

powder of a suitable glass composition that sinter to the full density in the glassy state and then crystallizes. The devitrification of glass greatly increases the viscosity of the system during firing, making it stable against further heat treatments. During the sintering, the glass devitrifies to low loss crystalline phases. Thus during the heat treatment complete densification as well as sufficient crystallization will be achieved. Typical example is $MgO\text{-}Al_2O_3\text{-}SiO_2$ glass system having cordierite as the major crystalline phase (Knickerbocker *et al.*, 1993).

In the second approach, the glass-ceramic composite is a mixture of glass and ceramic powder in nearly equal proportion. When sintered at a temperature near to 900 ^oC the composition becomes a continuous vitreous network with the crystalline phases dispersed in it. The densification occurs due to the viscous flow of the glass. In most case reaction takes place between the glass and ceramic producing new crystalline phases. Such reaction products usually improve the properties. For example when the composition containing 55 wt. % alumina and 45 wt.% lead borosilicate glass is sintered at 900 ^oC, anorthite crystallization takes place, due to the chemical relation between alumina and lead borosilicate glass. Anorthite is phase with low ε_r and low CTE (Shimada *et al.*, 1983; Shimada *et al.*, 1990; Buchanan, 2004).

In the third approach (glass + ceramic) very small amount of a low softening point glass will be added to the ceramic to densify it. During heating, the glass becomes liquid phase and fills the capillary pore channels between the ceramic grains. The subsequent liquid phase assisted sintering densifies the ceramic (Kemethmueller *et al.*, 2007). The amount of glass required to achieve densification decreases with increasing the particle size ratio between ceramic filler and glass. The selection of glass materials is very important to the sintering process. The main requirement is that the glass in liquid phase should wet the grains of the ceramics. The use of glasses is found to be an effective way to decrease the firing temperature and most of the LTCC materials developed so far are glass-ceramic compositions (Sebastian *et al.*, 2008).

(b) Wet chemical processing

It has been observed that use of nano-sized particles prepared through wet chemical processing lowers the sintering temperature (Liang *et al.*, 2003; Sanoj *et*

al., 2009; Vidya *et al.*, 2012). However in most cases this method is not effective in reducing the sintering temperature to such an extent that the ceramic can be safely co-fired with the low resistivity metals. Also the chemical processing is complicated and costly. Hence chemical synthesis is not commonly used in the development of LTCC.

(c) Glass free LTCC

The commonly used way to produce LTCC is the use of glass-ceramic compositions. However there are several disadvantages for this method. Usually the dielectric loss of glass phases is large compared to the crystalline phases. Hence it is necessary to minimize the amount of glass in the LTCC composition to get good microwave dielectric properties. The developments of glass-ceramic compositions require initial glass preparation. The glass preparation involves melting of the mixture of raw materials in the temperature range 900-1500 ^{o}C, quenching and pulverization. The high temperature treatment may cause the volatilization of the constituents like Bi_2O_3, B_2O_3, PbO and Li_2O resulting in the unexpected variations in the properties of the final LTCC composition (Jantunen *et al.*, 2000). After firing, a typical glass-ceramic LTCC consists of crystalline phases, residual glass and phase for the modification of the dielectric properties (like $SrTiO_3$, TiO_2 etc.). Unfortunately, the presence of several phases in the LTCC tape increases the probability of chemical reaction between the substrate and the metal electrode (Valant *et al.*, 2004). In addition, presence of glass phase in the LTCC substrate may bring about cracks while soldering due to the CTE mismatch of glass and ceramic if the amount of glass is greater than 5 wt.% (Bian *et al.*, 2005). Considering all these factors, we can say that the development of new ceramic compositions that can be sintered at low temperature without any glass addition is greatly appreciable.

1.5.3 Other applications of LTCC technology

Apart from the electronic packaging applications, LTCC technology finds many other applications. This technology is now being applied for the production of sensors and actuators due to its good electrical and mechanical properties, high reliability and stability as well as possibility of making three

dimensional integrated microstructures (Golonka, 2006). The application of LTCC to micro-high-performance liquid chromatography (μ-HPLC) demonstrates performance advantages at very high pressures (Peterson *et al.*, 2005). Nowadays LTCC technology is widely used in the development of micro-fluidic systems, miniature fuel cells, Micro Total Analysis Systems (μTAS), Polymerase Chain Reactors (PCR), chemical micro reactors, photonic devices and Micro-Electro Mechanical Systems (MEMS) packaging (Chou *et al.*, 2002; Golonka *et al.*, 2005). Another interesting application of LTCC is in the development of three-dimensional shells used for example in spherical stepper motor or radar sensor (Li *et al.*, 2002).

1.6 Composites

The term 'composite' refers to a combination of two or more materials, differing in form or composition on a macro scale. The constituents do not dissolve or merge and retain their identity. In modern usage, composites are made by dispersing filler such as particles, flakes or fibres in a matrix of polymer, metal or glass. By combining two or more constituents, it is possible to create materials with unique properties that cannot be achieved in another way. For this, identification of the important variables controlling the properties is of great importance in the successful manufacturing of a composite. The connectivity of the phases in the composite also plays a crucial role in determining the properties (Dias *et al.*, 1996).

1.6.1 Composite properties

Generally the physical and chemical properties of composites are classified into three.

(a) Sum properties

Sum properties are those properties in which the property coefficient of the composite depends on the corresponding coefficients of its constituents. Usually the property coefficient will be in between those of the constituent phases. The stiffness and relative permittivity are the best examples for sum properties.

(b) Combination properties

Combination properties depend on two or more different coefficients of the constituents. For example acoustic velocity depends on modulus of elasticity and

density of the material and the mixing rules for these two properties are often different. Hence the acoustic velocity of a composite can be smaller than those of its constituent phases. Thus the combination properties involve more than one coefficient which average in a different way.

(c) Product properties

Product properties are more complex. The different properties of the constituents combine to yield a new property, a product property. For example in a magneto-electric composite, the piezoelectric effect of on phase acts on the magnetostrictive effect of the second phase to produce a composite magneto-electric effect which is a product property. In such cases, the interaction between the constituent phases produces unexpected properties of the composite. Sometimes, product properties are found in composites that are entirely absent in the phases making up the composite (Newnham, 1986).

1.6.2 Connectivity

Connectivity is a key feature in the development of a composite since physical properties of the composites rely largely on the manner in which connections are made. The spatial arrangement of components in a multiphase composite is of considerable importance since it controls the mechanical, electrical and thermal fluxes between the phases. Thus, the development of composites with required properties involve choosing the constituent phases with the right properties as well as coupling them in the best possible manner (Dias *et al.*, 1996). Each phase in a composite may be self connected in zero, one, two or three dimensions. In a two phase composite there are 10 possible connectivities designated as 0-0, 0-1, 0-2, 0-3, 1-1, 1-2, 1-3, 2-2, 2-3 and 3-3 connectivity. These connectivity patterns are illustrated in Fig. 1.11 using cube as building block. In general for a composite containing n phases there are (n+3)!/3!n! connectivity patterns (Newnham *et al.*, 1978). The most commonly studied composites are 0-3 and 1-3 configurations. Composites with 0-3 connectivity can be easily prepared at relatively low cost (Dias *et al.*, 1996).

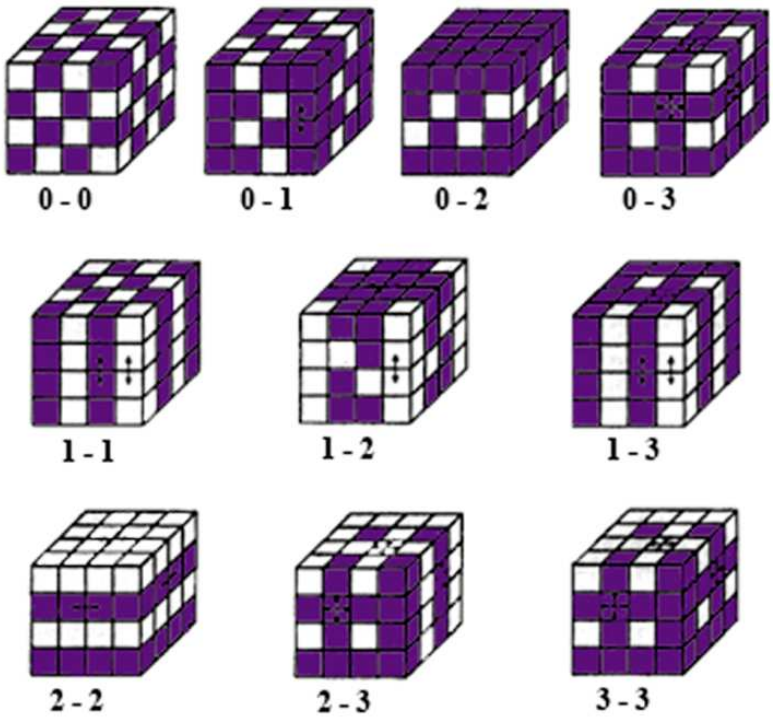

Figure 1.11 Connectivity patterns in a two phase composites system (Dias *et al.*, 1996)

Several methods have been developed for the preparation of two phase composites like extrusion, tape casting and replamine method. Composite with 1-3 connectivity can be prepared through extrusion. A ceramic slip is extruded through a die to produce a three dimensionally connected pattern with one dimensional holes, which can be filled later with a different material. A 2-2 pattern can be produced by tape casting and stacking alternate layers of two different materials. In this arrangement both the phases are self connected in two dimensions (x-y directions), however, not connected in the direction perpendicular to the layers (z- direction). In 2-3 pattern one phase is two dimensionally connected while the second phase is connected three dimensionally with each other. This pattern can be considered as a modified form of the 2-2 composite. In 2-2 pattern if holes are present in the layers of one phase, layers of second phase can connect through the holes to get three dimensional connectivity (Newnham *et al.*, 1980).

1.6.3 Polymer-ceramic composites

Polymer-ceramic composites are one of the important classes of composites. In a polymer-ceramic composite, the physical properties of the polymer matrix will be modified with suitable ceramic fillers. Polymer-ceramic composites can have thermoplastic or thermosetting matrices. Thermoplastics are polymers that melts on heating and solidify to a rigid state when cooled without undergoing any chemical change. Polymers that are not cross linked are thermoplastics. Thermosetting polymers on the other hand irreversibly cure to a rigid form. Cross-linked polymers are thermosets. The curing may be carried out by heating or through some chemical processing. Thermoplastics have the advantage that they can be reworked by heating for the purpose of repair, whereas thermosetting matrices cannot be reworked (Chung, 2000). Most thermoplastics are high molecular weight polymers whose chains associate through weak Van der Waals forces (polyethylene); stronger dipole-dipole interactions and hydrogen bonding (nylon); or even stacking of aromatic rings (polystyrene). There are two types of polymers amorphous and semicrystalline. None of the polymer is completely crystalline. Semicrystalline polymers contain crystalline and amorphous regions in the polymer chain. In crystalline regions the chain can neatly fold over on it. In amorphous regions, on the other hand chain folding does not occur. Bulky side groups in the chain inhibit the folding and increase the amorphous nature (Murray *et al.*, 2008).

1.6.4 Polymer-ceramic composites for electronic applications

Composites are traditionally used as structural materials. With the rapid growth of electronic industry composites are finding more and more electronic applications. The importance of polymers in electronic applications lies in the fact that, although they are not inherently functional, they can be made functional and their soft or flexible nature enables the molding in a variety of different shapes. In addition they are inexpensive, corrosion resistant and they have low density (Murray *et al.*, 2008). Polymer matrix composites find a wide range of applications in microelectronics like interconnections, substrates, encapsulations, interlayer dielectrics, die attach, electrical contacts, connectors, thermal interface materials, heat sinks, lids, housings etc. (Chung, 2000). Recently, there is an increasing interest

in polymer ceramic composites for microwave applications because they enable inexpensive industrial level realization of microwave devices and packages with advanced electric and mechanical properties.

Generally polymers have low processing temperature and many of them have good microwave dielectric properties. However, the low thermal conductivity and high coefficient of thermal expansion of polymers are unfavorable. Ceramic–polymer composites with 0–3 connectivity are attractive materials for producing microelectronic packages that combine the electrical properties of ceramics and the mechanical flexibility, chemical stability, and processing possibilities of polymers. Recently, a large number of polymer-ceramic composites have been introduced for telecommunication and microelectronic applications. The composites with a three-dimensionally connected polymer matrix loaded with isolated ceramic particles called composites of 0-3 connectivity is attractive for practical applications. Composites of 0-3 connectivity enable flexible forms and very different shapes with very inexpensive fabrication methods like simple mixing and molding. Polymer-ceramic composites used in microelectronic packaging have to simultaneously fulfill diverse requirements such as low dielectric loss (tan δ), moderate relative permittivity (ε_r), low temperature coefficient of relative permittivity (τ_ε), low moisture absorption, low coefficient of thermal expansion and high dimensional stability and mechanical stiffness. The processing, design aspects and requirements for polymer-ceramic composites for microwave applications are discussed in the recent review “Polymer–Ceramic Composites of 0–3 Connectivity for Circuits in Electronics: A Review” authored by Sebastian and Jantunen (Sebastian *et al.*, 2010).

1.6.5 Mechanically flexible composites

Mechanically flexible electronic systems find applications in various fields including communication, automotive, biomedical and aerospace. In a near future flexible electronics will replace several conventional electronic circuits. The development of technologies based on organic materials, printed polymers, inkjet print chemicals, carbon nanotubes and thin film semiconductors contributed to the evolution of flexible electronics. The progress in these areas have generated several new applications like flexible displays, flexible and conformal antenna arrays, solar

cell arrays, radio-frequency identification (RFID) tags, flexible batteries, electronic clothing and biomedical devices (Park *et al.*, 2008; Siegel *et al.*, 2010).

Electronic circuit printed on a flexible dielectric substrate constitutes the base of flexible electronics. Such electronic assemblies should have good flexibility and stretchability, so that they can take the shape of the object in which they are integrated giving more comfort. Examples for such systems are implants, intelligent textiles, portable electronic equipments like mobile phones and navigation systems, robotics etc. (De Geyter *et al.*, 2008). In addition to being readily bendable, the flexible substrate must have good dielectric and thermal properties. Unfortunately, there is no single phase flexible material meeting all these requirements. Some of the elastomers show exceptional dielectric properties as well as flexibility. But they have large coefficient of thermal expansion and poor thermal conductivity which are undesirable for substrate applications. On the other hand, dielectric ceramics are well known for their good dielectric properties, low thermal expansion and moderately high thermal conductivity. But their inherent brittleness precludes them from direct use. Hence neither elastomers nor ceramics can be used as such for the flexible substrate applications. The most convenient way to get all the requisite properties together is by the formation of elastomer-ceramic composites (Thomas *et al.*, 2011).

Chapter 2

Synthesis and characterization

Detailed description of various steps involved in the preparation of dielectric ceramics, LTCC tapes and polymer-ceramic composites for microwave applications is given in this chapter. Various characterization techniques used to study the structure, microstructure, microwave dielectric properties, thermal and mechanical properties are also discussed

2.1 Ceramic processing

Most of the earth's solid surface is composed of natural ceramics and the earliest human beings used these materials for various purposes. Ceramic processing has very ancient history when someone found that clay could be hardened by fire and since that time pottery making has developed as an art. Remarkable progress in synthetic chemistry and related fields has made the synthesis of various ceramic materials possible. The preparation of these artificial materials required the development of ceramic processing from an art to a science. This development has supported the basis of so-called 'fine or advanced ceramics'. The functions of these materials depend on their morphology, over which control has been gained through advances in production processes. Ceramic fabrication is the combination of various process technologies to produce monolithic or composite ceramic components with a given shape, size and microstructure for a given composition. The microstructure governs the properties of ceramics to a large extent and the manufacturing process strongly influences the microstructure (Norton, 1970; Saito, 1985; Richerson, 2006).

Ceramics are prepared by powder metallurgical processes. The processing of ceramics into useful products involves alloying the powdered raw materials with additives, pressing followed by sintering and finishing. The final properties of a ceramic component rely on the nature of the raw materials used. The synthesis of specific powders with better control over the chemical and physical characteristics allows obtaining improved and reproducible properties. The are several methods for ceramic powder synthesis which can be broadly classified into (a) mechanical methods (b) solid state reaction methods and (c) chemical methods (Arai, 1996). In the mechanical methods, fine particles are produced from larger ones by mechanical forces, a process referred to as comminution. The process involves operations such as crushing, grinding and milling. Mechanical treatment of ceramic powders can reduce particle size and enables to obtain even nano-structured powders. Powders of traditional ceramics are usually prepared by mechanical methods from naturally occurring raw materials. The most commonly used method for the preparation of ceramic powders in bulk is by solid-state reaction, due to its simplicity and cost effectiveness. Several chemical methods like citrate gel, molten salt, co-

precipitation, sol-gel, hydrothermal and polymer precursor methods are available to prepare very fine ceramic powder (Johnson, 1985; Thirumal *et al.*, 2001). Nevertheless the sinterability of bulk ceramics prepared using chemically derived powders is found to be very poor and hence none of these techniques could give a higher quality factor for dielectric ceramics compared to those prepared through solid state route. Moreover the stringent operation conditions involved in the reaction sequence as well as the high cost of precursors limit the usage of chemical methods for the industrial fabrication of DRs and microwave substrates. Hence in the present study we employed the conventional solid state synthesis of ceramics for the fabrication of dielectric ceramics.

2.2 Solid state synthesis

The solid state ceramic route is the conventional and easiest way of synthesizing complex oxide materials. The method involves basically four steps (a) intimate mixing of the raw powders in stoichiometric ratio, (b) high temperature firing/calcination (c) intermediate grinding and (d) sintering. On heating at high temperatures, the new phase will be formed to reduce the free energy, at the points of contact through solid state diffusion (Fig. 2.1). This new product layer (of a few Å) subsequently acts as a potential barrier between the two grains and thus impeding further material transport. This demands the need of new point of contacts to be introduced which is usually achieved through grinding or ball milling (Kingery, 1960; West, 1984). The process steps involved in solid state route is discussed in detail below.

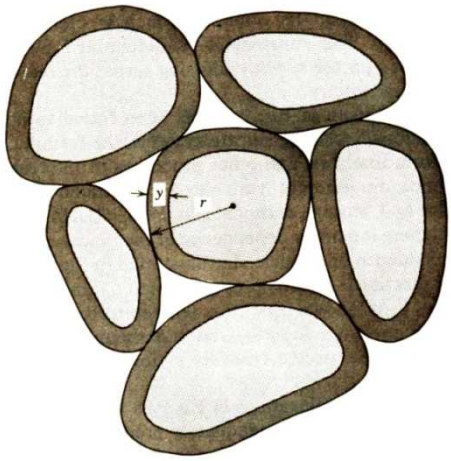

Figure 2.1 Schematic representation of reaction product layer formation (Kingery, 1960).

2.2.1 Selection and weighing of raw materials

The proper selection of raw materials requires an idea about the final material properties stipulated. For example, it has been observed that increased level of impurities is detrimental to the microwave dielectric properties (Alford *et al.*, 1996). Hence it is necessary to use high purity starting materials for the synthesis of microwave ceramics. Mainly oxides of the constituent cations are used as precursors in the solid state method. Sometimes, when the oxides are hygroscopic carbonates will be preferred. For example $MgCO_3$ could be used as a source of MgO which is less hygroscopic than MgO (West, 1984). In the present study, electronic balance with four decimal place accuracy is used for weighing the raw powders in stoichiometric ratio.

2.2.2 Mixing of raw materials

The objective of mixing is to increase the points of contact between reactant oxides, which in turn enhance the product layer formation. The process of mixing breaks the agglomerates so that the individual particles can move relative to one another. During the mixing, defects are introduced into the grains which enhance diffusion during the subsequent heat treatment. Therefore the mixture of powders is ground well and thoroughly mixed using distilled water or ethanol. Ball mills are used for the mixing purpose. In the present investigation, the mixture of constituent powders taken in polythene bottles and ball milled for sufficient duration in ethanol using Yttria Stabilized Zirconia (YSZ) balls. In the milling process, the particles experience mechanical stresses at their contact points due to the collisions with the milling medium, other particles and mill wall. The rate of milling is determined by the relative size, specific gravity and hardness of the media and particles. The shape of the milling media (balls) is an important factor in ball milling as it determines the final size distribution. Using spherical balls, the size distribution will be broad since two balls have only one point of contact between them. On the other hand, using cylindrical balls with ‘dome ends’ more uniform and narrow particle size distribution will be obtained (Rose *et al.*, 1958). This is due to the fact that cylindrical balls offer a line of contact between them.

2.2.3 Calcination

Calcination is the high temperature treatment of the starting raw materials to allow their reaction towards the desired compound. Calcination promotes the interaction between the constituents to yield a material that after grinding and compaction will sinter to a dimensionally, mechanically and electrically satisfactory body. The compound may not be fully formed during calcination and some further diffusion of ions may assist sintering (Herbert, 1985). The kinetics of solid state reactions that occur during calcination may be controlled by any one of the three processes: (i) the reaction at the interface between the reactant and the solid product, (ii) heat transfer to the reaction surface or (iii) gas diffusion or permeation from the reaction surface through the porous product layer. The heating programme of calcination is to be selected based on the form and reactivity of the reactants. If one or more of the reactants is an oxysalt e.g. $MgCO_3$, the mixture should be first heated at an appropriate temperature below the calcination temperature for a few hours so that decomposition of the reactants occur in a controlled manner (West, 1984).

2.2.4 Grinding

The calcined ceramic powder will contain large grains and agglomerates. On sintering, the agglomerates will grow together into larger particles producing porosity in the microstructure (Barsoum, 2003). Hence to achieve a dense defect free microstructure, the calcined powder should be ground into fine powder before sintering. The grinding process decreases the particle size, increases specific surface area and provides surface activation. For grinding small quantities (< 20 g), agate mortar with pestle is used. Agate is preferable since it is hard, unlikely to contaminate the powder and with its smooth, non-porous surface, is easy to clean afterwards. For quantities larger than 20 g, manual grinding is difficult and hence ball mill is used.

2.2.5 Addition of polymer binder

Binders are added to give enough strength to the green body while handling or green machining prior to densification. They coat on the ceramic particles and provide lubrication while pressing and temporary bonding after pressing. The

polymeric binders are normally burnt out before densification. Some binders leave carbon residue, especially when fired in reducing atmosphere (Richerson, 2006). The selection of binder must be based on compatibility with the ceramic and the purity requirements of the application. In modern ceramic technology, for die pressing, a narrow range of water-soluble organic binders, such as poly vinyl alcohol is most often applied (Onoda *et al.*, 1973). The binder concentration required is about 3 wt% in dry process, 3-17 wt% in wet processing and 7-20 wt% in plastic forming (Lampman *et al.*, 1991). The commonly used polymers for ceramic binding purpose are poly vinyl alcohol (PVA), poly ethylene glycol (PEG), methyl cellulose etc. (Alford *et al.*, 2000). The burnout of polymeric binders become complete by 600 to 700 ^{o}C in oxidizing atmosphere (Baklouti *et al.*, 2001).

2.2.6 Uniaxial pressing

The compaction of ceramic powder is an important stage in the ceramic processing. A typical compaction process involves three basic steps: (i) filling the mold or die with powder (ii) pressing the powder to a specific size and shape and (iii) ejecting the compact from the die. Uniaxial pressing is the most commonly used method for powder compaction. It involves the compaction of powder into a rigid die by applying pressure in a single axial direction through a rigid plunger or piston (Richerson, 2006). Compaction is done slowly to facilitate the escape of the entrapped air. The pressure applied should be sufficient for the pressed compact to achieve a density of about 60 % of that of the fully densified sample. This can be normally achieved at a pressure between 100 – 300 MPa, depending on the aspect ratio and other shape factors (Herbert, 1985). One of the major problems with uniaxial pressing is the nonuniform density of the compact. This may lead to warpage, distortion or cracking during sintering. The density variation occurs due to friction between the powder and the die wall and between powder particles, nonuniform fill of the die and the presence of hard agglomerates in the powder. The die wall and particle –particle friction can be reduced by using suitable lubricants and binders (Richerson, 2006). Stearic acid dissolved in Propane 2-ol can be used as a lubricant to reduce the die wall friction. Highly polished Tungsten Carbide or steel are used as the die material, which also helps in great deal to reduce the friction.

2.2.7 Solid state sintering

The word "sinter" comes from the German *Sinter* having the meaning “solid piece of matter remaining after combustion”. Sintering is a thermally activated transition of a powder or porous system to a thermodynamically more equilibrium state through a decrease of free surface energy. It involves heat treatment of powder compacts at elevated temperatures, where diffusional mass transport is appreciable which results in a dense polycrystalline solid. During this process removal of pores occurs combined with growth and strong bonding between adjacent particles.

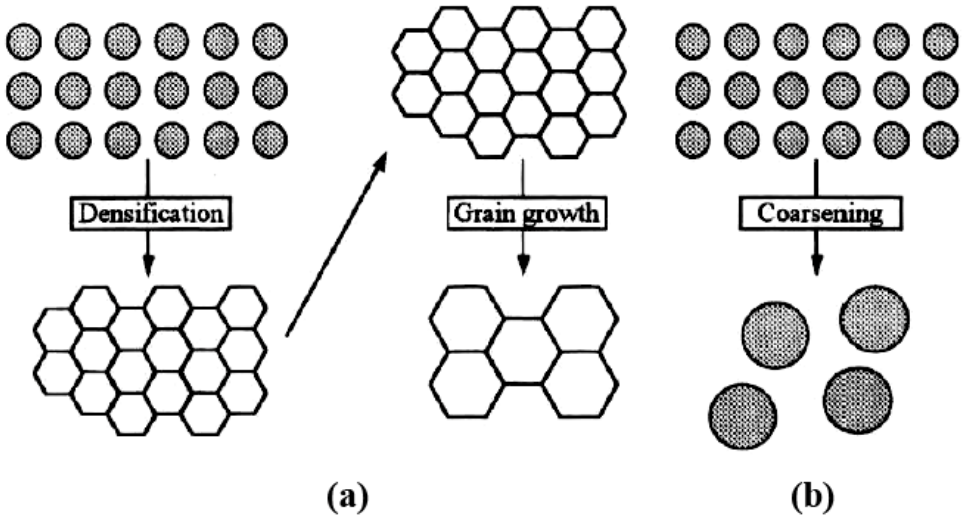

Figure 2.2 Schematic of (a) densification followed by grain growth (b) coarsening (Barsoum, 2003).

For sintering to happen, the following factors must be present: (1) a driving force, (2) a mechanism for material transport and (3) a source of energy to activate and sustain this material transport (Richerson, 2006). Sintering is accompanied by a decrease in surface area and hence the free energy of the system. The sources that bring about this lowering of free energy are identified as the driving forces for sintering. Three possible driving forces are (1) the curvature of the particle surfaces, (2) an externally applied pressure and (3) a chemical reaction. The mechanism of sintering is through material transport. In crystalline solids, material transport occurs predominantly by diffusion. There are several paths through which diffusion can occur. These paths define the mechanisms of diffusion and therefore the

mechanisms of sintering (Rahaman, 1999). Heat is the primary source of energy, in conjunction with energy gradients due to particle-particle contact and surface tension. There are mainly two types of sintering, solid state sintering in which only solid phases are present during sintering and liquid phase sintering where small amounts of liquid phase will be present at sintering temperature.

The reduction of the excess energy associated with surfaces while sintering can happen in two ways (1) reduction of the total surface area by an increase in the average size of the particles, which leads to coarsening (Fig. 2.2a), and/or (2) the elimination of solid/vapor interfaces and the creation of grain boundary area, followed by grain growth, which leads to densification (Fig. 2.2b) (Barsoum, 2003). There are several competing paths for the material transport to the neck area between two particles in contact. Some of these lead to densification which requires the centers of particles approach each other. The remaining transport mechanisms lead to coarsening in which growth of neck occurs thereby reducing the specific surface area without shrinkage. The various possible paths for material transport in the initial stage of sintering are given in Table 2.1 and are depicted in Fig. 2.3. Evaporation-condensation and surface diffusion are coarsening mechanisms. On the other hand grain boundary diffusion and lattice diffusion are densification mechanisms.

Table 2.1 Alternate paths for material transport during sintering (Chiang *et al.*, 1997).

Mechanism number	Transport path	Source of matter	Sink of matter
1	Surface diffusion	Surface	Neck
2	Lattice diffusion	Surface	Neck
3	Evaporation-condensation (Vapor transport)	Surface	Neck
4	Boundary diffusion	Grain boundary	Neck
5	Lattice diffusion	Grain boundary	Neck
6	Lattice diffusion	Dislocations	Neck

The various stages involved in the solid state sintering are shown in Fig. 2.4 below.

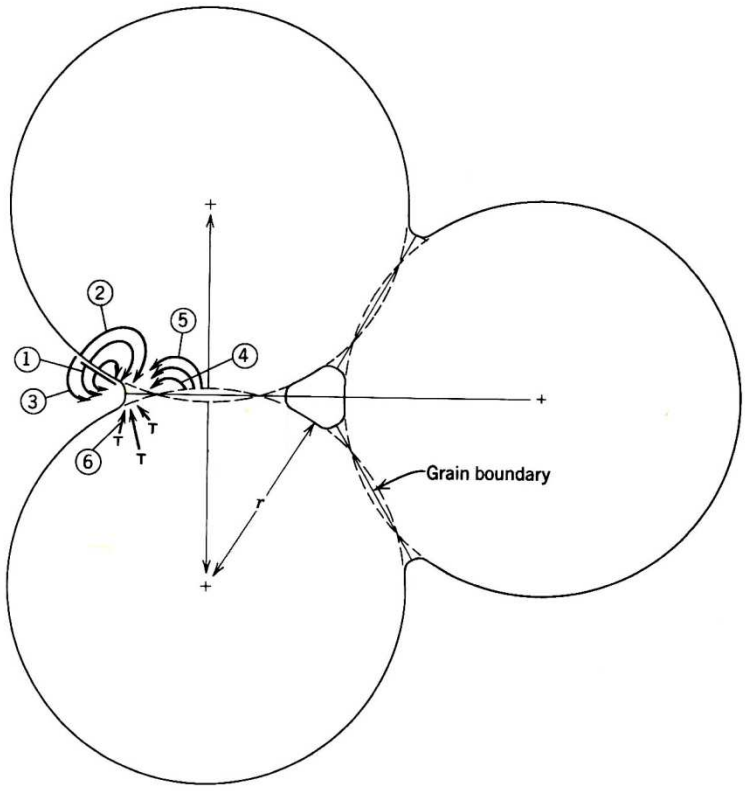

Figure 2.3 Different paths for material transport during sintering (Chiang *et al.*, 1997).

(a) Initial stage of sintering:

It involves rearrangement of particles and initial neck formation at the contact point between each particle. The rearrangement consists of slight movement or rotation of adjacent particles to increase the number of points of contact. After the initial stage, the densification of the sintering component increases by ~10% and it is reached very quickly after exposing powder to high temperature because of the large surface area and the high driving force for sintering (Kingery *et al.*, 1955).

(b) Intermediate stage of sintering:

The second stage of sintering is referred to as intermediate sintering. The physical changes that occur at this stage are: the size of the necks between the particles grow, porosity decreases and the centers of the original particles move closer together. The grain boundaries begin to move so that one grain begins to grow while the adjacent grain is consumed. This allows geometry changes that are

necessary to accommodate further neck growth and removal of porosity. Intermediate sintering continues as long as pore channels are interconnected and ends when pores become isolated. Most of the shrinkage during sintering occurs during this stage. During this stage the relative density increases to about 95% (Gupta, 1978).

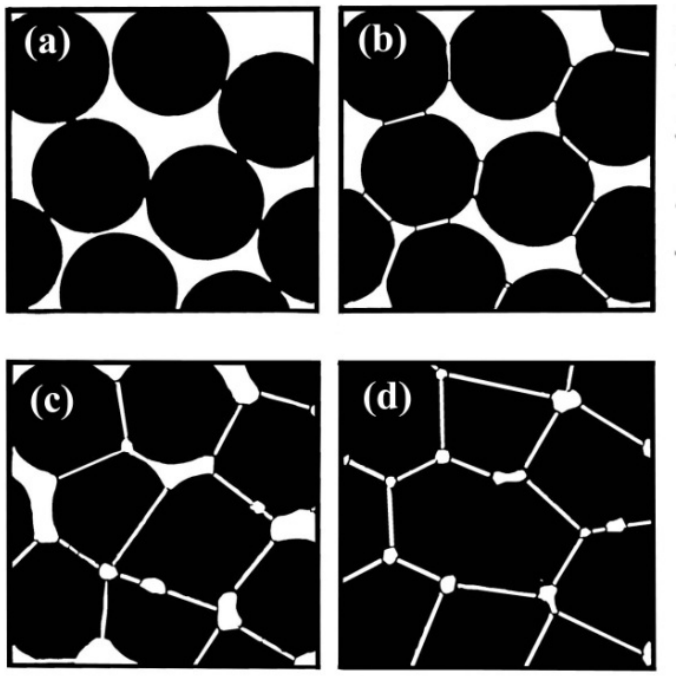

Figure 2.4 (a) & (b) Initial stage, (c) Intermediate stage and (d) Final stage of sintering (Lampman *et al.*, 1991).

(c) Final stage of sintering:

It involves the final removal of porosity by vacancy diffusion along the grain boundaries. Therefore the pores must remain close to the grain boundaries. Pore removal and vacancy diffusion are aided by the movement of grain boundaries and controlled grain growth. However, if grain growth is too rapid, the grain boundaries can move faster than the pores and leave them isolated inside the grain. Therefore, grain growth must be controlled to achieve maximum removal of porosity (Barsoum, 2003).

2.3 Casting of LTCC tapes

The first step in the production of multilayer ceramic modules is the casting of ceramic into thin tapes. In tape casting, also called the doctor-blade process, ceramic slurry is spread over a surface using a carefully controlled blade referred to as doctor blade (Rahaman, 1999). This method was introduced for ceramic materials for the first time by Glenn Howatt in 1947 (Howatt *et al.*, 1947) and ever since it has been used to produce multilayer capacitors, ceramic substrates, High Temperature Co-fired Ceramic (HTCC) and Low Temperature Co-fired Ceramic (LTCC) applications. The tape casting method is able to produce flexible, self-supporting green ceramic sheets with a wide thickness range (10 µm–1 mm). The tapes also have smooth surfaces suitable for accurate printing to form e.g. conductive patterns (Mistler *et al.*, 2000). The process flow chart for tape casting is shown in Fig. 2.5.

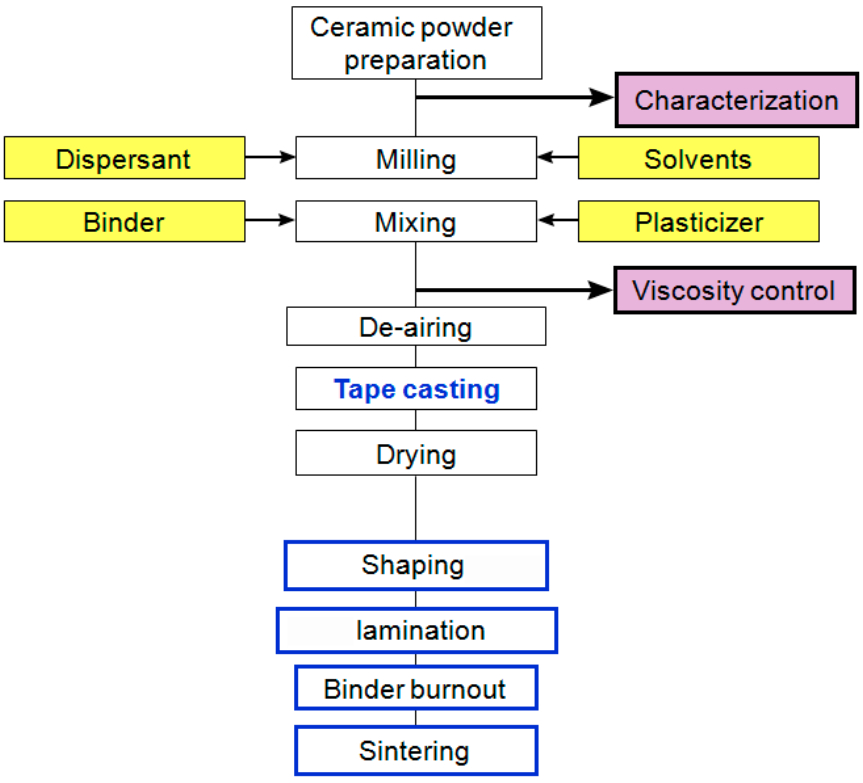

Figure 2.5 Process flow chart for tape casting.

Table 2.2 Composition of tape casting slurry (Buchanan, 2004).

Component	Function
Part 1	
Ceramic powder	Provide the desired material properties
Solvent	Solvate polymer binders, and functional additives; disperse powder particles
Dispersant	Disperse powder particles; control the degree of particle agglomeration
Part 2	
Binder	Interconnect powder particles; provide green tape strength; guarantee laminate formation
Plasticizer	Give flexibility to the green tape
Homogenizer	Makes the system uniform throughout and prevents skin formation

Tape casting involves the preparation of ceramic slurry with good flow properties and casting the slurry into thin tape. The tape casting slurry will be prepared by dispersing the ceramic powder in a suitable solvent using some dispersant followed by the addition of binder and plasticizer to increase the strength and flexibility of the final tape. Tape casting can be accomplished through aqueous or non-aqueous route. In aqueous route, water is used as the solvent for slurry preparation and in non-aqueous route some organic solvent will be used. Non-aqueous systems offer the advantage of fast and easy drying of the cast tapes. The solvent used must dissolve the dispersant and binder. Usually binary solvent systems are used due to their increased ability to dissolve different organic additives, greater control over the slurry rheology and drying speed. Mixture of ethanol and xylene is one of the commonly used binary system for tape casting. Conventionally fish oil has been used as the dispersant for tape casting as it works with most of the ceramic powder. The higher deflocculating ability of fish oil is due to the presence of a large variety of long chain fatty acids in it. Polymeric binder provides strength to the green tape by holding the ceramic particles together. Polyvinyl butyral (PVB) is a binder extensively used in tape casting systems. Plasticizers impart flexibility to the ceramic green tape. Plasticizers are classified as Type I and Type II depending on how they work to provide flexibility. Type I plasticizer softens the polymer chains of the binder and make the tape more stretchable without fracture. Butyl benzyl phthalate is suitable Type I plasticizer compatible with PVB. Type II plasticizer lubricates the tape matrix, thus providing flexibility. It also provides good flow properties to the slurry during casting. A homogenizer may also be added in the tape

casting slurry to avoid the skin formation while drying the tape (Moreno, 1992; Mistler *et al.*, 2000; Imanaka, 2005). The generally used ingredients of tape casting slurry and the function of each component are given in Table 2.2.

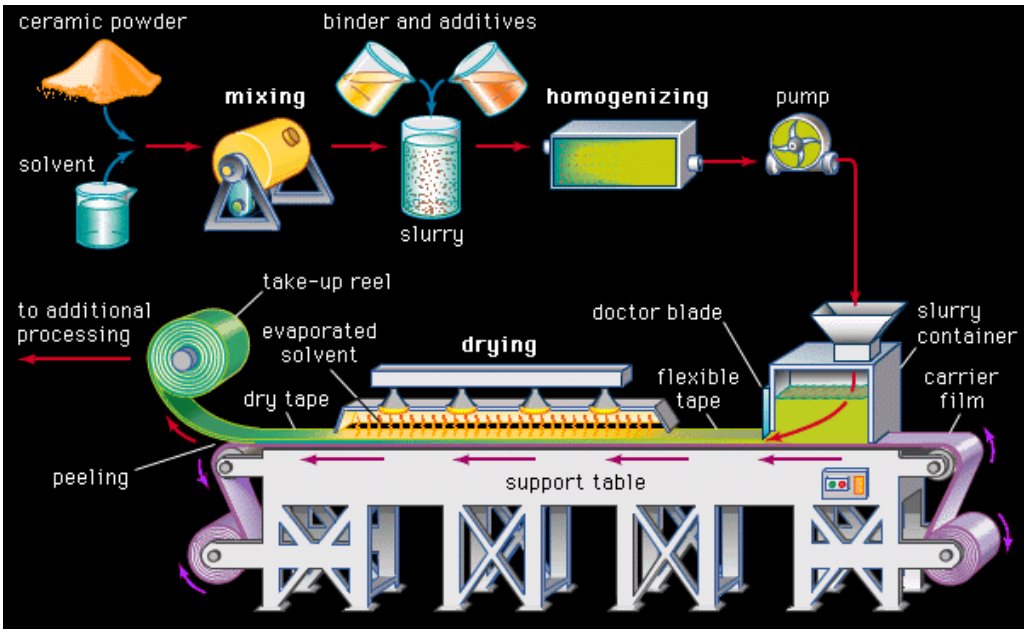

Figure 2.6 The tape casting process (courtesy: Britannica Encyclopedia).

The tape casting slurry will be prepared in a two stage process. In the first part the ceramic powder will be ball milled for 24 hours with the solvent and dispersant. In the second part Type I plasticizer, Type II plasticizer, binder and homogenizer will be added and ball milled for another 24 hours (Table 2.2). The slurry prepared should have low settling rate so that it will be stable until the casting is complete. The rate of settling increases with the particle size and density of the ceramic powder. Usually air bubbles will get entrapped within the slurry while milling and it may cause defects in the tape cast product. Air bubbles may produce pinholes in the tape which can lead to cracks upon drying. Hence the entrained air must be removed from the slip before casting. This can be done by de-airing the slip using low vacuum. The viscosity of the slip is also to be considered while de-airing. High viscosity slips are difficult to de-air and require more time and agitation during the process (Mistler *et al.*, 2000).

In tape casting there are four primary variables viz. slip viscosity, carrier speed, blade gap and reservoir head which control the tape thickness. The viscosity of the slip determines the extent of fluid flow through the blade gap due to the forces acting on it. A low viscosity slip will flow freely through the gap under the pressure of the reservoir. The viscosity of most of the tape casting slips is in the range 0.5 to 6 Pa.s at low shear rates. The speed of carrier motion should remain constant until the casting is complete to avoid the thickness variation. Increasing carrier speed with all other variables held constant will decrease tape thickness. The distance between the carrier and the bottom of the doctor blade (blade gap) is the most important variable in determining the tape thickness. Any change in the blade gap will bring about proportional changes in the slip velocity and thus affect the tape thickness. The pressure on the slip increases with the height of the slip in the reservoir (reservoir height) which in turn increases the slip velocity. A change in one of these four variables can be offset by an opposite change in one or more of the other variables. Usually, reservoir height and casting speed are held constant while the blade gap is varied to account for the changes in viscosity thereby yielding repeatable tape thickness (Mistler *et al.*, 2000).

Figure 2.7 Photographs of (a) tape casting machine and (b) cast LTCC tape.

The tape casting machine (Keko equipment, Slovenia) used and the LTCC tape developed in the present study are shown in Fig. 2.7 (a) and (b) respectively. Once the tape is cast, it will be allowed to dry either naturally or using

some hot air circulation depending on the solvents used in the tape casting slurry. The dried tapes will be used for further characterization.

2.4 Preparation of polymer-ceramic composites

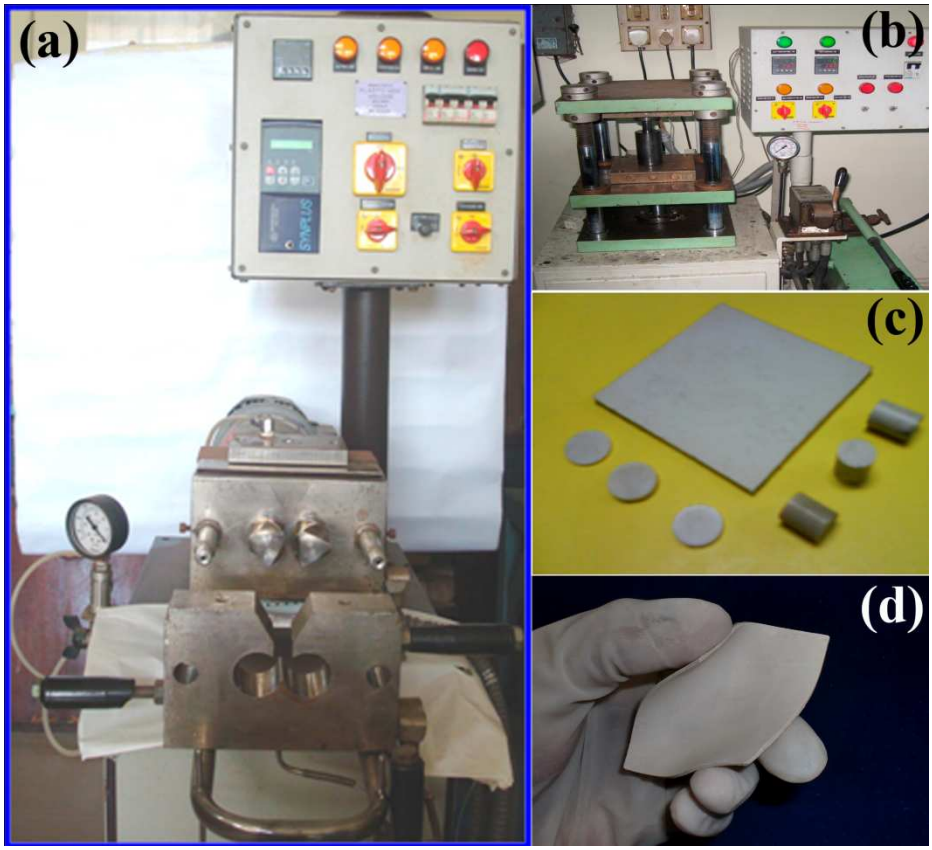

Figure 2.8 Photographs of Kneading machine (a), hot press (b), and polymer-ceramic composite samples (c, d).

Polymer-ceramic composites are prepared through sigma blending. The polymer and ceramic are mixed thoroughly in a kneading machine (sigma mixing). The kneading machine is a variable speed mixer having two counter rotating sigma blades with a gear ratio of 1:1.2 and heating facility up to 300 ^{o}C (Fig. 2.8). The counter rotating sigma blades ensure fine mixing by applying high shear force on the mixture. In the present study, composites based on High Density Polyethylene (HDPE) and butyl rubber has been prepared. For the preparation of HDPE based composites, desired amount of polymer (normally 15 g) is taken in Kneading machine and slowly the temperature is increased. As the temperature increases, the

polymer starts melting and viscous fluid is formed. Then the required amount of ceramic is added in small amounts keeping the temperature constant and rotating the sigma blades. The preparation temperature is about 180 ^{o}C. The mixing of Butyl rubber and ceramic is carried out in a similar way without heating. The HDPE-ceramic composites are then hot pressed at 180 ^{o}C for 30 minutes under a pressure of 20 MPa. For Butyl rubber-ceramic composites, hot molding conditions are 2 MPa pressure at 200 ^{o}C for 90 minutes. The hot press used (Fig. 2.8 (b)) and some of the samples prepared (Fig. 2.8 (c), (d)) are shown in Fig. 2.8.

2.5 Structural and microstructural characterization

2.5.1 Powder X-ray diffraction

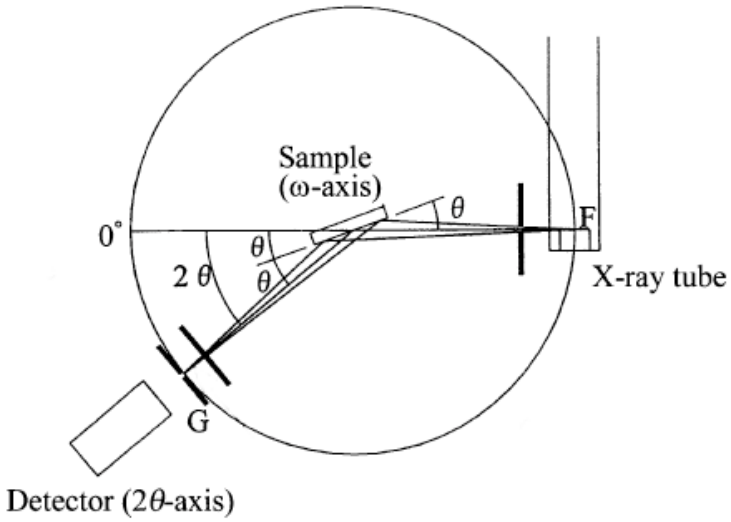

Figure 2.9 Schematic representation of an X-ray diffractometer (Waseda *et al.*, 2011).

The experimental technique which has been of the greatest significance in revealing the structure of crystals is undoubtedly X-ray diffraction. This technique is most useful for qualitative, rather than quantitative, analysis (although it can be used for both). X-rays incident on a sample will either be transmitted or scattered by the electrons of the atoms in the material. In general, the scattered waves interfere destructively with each other, with the exception of special orientations at which Bragg's law is satisfied. The direction and intensity of the scattered (diffracted)

beams depends on the orientation of the crystal lattice with respect to the incident beam. The crystal lattice consists of parallel rows of atoms separated by a unique distance (d-spacing), which are capable of diffracting X-rays. Intense reflected beams will be produced when the path differences between reflections from successive planes in a family is equal to whole number of wavelength (Hammond, 2009). The powdered sample provides (theoretically) all possible orientations of the crystal lattice. The powder should be ground extremely fine to a size of 10 μm or less for the accurate reproducibility of relative line intensities (Cullity, 1978).

The X-ray diffractometer is a precision instrument with two axes (ω and 2θ) of independent rotation. This equipment records the intensity data of a diffracted X-ray beam, as a function of angle, so as to satisfy Bragg's law under the condition of X-rays of known wavelength. The basic design of the diffractometer is shown in Fig. 2.9. The X-ray source (F) and detector (G) lie on the circumference of a circle centered at the sample holder (S). When the position of X-ray source is fixed and the detector is attached on the 2θ-axis, the powder sample is usually set on the ω-axis corresponding to the center of the diffractometer. During the course of measurements, the 2θ-axis rotates two times as much as the ω-axis. This is to maintain the experimental condition that the angle between the plane of the sample and direction of the incident X-ray beam is equal to that of direction of the diffracted beam, with reference to the direction of propagation of the incident X-ray beam (Waseda *et al.*, 2011). Diffraction data from many materials have been recorded in a computer searchable Powder Diffraction File (PDF). Comparing the observed data with that in the PDF allows the phases in the sample to be identified. In the present work powder XRD spectra are recorded using CuKα radiation (X'Pert PRO MPD X-ray diffractometer, PANalytical, Almelo, Netherlands).

2.5.2 Scanning electron microscopy

In light microscopy, a specimen is viewed through a series of lenses that magnify the visible-light image. However, the scanning electron microscope (SEM) does not actually view a true image of the specimen, but rather produces an electronic map of the specimen. The SEM is a microscope that uses electrons instead of visible light to form an image. In these microscopes the electron beam is focused

onto a small spot on the sample that is then scanned across the surface to build up a two dimensional image. The scanning electron microscope has many advantages over traditional microscopes. The SEM has a large depth of field, which allows more of a specimen to be in focus at one time (Reimer, 1985). The SEM also has much higher resolution, so closely spaced specimens can be magnified at much higher levels.

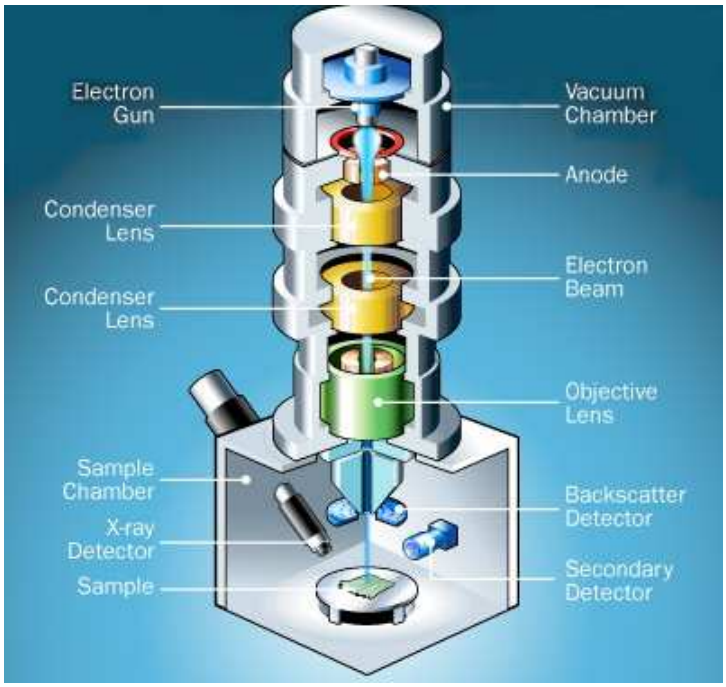

Figure 2.10 Schematic representation of SEM (courtesy: http://science.howstuffworks.com)

The interaction between primary electron beam and the sample produces secondary electrons, characteristic x-rays, and back scattered electrons. The SEM is capable of producing high-resolution images of a sample surface in its primary use mode, namely secondary electron imaging (SEI). The resolution of SEM can fall somewhere between less than 1 nm and 20 nm. An electrically conductive (usually gold) coating must be applied to electrically insulating samples. In the present study Scanning Electron Microscope of JEOL JSM-5600LV, Tokyo, Japan has been used for analyzing the microstructure of the samples prepared.

2.5.3 Atomic force microscopy

Atomic force microscopy is a very high resolution type of scanning probe microscopy used to exploit contact and non contact forces for imaging the surface topology of materials. The Atomic Force Microscope (AFM) consists of a cantilever with a sharp tip (probe) at its end that is used to scan the specimen surface. The cantilever is typically silicon or silicon nitride with a tip radius of curvature on the order of nanometers. When the tip is brought into proximity of a sample surface, forces between the tip and the sample lead to a deflection of the cantilever. A laser beam, which is deflected from the backside of the cantilever, is directed to a 4-segment positional photodetector, which is divided into segments for measurements of normal and lateral deflections of the cantilever. The AFM can be operated in a number of modes, depending on the application. In general, possible imaging modes are divided into static (also called contact) modes and dynamic (non-contact or "tapping") modes where the cantilever is vibrated. In tapping mode, the tip of the cantilever does not come in contact with the sample surface. Instead it is oscillated at a frequency slightly above its resonant frequency. The drop in vibration amplitude of the cantilever when the tip comes into interaction with a sample is used as a measure of these interactions (Yao *et al.*, 2005). AFM (NTEGRA, NT-MDT, Russia) operating in tapping mode regime is used in the present study to measure the surface roughness of ceramic green tapes.

2.6 Dielectric characterization

2.6.1 Radio frequency dielectric measurements

The dielectric properties of the samples upto 1MHz are measured using the parallel plate capacitor method with the aid of an LCR meter (HIOKI 3532-50 LCR Hi TESTER, Japan). The parallel plate capacitor method involves sandwiching a thin sheet of the material between two electrodes to form a capacitor. This is done by uniformly coating silver paste on both sides of cylindrical specimens of diameter ~ 10 mm and thickness ~ 1mm. LCR meter measures the complex impedance by auto balancing bridge technique from which the capacitance and loss tangent are calculated. Then relative permittivity is calculated using the equation

$$C = \frac{\varepsilon_r \varepsilon_o A}{d} \quad (2.1)$$

where C is the capacitance, ε_r and ε_o are the relative permittivity of material and free space respectively. A and d are the cross sectional area and thickness of the sample.

2.6.2 Measurement of microwave dielectric properties

In general, the methods for the measurement of microwave dielectric properties fall into two categories: non-resonant methods and resonant methods. Non-resonant methods are often used to get a general knowledge of electromagnetic properties over a frequency range. On the other hand, resonant methods are used to get accurate knowledge of dielectric properties at a single frequency or at several discrete frequencies. In non-resonant methods, the properties of materials are fundamentally deduced from their impedance and wave velocities in the material. Non-resonant methods mainly include reflection methods and transmission/reflection methods. In reflection methods, electromagnetic waves are directed to the sample and the properties of the sample are deduced from the reflection coefficient. In a transmission/reflection method, the material under test is inserted into a segment of transmission line and the properties of the materials are deduced on the basis of the reflection from the material and the transmission through the material. The transmission and reflection methods are used to measure the dielectric properties of medium and high loss materials (Krupka, 2006; Sebastian, 2008).

Resonant methods usually have higher accuracies and sensitivities than non-resonant methods, and are most suitable for low-loss samples. Resonant methods generally include resonator method and resonant-perturbation method. In resonator method, the test specimen acts as a resonator in the measurement circuit and the dielectric properties of the specimen are determined from its resonant frequency and quality factor. In a resonant perturbation method, the sample is inserted into a resonator, and the properties of the sample are calculated from the changes of the resonant frequency and the quality factor of the resonator caused by the sample (Chen *et al.*, 2004).

2.6.2.1 Network analyzer

Network Analyzer is the major instrument used in this investigation for the characterization of low loss microwave materials. In microwave engineering, network analyzers are the basic instrument used to analyze a wide variety of materials, components, circuits and systems. By measuring the amplitudes and phases of transmission and reflection coefficients, network analyzer reveals all the network characteristics of the analog circuits (Chen *et al.*, 2004). Network Analyzer is a swept frequency measurement equipment to completely characterize the complex network parameters in comparatively less time, without any degradation in accuracy and precision. Two types of network analyzers are available, scalar and vector network analyzers. Scalar network analyzer measures only the magnitude of reflection and transmission coefficients while the vector network analyzer measures both the magnitude and phase. Both the magnitude and phase behavior of a component can be critical to the performance of a communication system.

2.6.2.2 Measurement of relative permittivity (ε_r)

The relative permittivity of dielectric ceramics is often measured by the method developed by Hakki and Coleman (Hakki *et al.*, 1960) and modified by Courtney (Courtney, 1970). In this method a circular disc of material whose ε_r to be measured is inserted between two mathematically infinite conducting plates, as shown in Fig. 2.11. If the dielectric material is isotropic then the characteristic equation for this resonant structure operating in the TE_{0ml} mode may be written as

$$\alpha \frac{J_0(\alpha)}{J_1(\alpha)} = -\beta \frac{K_0(\beta)}{K_1(\beta)} \tag{2.2}$$

where $J_0(\alpha)$ and $J_1(\alpha)$ are Bessel functions of the first kind of orders zero and one respectively. The $K_0(\beta)$ and $K_1(\beta)$ are the modified Bessel functions of the second kind of order zero and one respectively. The parameters α and β are given by

$$\alpha = \frac{\pi D}{\lambda_0}\left[\varepsilon_r - \left(\frac{l\lambda_0}{2L}\right)^2\right]^{1/2} \tag{2.3}$$

$$\beta = \frac{\pi D}{\lambda_0}\left[\left(\frac{l\lambda_0}{2L}\right)^2 - 1\right]^{1/2} \qquad (2.4)$$

where l is the number of longitudinal variations of the field along the axis, L is the length of the DR, D the diameter of DR and λ_0 is the free space resonant wave length. The characteristic equation (2.2) is a transcendental equation and hence a graphical solution is necessary. Corresponding to each value of β there is infinite number of α_n that solves the characteristic equation. Hakki and Coleman obtained a mode chart showing the variation of α values as a function of β.

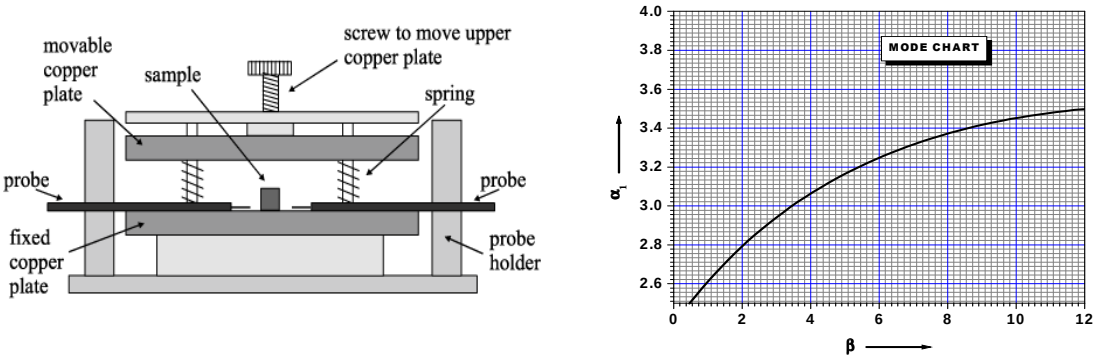

Figure 2.11 Hakki-Coleman method for measuring ε_r by end shorted method and mode chart of Hakki-Coleman giving α_1 as functions of β (Hakki *et al.*, 1960; Courtney, 1970).

The TE_{011} mode is used for the measurements since this mode propagates inside the sample but is evanescent outside it. Therefore a large amount of electrical energy can be stored in the high Q dielectric resonators (Kobayashi *et al.*, 1980). However, in the open space post resonator setup, a part of electrical energy is radiated out as evanescent field and hence the axial mode number is usually expressed as δ since it is less than 1 (ie., $TE_{01\delta}$). In the end shorted condition the E field becomes zero close to the metal wall and electric energy vanishes in the air gap (Cohn *et al.*, 1966). Courtney used two horizontally oriented E-field probes for coupling microwave to the DR instead of the iris coupling used by Hakki and Coleman. This increased range of frequencies that can be used for measurement (Courtney, 1970). Rewriting the equations (2.3) and (2.4) for TE_{011} mode we will get

$$\varepsilon_r = 1 + \left[\frac{c}{\pi D f_o}\right]^2 \left(\alpha_1^2 + \beta_1^2\right) \quad (2.5)$$

where f_o is the resonant frequency. The mode chart for α_1 is shown in Fig. 2.11.

In the experimental setup, a vector network analyzer is used for taking measurements at microwave frequencies. The specimen is placed approximately symmetrical with two E-probes. The resonant modes are visualized by giving a wide frequency range in the network analyzer. To select the TE_{011} resonance from the several modes having non-zero E_z components, the upper metal plate is slightly tilted to introduce an air gap. As the plate is tilted the entire TM modes move rapidly to the higher frequencies while the TE_{011} mode remains almost stationary. It is well known that in exact resonance technique, TE_{011} is least perturbed by the surroundings. After identifying the TE_{011} mode, span around that resonant peak is reduced as much as possible to get maximum resolution and the resonant frequency f_o is recorded. By knowing the diameter 'D' and length 'L' of the sample β is calculated using equation (2.4). From the mode chart, the value of α_1 corresponding to β_1 value is determined. Then ε_r is calculated using eqn. (2.5). The possible error in the measurement of ε_r is of the order of 0.3% (Sebastian, 2008).

2.6.2.3 Measurement of quality factor

There are several methods to measure the quality factor of dielectric ceramics. However, many of them fail to account for the practical effects introduced by a real measurement system such as noise, crosstalk, coupling losses, transmission line delay, and impedance mismatch. Inadequate accounting of these effects may lead to significant uncertainty in the Q-factor obtained. For a DR, the quality factor measured by the end shorted method of Hakki and Coleman will be very low due to the conduction and radiation losses (Sebastian, 2008). In order to reduce these effects, in the present study the unloaded quality factor (Q_u) of the DRs is measured using a transmission mode cavity proposed by Krupka et al. (Krupka *et al.*, 1998). The DR specimen to be characterized is placed inside a cylindrical copper cavity whose inner surface is silver coated to reduce radiation loss. The size of cavity is designed to be 3-5 times the size of the sample (Sebastian, 2008). Samples with

diameter/length (D/L) ratio of 1.8 - 2.2 are used to get maximum mode separation. The DR specimen is kept over a quartz spacer placed at the inner bottom surface, which enables to avoid the conduction loss. The cavity is provided with a tunable upper lid (Fig. 2.12 (a)). This enables to tune the height of air layer in the metallic cavity and hence to provide more accuracy in the determination of the resonant mode and quality factor.

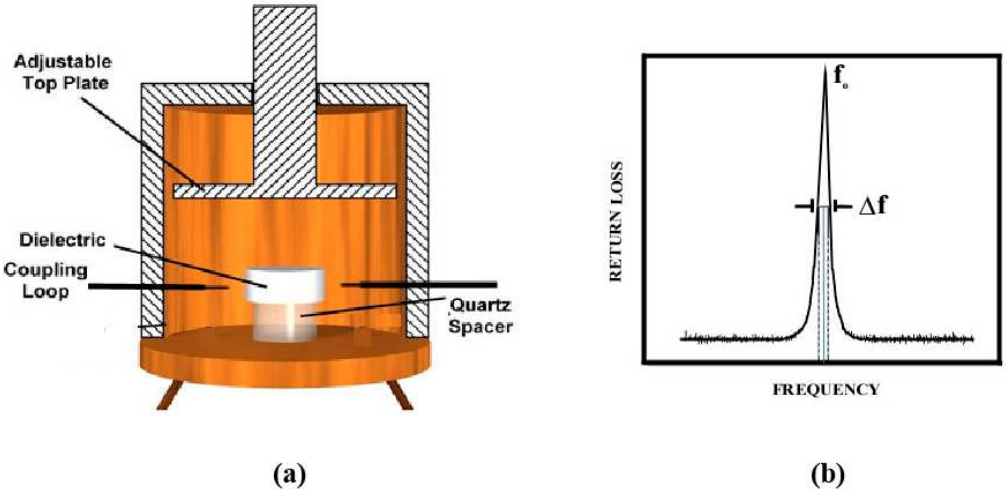

Figure 2.12 (a) resonant cavity for the measurement of Q factor and (b) method of calculating the half power bandwidth (Anjana, 2008).

Microwaves are fed into the sample by magnetic coupling using two loop coaxial antennas. The coupling is adjusted to be optimum. The spectrum of S_{21} (return loss) versus frequency can be observed in the network analyzer. In principle the cavity has infinite number of modes, when excited with microwaves. $TE_{01\delta}$ mode will be the fundamental mode with least perturbation when the tunable top lid is adjusted properly. After identifying the $TE_{01\delta}$ mode, the lid is fine tuned to get maximum separation between $TE_{01\delta}$ and any nearby cavity modes, to attain maximum possible accuracy in the Q_u measurement. The resonant frequency (f_o) and the half power (-3dB) bandwidth (Δf) of $TE_{01\delta}$ can be measured from the resonance spectrum as shown in Fig. 2.12 (b). Then the loaded quality factor can be calculated using the relation

$$Q_l = \frac{f_o}{\Delta f} \qquad (2.6)$$

If the couplings between the cavity and the two transmission lines are weak and equal, the unloaded quality factor (Q_u) can be calculated using the equation

$$Q_u = \frac{Q_l}{1-\beta} \tag{2.7}$$

where the coupling coefficient, $$\beta = 10^{(S_{21,f_o}/20)} \tag{2.8}$$

with $S_{21,fo}$ being the S_{21} value at the resonant frequency. The uncertainty in loss measurements using $TE_{01\delta}$ mode cavity method with optimized enclosures is of the order of 2×10^{-6} (Sebastian, 2008). In the microwave frequency range the quality factor decreases with frequency. Hence the quality factor of dielectric resonators is conventionally represented in terms of $Q_u \times f$, rather than Q_u.

2.6.2.4 Measurement of temperature coefficient of resonant frequency (τ_f)

The temperature **s**tability of resonant frequency of DR is a major concern in microwave devices. The temperature stability may be examined using the parameter τ_f defined as

$$\tau_f = \frac{1}{f_o}\frac{\Delta f_o}{\Delta T} \tag{2.9}$$

In order to measure τ_f, DR is kept in a cavity, and the peak corresponding to $TE_{01\delta}$ mode is observed in network analyzer. Then the entire set up is heated in the temperature range of 25 to 70 ^oC. The shift in the resonant frequency of $TE_{01\delta}$ with temperature is noted at regular intervals and the value of τ_f is calculated using the eqn. (2.9). The value of τ_f is usually expressed in parts per million per degree celsius (ppm/^oC).

2.6.2.5 Split Post Dielectric Resonator (SPDR) method

Split Post Dielectric Resonator method is suitable for the measurement of dielectric properties of samples in the form of a thin sheet (Krupka *et al.*, 1996). The SPDR mainly consists of two dielectric discs separated by a small air gap in a metal enclosure (Fig. 2.13). The dielectric discs are thin and the height of metal enclosure

is relatively small, so the evanescent electromagnetic field is strong not only in the air-gap region outside the cavity but also in the cavity region for radii greater than the radius of the dielectric resonator. Therefore the electromagnetic fields are also attenuated in the cavity so it is not necessary to take them into account in the air gap. This simplifies the numerical analysis and reduces possible radiation. The SPDR usually operates in $TE_{01\delta}$ mode. The sample under test is placed in the gap between the two parts of the resonator, usually at the place of maximum electric field. The loading of a dielectric sheet sample changes the resonant properties of a split resonator, and the dielectric properties of the sample can be derived from the resonant properties of the resonator loaded with sample and the dimensions of the resonator and the sample (Chen *et al.*, 2004).

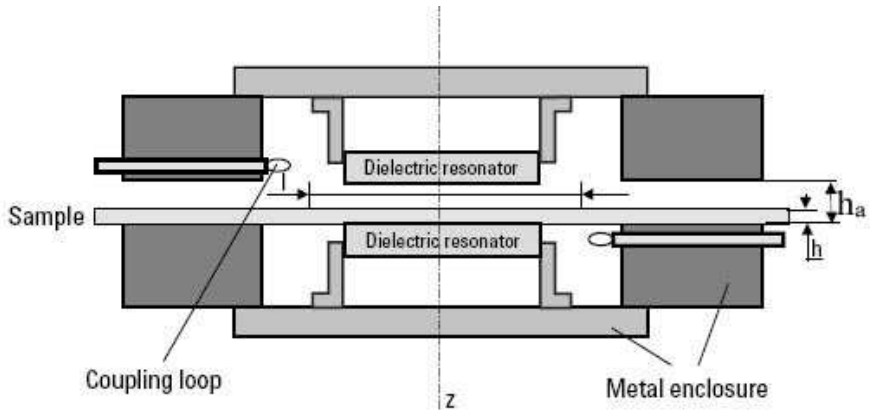

Figure 2.13 Schematic diagram of an SPDR (Sebastian, 2008).

The real part of complex relative permittivity can be calculated from the measured resonant frequency and sample thickness as an iterative solution to the equation

$$\varepsilon_r = 1 + \frac{f_o - f_s}{h f_o K_\varepsilon(\varepsilon_r, h)} \tag{2.10}$$

where h is the thickness of the sample t, f_o is the resonant frequency of empty SPDR, f_s is the resonant frequency of the resonant fixture with dielectric sample and K_ε is a function of ε_r and h. K_ε was computed for a number of ε_r and h for a given resonant

fixture and tabulated. Then the relative permittivity of the test specimen is evaluated using some iterative procedure (Krupka *et al.*, 2001). The dielectric loss tangent calculated using the equation

$$\tan\delta = (Q_u^{-1} - Q_{DR}^{-1} - Q_c^{-1})/p_{es} \tag{2.11}$$

with

$$p_{es} = h\varepsilon_r K_1(\varepsilon_r, h) \tag{2.12}$$

$$Q_c = Q_{c0} K_2(\varepsilon_r, h) \tag{2.13}$$

$$Q_{DR} = Q_{DR0}\left(\frac{f_o}{f_s}\right)\left(\frac{p_{eDR0}}{p_{eDR}}\right) \tag{2.14}$$

where p_{es} and p_{eDR0} are the electric-energy filling factors of the test specimen and the empty SPDR respectively; p_{eDR} is the electric-energy filling factor of the dielectric split resonator containing the sample; Q_{c0} is the quality factor depending on metal losses for empty resonant fixture; Q_{DR0} is the quality factor depending on dielectric losses in dielectric posts for empty resonant fixture; and Q_u is the unloaded quality factor of the resonant fixture containing the dielectric sample. The values of p_{eDR}, p_{es} and Q_c for a given resonant structure can be calculated using numerical techniques. The sample should be flat and must be positioned such that it extends beyond the diameter of two cavity sections. The uncertainty in the measurement of ε_r is about 0.3%. The resolution for loss tangent measurements is ~ 2×10^{-5} (Krupka *et al.*, 2001).

2.7 Thermal characterization

Thermal analysis includes the techniques in which some physical parameter of the system is determined and recorded as a function of temperature. Some of the thermal characterization methods adopted in the present investigation are discussed below.

2.7.1 Thermo gravimetric analysis (TGA)

On heating, losses in weight of the material may occur due to the burning out of organic matter and by dissociation or reduction of ceramic; gains in weight may accompany their oxidation. The thermo gravimetric technique provides a simple and accurate method of obtaining quantitative data on these aspects of the effect of heat. This method involves the continuous measurement of the weight of the sample subjected to a selected firing profile that is usually linear (Pennisi, 1991).

2.7.2 Dilatometry

The shrinkage of ceramic while sintering can be measured by following the change of length in a particular direction as a function of temperature without any stress imposed other than the sample's mass (Cahn *et al.,* 1992). The data obtained includes the shrinkage of a composition and more importantly the onset and completion of the sintering cycle. The thermal expansion of the samples, which is an important parameter for electronic packaging application of the dielectric materials, is also studied using the dilatometer. The value of linear coefficient of thermal expansion can be calculated using equation (1.32). In the present study, Dilatometer DIL 402 PC, NETZSCH (Selb, Germany) is employed for both thermal expansion and shrinkage measurements.

2.7.3 Thermal conductivity

The thermal conductivity (λ) of the materials can be calculated from the thermal diffusivity (α), specific heat capacity (C_p) and density (ρ) using the equation

$$\lambda = \alpha \rho C_p \qquad (2.15)$$

The laser flash method can be used to measure the thermal diffusivity. The method involves subjecting one face of the sample to a laser flash and monitoring the transient temperature response of the opposite face. The thermal diffusivity value is calculated from the specimen thickness and the time required for the rear face temperature rise to reach certain percentages of its maximum value (Hasselman *et al.,* 1985). The heat capacity of the sample is also measured simultaneously by

comparing the temperature rise in the sample with that in a reference material (Parker *et al.*, 1961). When the thermal diffusivity of the specimen is to be determined over a temperature range, the measurement must be repeated at each temperature of interest. In the present study thermal conductivity is measured using a laser flash thermal properties analyzer (Flash Line 2000, Anter corporation, Pittsburgh, USA).

2.8 Tensile properties

Among the various tests used to evaluate mechanical properties of materials, tensile test in which the sample is pulled to failure in a relatively short period of time, is perhaps the most useful. In this test the sample is elongated at a constant rate and the load required to produce a given elongation is measured as a dependent variable. A stress-strain curve may be plotted from the results of a tension test which may reveal the toughness of the material (Hayden *et al.*, 1984). In the present study the tensile properties of the samples are measured using a Universal Testing Machine (Hounsfield, H5K-S UTM, Redhill, UK).

Chapter 3

Microwave dielectric properties of some rare earth apatites

This chapter deals with the preparation and characterization of a series of rare earth apatites $Ca_{2+x}RE_{8-x}(SiO_4)_{6-x}(PO_4)_xO_2$ [RE= La, Pr, Nd, Sm, Eu, Gd and Tb] (x= 0, 2, 4 and 6). The structure and microstructure of the ceramics are analyzed using the powder X-ray diffraction and SEM respectively. $Ca_4La_6(SiO_4)_4(PO_4)_2O_2$ has good microwave dielectric properties. Effect of isovalent substitutions of Sr^{2+}, Pr^{3+}, $(GeO_4)^{4-}$ and $(VO_4)^{3-}$ in the respective divalent, trivalent cationic and tetravalent, trivalent anionic sites of $Ca_4La_6(SiO_4)_4(PO_4)_2O_2$ is also studied. The partial substitution of Pr^{3+} for La^{3+} is found to be effective in tuning the τ_f without much affecting ε_r and $Q_u \times f$.

3.1 Introduction

Wireless communication using microwaves opened up a new era of information exchange. Dielectric ceramics have played a pivotal role in universalizing the microwave communication systems by making them more efficient, miniaturized and cheaper. The continuing developments in wireless technology demand low cost ceramics with excellent microwave dielectric properties. Dielectric ceramics function as resonator oscillators, filters, antennas and substrates in microwave modules. The relative permittivity (ε_r) of the ceramic has a major role in determining the function of a ceramic in a microwave communication system. Microwave dielectric resonators should have high relative permittivity for miniaturization. For the ceramic to be used as a substrate, it should have a low value of ε_r (< 15). The carrier frequency for several wireless systems is approaching towards the millimeter wave region, as the lower frequencies are getting congested. For instance, frequencies above 20 GHz in Local Multipoint Distribution Service (LMDS) systems (Kim, 2000), 20/30 GHz in Ka-band satellite systems (Castanet *et al.*, 2002), 24 GHz in ultra wide band short range radar (SRR) systems and 77 GHz in long range radar (LRR) systems for automotive applications (Strohm *et al.*, 2005) are being used. Millimeter wave frequency bands offer large transmission bandwidths and efficient frequency reuse (Khawaja *et al.*, 2008). Low permittivity ceramics are required for the dielectric resonators operating at higher frequencies. So far, several ceramics with good microwave dielectric properties have been developed (Sebastian, 2008). However, attempts are still continuing to develop new materials with diverse values of ε_r and a better balance between the requisite properties.

Generally aluminates and silicates are found to have low relative permittivity suitable for substrate applications (Tsunooka *et al.*, 2003; Surendran *et al.*, 2004; Surendran *et al.*, 2005; Sebastian, 2008; Joseph *et al.*, 2010). The phosphates also show relatively low permittivity. However, only limited exploration of the microwave dielectric properties of phosphates has been reported. The pyrophosphates $A_2P_2O_7$ (A = Ca, Sr, Ba; Mg, Zn, Mn) have good microwave dielectric properties with ε_r varying from 6.1 to 8.4, $Q_u \times f$ varying from 12300 to

53500 GHz and τ_f from -23 to -746 ppm/^oC (Bian *et al.*, 2004). Rare earth orthophosphates $RePO_4$ form another class of microwave dielectrics with ε_r in the range 7.8-11.1 (Cho *et al.*, 2009). The composition $YbPO_4$ has the highest $Q_u \times f$ of 71650 GHz and $DyPO_4$ has the lowest τ_f of -17 ppm/^oC. $Ba_4Ti_3P_2O_{15}$ has been observed to possess good microwave dielectric properties: ε_r = 20.7, $Q_u \times f$ = 42200 GHz and τ_f = + 37 ppm/^oC (Zhou *et al.*, 2010). The ceramics in the series $BaNb_{(2-x)}Ta_xP_2O_{11}$ (x = 0 to 2) are also found to have good microwave dielectric properties (ε_r = 12.9 to 25.3, $Q_u \times f$ = 5300 to 28900 GHz and τ_f = +46 to -29 ppm/^oC) (Thomas *et al.*, 2012).

3.2 Phosphates

Phosphates are the compounds in which each phosphorus atom is surrounded by four oxygen atoms to form PO_4 tetrahedron. Phosphorus exhibits sp^3 -bonding in the phosphates. By sharing oxygen atoms between the tetrahedra, chains, rings and branched polymers of interconnected PO_4 tetrahedra can be produced (Wazer, 1958). Crystalline phosphates can be classified into (a) linear phosphates and polyphosphates (b) cyclic phosphates and (c) ultraphosphates. The linear polyphosphates contain $(P_nO_{3n+1})^{(n+2)-}$ anion, where n is the number of tetrahedra. They include: (1) orthophosphates containing $(PO_4)^{3-}$ ion (2) pyrophosphates containing $(P_2O_7)^{4-}$ ion and (3) triphosphates containing $(P_3O_{10})^{5-}$ ion (Sneed *et al.*, 1956).

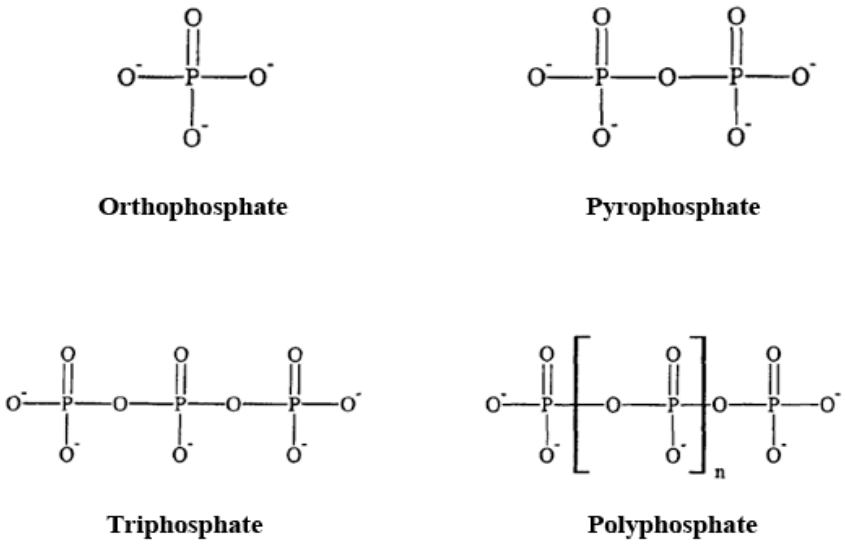

Figure 3.1 Linear polyphosphate ions (Rashchi *et al.*, 2000).

It is also possible for the PO_4 tetrahedra to link together to form cyclic anions which results in cyclic phosphates (Sneed *et al.*, 1956). The general formula for their anions is $(P_nO_{3n})^{n-}$ and the cyclic phosphates are known for n = 3, 4, 5, 6, 8, 9, 10, and 12 (Durif, 2005). In ultraphosphates, at least some of the PO_4 tetrahedra share three oxygen atoms to form cages, sheets or three dimensional structures (Rashchi *et al.*, 2000). The phosphorus containing minerals are orthophosphates containing isolated PO_4 tetrahedra (Wazer, 1958).

3.3 Apatites

Apatites have long been studied for their catalytic activity, luminescent properties and biological applications (Wanmaker *et al.*, 1971; Monma, 1982; Hench, 1991). They form a large family of compounds with general formula $M_{10}(RO_4)_6X_2$ with M being a monovalent to trivalent cation (Na^+, K^+, Ca^{2+}, Sr^{2+}, La^{3+}, Pr^{3+}, etc.), (RO_4) a trivalent or tetravalent anion ($(PO_4)^{3-}$, $(VO_4)^{3-}$, $(SiO_4)^{4-}$ etc.) and X a monovalent or divalent anion (OH^-, F^-, Cl^-, O^{2-} etc.). Apatites have hexagonal structure and belong to $P6_3/m$ space group (Serret *et al.*, 2000; Ardanova *et al.*, 2010). The structure consists of isolated RO_4 tetrahedra arranged in such a way to form two distinct channels running along the c- direction. The smaller channel is occupied by the M cations. On the other hand the larger channel contains a ring of M cations with the X anion occupying the positions in the channel centre (Fig. 3.2). Thus the M cation has two possible sites, M(I) with 9-fold coordination (4*f*) and M(II) with 7-fold coordination (6*h*) (Serret *et al.*, 2000; Tolchard *et al.*, 2005). The average covalency of M(II) site is higher than that of M(I) site (Boyer *et al.*, 2000). Large number of possible substitutions in their sites makes apatites attractive class of materials for functional applications.

The distribution of cations between the two non-equivalent M sites has been addressed in several studies (Schroeder *et al.*, 1978; Hughes *et al.*, 1991(a); Hughes *et al.*, 1991(b)). In the rare earth oxy-apatites $M_2RE_8(SiO_4)_6O_2$ (M = Mg, Ca, Sr, Ba) Felsche suggested that Mg and Ca ions can occupy M(II) sites whilst larger Sr and Ba ions occupy only the M(I) site (Felsche, 1972). Later Blasse predicted that alkaline-earth ions reside in M(I) site except when the RE^{3+} ions are large (eg. La^{3+}) and M^{2+} ions are small (eg. Mg^{2+}) where M^{2+} ions may be accommodated in M(II)

also (Blasse, 1975). The structural refinement of $Ca_2La_8(SiO_4)_6O_2$ has shown that M(II) sites are solely occupied by La^{3+} ions, whereas M(I) sites are occupied equally by La^{3+} and Ca^{2+} ions (Schroeder *et al.*, 1978). Similar results have been obtained for $(Sr_2RE_2)(RE_6)(SiO_4)_6O_2$ (RE = La, Pr, Tb, and Y) apatites also (Leu *et al.*, 2011). It has been reported that in $Ca_8La_2(PO_4)_6O_2$ apatite La^{3+} ions occupy only the M(II) position whereas Ca^{2+} ions occupy both M(I) and M(II) sites (Serret *et al.*, 2000).

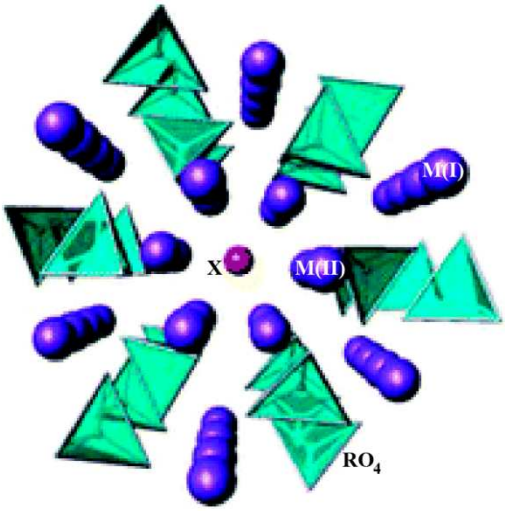

Figure 3.2 The apatite structure $M_{10}(RO_4)_6X_2$ (Kendrick *et al.*, 2007).

3.4 Microwave dielectric properties of $Ca_{2+x}RE_{8-x}(SiO_4)_{6-x}(PO_4)_xO_2$ [RE= La, Pr, Nd, Sm, Eu, Gd and Tb] (x= 0, 2, 4 and 6) apatites

The present work is focused on the development of some rare earth bearing oxyapatites for microwave applications.

3.4.1 Experimental

$Ca_{2+x}RE_{8-x}(SiO_4)_{6-x}(PO_4)_xO_2$ (x=0, 2, 4 and 6) ceramics were prepared by the solid state ceramic route. High purity $CaCO_3$ (99+ %, Sigma-Aldrich, St. Louis, MO, USA), Pr_6O_{11}, Eu_2O_3, Gd_2O_3, Tb_2O_3 (99%, Treibacher, Althofen, Austria), La_2O_3 (99%, Indian Rare Earths Ltd., Kerala, India), Nd_2O_3 (99.9%, Indian Rare Earths), Sm_2O_3 (99%, Indian Rare Earths), SiO_2 (99.6%, Sigma-Aldrich) and $NH_4H_2PO_4$ (98+ %, Sigma-Aldrich) were weighed as per the stoichiometric ratio required and ball milled in ethanol for 24 hours with yittria stabilized zirconia balls.

The slurry was then dried in hot air oven and pre-heated at 1000 ^{o}C. The powder was then ground and calcined in the temperature range 1250-1450 ^{o}C. Calcined powder was ground into fine powder. It was then mixed with 4 wt% PVA (molecular weight 22000, BDH Lab suppliers, Poole, U. K.) and again dried and ground well. Cylindrical disks of 11 mm diameter and 5-6 mm height were produced in a uniaxial press by applying a pressure of 100 MPa. The compacts were then sintered at temperatures in the range 1375-1675^{o}C for 4 hours with an intermediate soaking at 600 ^{o}C to expel the binder (PVA).

The densities of the sintered samples were measured by Archimedes method. The crystal structure of the sintered and powdered samples was studied by recording the X-ray diffraction (XRD) pattern using CuKα radiation (X'Pert PRO MPD X-ray diffractometer, PANalytical, Almelo, Netherlands). The surface morphology of the thermally etched samples was analyzed using a Scanning Electron Microscope (SEM) (JOEL-JSM 5600 LV, Tokyo, Japan). The microwave dielectric properties were measured using Vector Network Analyzer (Model No: E8362B, Agilent Technologies, Santa Clara CA, US) in the frequency range 8-15 GHz as described in chapter 2.

3.4.2 Results and discussion

The sintering temperatures of the ceramics are optimized for maximum densification and best microwave dielectric properties. Figure 3.3 shows the variation of bulk density and microwave dielectric properties with sintering temperature of a representative material $Ca_8La_2(PO_4)_6O_2$. From Fig. 3.3 (a) it can be observed that the density first increases with sintering temperature, reaches the maximum value at 1425 ^{o}C and then decreases with the increase in sintering temperature. The initial increase in density is due to the grain growth and removal of porosity. The decrease in density above 1425 ^{o}C may be due to the exaggerated grain growth (Lal *et al.*, 1989). The variation in ε_r and $Q_u \times f$ with sintering temperature follows the same trend as that of the density (Fig. 3.3 (b)). Both the values of ε_r and $Q_u \times f$ are directly related to the densification of the dielectric

ceramic (Sebastian, 2008). The maximum value of ε_r and $Q_u \times f$ obtained are 11.6 and 12700 GHz respectively when sintered at 1425 ^oC.

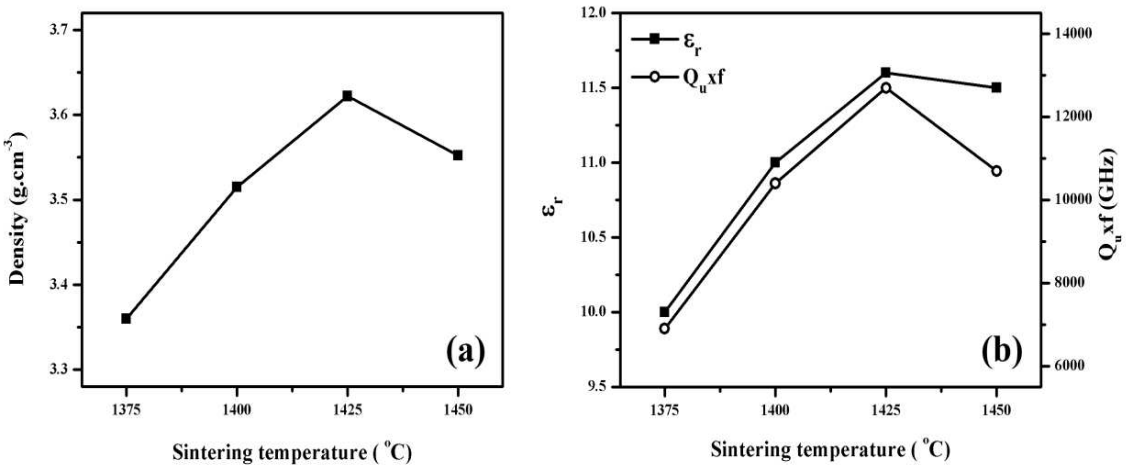

Figure 3.3 Variation of (a) density and (b) ε_r and $Q_u \times f$ with the sintering temperature

Figures 3.4, 3.5 and 3.6 show the powder XRD patterns of $Ca_{2+x}RE_{8-x}(SiO_4)_{6-x}(PO_4)_xO_2$ ceramics. The major peaks are indexed for the end members of each rare earth series using the standard JCPDS files (file no: 29-0337, 33-0287, 29-0362, 33-0298, 28-0228, 32-0175, 29-0365, 29-0320, 33-0275, 28-0212, 32-0163, 29-0386, 38-0256). The XRD pattern for $Ca_8Sm_2(PO_4)_6O_2$ (Fig. 3.5 (b)) is not indexable using the corresponding JCPDS file (file no: 38-0255). Also no quality mark has been assigned for this JCPDS file. Hence the peaks are indexed using the JCPDS file for $Ca_2Sm_8(SiO_4)_6O_2$ (file no: 29-0365) which is one of the end members of the Sm series (Fig. 3.5 (b)). Similarly the JCPDS file used for indexing the peaks of $Ca_8Tb_2(PO_4)_6O_2$ has no assigned quality mark and some minor peaks are not indexable using this file (Fig. 3.6 (b)). However all these peaks can be well indexed using the JCPDS file for $Ca_2Tb_8(SiO_4)_6O_2$ which is the other end member of Tb series (Fig. 3.6 (b)). The ceramics crystallize with hexagonal symmetry and belong to $P6_3/m$ space group. From Fig. 3.4, 3.5 and 3.6, it is obvious that all the XRD patterns are similar except for the small shift towards the higher angles with the increase in the value of x. It is also noteworthy that the magnitude of peak shift decreases with the decrease in ionic radius of the RE ion. For smaller RE ions like Gd and Tb only marginal shift in peak positions with the value of x can be observed

(Fig. 3.6 (a) and 3.6 (b)). An unidentified minor intensity peak is observed in the XRD patterns of $Ca_8Nd_2(PO_4)_6O_2$ (x = 6) and $Ca_6Sm_4(SiO_4)_2(PO_4)_4O_2$ (x = 4) indicated using asterisks in Fig. 3.5 (a) and Fig. 3.5 (b) respectively.

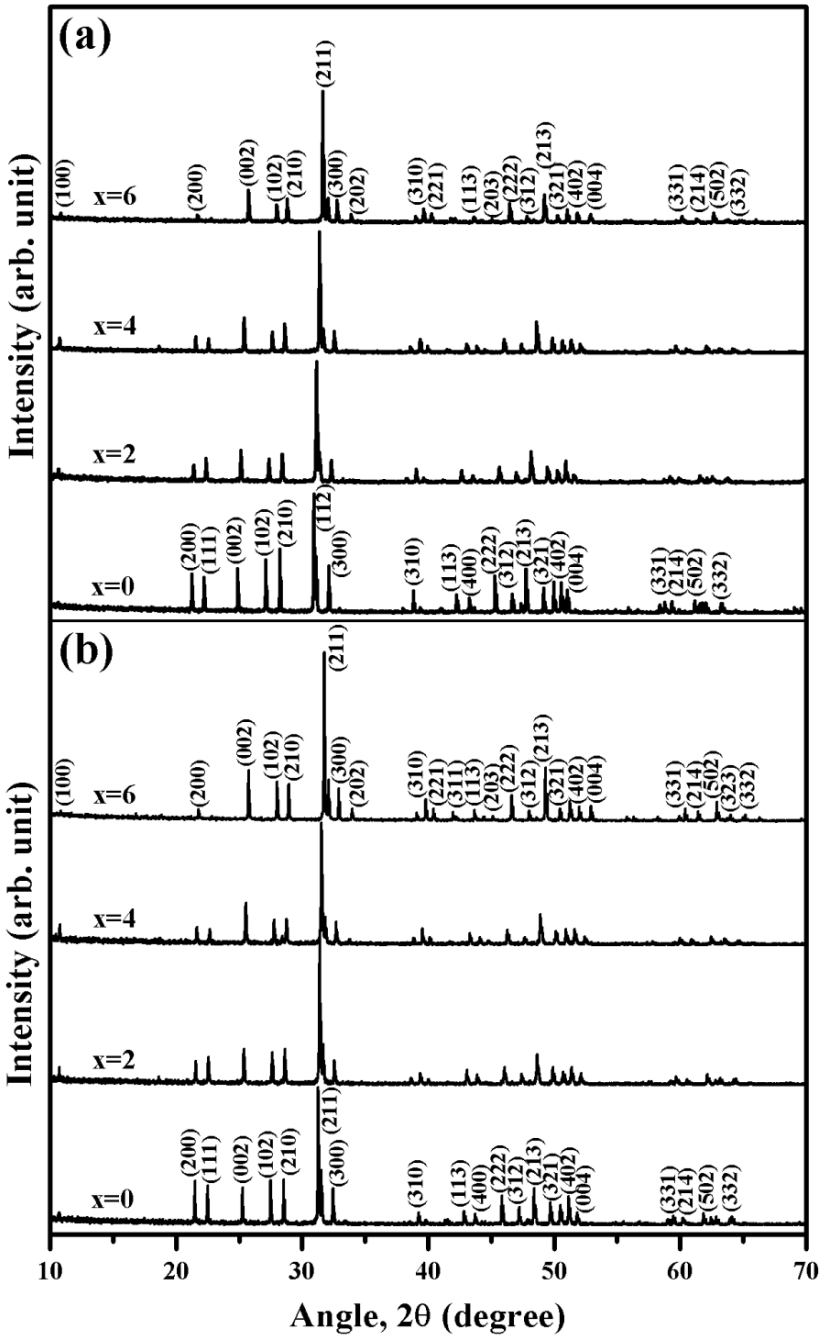

Figure 3.4 Powder XRD patterns of $Ca_{2+x}RE_{8-x}(SiO_4)_{6-x}(PO_4)_xO_2$ ceramics for the RE ions (a) La and (b) Pr.

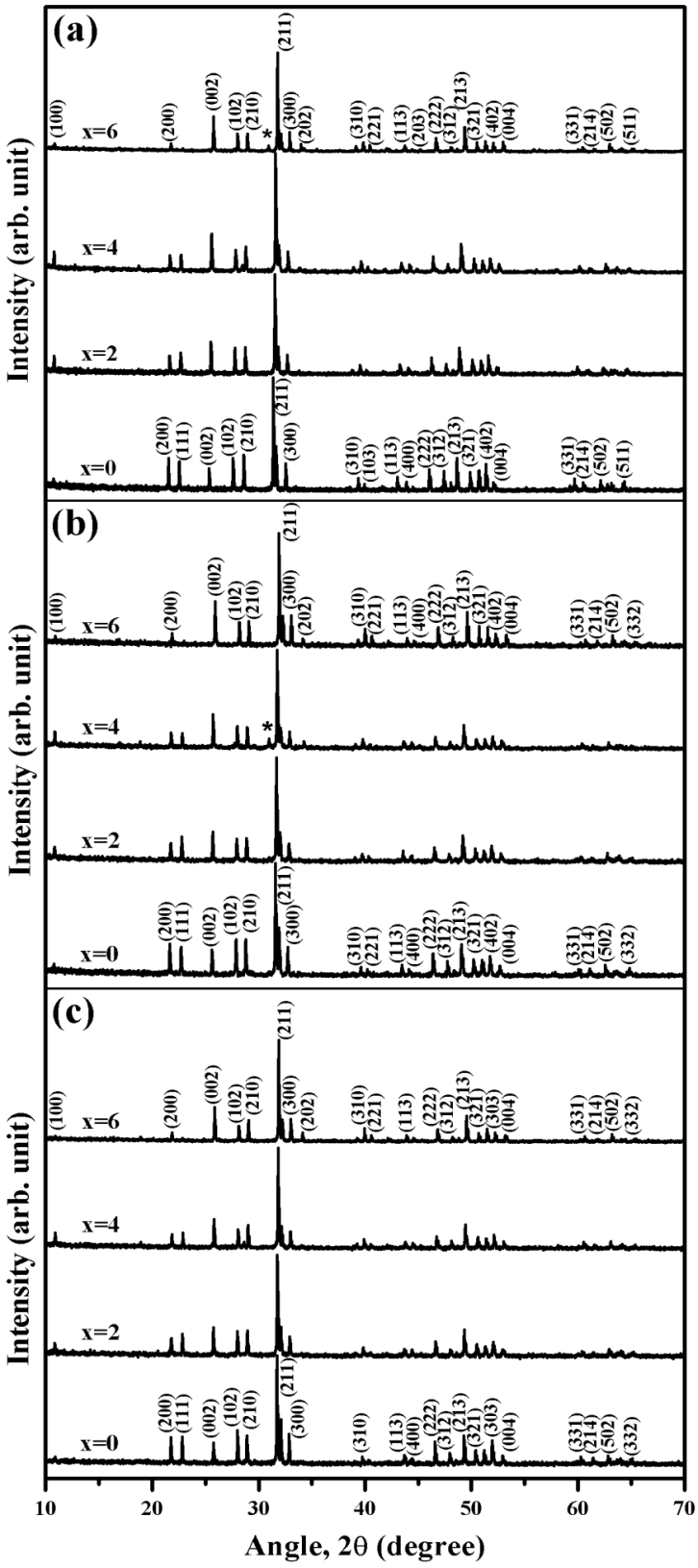

Figure 3.5 Powder XRD patterns of $Ca_{2+x}RE_{8-x}(SiO_4)_{6-x}(PO_4)_xO_2$ ceramics for the RE ions (a) Nd, (b) Sm and (c) Eu.

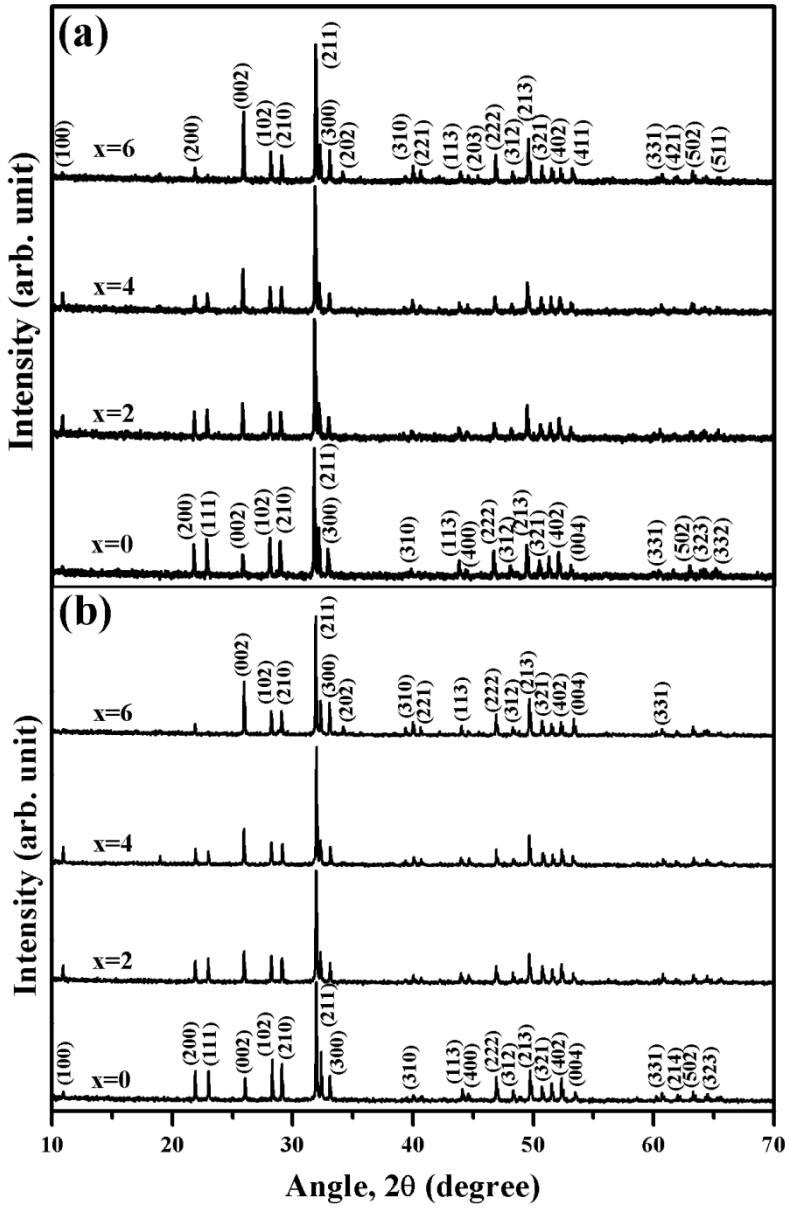

Figure 3.6 Powder XRD patterns of $Ca_{2+x}RE_{8-x}(SiO_4)_{6-x}(PO_4)_xO_2$ ceramics for the RE ions (a) Gd and (b) Tb.

The lattice parameters calculated from the XRD pattern using the equation (Cullity, 1978)

$$\frac{1}{d^2} = \frac{4}{3}\left[\frac{h^2+hk+k^2}{a^2}\right] + \frac{l^2}{c^2} \tag{3.1}$$

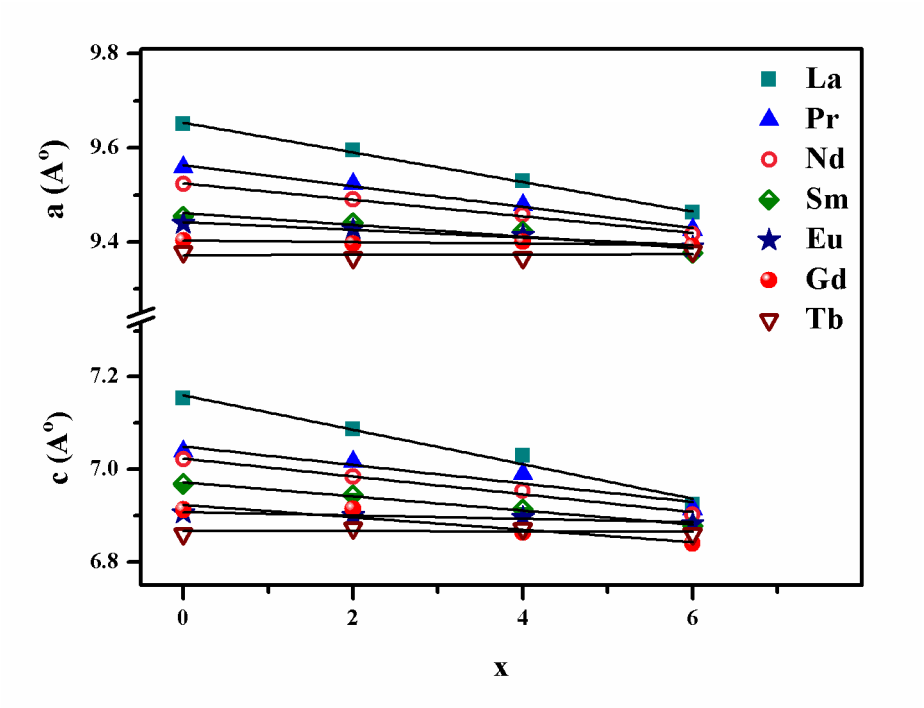

Figure 3.7 Lattice parameter variation of $Ca_{2+x}RE_{8-x}(SiO_4)_{6-x}(PO_4)_xO_2$ with the value of x

where d is the interplanar spacing, a and c are the lattice parameters and (*hkl*) the Miller indices. Figure 3.7 shows the variation of lattice parameters with the value of x for all the rare earth series studied. The lattice parameters 'a' and 'c' decreases gradually with x for the series containing larger RE ions (La to Eu). However the slope of both the lattice parameter variation decreases with the decrease in ionic radius of rare earth ion. Finally for smaller RE ion (Tb) the lattice parameter variation with x becomes marginal. It is also noteworthy that the lattice parameter 'c' varies irregularly with x for $Ca_{2+x}Gd_{8-x}(SiO_4)_{6-x}(PO_4)_xO_2$ although the variation is small. It has been reported earlier that for apatites, lattice parameter variation is sensitive to the distribution of cations among the M(I) and M(II) sites (Felsche, 1972). From Fig. 3.7 it is also obvious that the variation of lattice parameters for $Ca_{2+x}RE_{8-x}(SiO_4)_{6-x}(PO_4)_xO_2$ with the change in RE ion is more pronounced at the silicate end (x = 0) compared to the phosphate end (x = 6). The number of RE ions per unit cell decreases as the value of x increases and hence the effect of RE substitution on the lattice parameters may be relatively low for higher values of x.

The unit cell volume for the $Ca_{2+x}RE_{8-x}(SiO_4)_{6-x}(PO_4)_xO_2$ ceramics is calculated using the relation (Cullity, 1978)

$$V = \frac{\sqrt{3}a^2c}{2} \tag{3.2}$$

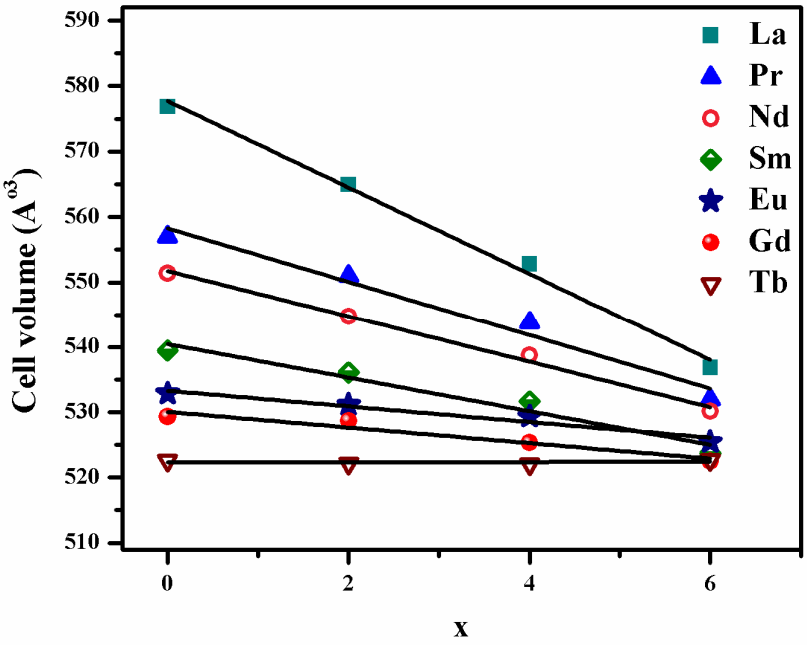

Figure 3.8 Variation of unit cell volume with the value of x

Figure 3.8 shows the variation of unit cell volume with x. The unit cell volume varies with x in a similar way as does the lattice parameters. Considerable lattice contraction occurs with the increase in x for $Ca_{2+x}La_{8-x}(SiO_4)_{6-x}(PO_4)_xO_2$. However, the variation of cell volume with x diminishes as La is replaced with smaller RE ions and the variation becomes negligible for Tb series (Fig. 3.8).

The optimized sintering temperature (T_s), relative density and the linear coefficient of thermal expansion (CTE) of all the compositions are given in Table 3.1. The optimized sintering temperature varies non-linearly as the value of x increases with a maximum at x = 4 for all the RE series. The compositions in La and Pr series show good densification (≥ 96%) for all the values of x (Table 3.1). Similarly Nd series shows a densification ≥ 96% upto x = 4. The ceramics in $Ca_{2+x}Sm_{8-x}(SiO_4)_{6-x}(PO_4)_xO_2$ series show a densification ~ 94%. For $Ca_{2+x}Eu_{8-x}(SiO_4)_{6-x}(PO_4)_xO_2$ the relative density varies in between 94.5% and 96.9%. $Ca_8Gd_2(PO_4)_6O_2$, $Ca_2Tb_8(SiO_4)_6O_2$ and $Ca_8Tb_2(PO_4)_6O_2$ show relatively poor densification of around 93%. The $Ca_{2+x}RE_{8-x}(SiO_4)_{6-x}(PO_4)_xO_2$ ceramics show

low thermal expansion (CTE ≤ 7 ppm/^{o}C) as evident from Table 3.1. From Table 3.1 it is also obvious that the value CTE increases with x for all the RE series.

Table 3.1 Optimized sintering temperature, relative density and CTE of $Ca_{2+x}RE_{8-x}(SiO_4)_{6-x}(PO_4)_xO_2$ ceramics

RE^{3+} ion	**x**	**T_s (^{o}C)**	**Relative density (%)**	**CTE (ppm/^{o}C)**
La	0	1475	96.7	3
	2	1475	98.7	5
	4	1675	97.5	5
	6	1425	97.6	7
Pr	0	1425	97.1	3
	2	1400	96.0	4
	4	1550	96.6	5
	6	1475	96.5	7
Nd	0	1375	97.1	3
	2	1400	96.0	3
	4	1575	97.5	4
	6	1475	93.7	6
Sm	0	1400	94.2	3
	2	1375	94.1	4
	4	1575	94.4	4
	6	1475	94.3	6
Eu	0	1425	95.0	3
	2	1425	94.5	4
	4	1575	95.2	5
	6	1475	96.9	6
Gd	0	1450	94.8	3
	2	1450	94.7	3
	4	1575	96.8	5
	6	1500	93.4	6
Tb	0	1525	92.8	2
	2	1500	94.7	4
	4	1575	96.8	5
	6	1550	92.9	5

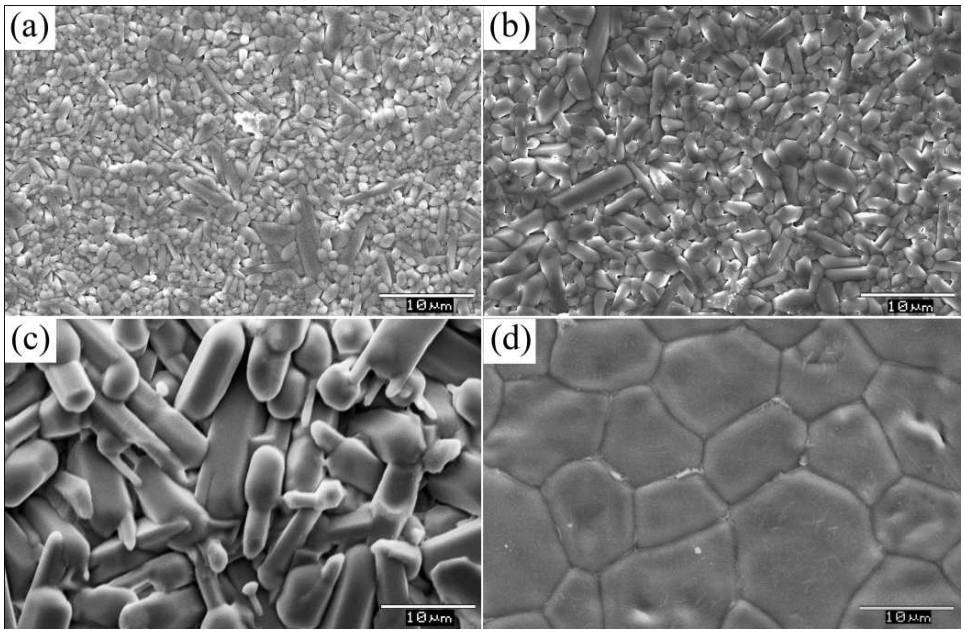

Figure 3.9 SEM images of $Ca_{2+x}La_{8-x}(SiO_4)_{6-x}(PO_4)_xO_2$ with (a) x = 0 sintered at 1475 ^oC/4h, (b) x = 2 sintered at 1475 ^oC/4h, (c) x = 4 sintered at 1675 ^oC/4h and (d) x = 6 sintered at 1425 ^oC/4h.

The microstructure of $Ca_{2+x}La_{8-x}(SiO_4)_{6-x}(PO_4)_xO_2$ ceramics is shown in Fig. 3.9. The microstructure of the composition with x = 0 (Fig. 3.9 (a)) contains grains of size randomly varying from less than 1 µm to ~ 8 µm. For x = 2 (Fig. 3.9 (b)) also the grain distribution follows somewhat similar trend with largest grain size being 10 µm. The SEM image of the surface of the ceramic with x = 4 (Fig. 3.9 (c)) shows still larger grains of size greater than 10 µm. Grains of size larger than 15 µm can be observed in the surface morphology of the composition with x = 6 (Fig. 3.9 (d)). From Fig. 3.9, it is obvious that the average grain size increases with increasing value of x.

Figure 3.10 shows the SEM images of $Ca_{2+x}Pr_{8-x}(SiO_4)_{6-x}(PO_4)_xO_2$ (x = 2 and 6) (Fig. 3.10 (a), (b)), $Ca_{2+x}Sm_{8-x}(SiO_4)_{6-x}(PO_4)_xO_2$ (x = 2 and 6) (Fig.3.10 (c), (d)) and $Ca_{2+x}Tb_{8-x}(SiO_4)_{6-x}(PO_4)_xO_2$ (x = 2 and 6) (Fig. 3.10 (e), (f)). The compositions with x = 2 contain smaller grains compared to those with x = 6. The surface morphology of $Ca_4Pr_6(SiO_4)_4(PO_4)_2O_2$ (Fig. 3.10 (a)) $Ca_4Sm_6(SiO_4)_4(PO_4)_2O_2$ (Fig. 3.10 (c)) and $Ca_4Tb_6(SiO_4)_4(PO_4)_2O_2$ (Fig. 3.10 (e)) reveals the presence rod shaped grains similar to those observed in Fig. 3.9 (a), (b)

and (c). For $Ca_8Pr_2(PO_4)_6O_2$ (Fig. 3.10 (b)), $Ca_8Sm_2(PO_4)_6O_2$ (Fig. 3.10 (d)) and $Ca_8Tb_2(PO_4)_6O_2$ (Fig. 3.10 (f)) the grain morphology changes to polygonal similar to $Ca_8La_2(PO_4)_6O_2$ (Fig. 3.9 (d)). The $Ca_8Tb_2(PO_4)_6O_2$ ceramic has got a poor microstructure (Fig. 3.10 (d)) with a secondary growth on some grains. However, no information about such a secondary phase is available from XRD pattern (Fig. 3.6 (b)). Hence further studies are required to resolve it.

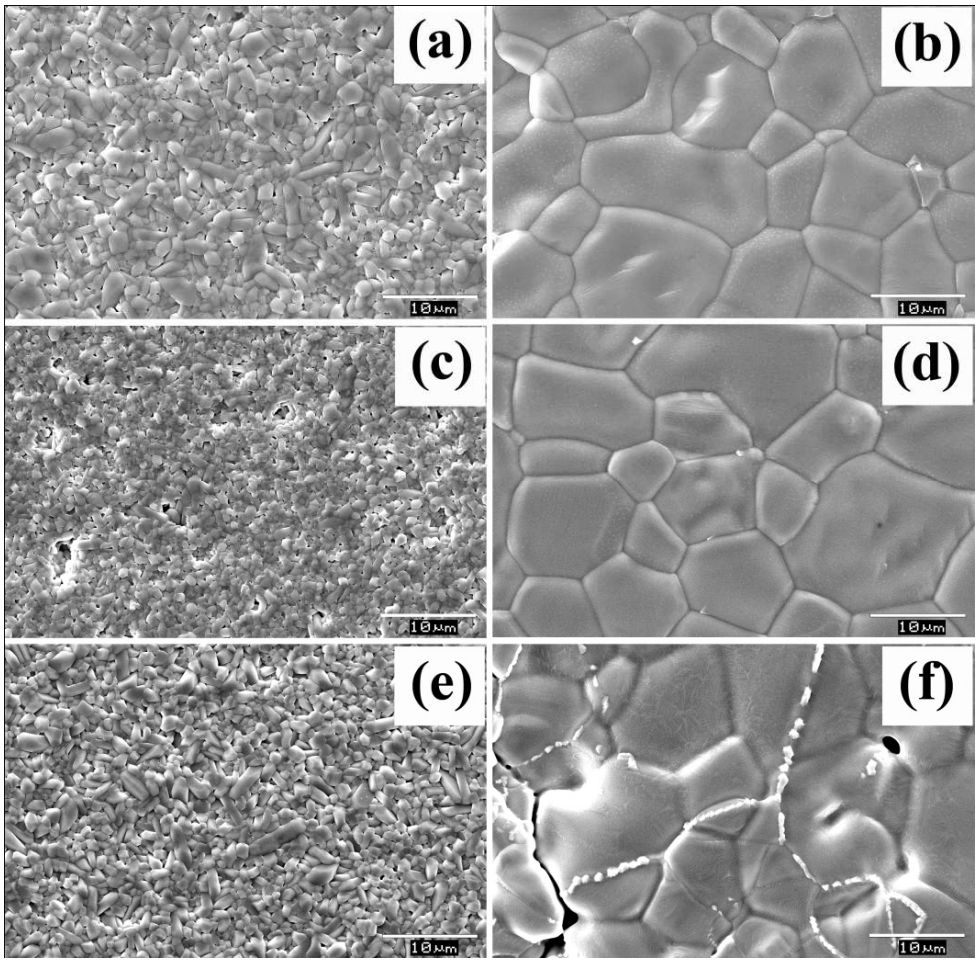

Figure 3.10 SEM images of $Ca_{2+x}RE_{8-x}(SiO_4)_{6-x}(PO_4)_xO_2$ with (a) RE= Pr, x=2, (b) RE= Pr, x=6, (c) RE= Sm, x= 2, (d) RE= Sm, x= 6, (e) RE= Tb, x= 2 and (f) RE= Tb, x=6.

The relative permittivity of $Ca_{2+x}RE_{8-x}(SiO_4)_{6-x}(PO_4)_xO_2$ ceramics at microwave frequencies ($\varepsilon_{r,measured}$) are given in Table 3.2. The relative permittivity depends on porosity within the sample. Hence the values of relative permittivity corrected for porosity ($\varepsilon_{r,corrected}$) using Penn equation (Eqn. 1.21) are also given in

Table 3.2. Table 3.2 also gives the values of relative permittivity ($\varepsilon_{r,calculated}$) predicted using Clausius-Mosotti equation (Eqn. 1.18) for comparison.

Table 3.2 Dielectric polarizability, molar volume and relative permittivity of the ceramics

RE ion	x	α_D (Å^3)	V_m (Å^3)	$\varepsilon_{r,\ measured}$	$\varepsilon_{r,\ corrected}$	$\varepsilon_{r,\ calculated}$
La	0	102.36	576.86	13.7	14.3	9.7
	2	99.74	564.97	13.8	14.0	9.5
	4	97.12	552.82	12.3	12.7	9.4
	6	94.50	536.85	11.6	12.0	9.4
Pr	0	106.36	556.94	14.8	15.4	13.0
	2	102.74	551.02	13.7	14.5	11.7
	4	99.12	543.80	12.5	13.1	10.7
	6	95.50	532.00	10.9	11.4	10.1
Nd	0	103.88	551.41	14.2	14.8	12.2
	2	100.88	544.71	13.2	14.0	11.4
	4	97.88	538.72	11.9	12.3	10.6
	6	94.88	530.14	10.3	11.2	10.0
Sm	0	101.72	539.43	13.5	14.7	12.3
	2	99.26	536.09	12.2	13.2	11.4
	4	96.80	531.67	11.4	12.3	10.6
	6	94.34	523.75	10.3	11.1	10.2
Eu	0	100.04	532.86	13.7	14.7	12.0
	2	98.00	531.12	12.5	13.5	11.2
	4	95.96	529.35	11.3	12.1	10.5
	6	93.92	525.47	10.4	10.8	9.9
Gd	0	98.76	529.33	13.1	14.1	11.7
	2	97.04	528.70	12.0	12.9	11.0
	4	95.32	525.36	11.3	11.8	10.5
	6	93.60	522.49	9.7	10.6	10.0
Tb	0	97.80	522.56	12.5	13.8	11.9
	2	96.32	522.14	12.0	12.9	11.2
	4	94.84	522.06	11.4	11.9	10.5
	6	93.36	522.71	9.2	10.1	9.9

The porosity corrected value of ε_r decreases gradually with the increase of x. This may be mainly due to the decrease in number of RE^{3+} ions with relatively large ionic polarizability (Shannon, 1993) in the unit cell as the value of x increases. From Table 3.2, it is obvious that the variation of both $\varepsilon_{r,corrected}$ and $\varepsilon_{r,calculated}$ with x follows the same trend for all the RE series although the numerical values are not close to each other. It is also noteworthy that the difference in $\varepsilon_{r,corrected}$ and $\varepsilon_{r,calculated}$ decreases when La is replaced with other RE ions for all the values of x and the difference is found to be minimum for $Ca_{2+x}Tb_{8-x}(SiO_4)_{6-x}(PO_4)_xO_2$. Clausius-Mosotti equation is strictly valid for the materials with cubic symmetry (Shannon *et al.*, 1992). Several other factors like conductivity, presence of impurities, rattling or compressed cations, error in the determination of molar volume etc. may also bring about considerable difference in observed and calculated values as discussed earlier in Chapter 1.

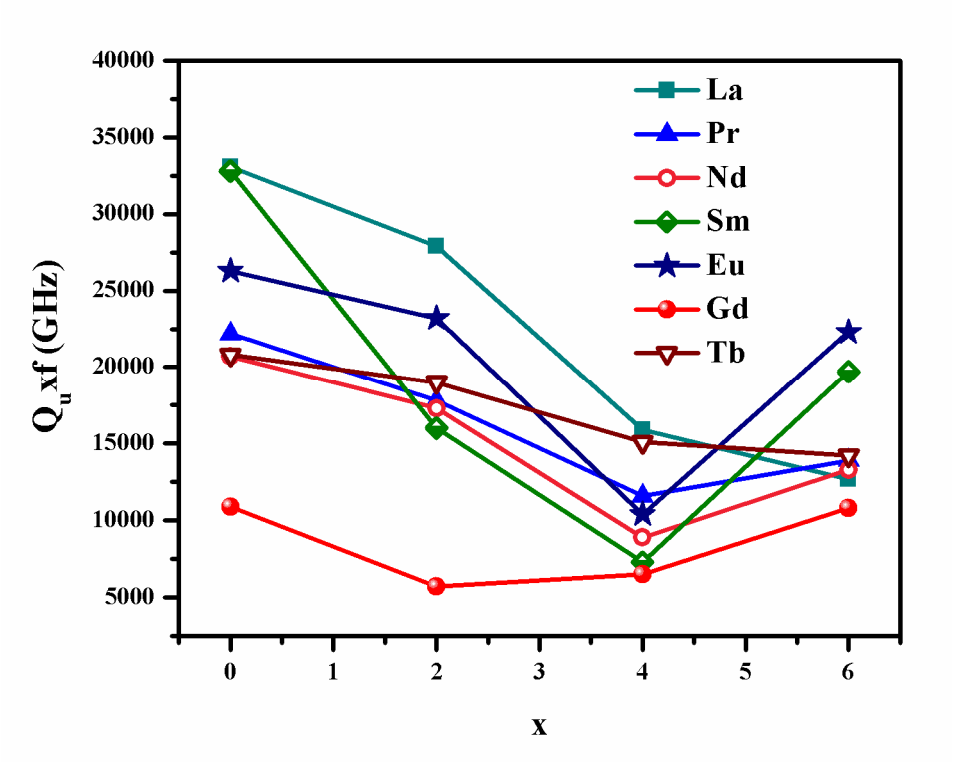

Figure 3.11 Variation of $Q_u \times f$ with x for $Ca_{2+x}RE_{8-x}(SiO_4)_{6-x}(PO_4)_xO_2$ ceramics

Figure 3.11 depicts the variation of $Q_u \times f$ as a function of x for $Ca_{2+x}RE_{8-x}(SiO_4)_{6-x}(PO_4)_xO_2$. For $Ca_{2+x}La_{8-x}(SiO_4)_{6-x}(PO_4)_xO_2$, $Q_u \times f$ decreases

gradually from 33100 GHz (at x = 0) to 12700 GHz (at x = 6). Similarly for $Ca_{2+x}Tb_{8-x}(SiO_4)_{6-x}(PO_4)_xO_2$ the quality factor decreases from 20800 GHz (at x = 0) to 14200 GHz (at x = 6). For $Ca_{2+x}RE_{8-x}(SiO_4)_{6-x}(PO_4)_xO_2$ with RE = Pr, Nd, Sm and Eu, $Q_u \times f$ decreases with x, reaches the minimum value at x= 4 and then increases for x = 6 (Fig. 3.11). The variation of $Q_u \times f$ for $Ca_{2+x}Gd_{8-x}(SiO_4)_{6-x}(PO_4)_xO_2$ also follows a similar trend showing the minimum value at x = 2. The variation in $Q_u \times f$ with x is small for the Gd series compared to the other series. Reasonably good quality factor ($Q_u \times f > 20000$ GHz) is obtained for the compositions $Ca_{2+x}La_{8-x}(SiO_4)_{6-x}(PO_4)_xO_2$ (x = 0, 2), $Ca_2Pr_8(SiO_4)_4O_2$ (x = 0), $Ca_2Nd_8(SiO_4)_4O_2$ (x = 0), $Ca_2Sm_8(SiO_4)_4O_2$ (x = 0), $Ca_{2+x}Eu_{8-x}(SiO_4)_{6-x}(PO_4)_xO_2$ (x = 0, 2 and 6), and $Ca_2Tb_8(SiO_4)_4O_2$ (x = 0). Among the various RE series studied, the Gd series show relatively poor quality factor with the maximum value being 10900 GHz for $Ca_2Gd_8(SiO_4)_4O_2$ (x = 0). Earlier Thomas et al. made a similar observation in $SrRE_4Si_3O_{13}$ apatites (Thomas *et al.*, 2009). Quality factor of dielectric ceramics depends on several intrinsic parameters arising from the anharmonic interaction of electromagnetic field with the phonons and extrinsic parameters like porosity, impurities, defects etc. (Breeze *et al.*, 2009).

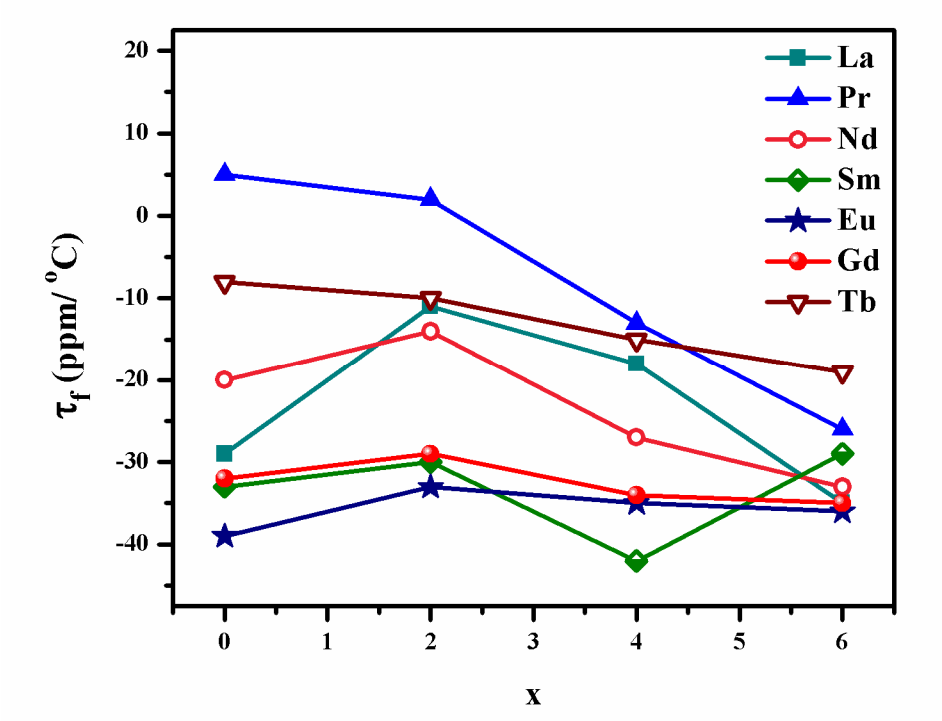

Figure 3.12 Variation of τ_f with x for $Ca_{2+x}RE_{8-x}(SiO_4)_{6-x}(PO_4)_xO_2$ ceramics

The variation of τ_f with x for the ceramics is shown in Fig. 3.12. All the ceramics except $Ca_{2+x}Pr_{8-x}(SiO_4)_{6-x}(PO_4)_xO_2$ (x = 0, 2) show negative value of τ_f. For $Ca_{2+x}Pr_{8-x}(SiO_4)_{6-x}(PO_4)_xO_2$ value of τ_f decreases with x from 5 ppm/^oC at x = 0 and shows negative value from x = 4 onwards. From Fig. 3.12 it can be observed that for the ceramics containing La, Nd, Eu and Gd, magnitude of τ_f decreases initially with x up to x = 2 and then increases from x = 4 onwards. The value of τ_f decreases linearly with x for $Ca_{2+x}Tb_{8-x}(SiO_4)_{6-x}(PO_4)_xO_2$. For $Ca_{2+x}Sm_{8-x}(SiO_4)_{6-x}(PO_4)_xO_2$ the τ_f shows irregular variation with x (Fig. 3.12). For $Sr_2RE_8(SiO_4)_6O_2$ apatites, it has been shown earlier that the value of τ_f depends on the possible lattice distortion (Leu *et al.*, 2011). In the present study, lowest values of τ_f (with the magnitude ≤ 15 ppm/^oC) are obtained for $Ca_4La_6(SiO_4)_4(PO_4)_2O_2$ (x = 2), $Ca_{2+x}Pr_{8-x}(SiO_4)_{6-x}(PO_4)_xO_2$ (x = 0, 2 and 4), $Ca_4Nd_6(SiO_4)_4(PO_4)_2O_2$ (x = 2) and $Ca_{2+x}Tb_{8-x}(SiO_4)_{6-x}(PO_4)_xO_2$ (x = 0, 2 and 4). Among the various compositions developed, $Ca_4La_6(SiO_4)_4(PO_4)_2O_2$ is found to have good densification (98.7%) and microwave dielectric properties (ε_r = 13.8, $Q_u \times f$ = 27900 GHz and τ_f = -11 ppm/^oC). Such an inherently low value of τ_f is very attractive for practical applications.

3.5 Effect of isovalent substitutions on the microwave dielectric properties of $Ca_4La_6(SiO_4)_4(PO_4)_2O_2$ apatite

The present study investigates how the microwave dielectric properties of $Ca_4La_6(SiO_4)_4(PO_4)_2O_2$ changes with the isovalent substitutions for the cations: Ca^{2+}, La^{3+} and for the anions: $(SiO_4)^{4-}$, $(PO_4)^{3-}$. The compositions studied are $(Ca_{4-x}Sr_x)La_6(SiO_4)_4(PO_4)_2O_2$ (x = 0, 2, 4), $Ca_4(La_{6-x}Pr_x)(SiO_4)_4(PO_4)_2O_2$ (x = 0, 2, 4, 6), $Ca_4La_6(SiO_4)_{4-x}(GeO_4)_x(PO_4)_2O_2$ (x = 0, 2, 4) and $Ca_4La_6(SiO_4)_4(PO_4)_{2-x}(VO_4)_xO_2$ (x = 0, 1, 2).

3.5.1 Experimental

The ceramics were prepared by the solid state ceramic route. High purity carbonates and oxides viz. $CaCO_3$ (99+%, Sigma-Aldrich), $SrCO_3$ (99.9+%, Sigma-Aldrich), La_2O_3 (99%, Indian Rare Earths Ltd., Kerala, India), Pr_6O_{11} (99%, Treibacher, Althofen, Austria), SiO_2 (99.6%, Sigma-Aldrich), GeO_2 (99.98%, Alfa Aesar, Lancashire, UK), $NH_4H_2PO_4$ (98+%, Sigma-Aldrich) and V_2O_5 (98+%,

Sigma-Aldrich) were used as precursors. Cylindrical samples of required dimensions were prepared as described earlier (section 3.4.1). The dimensions of the prepared samples were: diameter = 11 mm, thickness = 5-6 mm (for microwave measurements) and diameter = 8 mm, thickness = 12-13 mm (for thermal expansion measurements). The compacts were then sintered in air at temperatures in the range 1350-1600 ^{o}C for 4 hours with an intermediate dwell at 600 ^{o}C for the complete binder (PVA) burn out. The characterization techniques are same as those discussed in section 3.4.1.

3.5.2 Results and discussion

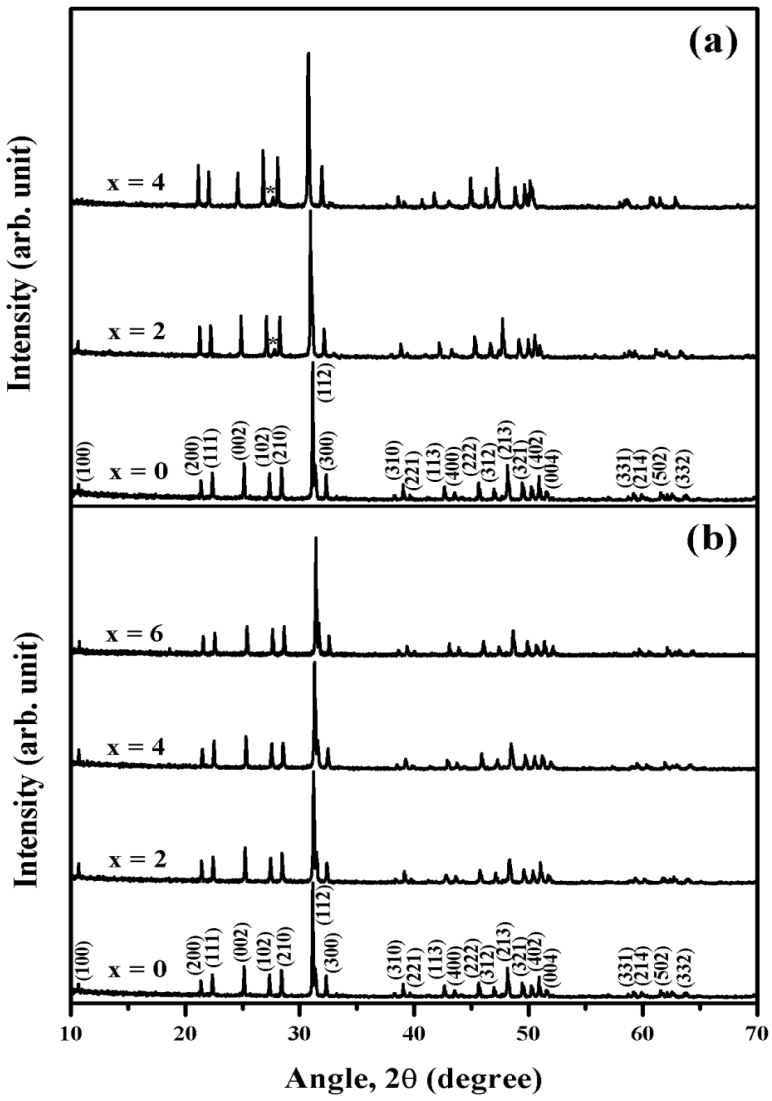

Figure 3.13 Powder XRD patterns of (a) $(Ca_{4-x}Sr_x)La_6(SiO_4)_4(PO_4)_2O_2$ and (b) $Ca_4(La_{6-x}Pr_x)(SiO_4)_4(PO_4)_2O_2$ ceramics.

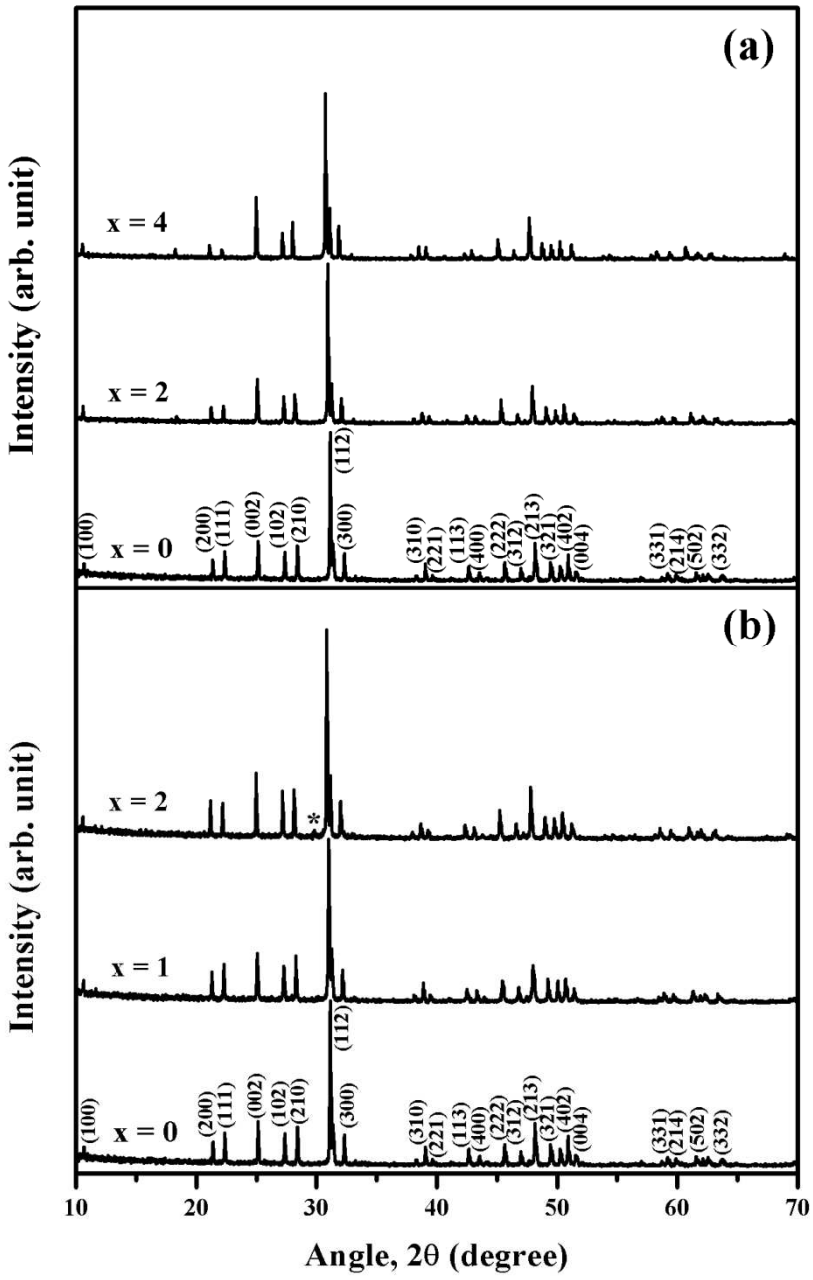

Figure 3.14 Powder XRD patterns of (a) $Ca_4La_6(SiO_4)_{4-x}(GeO_4)_x(PO_4)_2O_2$ and (b) $Ca_4La_6(SiO_4)_4(PO_4)_{2-x}(VO_4)_xO_2$.

The powder XRD patterns of the ceramics are shown in Fig. 3.13 and 3.14. Major peaks are indexed using the standard JCPDS files for $Ca_2La_8(SiO_4)_6O_2$ (file no: 29-0337) and $Ca_8La_2(PO_4)_6O_2$ (file no: 33-0287) with hexagonal symmetry and belonging to $P6_3/m$ space group. An unidentified peak can be obseved at $2\theta \sim 27.7^o$ in the XRD patterns of $Ca_2Sr_2La_6(SiO_4)_4(PO_4)_2O_2$ and $Sr_4La_6(SiO_4)_4(PO_4)_2O_2$

(indicated using *asterisks* in Fig. 3.13 (a)). Similarly an extra peak is present at $2\theta \sim 30^{o}$ in the XRD pattern of $Ca_4La_6(SiO_4)_4(VO_4)_2O_2$ (Fig. 3.14 (b)). Such peaks may arise due to the ionic ordering within the apatite lattice (Cullity, 1978; Pasero *et al.*, 2010) or due to the presence of small amount of impurity phases. However further studies are required to determine the exact origin of these peaks. It is also noteworthy that all these peaks have very low relative intensity (≤ 4 %). From Fig. 3.13 and 3.14 it is obvious that the XRD patterns for all the compositions are similar with an expected shift in peak positions due to substitution.

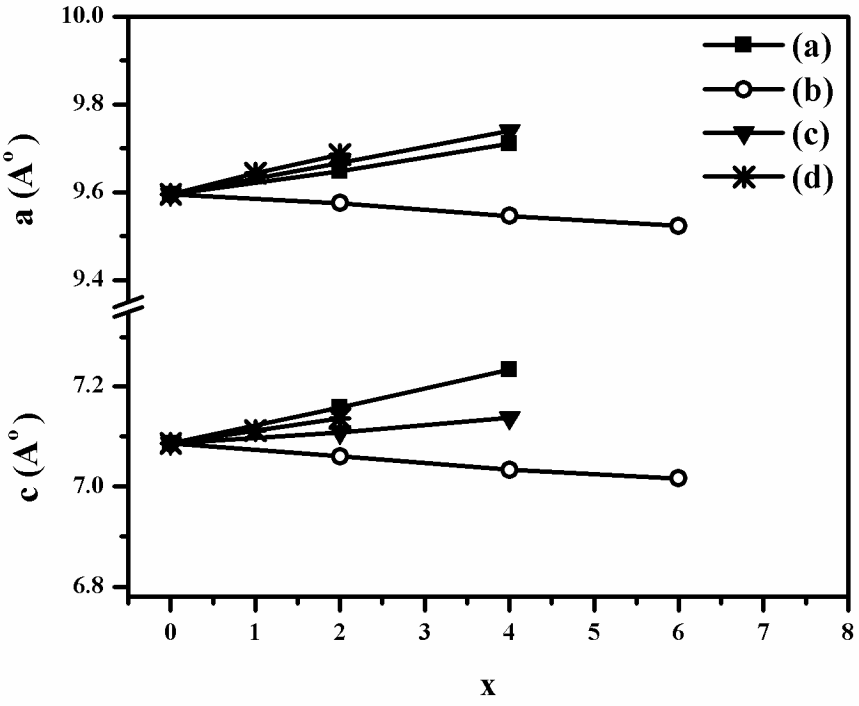

Figure 3.15 Variation of lattice parameters with x for (a) $(Ca_{4-x}Sr_x)La_6(SiO_4)_4(PO_4)_2O_2$, (b) $Ca_4(La_{6-x}Pr_x)(SiO_4)_4(PO_4)_2O_2$, (c) $Ca_4La_6(SiO_4)_{4-x}(GeO_4)_x(PO_4)_2O_2$ and (d) $Ca_4La_6(SiO_4)_4(PO_4)_{2-x}(VO_4)_xO_2$ ceramics.

The lattice parameters are calculated from the XRD data using the relation (3.1). Figure 3.15 shows the variation of lattice parameters with the value of x. The lattice parameters increase gradually with the substitution of Sr^{2+}, $(GeO_4)^{4-}$ and $(VO_4)^{3-}$ for Ca^{2+}, $(SiO_4)^{4-}$ and $(PO4)^{3-}$ respectively. This is due to the large ionic radii of the substituent ions compared to the existing ions (Shannon, 1976) and the resulting lattice expansion. On the other hand the lattice parameters decrease with

the substitution of Pr^{3+} for La^{3+} due to the relatively small ionic radius of Pr^{3+} (Shannon, 1976). For all the substitutions, the lattice parameters show linear dependence on the value of x (Vegard's law) indicating the formation of solid solutions (Azdouz *et al.*, 2010).

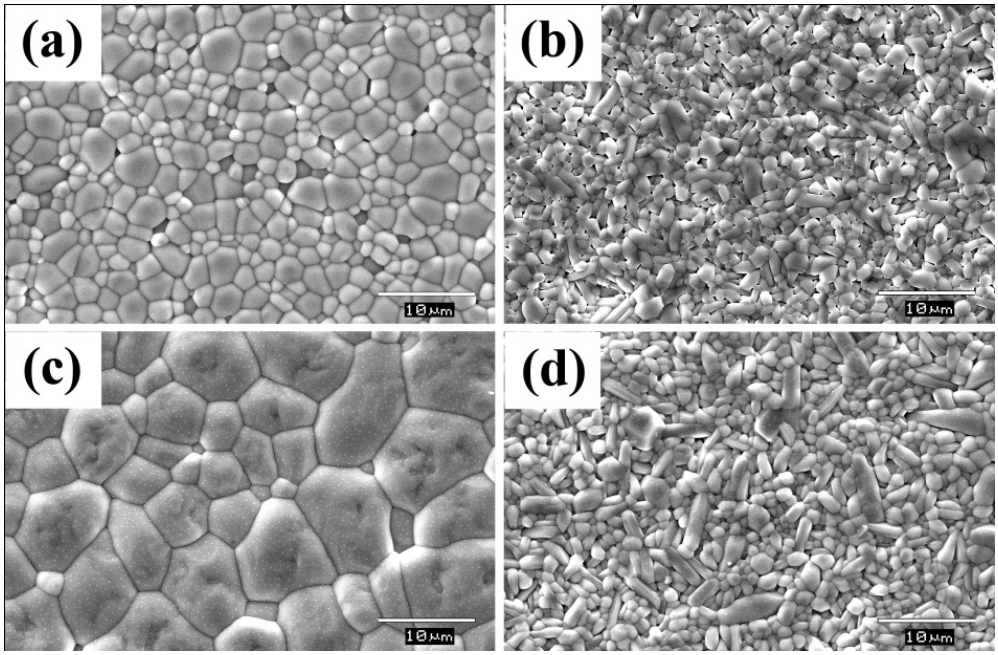

Figure 3.16 SEM images of (a) $Sr_4La_6(SiO_4)_4(PO_4)_2O_2$ (b) $Ca_4Pr_6(SiO_4)_4(PO_4)_2O_2$, (c) $Ca_4La_6(GeO_4)_4(PO_4)_2O_2$ and (d) $Ca_4La_6(SiO_4)_4(VO_4)_2O_2$.

The dielectric properties of sintered ceramics depend on the microstructure. A dense, defect free microstructure is essential for good microwave dielectric properties (Park *et al.*, 2001). Figure 3.16 shows the SEM images of the compositions derived from $Ca_4La_6(SiO_4)_4(PO_4)_2O_2$ by fully replacing Ca^{2+} with Sr^{2+} (Fig. 3.16 (a)), La^{3+} with Pr^{3+} (Fig. 3.16 (b)), $(SiO_4)^{4-}$ with $(GeO_4)^{4-}$ (Fig. 3.16 (c)) and $(PO_4)^{3-}$ with $(VO_4)^{3-}$ (Fig. 3.16 (d)). The SEM images of the compositions with Sr^{2+} and $(GeO_4)^{4-}$ (Fig. 3.16 (a) and 3.16 (c)) reveal dense microstructures with well packed polygonal grains. For $Sr_4La_6(SiO_4)_4(PO_4)_2O_2$ the grain size varies from < 1μm to ~5 μm. $Ca_4La_6(GeO_4)_4(PO_4)_2O_2$ shows broader grain size distribution with the size varying from ~1 μm to ~15 μm. The microstructure of $Ca_4Pr_6(SiO_4)_4(PO_4)_2O_2$ (Fig. 3.16 (b)) and $Ca_4La_6(SiO_4)_4(VO_4)_2O_2$ (Fig. 3.16(d))

shows rather elongated grains with the maximum grain size of ~5 μm and ~8 μm respectively.

Table 3.3 Sintering temperature, relative density, CTE and water absorption of the ceramics

Material	x	T_s (^oC)	Relative density (%)	CTE (ppm/^oC)	Water absorption (wt. %)
$(Ca_{4-x}Sr_x)La_6(SiO_4)_4(PO_4)_2O_2$	0	1475	98.7	5	0.00
	2	1575	98.4	4	0.00
	4	1600	98.0	4	0.01
$Ca_4(La_{6-x}Pr_x)(SiO_4)_4(PO_4)_2O_2$	0	1475	98.7	5	0.00
	2	1400	97.9	4	0.02
	4	1375	97.2	4	0.02
	6	1400	96.0	4	0.02
$Ca_4La_6(SiO_4)_{4-x}(GeO_4)_x(PO_4)_2O_2$	0	1475	98.7	5	0.00
	2	1550	94.9	4	0.39
	4	1550	98.2	4	0.01
$Ca_4La_6(SiO_4)_4(PO_4)_{2-x}(VO_4)_xO_2$	0	1475	98.7	5	0.00
	1	1375	97.9	4	0.01
	2	1350	98.5	4	0.00

Table 3.3 gives the optimized sintering temperature (T_s), relative density, linear coefficient of thermal expansion (CTE) and water absorption of all the compositions studied. The substitution of Sr^{2+} and $(GeO_4)^{4-}$ increases the sintering temperature. On the other hand, sintering temperature decreases with the substitution of Pr^{3+} and $(VO_4)^{3-}$. The relative density decreases for all the substitutions. However, the variation in relative density is marginal for Sr^{2+} substitution and all the compositions in this series maintain a densification ≥ 98%. From Table 3.3, it is obvious that variation of relative density has a non linear dependence on the value of x for $(GeO_4)^{4-}$ and $(VO_4)^{3-}$ substitution. The ceramics show only a small thermal expansion with the values of CTE in the range 4-5 ppm/^{o}C (Table 3.3). The presence of water content within the sample is detrimental to the dielectric properties (Sebastian, 2008). From Table 3.3 it is clear that all the compositions shows negligible tendency for water absorption with the exception for

$Ca_4La_6(SiO_4)_2(GeO_4)_2(PO_4)_2O_2$ which shows relatively large water absorption (0.39 %). The water absorption characteristics can be correlated with the relative density of the samples, poor densification leads to high water absorption.

Table 3.4 Dielectric polarizability, molar volume and relative permittivity of the ceramics

Material	**x**	α_D **(Å^3)**	V_m **(Å^3)**	$\varepsilon_{r,\ measured}$	$\varepsilon_{r,\ corrected}$	$\varepsilon_{r,\ calculated}$
$(Ca_{4-x}Sr_x)La_6(SiO_4)_4(PO_4)_2O_2$	0	99.74	564.97	13.8	14.0	9.5
	2	101.90	577.03	13.4	13.7	9.5
	4	104.06	590.59	12.7	13.0	9.5
$Ca_4(La_{6-x}Pr_x)(SiO_4)_4(PO_4)_2O_2$	0	99.74	564.97	13.8	14.0	9.5
	2	100.74	560.55	13.8	14.2	10.1
	4	101.74	555.03	13.8	14.3	10.9
	6	102.74	551.02	13.7	14.5	11.7
$Ca_4La_6(SiO_4)_{4-x}(GeO_4)_x(PO_4)_2O_2$	0	99.74	564.97	13.8	14.0	9.5
	2	101.26	575.26	13.9	14.9	9.4
	4	102.78	586.24	15.2	15.6	9.3
$Ca_4La_6(SiO_4)_4(PO_4)_{2-x}(VO_4)_xO_2$	0	99.74	564.97	13.8	14.0	9.5
	1	101.44	572.65	14.2	14.6	9.6
	2	103.14	579.68	14.5	14.8	9.8

The experimentally measured values of relative permittivity ($\varepsilon_{r,\ measured}$) at microwave frequencies and the ε_r corrected for porosity ($\varepsilon_{r,\ corrected}$) using Penn equation (eqn. 1.21) are given in Table 3.4. The values of relative permittivity calculated using Clausius-Mosotti equation (eqn. 1.18) are also given in Table 3.4. In Table 3.4, V_m is the molar volume calculated from the powder XRD pattern (Vineis *et al.*, 1996) and α_D is dielectric polarizability calculated using the individual ion dielectric polarizabilities (Shannon, 1993; Vineis *et al.*, 1996). The values of V_m, α_D and calculated relative permittvity ($\varepsilon_{r,\ calculated}$) are also given in Table 3.4. From Table 3.4 it is obvious that $\varepsilon_{r,\ measured}$ decreases gradually with x for Sr^{2+} substitution. On the other hand $\varepsilon_{r,\ measured}$ increases with the substitution of $(GeO_4)^{4-}$ and $(VO_4)^{3-}$. The experimentally measured values of ε_r do not show considerable variation with Pr^{3+} substitution. However $\varepsilon_{r,\ corrected}$ increases slowly with x for Pr^{3+} substitution. From Table 3.4 it is clear that there is a considerable difference in the calculated and

measured values of ε_r for all the compositions. It is also noteworthy that the variation of $\varepsilon_{r,\ corrected}$ and $\varepsilon_{r,\ calculated}$ does not follow the same trend for Sr^{2+} and $(GeO_4)^{4-}$ substitutions. Clausius-Mosotti equation is best suited for the compounds with cubic symmetry (Shannon *et al.*, 1992) and any deviation from this may produce deviations in the estimated values. Furthermore, it has been reported that a misfit between the calculated and measured values of ε_r can occur due to the ionic or electronic conductivity, presence of H_2O or CO_2 in channels, dipolar impurities, presence of rattling or compressed cations etc. (Shannon, 1993).

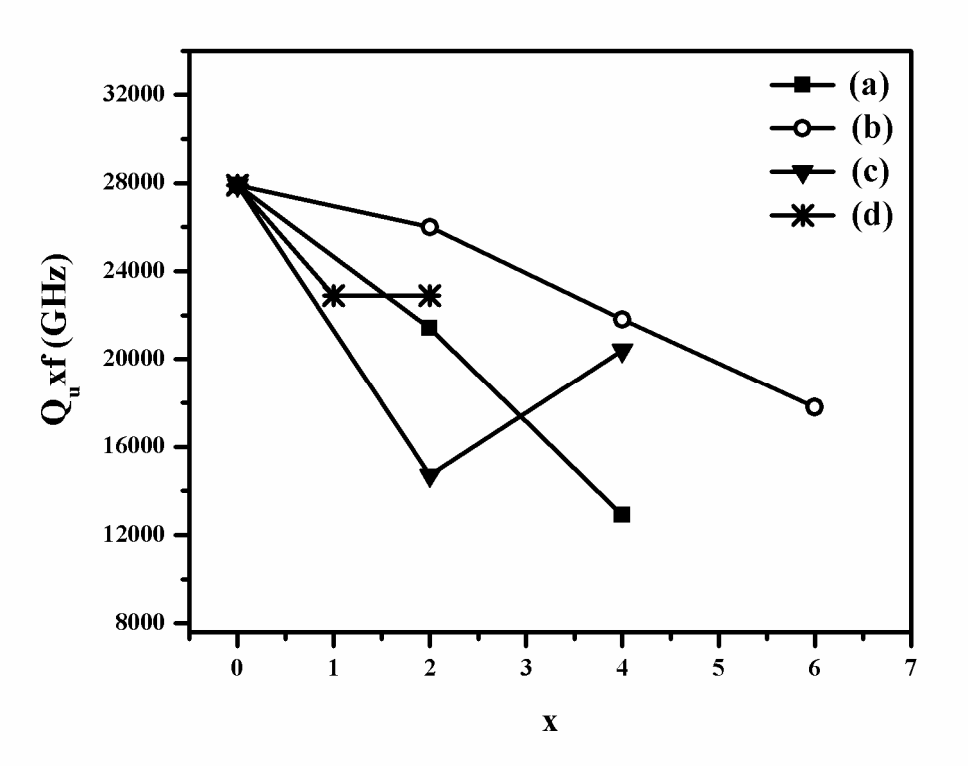

Figure 3.17 Dependence of $Q_u \times f$ on the value of x for (a) $(Ca_{4-x}Sr_x)La_6(SiO_4)_4(PO_4)_2O_2$, (b) $Ca_4(La_{6-x}Pr_x)(SiO_4)_4(PO_4)_2O_2$, (c) $Ca_4La_6(SiO_4)_{4-x}(GeO_4)_x(PO_4)_2O_2$ and (d) $Ca_4La_6(SiO_4)_4(PO_4)_{2-x}(VO_4)_xO_2$ ceramics.

Figure 3.17 shows the variation of quality factor ($Q_u \times f$) with x for all the four isovalent substitutions. The quality factor is dependent on several intrinsic factors like the anharmonicity in the interaction between electric field with the phonon system of the dielectric and extrinsic factors like imperfections in crystal lattice, order-disorder, impurities, porosity, micro cracks etc. (Sebastian, 2008). The presence of porosity and the subsequent moisture absorption will reduce the quality

factor to a considerable extent. In the present study the variation of relative density (and hence the porosity) with Sr^{2+} substitution is very small (Table 3.3). Nevertheless, $Q_u \times f$ shows a substantial decrease from 27900 GHz to 12900 GHz as the value of x increases from 0 to 4 (Fig. 3.17 (a)). Hence some other extrinsic factors might be responsible for such a behavior. In apatite structure, the divalent cation has two possible sites 4f with ninefold coordination and 6h with sevenfold coordination (Chartier *et al.*, 2001). The ordering of the ions among these sites may have some influence on the dielectric response of the system (Thomas *et al.*, 2009). From Fig. 3.17 (b), it can be observed that $Q_u \times f$ decreases from 27900 GHz at x = 0 to 17800 GHz at x = 6 with the Pr^{3+} substitution. The gradual decrease in $Q_u \times f$ with Pr^{3+} substitution may presumably due to the corresponding decrease in relative density (Table 3.3). $(GeO_4)^{4-}$ substitution first decreases $Q_u \times f$ from 27900 GHz for x = 0 to 14700 GHz for x = 2 and then increases to 20400 GHz for x = 2 (Fig. 3.17 (c)). $Q_u \times f$ decreases initially with the $(VO_4)^{3-}$ substitution and saturates at 22900 GHz from x = 1 onwards (Fig. 3.17 (d)). The non linear variation of $Q_u \times f$ with x for $(GeO_4)^{4-}$ and $(VO_4)^{3-}$ substitutions may be correlated with the non linearity in the variation of relative density (Table 3.3). It has been reported earlier that the post-sinter annealing is effective in several systems to develop an ordered structure and thereby an increase in $Q_u \times f$ (Sebastian, 2008). In the present study, the sintered samples are annealed at a temperature 200 ^oC less than that of the sintering temperature for 10 hours and again the microwave dielectric properties are measured. However no appreciable increase has been observed in the properties after annealing.

The variation of τ_f with the substitutions is shown in Fig. 3.18. The τ_f increases linearly with x for Sr^{2+} and $(VO_4)^{3-}$ substitution (Fig. 3.18 (a) and 3.18 (d)). On Pr^{3+} substitution, the magnitude of τ_f decreases gradually from – 11 ppm/^oC at x = 0 and reaches a value of + 2 ppm/^oC at x = 6 (Fig. 3.18 (b)). The value of τ_f shows slightly non linear variation upon $(GeO_4)^{4-}$ substitution (Fig. 3.18 (c)) with the values lying between -11 ppm/^oC and -13 ppm/^oC. The partial substitution of Pr^{3+} for La^{3+} in $Ca_4La_6(SiO_4)_4(PO_4)_2O_2$ effectively reduces the τ_f without much altering the values of ε_r and $Q_u \times f$. Among the various compositions developed,

$Ca_4(La_4Pr_2)(SiO_4)_4(PO_4)_2O_2$ shows good microwave dielectric properties with ε_r = 13.8, $Q_u \times f$ = 26000 GHz and τ_f = -7 ppm/^oC.

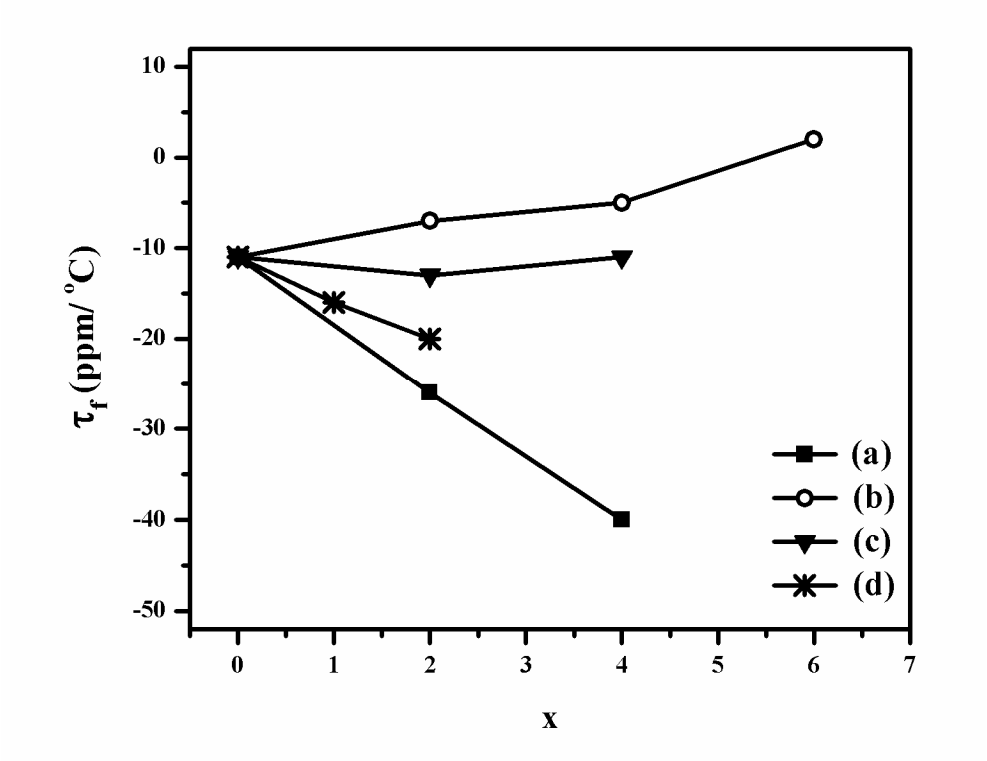

Figure 3.18 Variation of τ_f with x for (a) $(Ca_{4-x}Sr_x)La_6(SiO_4)_4(PO_4)_2O_2$, (b) $Ca_4(La_{6-x}Pr_x)(SiO_4)_4(PO_4)_2O_2$, (c) $Ca_4La_6(SiO_4)_{4-x}(GeO_4)_x(PO_4)_2O_2$ and (d) $Ca_4La_6(SiO_4)_4(PO_4)_{2-x}(VO_4)_xO_2$ ceramics

3.6 Conclusions

The $Ca_{2+x}RE_{8-x}(SiO_4)_{6-x}(PO_4)_xO_2$ [RE = La, Pr, Nd, Sm, Eu, Gd and Tb] (x = 0, 2, 4 and 6) ceramics have been prepared by the solid state ceramic technique. Sintering temperature has been optimized for maximum densification and good microwave dielectric properties. The compositions containing larger rare earth ions show highest densification. The crystal structure of the ceramics has been analyzed using powder XRD. The ceramics have hexagonal symmetry and belong to $P6_3/m$ space group. The microstructural analysis using SEM showed an increase in the average grain size with x. The measured values of relative permittivity have been compared with the values calculated using Clausius-Mosotti equation. For majority of the compositions studied, both $Q_u \times f$ and τ_f vary non-linearly with the value of x. The composition $Ca_4La_6(SiO_4)_4(PO_4)_2O_2$ is found to have the highest densification

(98.7%) and good microwave dielectric properties with ε_r = 13.8, $Q_u \times f$ = 27900 GHz and τ_f = -11 ppm/^oC.

The isovalent substitutions of Sr^{2+}, Pr^{3+}, $(GeO_4)^{4-}$ and $(VO_4)^{3-}$ in the respective cationic and anionic sites of $Ca_4La_6(SiO_4)_4(PO_4)_2O_2$ have been accomplished. The ceramics have been prepared through the solid state ceramic route. The powder XRD data reveals the complete solid solubility of Sr^{2+}, Pr^{3+}, $(GeO_4)^{4-}$ and $(VO_4)^{3-}$ in the respective divalent, trivalent cationic and tetravalent, trivalent anionic sites of $Ca_4La_6(SiO_4)_4(PO_4)_2O_2$. Most of the compositions show good densification ≥ 96%. The relative permittivity decreases with Sr^{2+} substitution, increases with $(GeO_4)^{4-}$ and $(VO_4)^{3-}$ substitutions and remains almost the same on Pr^{3+} substitution. $Q_u \times f$ is found to be decreasing with all the substitutions. Only the substitution of Pr^{3+} for La^{3+} improves the τ_f. $Ca_4(La_4Pr_2)(SiO_4)_4(PO_4)_2O_2$ has got promising microwave dielectric properties with ε_r = 13.8, $Q_u \times f$ = 26000 GHz and τ_f = -7 ppm/^oC. The compositions developed exhibit rather low values of linear coefficient of thermal expansion in the range 4-5 ppm/^oC.

Chapter 4

Development of Phosphate based dielectric ceramics and tapes for LTCC applications

Development of some phosphate based glass free LTCC compositions and tape is discussed in this chapter. The ceramics developed are $LiMg_{(1-x)}Zn_xPO_4$ (x = 0 to 1) with sintering temperature ≤ 950 ^oC. The ceramic with x = 0.1 ($LiMg_{0.9}Zn_{0.1}PO_4$) sintered at 925 ^oC shows the best microwave dielectric properties (ε_r = 6.7, $Q_u \times f$ = 99700 GHz and τ_f = -62 ppm/^oC). The slightly large τ_f of the ceramics is adjusted nearly to zero with the addition of TiO_2. The ceramics are found to be chemically compatible with silver. The tape casting slurry of $LiMgPO_4$ with typical pseudoplastic behavior has been prepared and cast into thin tapes of thickness 70 μm. The thermo-laminated tape (4 layers) sintered at 950 ^oC shows good microwave dielectric properties: ε_r = 6.4 and tan δ = 0.0002.

4.1 Introduction

The past two decades have witnessed revolutionary changes in wireless communication which stimulated the development of new technologies. Low Temperature Co-fired Ceramic (LTCC) technology has emerged as the paramount technology for the production of miniaturized microwave devices at a relatively low cost. LTCC technology offers high level of passive integration, performance stability and reliability. The ceramic system used for LTCC applications should meet the requirements such as low relative permittivity, low dielectric loss, temperature stability of dielectric properties, low coefficient of thermal expansion and high thermal conductivity. Most importantly the ceramic should be chemically compatible with silver and its sintering temperature must be less than the melting point of silver (961 ^{o}C) which is the most commonly used electrode material (Sebastian *et al.*, 2008). Low bulk density of the ceramic is also desirable for the production of light weight electronic modules. These stringent requirements limit the number of materials available for practical applications.

Most of the conventional ceramics with good microwave dielectric properties have very high sintering temperature which is unsuitable for LTCC applications. However, the sintering temperature can be lowered by the liquid phase sintering through the addition of glasses with low melting point (Sebastian *et al.*, 2008). Another method to produce LTCC is through the glass-ceramic route (Tummala, 1991). In both the above mentioned approaches, presence of amorphous phase in the system may degrade the microwave dielectric properties and enhance the possibility of chemical reaction between the substrate and metal electrode (Bian *et al.*, 2011). The presence of glass phase may also reduce the ease of processing while tape casting. It is also possible to lower the sintering temperature by using fine powders prepared through wet chemical processing. However, the chemical synthesis is complicated and expensive (Li *et al.*, 2009). Therefore a glass free ceramic with good microwave dielectric properties is desirable for LTCC applications.

Several glass free ceramics have been reported in the literature for LTCC applications. Among them Te and Bi based ceramics are found to have very low

sintering temperature (< 850 ^{o}C) (Udovic *et al.*, 2001; Valant *et al.*, 2001; Udovic *et al.*, 2004; Valant *et al.*, 2004; Kwon *et al.*, 2005; Kwon *et al.*, 2007; Subodh *et al.*, 2007; Li *et al.*, 2009; Zhou *et al.*, 2009; Zhou *et al.*, 2010). However, most of the Te-based systems are reactive with silver which limits their practical applications. It should also be noted that any densification of ceramics below 800 ^{o}C may prevent the complete evaporation of organics added for tape casting and leave out residual carbon which is detrimental to the microwave dielectric properties (Tummala, 1991). Li_3NbO_4 ceramic sintered at 930 ^{o}C is found to have good microwave dielectric properties (ε_r= 15.8, $Q_u \times f$ = 55000 GHz and τ_f = - 49 ppm/^{o}C). The ceramic is also found to be chemically compatible with silver (Ag) (Zhou *et al.*, 2008). Recently, Bian et al. reported the microwave dielectric properties of $(La_{0.5}Na_{0.5})_{1-x}(Li_{0.5}Nd_{0.5})_xWO_4$ ceramics. The composition with x=0.3 sintered at 800 ^{o}C has remarkable dielectric properties: ε_r = 12.7, $Q_u \times f$ = 23500 GHz and τ_f = -1.4 ppm/°C at microwave frequency. However, the ceramic is found to be reactive with Ag (Bian *et al.*, 2011). $Ca_{1-x}(Li_{0.5}Nd_{0.5})_xWO_4$ scheelites constitute another class of glass-free LTCC. $Ca_{0.8}(Nd_{0.5}Li_{0.5})_{0.2}WO_4$ has an ε_r of 11.7, $Q_u \times f$ of 36700 GHz, and τ_f of 5.4 ppm/°C and is chemically compatible with Ag (Bian *et al.*, 2012).

A few glass free phosphates are also reported to be suitable for LTCC applications. Bian et al. studied the microwave dielectric properties of AMP_2O_7 (A=Ca, Sr; M=Zn, Cu) (Bian *et al.*, 2005). The ceramics can be sintered at a low temperature (≤ 950 ^{o}C) and possess low relative permittivity (ε_r < 8). $SrCuP_2O_7$ sintered at 925 ^{o}C has the highest $Q_u \times f$ greater than 100000 GHz and lowest τ_f of -62 ppm/^{o}C. Nevertheless all the compositions react with silver. Cho et al. reported the microwave dielectric properties of $BiPO_4$ which has a low sintering temperature of 950 ^{o}C. The ceramic has an ε_r of 22, $Q_u \times f$ of 32500 GHz and a τ_f of -79 ppm/^{o}C (Cho *et al.*, 2006).

4.2 Microwave dielectric properties of $LiMg_{(1-x)}Zn_xPO_4$ (x = 0 to 1) and the development of new temperature stable glass free LTCC

The present work investigates the microwave dielectric properties of olivine type $LiMgPO_4$ and the effect of Zn^{2+} substitution for Mg^{2+} on its microwave dielectric properties with an objective to develop new low cost, light weight, glass

free ceramics having excellent microwave dielectric properties for LTCC applications.

4.2.1 Experimental

$LiMg_{(1-x)}Zn_xPO_4$ ceramics were prepared by the solid state ceramic route. High purity Li_2CO_3 (99+ %, Sigma-Aldrich, St. Louis, MO), $(MgCO_3)_4.Mg(OH)_2.5H_2O$ (99 %, Sigma-Aldrich), ZnO (99.9%, Sigma-Aldrich) and $NH_4H_2PO_4$ (98+ %, Sigma-Aldrich) were used as raw materials. The ceramics were pre-heated at 500 ^oC for 4 hours and then calcined at temperatures in the range 700-750 ^oC for 4 hours with intermediate grinding. Calcined powder was ground into fine powder. The fine powder obtained was mixed with different volume fractions (V_f) of TiO_2 (99.8 %, Sigma-Aldrich) in ethanol using an agate mortar and pestle. Cylindrical disks having 11 mm diameter and 5-6 mm thickness were prepared through the same procedure described earlier in Chapter 3. The samples were then sintered at temperatures in the range 825 ^oC to 975 ^oC for 4 hours with an intermediate soaking at 600 ^oC for binder (PVA) burn out. In order to study the chemical compatibility of the ceramic with Ag, the $LiMgPO_4$ + 0.15 V_f TiO_2 and $LiMg_{0.9}Zn_{0.1}PO_4$ + 0.12 V_f TiO_2 composites were further mixed with 20 wt% Ag powder (< 45 mm, 99.99+ %, Sigma-Aldrich) and sintered at 950 ^oC for 6 hours.

The structure, microstructure and dielectric properties of the ceramics were studied using the methods already described in Chapters 2 and 3. The shrinkage characteristics and linear coefficient of thermal expansion of the samples were determined using a Dilatometer (Netzsch DIL 402 PC, Selb, Germany).

4.2.2 Results and discussion

The shrinkage characteristics of $LiMg_{(1-x)}Zn_xPO_4$ ceramics are shown in Fig. 4.1. For all the compositions the onset of shrinkage is above 600 ^oC. Hence, all the samples are initially kept at 600 ^oC for 30 min. in the course of sintering for the complete removal of binder prior to densification. From Fig. 4.1 it is clear that both the onset of shrinkage and the temperature at which shrinkage completes decreases with the value of x. It is also noteworthy that the shrinkage of the ceramics completes at a temperature ≤ 950 ^oC.

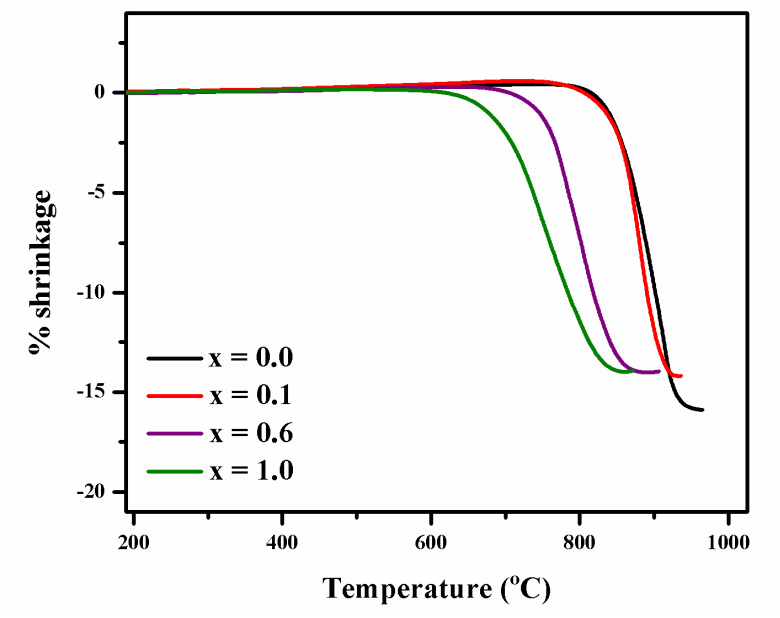

Figure 4.1 Shrinkage characteristics of $LiMg_{(1-x)}Zn_xPO_4$ ceramics

Figure 4.2 shows the variation of optimized sintering temperature of $LiMg_{(1-x)}Zn_xPO_4$ ceramics with the value of x. The sintering temperature decreases gradually from 950 °C at x = 0 to 825 °C at x = 1. Hence it is clear that the Zn^{2+} substitution for Mg^{2+} effectively lowers the sintering temperature. It is also interesting to note that all the compositions can be sintered at temperatures ≤ 950 °C without any sintering aid which is favorable for LTCC applications.

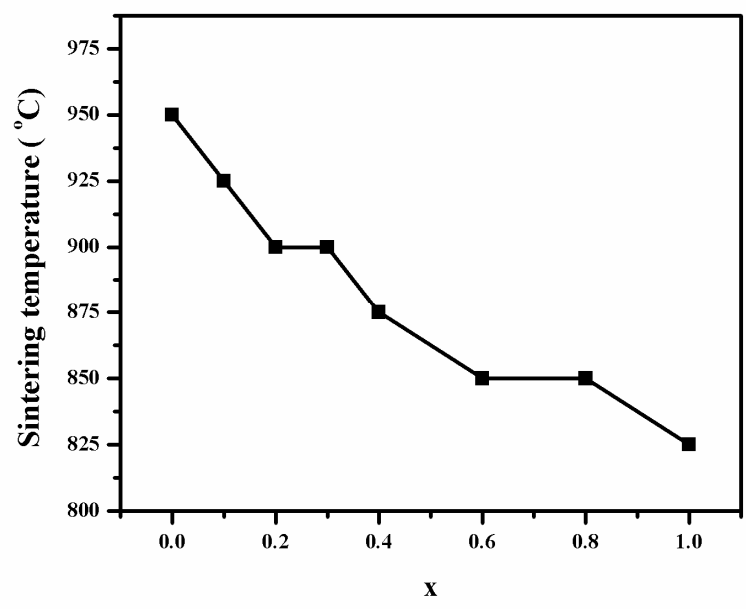

Figure 4.2 Sintering temperature of $LiMg_{(1-x)}Zn_xPO_4$ ceramics as a function of x

Figure 4.3 shows the powder XRD patterns of $LiMg_{(1-x)}Zn_xPO_4$ (x = 0 to 1) ceramics. The peaks corresponding to the composition with x = 0 are indexed using the standard JCPDS file for $LiMgPO_4$ (file no: 32-0574) with orthorhombic structure and belonging to Pmnb space group. Similarly the peaks corresponding to the composition with x=1.0 can be well indexed using the JCPDS file for $LiZnPO_4$ (file no: 84-2136) with monoclinic structure and Cc space group. From Fig. 4.3, it is obvious that the compositions up to x = 0.2 form solid solutions having orthorhombic structure. However, for the compositions from x = 0.3 onwards, a new peak starts forming at $2\theta \sim 22^o$ which corresponds to the major intensity peak of $LiZnPO_4$. As x increases, the peaks of the orthorhombic phase weaken and that of the monoclinic phase becomes stronger. For x=0.3 to 0.8, the ceramics exist as a mixture of orthorhombic and monoclinic phases and transform completely to monoclinic at x=1 ($LiZnPO_4$).

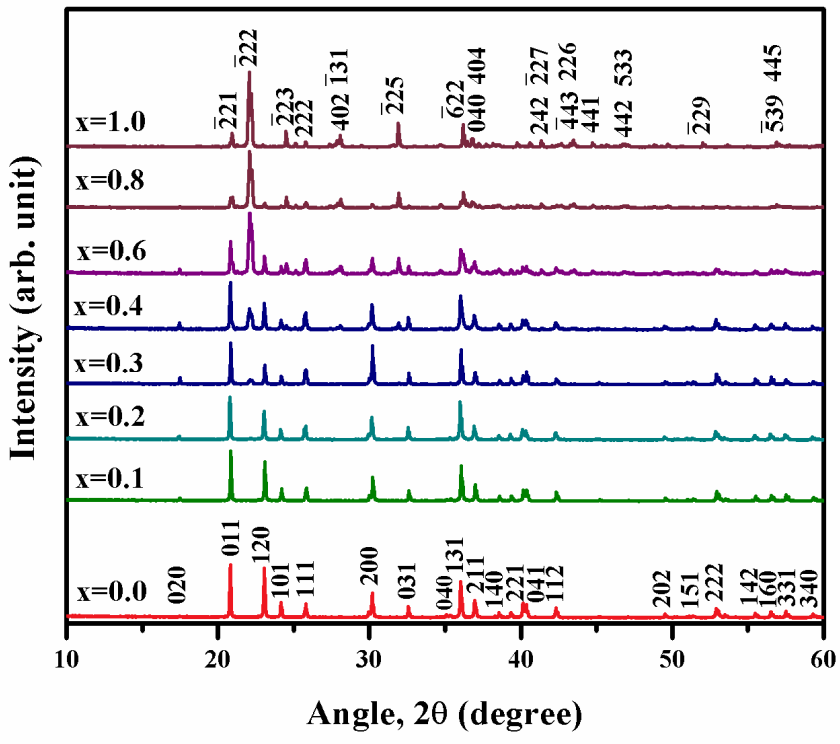

Figure 4.3 Powder XRD patterns of $LiMg_{(1-x)}Zn_xPO_4$ ceramics

The SEM images of the sintered and thermally etched surfaces of the ceramics with x = 0.0, 0.1, 0.8 and 1.0 are shown in Fig. 4.4 (a), 4.4 (b), 4.4 (c) and

4.4 (d) respectively. The images reveal a microstructure containing grains of size randomly varying from ~1 μm to >10 μm. From the surface morphology of the composition with x = 0.8 (Fig. 4.4 (c)) it is obvious that the ceramic is mixture of two phases.

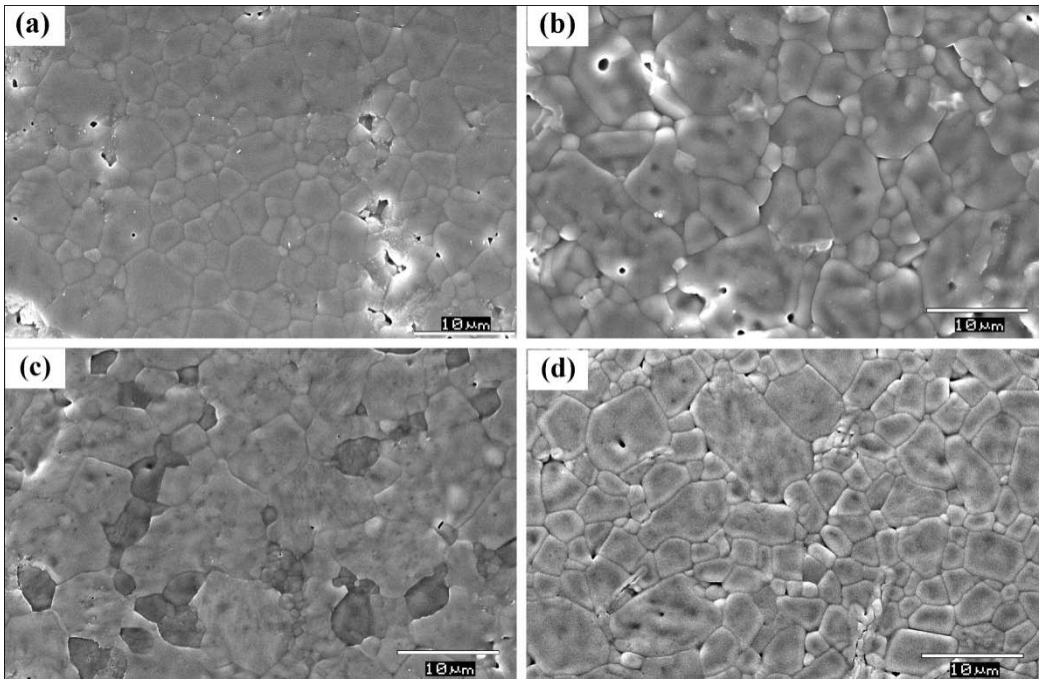

Figure 4.4 SEM images of $LiMg_{(1-x)}Zn_xPO_4$ ceramics with (a) x = 0.0, (b) x = 0.1, (c) x = 0.8 and (d) x = 1.0

The bulk density, linear coefficient of thermal expansion (CTE) and the dielectric properties at 1 MHz of the ceramics are given in Table 4.1. The relative densities of the compositions from x = 0.3 to x = 0.8 are not calculated as they are found to contain more than one phase. From Table 4.1, it is clear that CTE of the ceramics decreases from 11 ppm/^oC at x = 0 to 5 ppm/^oC at x = 1. The relative permittivity at 1 MHz increases gradually from 7.1 at x = 0 to 7.4 at x = 0.2 and saturates up to x = 0.4, then goes on decreasing from x = 0.6 onwards. The initial increase in ε_r may be attributed to the large ionic polarizability of Zn^{2+} (2.04 $Å^3$) compared to Mg^{2+} (1.32 $Å^3$) (Shannon, 1993) and to the fact that Zn^{2+} gets partially substituted for Mg^{2+} in the orthorhombic lattice. However, as the value of x increases further the amount of monoclinic phase in the sample also increases and causes to reduce the value of ε_r. Lowest value of 5.2 is obtained for ε_r at x = 1.0

which is purely monoclinic in structure. The ceramics show very low dielectric loss (tan δ) of the order of 10^{-4} at 1 MHz (Table 4.1). It is also noteworthy that the compositions with x = 0.1 and 0.2 exhibit lowest dielectric loss (tan $\delta = 2\times10^{-4}$).

Table 4.1 Density, CTE and dielectric properties at 1 MHz of $LiMg_{(1-x)}Zn_xPO_4$ ceramics

x	Bulk density ($g.cm^{-3}$)	Relative density (%)	CTE (ppm/ ^oC)	ε_r	Tan δ
0.0	2.825	95.0	11	7.1	7×10^{-4}
0.1	2.916	94.9	10	7.3	2×10^{-4}
0.2	2.968	93.9	10	7.4	2×10^{-4}
0.3	3.075	-	10	7.4	6×10^{-4}
0.4	3.129	-	10	7.4	7×10^{-4}
0.6	3.116	-	8	6.1	7×10^{-4}
0.8	2.986	-	7	5.6	9×10^{-4}
1.0	3.050	92.0	5	5.2	7×10^{-4}

Figure 4.5 depicts the microwave dielectric properties of $LiMg_{(1-x)}Zn_xPO_4$ ceramics. The values of ε_r and $Q_u\times f$ as a function of x are shown in Fig. 4.5 (a). The variation in ε_r follows somewhat similar trend as that obtained at 1 MHz. The values of ε_r obtained at microwave frequencies are slightly lower than that at 1 MHz. This may be due to the fact that some of the polarization mechanisms become inactive as the frequency increases from MHz to GHz range (Joseph *et al.*, 2011). From Fig. 4.5 (a) it can be observed that the quality factor ($Q_u\times f$) increases from 79100 GHz at x = 0.0 to 99700 GHz at x = 0.1. Some of the early reports show such an increase in $Q_u\times f$ due to Zn^{2+} substitution (Yokoi *et al.*, 2007; Zheng *et al.*, 2007; George *et al.*, 2010). From x = 0.2 onwards $Q_u\times f$ decreases gradually up to x = 0.8 and then increases for x = 1.0. The value of $Q_u\times f$ depends largely on the extrinsic factors like porosity and phase purity (Guo *et al.*, 2006). In the present study, the decrease in $Q_u\times f$ as the value of x increases from 0.1 to 0.2 may be due to the decrease in relative density (Table 4.1). Further, as the value of x increases from 0.2 to 0.8, the

amount of secondary phase (monoclinic phase) in the sample also increases which is evident from the XRD patterns as well as SEM images (Fig. 4.3 and Fig. 4.4) and this may be the reason for the decrease in $Q_u \times f$ up to x = 0.8. At x = 1.0, the material becomes purely monoclinic $LiZnPO_4$ and hence $Q_u \times f$ increases. Highest $Q_u \times f$ of 99700 GHz is obtained for x = 0.1 ($LiMg_{0.9}Zn_{0.1}PO_4$) which is highly appreciable for microwave applications. The variation of τ_f with x is shown in Fig. 4.5 (b). The value of τ_f increases steadily from -55 ppm/^oC for x = 0.0 to -80 ppm/^oC for x = 1.0.

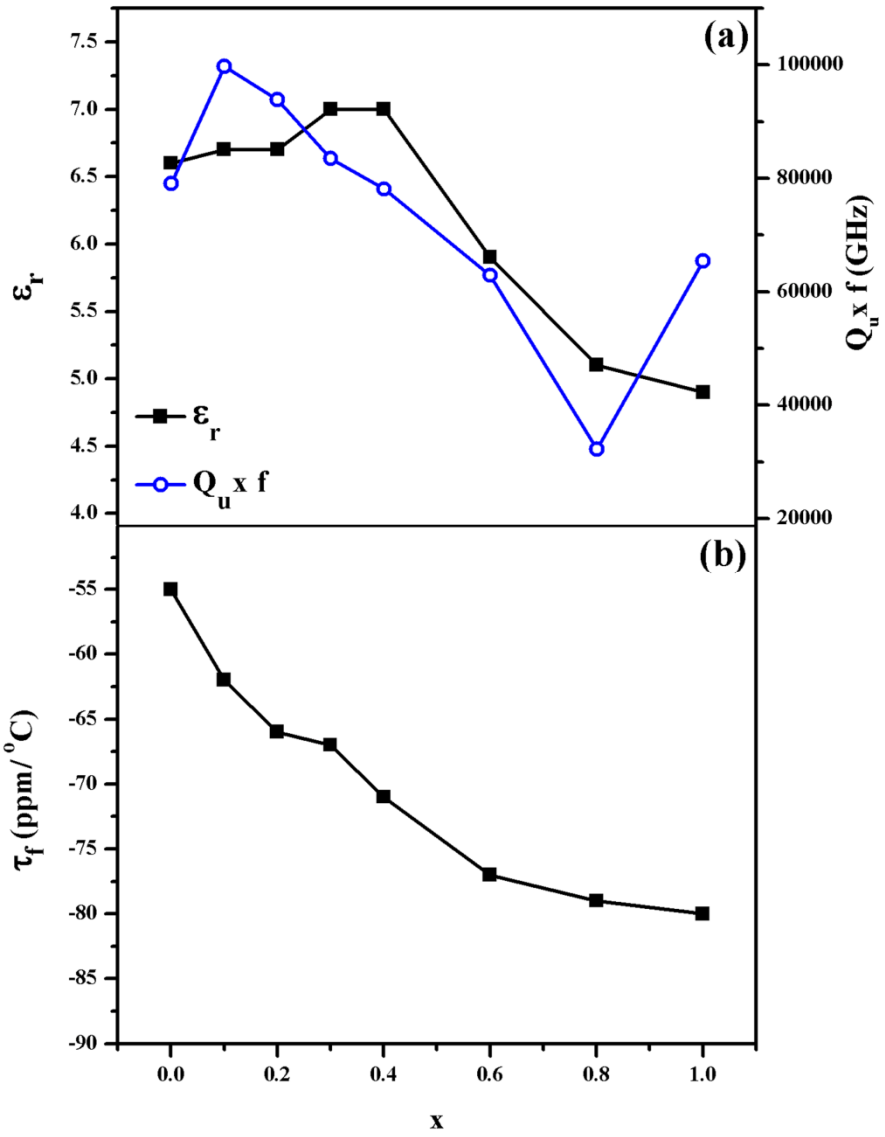

Figure 4.5 Variation of (a) ε_r and $Q_u \times f$ and (b) τ_f of $LiMg_{(1-x)}Zn_xPO_4$ ceramics with the value of x

4.2.2.1 Tuning the τ_f by TiO_2 addition

The ceramics developed in the present study have good microwave dielectric properties. However, the temperature stability of resonant frequency is poor ($|\tau_f| \geq$ 55 ppm/^oC) for practical applications. The value of τ_f can be tuned nearly to zero by making composite with a suitable ceramic having large positive τ_f like TiO_2 (τ_f = +450 ppm/^oC). In the present study, rutile type TiO_2 is used for tuning the τ_f since it has been reported more effective in improving the microwave dielectric properties compared to the anatase (Tsunooka *et al.*, 2003). The compositions with x = 0 ($LiMgPO_4$) and x = 0.1 ($LiMg_{0.9}Zn_{0.1}PO_4$) have been selected to study the effect of TiO_2 addition.

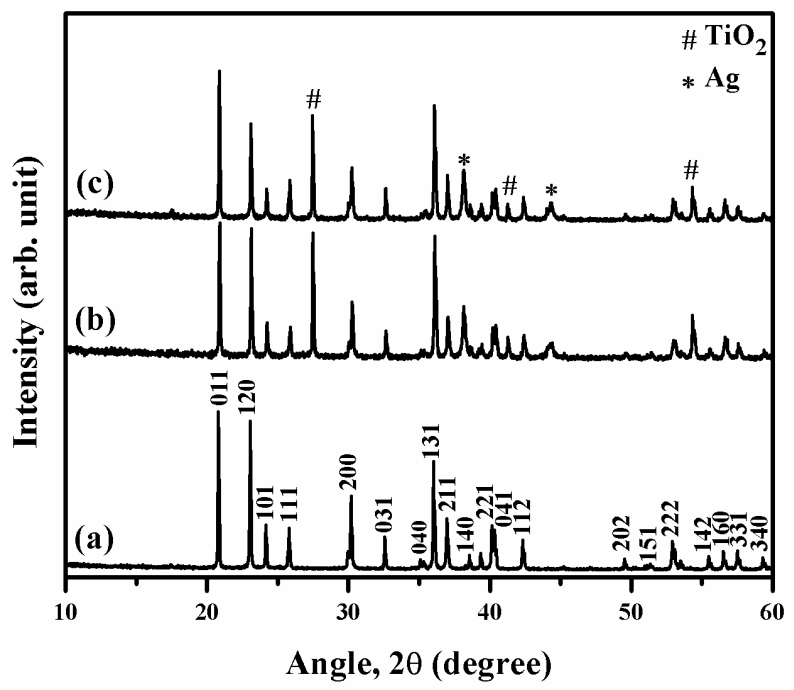

Figure 4.6 Powder XRD patterns of (a) $LiMgPO_4$, (b) $LiMgPO_4$+0.15 v_f TiO_2+20 wt% Ag and (c) $LiMg_{0.9}Zn_{0.1}PO_4$+0.12 V_f TiO_2+20 wt% Ag sintered at 950 ^oC

The powder XRD patterns of $LiMgPO_4$+0.15 V_f TiO_2 and $LiMg_{0.9}Zn_{0.1}PO_4$+0.12 V_f TiO_2 composites co-fired with 20 wt.% Ag are shown in Fig. 4.6 (b) and 4.6 (c) respectively. The XRD pattern corresponding to the parent composition ($LiMgPO_4$) is also plotted for comparison (Fig. 4.6 (a)). In Fig. 4.6 (b)

and 4.6 (c) peaks corresponding to all the three phases can be well indexed using standard JCPDS files (file no: 21-1276 for TiO_2 and 04-0783 for Ag) and no additional peaks are present. If the components react with each other producing secondary phase, it may degrade the dielectric properties (Tsunooka *et al.*, 2003; Cho *et al.*, 2005).

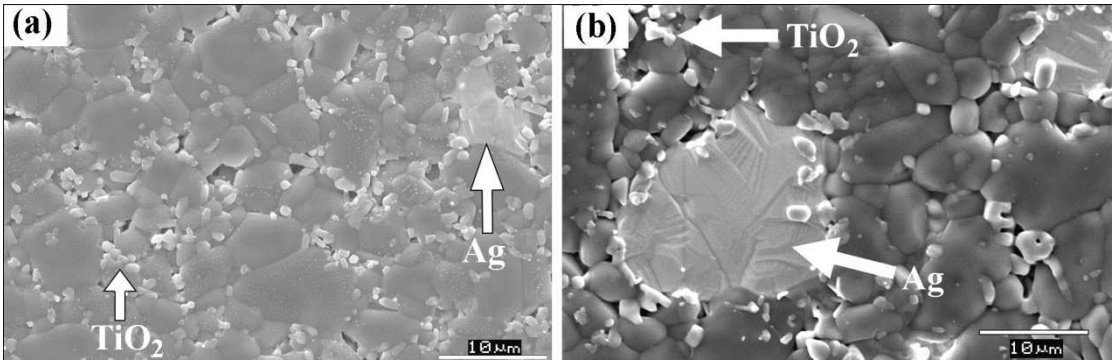

Figure 4.7 SEM images of (a) $LiMgPO_4$+0.15 v_f TiO_2+20 wt% Ag and (b) $LiMg_{0.9}Zn_{0.1}PO_4$+0.12 V_f TiO_2+20 wt% Ag sintered at 950 ^oC

Figure 4.7 (a) and 4.7 (b) shows the SEM images of $LiMgPO_4$+0.15 V_f TiO_2 and $LiMg_{0.9}Zn_{0.1}PO_4$+0.12 V_f TiO_2 composites co-fired with 20 wt.% Ag respectively. In Fig. 4.7 (a) and 4.7 (b) all the three constituent phases can be separately identified which indicates that no significant reaction occurs between these phases. From the microstructures it is obvious that TiO_2 remain as small particles. The sintering temperature of TiO_2 is very high (~1500 ^oC) and hence no substantial grain growth occurs for TiO_2 at 950 ^oC.

Table 4.2 Microwave dielectric properties of $LiMgPO_4$-TiO_2 composites

V_f of TiO_2	T_s (^oC)	Relative density (%)	ε_r	$Q_u \times f$ (GHz)	Experimental τ_f (ppm/^oC)	Calculated τ_f (ppm/^oC)
0.00	950	95.0	6.6	79100	-55	-55
0.10	950	95.0	9.3	45400	-12	-5
0.12	950	95.0	10.0	26900	+1	6
0.15	950	93.0	11.4	21100	+4	21

The sintering temperature, relative density and microwave dielectric properties of $LiMgPO_4$-TiO_2 composites are summarized in Table 4.2. All the composites show good densification of about 95% except for 0.15 volume fraction of TiO_2, which shows a densification of 93%. Relative permittivity of the composites increases gradually with the increase in volume fraction of TiO_2, since TiO_2 has a large value of ε_r (≈100). A reduction in $Q_u \times f$ occurs with the increase in TiO_2 volume fraction. This may be mainly due to the comparatively low $Q_u \times f$ (< 30000) of TiO_2 (Templeton *et al.*, 2000) and inhomogenity produced by the mixing of two materials with largely different ε_r values. Non-uniform mixing of phases can also have detrimental effects on $Q_u x f$. The τ_f is increased from -55 ppm/^oC to +3 ppm/^oC with the addition of 0.15 volume fraction of TiO_2. The composite containing 0.12 volume fraction of TiO_2 shows an excellent value of τ_f (+1 ppm/^oC). The value of τ_f for the composites can be calculated using the mixture rule (Dong *et al.*, 2008),

$$\tau_{f,composite} = V_{f1}\tau_{f1} + V_{f2}\tau_{f2} \quad (4.1)$$

where V_{f1} and V_{f2} are the volume fractions of $LiMgPO_4$ and TiO_2 and τ_{f1} and τ_{f2} are their temperature coefficients of resonant frequency respectively. The values of τ_f calculated using equation (4.1) are also given in Table 4.2. The experimental and calculated τ_f are in good agreement upto V_f = 0.12. However, for V_f = 0.15, experimental value of τ_f deviates considerably from the theoretical value. The variation can be attributed to the relatively poor densification of this sample.

Table 4.3 Microwave dielectric properties of $LiMg_{0.9}Zn_{0.1}PO_4$-TiO_2 composites

V_f of TiO_2	**T_s (^oC)**	**Relative density (%)**	**ε_r**	**$Q_u \times f$ (GHz)**	**Experimental τ_f (ppm/^oC)**	**Calculated τ_f (ppm/^oC)**
0.00	925	94.9	6.7	99700	-62	-62
0.10	950	95.6	9.5	69500	-15	-11
0.12	950	95.5	10.1	52900	-5	-1
0.15	975	93.3	11.7	49800	+17	+15

The microwave dielectric properties of $LiMg_{0.9}Zn_{0.1}PO_4$-TiO_2 composites are given in Table 4.3. With the addition of TiO_2, the sintering temperature increases slightly due to the high sintering temperature of TiO_2. The sintering temperature for the composite with 0.15 V_f TiO_2 is 975 ^oC which is not suitable for LTCC applications. On the other hand, composites containing up to 0.12 V_f TiO_2 can be well sintered below the melting point of Ag. The value of ε_r increases with the volume fraction of TiO_2 due to the large relative permittivity of TiO_2. The quality factor decreases gradually from 99700 GHz for $LiMg_{0.9}Zn_{0.1}PO_4$ to 49800 GHz for the composite with 0.15 V_f TiO_2. The value of τ_f varies from -62 ppm/^oC to +17 ppm/^oC as the V_f of TiO_2 increases from 0 to 0.15. The calculated values of τ_f are also given in Table 4.3. The experimentally observed values of τ_f are found to be in agreement with the theoretical ones. $LiMg_{0.9}Zn_{0.1}PO_4$ co-fired with 0.12V_f TiO_2 at 950 ^oC shows the best microwave dielectric properties with ε_r =10.1, $Q_u \times f$ = 52900 GHz and τ_f = -5 ppm/^oC. The excellent microwave dielectric properties and the glass-free nature make this composition competitive with the commercially available LTCC substrates (Sebastian *et al.*, 2008).

Table 4.4 Comparison of newly developed LTCC with commercial products (Imanaka, 2005; Sebastian *et al.*, 2008)

Product/Composition	**Supplier**	**ε_r**	**$Q_u \times f$**
$LiMgPO_4$	(Present work)	6.6	79100
$LiMg_{0.9}Zn_{0.1}PO_4$	(Present work)	6.7	99700
$LiMg_{0.8}Zn_{0.2}PO_4$	(Present work)	6.7	93900
$LiMgPO_4$+0.12 V_f TiO_2	(Present work)	10.0	26900
$LiMg_{0.9}Zn_{0.1}PO_4$+ 0.12 V_f TiO_2	(Present work)	10.1	52900
MLS-41(Nd_2O_3–TiO_2–SiO_2)	NEC glass	19.0	1200
G55 (BSG+SiO_2+Al_2O_3+cordierite)	Kyocera	5.7	8000
A6-M	Ferro	5.9	1500
GC-11	NGK	7.9	600
943	DuPont	7.8	2000
951	DuPont	7.8	900

Table 4.4 gives a comparison of ε_r and $Q_u \times f$ of the LTCC developed in the present study with that of some commercially available products. From Table 4.4 it is clear that the microwave dielectric properties of the present materials are superior to the commercial ones. The glass free nature of our materials is the main reason for their very large $Q_u \times f$ compared to that of the commercially available LTCC.

4.3 Casting and characterization of $LiMgPO_4$ glass free LTCC tape for microwave applications

4.3.1 Introduction

Multilayer Ceramic Modules (MCMs) form the core structures of high performance electronic systems especially in telecommunication. Low Temperature Cofired Ceramic (LTCC) technology is essential for the fabrication of high performance MCMs with high circuit density at low cost. The development of flexible LTCC green tapes is one of the critical technological issues in practical applications. Most of the materials reported for LTCC substrate applications are glass-ceramic composites due to the requirement of low temperature sintering (Sebastian *et al.*, 2008). The presence of glass phase in LTCC compositions makes the tape casting process more difficult and may produce undesired variations in the final properties (Jantunen *et al.*, 2000). The present work investigates the dispersion and tape casting of $LiMgPO_4$ ceramic with an objective to develop a low loss glass free LTCC tape for microwave applications.

4.3.2 Experimental

The $LiMgPO_4$ (LMP) ceramic was synthesized through the solid state ceramic route. LMP powder calcined at 800 ^oC for 4hours was ground into fine powder. The average particle size of the ceramic was determined by Dynamic Light Scattering (Zetasizer Nanoseries: ZEN 3600, Malvern, Worcestershire, UK). BET surface area of the powder was measured by nitrogen adsorption using surface area analyzer (Gemini 2375, Micromeritics, Norcross, USA). The thermal conductivity was measured using a laser flash thermal properties analyzer (Flash Line 2000, Anter corporation, *Pittsburgh,* USA) (Alm *et al.*, 2005). For the thermal

conductivity measurement specific heat capacity of reference material (alumina) as a function of temperature was taken from literature (Douglas *et al.*, 1956).

Mixture of ethanol and xylene in the ratio 50:50 was used as the solvent for the preparation of tape casting slurry. Initially dispersion studies were carried out with 37 wt.% ceramic loading and varying wt.% of dispersant. Fish oil (Arjuna natural extracts, Kerala, India) was used as the dispersant and the wt.% was calculated relative to the weight of the powder. The powder was ball milled in the solvent with dispersant for 24 hours. The shear viscosity of the slurry was measured using a rheometer (Brookfield, R/S Plus, Massachusetts, USA). For sedimentation analysis, 10 ml of the slurry was transferred into graduated measuring cylinder and allowed to settle. The sediment height (H) was then measured at regular intervals of time and the ratio of sediment height to the initial height (H/H_o) was calculated. The tape casting slurry was prepared in a two stage process. In the first stage the LMP powder was ball milled for 24 hours with the solvent (xylene/ethanol) and fish oil. In the second stage Type I plasticizer, Type II plasticizer, binder and homogenizer were added and ball milled for another 24 hours. Butyl benzyl phthalate (Sigma-Aldrich), polyethylene glycol (Sigma-Aldrich), polyvinyl butyral (Butvar B-98, Sigma-Aldrich) and cyclohexanone (Sigma-Aldrich) were respectively used as Type I plasticizer, Type II plasticizer, binder and homogenizer. The final slurry was then degassed in a vacuum desiccator for 5 minutes to remove the air bubbles and cast using a tape casting machine (Keko equipment, Zuzemberk, Slovenia). The casting was carried out on a Mylar film using a doctor blade system. The cast tape was then allowed to dry at room temperature.

Tensile strength of the LMP green tape was measured using a Universal Testing Machine (Hounsfield, H5K-S UTM, Redhill, UK) at a crosshead speed of 5 mm/min. The specimen gauge length was 40 mm, width 10 mm and thickness 0.07 mm. The surface roughness of the green tape was measured using an Atomic Force Microscope (AFM) (NTEGRA, NT-MDT, Russia) operating in the tapping mode regime. Images were acquired with a scan size of 50 μm × 50 μm and scan rate of 1.01 Hz. The thermogravimetric analysis (TGA) of the LMP green tape was conducted using a thermogravimetric analyzer (PerkinElmer, Waltham, USA). For

further characterization, square pieces of area 50 × 50 mm^2 were cut from the green tape and laminated together. The lamination was done in a uniaxial press by applying a pressure of 5 MPa and a temperature of 70 ^oC for 30 minutes. The laminated tape was sintered at 950 ^oC for 2 hours. While sintering, the laminate was kept in between two thin platinum plates in order to avoid warping. The density of tapes was measured using Archimedes method. The microstructure of the tapes was analyzed using SEM. The microwave dielectric properties were measured in a Split Post Dielectric Resonator operating at 5.155 GHz with the aid of a vector network analyzer (8753ET, Agilent Technologies, Santa Clara, CA) as discussed earlier in Chapter 2.

4.3.3 Results and discussion

The average particle size and BET surface area of the LMP powder are given in Table 4.5 below.

Table 4.5 Characteristics of $LiMgPO_4$ powder

Calcination temperature (^oC)	**Average particle size (μm)**	**BET surface area (m^2g^{-1})**
800	1.1	2.7

The variation of thermal conductivity of LMP with temperature is shown in Fig. 4.8. The ceramic shows a thermal conductivity of 7.1 $Wm^{-1}K^{-1}$ at room temperature which decreases gradually with the increase in temperature. In dielectric materials, primary carriers of thermal energy are phonons and the thermal conductivity is proportional to the mean free path for phonon collisions. For ceramics, the phonon mean free path decreases with the increase in temperature above room temperature resulting in a decrease of thermal conductivity (Kingery, 1960).

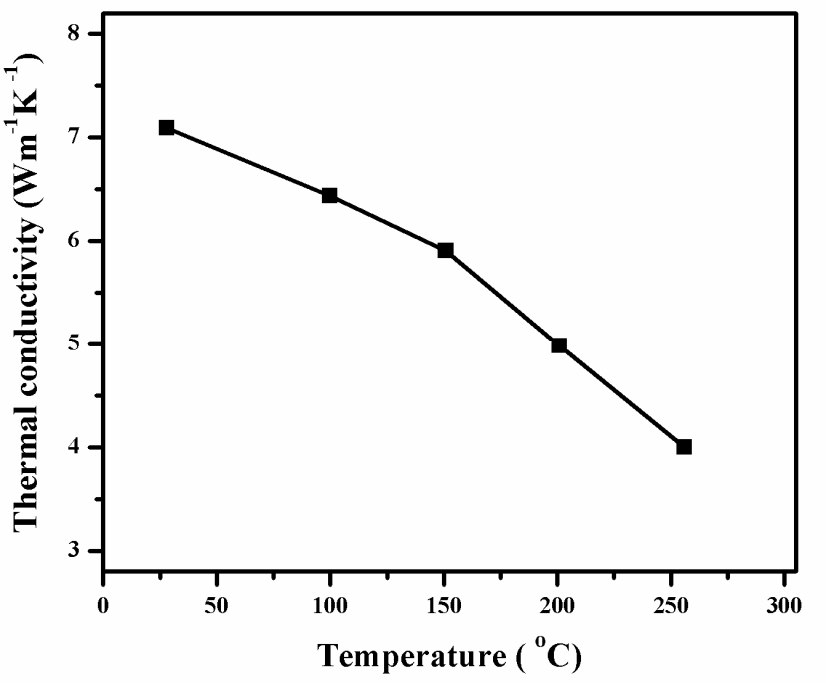

Figure 4.8 Variation of thermal conductivity of $LiMgPO_4$ with temperature

For the successful tape casting well dispersed, stable ceramic slurry is essential. Hence the amount of dispersant required to keep the particles deflocculated in the slurry has to be optimized first. The viscosity of well dispersed slurry will be lower due the presence of interparticulate fluid layer which offers increased mobility to the particles (Mukherjee *et al.*, 2001; Lee *et al.*, 2009). Figure 4.9 shows the variation of viscosity with shear rate of the slurries prepared by loading 37 wt.% LMP powder in the ethanol/xylene (in the ratio 50:50 by weight) solvent for the amount of dispersant (fish oil) varying from 1 to 3 wt.%. The fish oil keeps the ceramic particles deflocculated through steric stabilization (Calvert *et al.*, 1986). The viscosity of the slurries decreases with increase in shear rate, a behavior called shear thinning (pseudoplastic). In concentrated suspensions, even after the use of optimum amount of proper dispersant, some agglomerates will be formed (Mukherjee *et al.*, 2001). The shear thinning behavior is a result of the gradual breaking of these agglomerates under the shear stress (Li *et al.*, 2009). From Fig. 4.9, it is obvious that the viscosity (at low shear rates) decreases with the increasing amount of dispersant. This trend continues up to 2 wt.% of dispersant, beyond that the viscosity increases. Hence the amount of dispersant required to yield lowest

viscosity is 2 wt.%. The relatively higher viscosity of the slurries with lower dispersant concentration may be due to the insufficient amount of dispersant to completely cover the particle surface and the resulting flocculation. On the other hand when the amount of dispersant exceeds the optimum value, viscosity increases due to bridging flocculation or depletion flocculation (Palmqvist *et al.*, 2006).

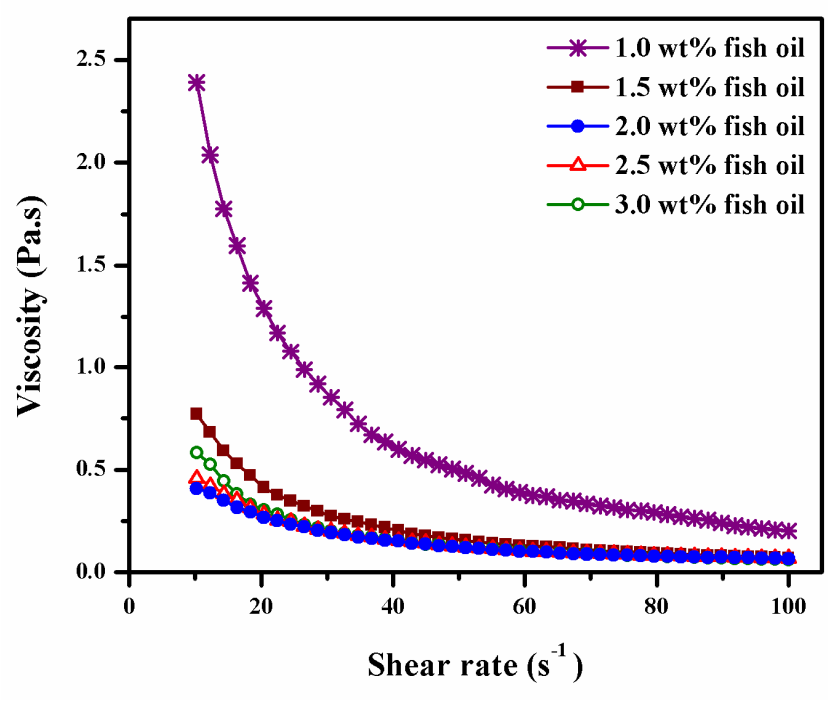

Figure 4.9 Variation of viscosity with shear rate at different concentrations of dispersant

Sedimentation analysis is a well known technique to estimate the dispersion stability and final packing. When ceramic particles are dispersed in a solvent and the suspension is kept undisturbed, the particles start to settle under the influence of gravitational force. The sedimentation velocity is proportional to the square of the particle diameter (Stokes' law) (Lee *et al.*, 2009). Therefore, less dispersed particles will settle down at a faster rate due to the larger effective diameter. On the other hand, in well dispersed slurry particles will settle at a slower rate and attain good packing density. Figure 4.10 shows the relative sediment height (H/H_o) of the suspensions containing 37 wt.% LMP for varying amounts of dispersant as a function of time. The suspension containing 2 wt.% dispersant has the lowest rate of sedimentation and highest final packing. Other compositions show relatively fast

sedimentation. The observations can be correlated to the results of viscosity measurements. From the viscosity measurements and sedimentation analysis, it can be concluded that 2 wt.% of fish oil is the optimum amount required to keep the LMP particles deflocculated in the solvent system taken.

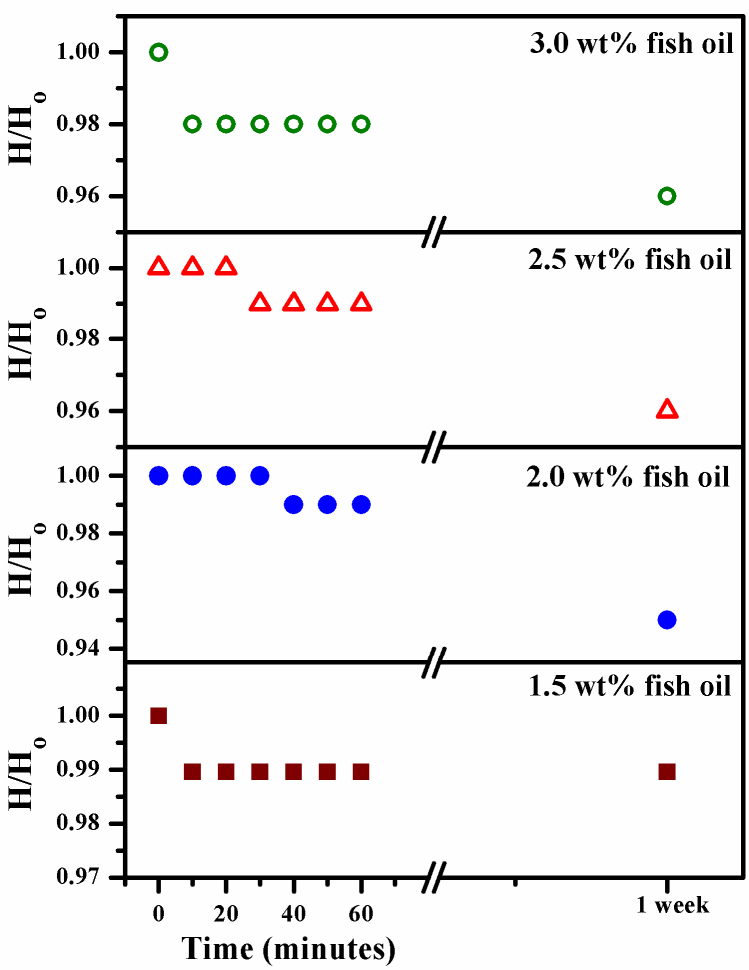

Figure 4.10 Relative sediment height as a function of time for different concentrations of dispersant

The composition of the LMP tape casting slurry is given in Table 4.6. The maximum powder loading achieved in the first stage is 40 wt.%. However, relative to the total weight of the final slurry wt.% of LMP is 34.87 as given in Table 4.6. Similarly the amount of fish oil relative to the total weight is given in the Table 4.6. The maximum powder loading attainable depends on the density and particle size of the powder and the effectiveness of dispersant. The powder loading in tape casting slurry may vary from ~ 20 to 90 wt.% (Mistler *et al.*, 2000). The lower filler loading

may lead to cracking of the tape while drying due to the larger volumetric shrinkage. However, increasing the amount of binder and Type II plasticizer will prevent cracking by increasing the matrix strength and allowing more plastic deformation respectively (Mistler *et al.*, 2000). In the present study, wt.% of both the binder and Type II plasticizer are large (Table 2) compared to many of the previously reported tape casting slurry compositions (Mistler *et al.*, 2000; Jantunen *et al.*, 2004; Honkamo *et al.*, 2009; Joseph *et al.*, 2011).

Table 4.6 Composition of $LiMgPO_4$ tape casting slurry

Component	Composition (wt.%)	Function
First stage		
$LiMgPO_4$	34.87	
Fish oil	0.70	Dispersant
Xylene	26.16	Solvent
Ethanol	26.16	Solvent
Second stage		
Polyvinyl butyral, grade B-98	5.23	Binder
Butyl benzyl phthalate	2.61	Plasticizer (Type I)
Polyethylene glycol	3.92	Plasticizer (Type II)
Cyclohexanone	0.35	Homogenizer

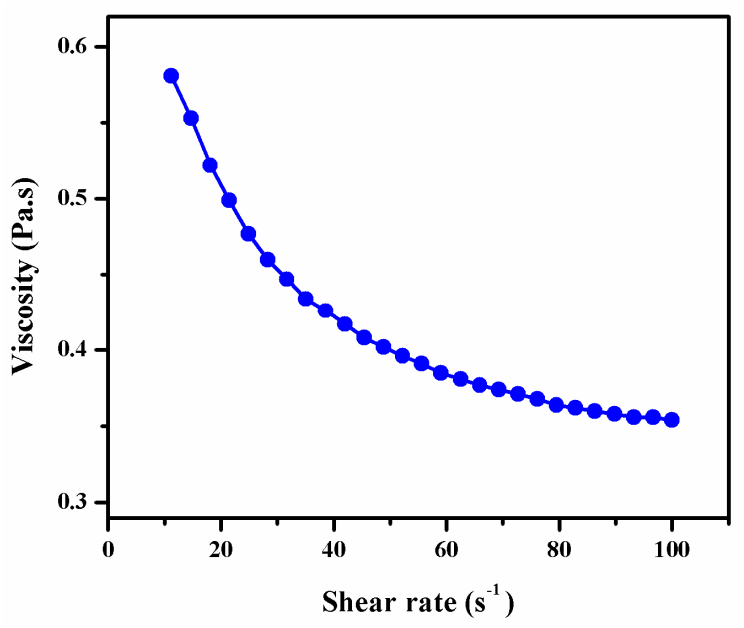

Figure 4.11 Viscosity of $LiMgPO_4$ tape casting slurry as a function of shear rate

Figure 4.11 shows the viscosity of the final slurry as a function of shear rate. The slurry shows typical pseudoplastic behavior. For the tape casting slurry the

pseudoplastic behavior is essential so that the viscosity will decrease while passing through the blade gap due to the shear force and the viscosity will increase immediately after the blade preventing the unwanted flow after casting (Moreno, 1992; Bitterlich *et al.*, 2002).

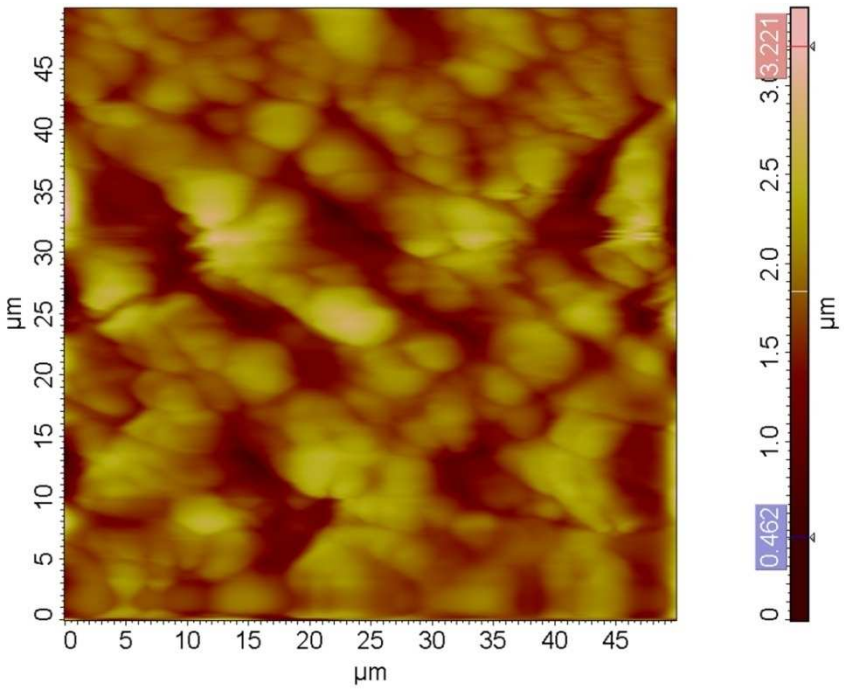

Figure 4.12 AFM image of $LiMgPO_4$ green tape

The tensile strength and surface roughness of the green tape are the two parameters of major concern while handling and printing the circuit patterns. The LMP green tape shows a tensile strength of 0.22 MPa. The AFM image of the surface of the green tape is shown in Fig. 4.12. The green tape has an average surface roughness (S_a) of 0.25 µm. The lamination pressure for the LMP tape (5 MPa) is found to be low compared to the commonly used value (~ 20 MPa) (Honkamo *et al.*, 2009; Joseph *et al.*, 2011). This may be due to the increased amount of polymers present in the LMP green tape which are responsible for thermo-lamination. It has been reported earlier that a pressure in the range 3 to 30 MPa may be used for laminating the ceramic tapes (Piwonski *et al.*, 1999). It is also noteworthy that a low lamination pressure is advantageous to avoid the deformation

and sagging of the circuit patterns that will be printed on the tape before lamination (Khoong *et al.*, 2009).

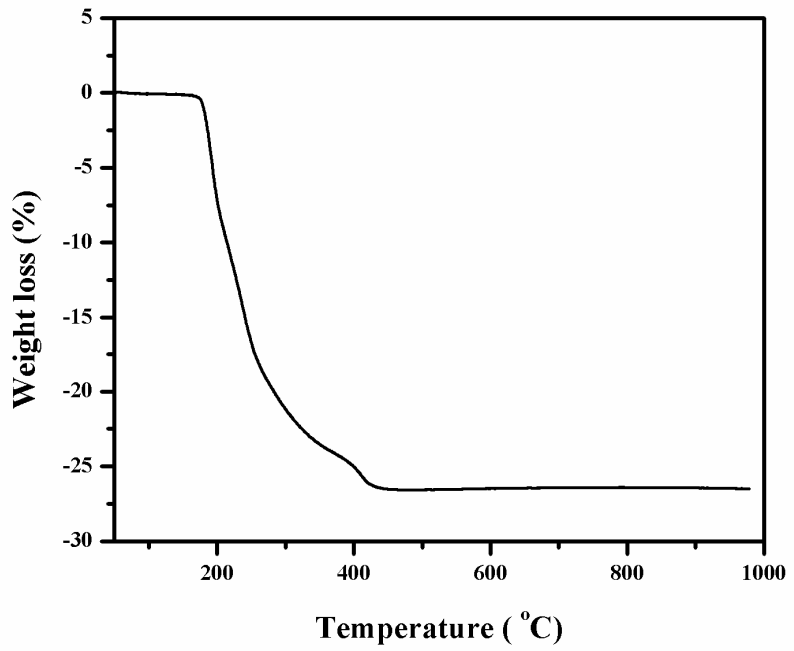

Figure 4.13 TG curve of $LiMgPO_4$ tape

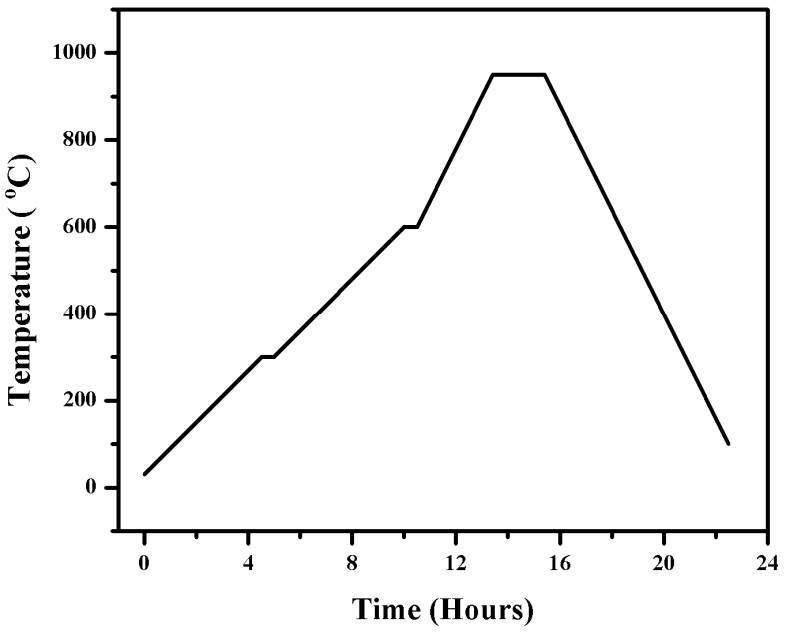

Figure 4.14 Sintering profile for $LiMgPO_4$ tape

Figure 4.13 shows the TG curve of thermo-laminated tape (4 layers) in air. From Fig. 4.13 it is evident that the burnout process of organic additives extends from about 175 ^{o}C to 450 ^{o}C. Initially there is a rapid weight loss of around 17% up to 250 ^{o}C followed by a slow weight loss up to 450 ^{o}C. The burnout process is completed at 450 ^{o}C with a total weight loss of ~ 27%. The weight loss at lower temperatures may be due to the evaporation of low molecular weight additives like dispersant and plasticizer. The weight loss at higher temperatures may be attributed to the binder burnout (Geffroy *et al.*, 2007; Luftl *et al.*, 2011; Vozdecky *et al.*, 2011). In order to get good microwave dielectric properties after sintering the tape, the organic additives have to be removed prior to densification (Tummala, 1991). If a fast heating rate is employed, chances are there for the formation of cracks or bubbles and the delamination of stacked layers of the tape (Zeng *et al.*, 2000; Kinemuchi *et al.*, 2006). Based on these facts and the results of TGA, a sintering profile is created as shown in Fig. 4.14. A slow heating rate of 1 ^{o}C/min. is given upto 600 ^{o}C with two intermediate dwells at 300 ^{o}C and 600 ^{o}C, 30 minutes each for the complete burnout of organics. Heating rate of 2 ^{o}C is employed upto 950 ^{o}C and the sample is cooled at a rate of 2 ^{o}C after the dwell at 950 ^{o}C for 2 hours.

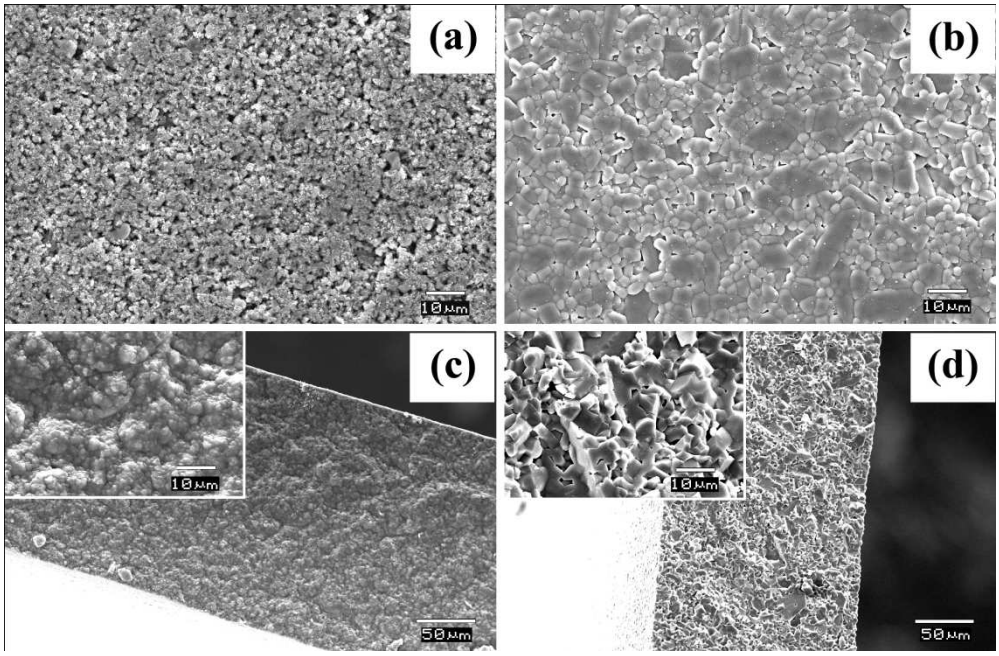

Figure 4.15 SEM images of the surface of (a) green tape, (b) sintered tape and fractured surface of (c) thermo-laminated stack (4 layers) (magnified image in the inset), (d) sintered stack (magnified image in the inset)

Figure 4.15 (a) and (b) shows the SEM images of the surface of green and sintered tapes respectively. Similarly Fig. 4.15 (c) and (d) shows the SEM images of the cross section of thermo-laminated stack (4 layers) before and after sintering respectively. The surface morphology of green tape reveals more or less uniformly distributed LMP ceramic particles connected through polymer bridges and some porosity. Substantial grain growth occurs during sintering and hence the microstructure of the sintered tape (Fig. 4.15 (b)) shows well packed grains with fractional porosity. In the SEM image of the cross section of thermo-laminated stack (Fig. 4.15 (c)), no interlayer boundary is visible. This means that under the conditions of thermo-lamination, the polymer in the matrix softens and the layers diffuse one into another making the laminate homogeneous (Salam *et al.,* 2000). From the microstructure of the fractured surface of the sintered stack (Fig. 4.15 (d)), it is clear that the stack densify to form a single module.

Table 4.7 Microwave dielectric properties of $LiMgPO_4$ tape

Material	**Number of layers**	**Thickness (μm)**	**Relative density** (%)	**Dielectric properties at 5 GHz**	
				ε_r	**tan δ**
Green tape	1	70	56.0	3.2	0.0688
Laminated stack	4	240	66.7	4.1	0.0680
Sintered stack	4	190	97.4	6.4	0.0002

The microwave dielectric properties of the green as well as sintered tapes are given in Table 4.7. The green tape shows low relative permittivity and high dielectric loss due to the presence of considerable amount of organic additives. The relative permittivity of the tape increases slightly after thrmo-lamination with a marginal decrease in tan δ. This may be due to the increase in relative density due to thermo-lamination. During thermo-lamination, the polymer present in the green tape softens and under the pressure applied the laminate shrinks bringing the ceramic particles close to each other which make the laminate denser. The laminate of LMP sintered at 950 ^{o}C/2h shows good densification of 97.4 % due to grain growth and the subsequent removal of porosity. The sintered laminate also shows good

microwave dielectric properties with an ε_r = 6.4 and tan δ = 0.0002 at 5GHz. The improvement in microwave dielectric properties on sintering may be ascribed to the removal of organics and the increase in densification.

Table 4.8 Comparison of fired properties of LMP tape with that of commercial LTCC tapes

Property	**$LiMgPO_4$**	**DuPont™ 951**	**DuPont™ 9K7**	**Ceram*tape GC***
Density ($g.cm^{-3}$)	2.75	3.10	3.10	2.92
ε_r	6.4	7.8	7.1	7.9
Tan δ	2×10^{-3}	1.4×10^{-2}	1×10^{-3}	$< 2\times10^{-3}$
CTE (ppm/^oC)	11	5.8	4.4	5.3
TC ($Wm^{-1}K^{-1}$)	7.1	3.3	4.6	2.2

Table 4.8 compares the fired properties of LMP tape with that of some commercial LTCC tapes. From Table 4.8, it is clear that the properties of LMP tape are comparable to that of the commercial products.

4.4 Conclusions

The microwave dielectric properties of $LiMg_{(1-x)}Zn_xPO_4$ (x = 0.0 to 1.0) ceramics have been investigated. The ceramics retain the orthorhombic structure up to x = 0.2. The compositions with $x \geq 0.3$ exist as a mixture of orthorhombic and monoclinic phases. As the value of x increases, the amount of monoclinic phase increases. At x = 1.0, the structure is completely transformed from orthorhombic to monoclinic. $LiMg_{0.9}Zn_{0.1}PO_4$ shows the highest $Q_u\times f$ of 99700 GHz. The ceramics show slightly large negative τ_f ($\geq$ -55 ppm/^oC). For the compositions $LiMgPO_4$ and $LiMg_{0.9}Zn_{0.1}PO_4$ the τ_f has been tuned nearly to zero through TiO_2 addition. The $LiMgPO_4$-TiO_2 composite with 0.12 volume fraction of TiO_2 has ε_r = 10, $Q_u\times f$ = 26900 GHz and τ_f = +1 ppm/^oC. $LiMg_{0.9}Zn_{0.1}PO_4$ + 0.12 V_f TiO_2 has also got good microwave dielectric properties with ε_r = 10.1, $Q_u\times f$ = 52900 GHz and τ_f = -5 ppm/^oC. The analysis of XRD pattern and microstructure reveals the chemical compatibility between the composites and the commonly used electrode material Ag. The good microwave dielectric properties, glass free nature and low bulk density makes the ceramics more attractive for practical applications.

$LiMgPO_4$ ceramic prepared by the solid state ceramic route has been used for the preparation of tape casting slurry. The $LiMgPO_4$ powder has an average particle size of 1.1 μm and BET surface area of 2.7 m^2g^{-1}. Dispersion studies based on the viscosity measurements and sedimentation analysis revealed that 2 wt.% of fish oil is the optimum amount of dispersant required. Pseudoplastic slurry of $LiMgPO_4$ has been prepared with the addition of suitable organic additives. Tapes of 70 μm thickness have been fabricated by the doctor blade technique. The cast green tape shows a tensile strength of 0.22 MPa and average surface roughness of 0.25 μm. The green tape has an ε_r of 3.2 and tan δ of 0.0688 at 5 GHz. The microwave dielectric properties have been improved after sintering. The stack (4 layers) of $LiMgPO_4$ tapes has got good microwave dielectric properties with ε_r = 6.4 and tan δ = 0.0002 when sintered at 950 ^oC/2h. The ceramic has a coefficient of thermal expansion of 10.5 ppm/^oC and thermal conductivity of 7.1 $Wm^{-1}K^{-1}$. The glass-free nature and the good microwave dielectric properties obtained for the final tape makes the newly developed tape casting formulation attractive for LTCC applications.

Chapter 5

Polymer matrix composites for microwave substrate applications

Preparation and characterization of some polymer-ceramic composites is discussed in this chapter. High density polyethylene (HDPE) and mechanically flexible butyl rubber (BR) have been selected as polymer matrices. $Ca_4La_6(SiO_4)_4(PO_4)_2O_2$ (CLSP) ceramic has been used as filler. The HDPE-CLSP composite with highest filler loading of 0.4 volume fraction shows an ε_r of 5.1 and tan δ of 2.3×10^{-3} at 5 GHz. Similarly BR+0.4 V_f CLSP composite has ε_r = 5.1 and tan δ = 1.6×10^{-3}. Experimentally observed values of relative permittivity of the composites have been compared with the values calculated using various theoretical models. The coefficient of linear thermal expansion of the composites has been observed to decrease with filler loading. The BR-CLSP composites show good flexibility even at higher filler loading.

5.1 Introduction

In recent years, wireless communication using microwaves has been emerged the prominent way of information exchange. The widespread use of wireless communication transformed the microwave electronics market into a consumer driven one. This necessitated the establishment of a balance between performance and cost of the product (Bhattacharya *et al.*, 2001). Consequently, high performance dielectric ceramics used as substrates in microwave modules have been largely replaced with cheaper polymer based substrates having reasonably good performance (Buchanan, 2004). Many of the polymers satisfy the criteria of low relative permittivity (ε_r) and low dielectric loss (tan δ) essential for substrate applications (Sebastian *et al.*, 2010). In addition they are light weight, flexible and easily machinable as compared to ceramics. However, unlike ceramics polymers exhibit high thermal expansion and low thermal conductivity which are not favorable for substrate applications (Rimdusit *et al.*, 2000; Sebastian *et al.*, 2010). Polymer-ceramic composites are capable to deliver balanced mechanical, thermal and dielectric properties at a relatively low cost. The ability to tune the physical properties of polymer-ceramic composites by varying ceramic filler loading is also advantageous for practical applications.

5.2 HDPE matrix composites filled with $Ca_4La_6(SiO_4)_4(PO_4)_2O_2$ for microwave substrate applications

Several polymer-ceramic composites have been developed for microwave substrate applications (Sebastian *et al.*, 2010). Polytetrafluoroethylene (PTFE) is the mostly studied polymer for microwave applications due to its extremely low loss. However the preparation of PTFE based laminates is difficult due to its high melting point and high melt viscosity (Murali *et al.*, 2009; Sebastian *et al.*, 2010). The other commonly used polymers for substrate applications are epoxy, high density polyethylene (HDPE), Polystyrene (PS) etc. (Sebastian *et al.*, 2010). Among them HDPE is an easily processable polymer with good microwave dielectric properties (ε_r = 2.3, tan δ = 6×10^{-4}) (Thomas *et al.*, 2009). HDPE is a non polar, semi-crystalline polymer composed of (-CH_2-CH_2-) (Bur, 1985). It is a thermoplastic and hence can be easily remolded into various shapes. The development of HDPE based

microwave dielectric composites has been addressed in some of the earlier works (Subodh *et al.*, 2009; Thomas *et al.*, 2009; Anjana *et al.*, 2010; George *et al.*, 2010; George *et al.*, 2010; Sebastian *et al.*, 2010; Joseph *et al.*, 2012). HDPE matrix composites loaded with $Sm_2Si_2O_7$ show good dielectric properties (ε_r = 2.8-5.3 and tan $\delta = 3.0\times10^{-3} – 9.1\times10^{-3}$) at 8 GHz (Thomas *et al.*, 2009). The composites have water absorption in the range 0.2 to 0.3 %. The HDPE-$Sm_2Si_2O_7$ composite containing maximum filler loading of 0.5 volume fraction (V_f) has got the lowest linear coefficient of thermal expansion (CTE) of 60 ppm/^oC and highest thermal conductivity (TC) of 3 $Wm^{-1}K^{-1}$ (Thomas *et al.*, 2009). Subodh et al. studied the dielectric response of HDPE-$Sr_9Ce_2Ti_{12}O_{36}$ composites (Subodh *et al.*, 2009). The composites with maximum filler loading of 0.4 V_f show rather high relative permittivity of 12.1 and low dielectric loss (tan $\delta = 4\times10^{-3}$) at 8 GHz. HDPE-CeO_2 composites have ε_r in the range 2.8-6.9 and tan δ in the range 3.6×10^{-3}–8.5×10^{-3} at 7 GHz (Anjana *et al.*, 2010). HDPE-CeO_2 composite with maximum filler loading of 0.5 V_f has the lowest CTE of 88.5 ppm/^oC and tensile strength of 10.2 MPa. Lin et al. studied the dielectric and magnetic properties of HDPE filled with $Y_3Fe_5O_{12}$ (YIG) (Lin *et al.*, 2010). However, most of the HDPE-YIG composites show large dielectric loss (tan $\delta > 1\times10^{-2}$). The HDPE-Li_2MgSiO_4 composites have been reported to be suitable for microwave substrate applications (George *et al.*, 2010). For 0.4 V_f of Li_2MgSiO_4 filler loading the composite shows good microwave dielectric properties (ε_r = 3.5 and tan $\delta = 3.2\times10^{-3}$ at 5 GHz). The $Ca[(Li_{1/3}Nb_{2/3})_{1-x}Ti_x]O_{3-\delta}$ ceramic reinforced HDPE composites with ε_r = 3-9 and tan $\delta = 1.2\times10^{-3}$-$5.0\times10^{-3}$ form another class of polymer-ceramic composites suitable for microwave applications (George *et al.*, 2010). Recently, Joseph et al. reported the effect of $Sr_2ZnSi_2O_7$ filler loading on the mechanical, thermal and dielectric properties of HDPE (Joseph *et al.*, 2012). HDPE filled with 0.5 V_f of $Sr_2ZnSi_2O_7$ filler shows ε_r = 4.6 and tan $\delta = 3.6\times10^{-3}$ at 5.1 GHz. The composite also has a CTE of 76.2 ppm/^oC, TC of around 3 $Wm^{-1}K^{-1}$.

The present work is focused on the preparation and characterization of HDPE matrix composites filled with $Ca_4La_6(SiO_4)_4(PO_4)_2O_2$ (CLSP) ceramic. $Ca_4La_6(SiO_4)_4(PO_4)_2O_2$ which is a solid solution of oxyapatites $Ca_2La_8(SiO_4)_6O_2$ and

$Ca_8La_2(PO_4)_6O_2$ has been observed to have good microwave dielectric properties (ε_r = 13.8, $Q_u \times f$ = 27900 GHz and τ_f = -11 ppm/^oC) (Chapter 3).

5.2.1 Experimental

The $Ca_4La_6(SiO_4)_4(PO_4)_2O_2$ (CLSP) ceramic was prepared through solid state reaction. The powder obtained was pre-heated at 1000 ^oC and then calcined at 1400 ^oC for 4 hours with intermediate grinding. Calcined powder was ground into fine powder and sieved through 25 μm sieve. The composites were prepared by melt mixing different volume fractions (V_f) of CLSP filler with HDPE (Nikunj Industries, Mumbai, India) in a kneading machine at a temperature of 180 ^oC (see Chapter 2). The uniform mixtures so obtained were then hot pressed at 180 ^oC for 30 minutes under a pressure of 20 MPa.

The phase formation of the ceramic filler was identified by recording X-ray diffraction pattern with CuKα radiation. The bulk density of the composites was measured by the Archimedes method. The microstructure of the composites was studied using Scanning Electron Microscope (SEM). Water absorption characteristics of the composites were measured using samples with dimensions 50 mm×50 mm×2 mm. Each of the samples were weighed accurate to four decimal places and kept immersed in distilled water for 24 hours. The samples were then taken out and after removing the excess water from the surface, the weight was measured again. The water absorption was then calculated using the relation,

$$\text{Water absorption} = \frac{W_f - W_i}{W_i} \times 100 \qquad (5.1)$$

where W_i and W_f are the weights of the sample before and after water immersion respectively. The dielectric properties at 1 MHz were measured by parallel plate capacitor method using an LCR meter. Microwave dielectric properties were measured by Split Post Dielectric Resonator (SPDR) method. The linear coefficient of thermal expansion of the composites was measured in the temperature range 30-100 ^oC using a dilatometer. The tensile test of the composites was conducted using

dumb-bell shaped samples of width 4 mm and thickness 1.5-2 mm in a Universal Testing Machine.

5.2.2 Results and discussion

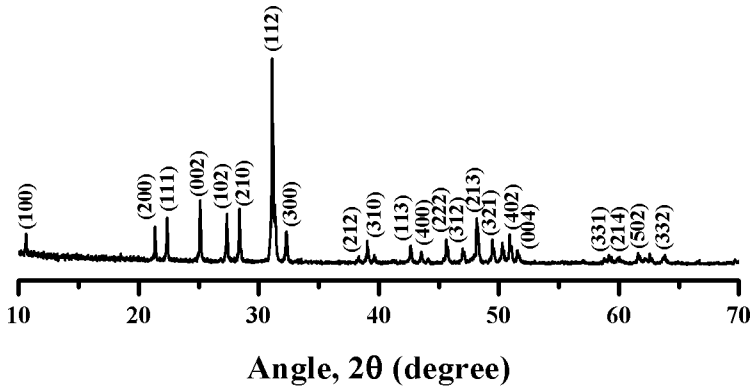

Figure 5.1 Powder XRD pattern of CLSP filler

The powder XRD pattern of $Ca_4La_6(SiO_4)_4(PO_4)_2O_2$ (CLSP) filler is shown in Fig. 5.1. The peaks are indexed using standard JCPDS files for $Ca_2La_8(SiO_4)_6O_2$ (file no: 29-0337) and $Ca_8La_2(PO_4)_6O_2$ (33-0287) with hexagonal structure and belonging to $P6_3/m$ space group. The CLSP ceramic shows good dielectric properties with ε_r = 13.8 and tan $\delta = 5\times10^{-4}$ when measured at around 5 GHz using an SPDR.

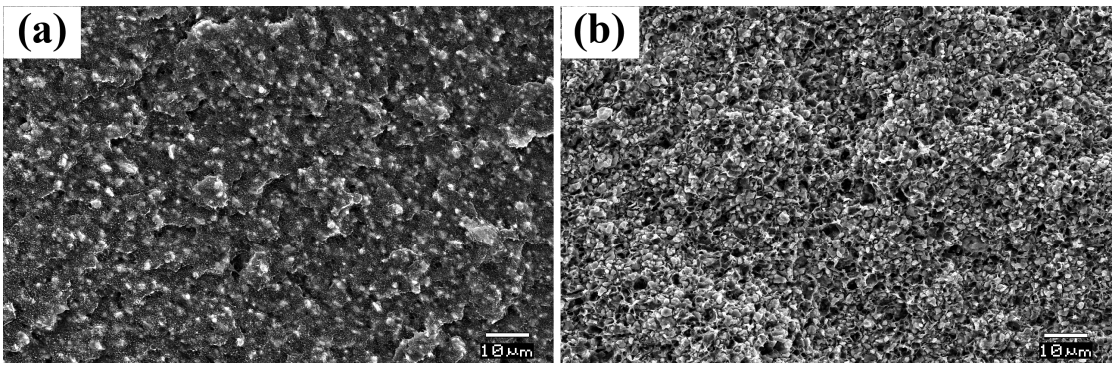

Figure 5.2 SEM images of fractured surfaces of (a) HDPE-0.2 V_f CLSP and (b) HDPE-0.4 V_f CLSP

Figure 5.2 (a) and (b) respectively shows the SEM images of the cross sections of composites loaded with 0.2 V_f and 0.4 V_f CLSP. In the microstructure of

PE+0.2 V_f CLSP composite, most of the filler particles remain isolated from each other with a polymer layer in between (Fig. 5.2 (a)). However, for the highest filler loading of 0.4 V_f the inter-particle distance decreases and the filler particles tend to agglomerate (Fig. 5.2 (b)). For polymer-ceramic composites there is a maximum limit of filler loading above which the processing becomes difficult and also results in poor mechanical properties (Xu *et al.*, 2006). In HDPE-CLSP composites, the maximum filler loading achieved is 0.4 V_f.

Table 5.1 Relative density, water absorption and dielectric properties at 1 MHz

V_f of filler	Relative density (%)	Water absorption (wt.%)	At 1 MHz	
			ε_r	tan δ
0.1	99.0	0.03	3.0	1.8×10^{-3}
0.2	98.8	0.03	3.7	2.4×10^{-3}
0.3	98.8	0.03	4.5	2.5×10^{-3}
0.4	98.3	0.04	5.4	2.5×10^{-3}

The relative density, water absorption and dielectric properties at 1 MHz are given in Table 5.1. The composites have high relative density (> 98 %) although the densification decreases slightly with filler loading (Table 5.1). In dielectric materials, moisture absorption will lead to the overall degradation of dielectric properties both at radio and microwave frequencies (Field, 1946; Tinga *et al.*, 1973; Bur, 1985). The absorbed water acts as an interlayer between the matrix and filler giving rise to an interfacial loss mechanism (Steeman *et al.*, 1991) at low frequencies. Similarly the dipole relaxation of absorbed water may produce additional loss at microwave frequencies (Xiang *et al.*, 2006). In addition, the vaporization of absorbed water owing to the heat generated during soldering may lead to delamination and cracking of the substrate (Amagai, 2002). Moisture absorption of less than 0.1 % has been reported to be ideal for electronic packaging (Rajesh *et al.*, 2009). From Table 5.1, it is obvious that HDPE-CLSP composites show negligible tendency for water absorption and the maximum water absorption being 0.04 wt.% for the composite containing 0.4 V_f CLSP. The relative permittivity

of HDPE-CLSP composites at 1 MHz increases gradually with filler volume fraction (Table 5.1) due to relatively large ε_r of the CLSP filler. Tan δ at 1 MHz increases from 1.8×10^{-3} for 0.1 V_f CLSP to 2.5×10^{-3} for 0.3 V_f CLSP and becomes steady on further increase in filler concentration. The increase in tan δ with filler V_f may be ascribed to the decreasing homogeneity with filler loading (Gemant, 1938).

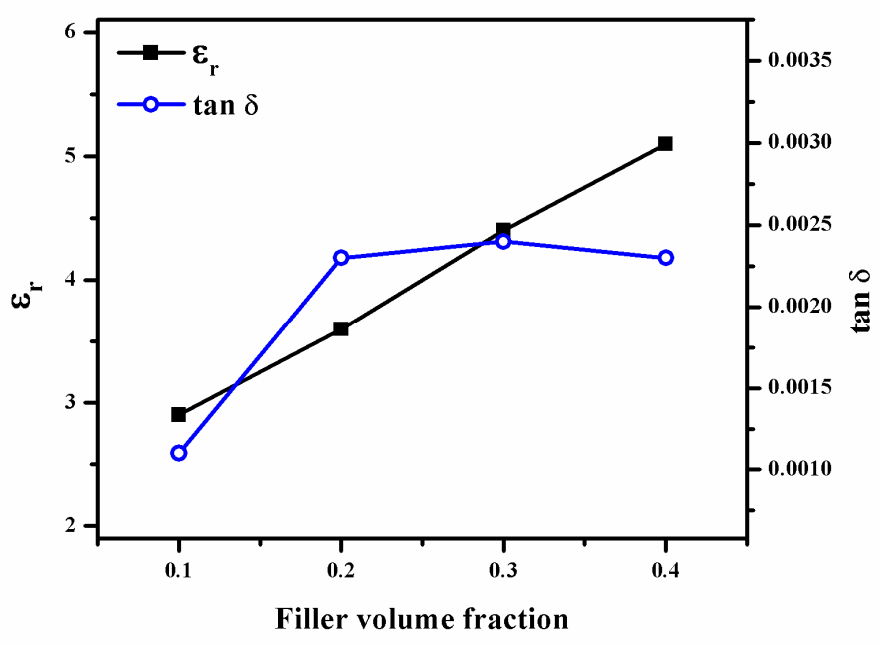

Figure 5.3 Dependence of microwave dielectric properties on filler concentration

Figure 5.3 shows ε_r and tan δ of the composites at 5 GHz as a function of filler volume fraction. The variation of both ε_r and tan δ with V_f of filler follows somewhat similar trend as that observed at 1 MHz. The composite with maximum filler loading of 0.4 V_f CLSP has $\varepsilon_r = 5.1$ and tan $\delta = 2.3 \times 10^{-3}$. In polyethylene, the major contributions towards dielectric loss come from branching, vinyl unsaturation and impurity dipolar structures introduced while processing (Curtis, 1962; Conklin, 1964). Several factors including the anharmonic interaction of electric field with the phonon system, imperfections in crystal lattice, order-disorder and impurities affect the microwave dielectric loss of ceramic filler (Sebastian, 2008). When the composite as a whole is considered, additional effects arising from heterogeneity,

porosity and matrix-filler interphase region may also come into play (Gemant, 1938; Todd *et al.*, 2003).

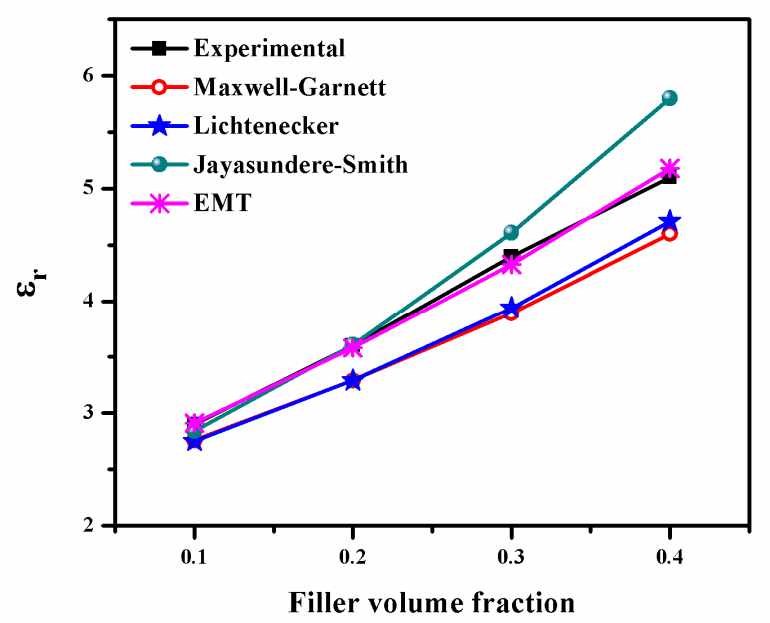

Figure 5.4 Comparison of theoretical and experimental values of ε_r at 5 GHz

Several theoretical models have been developed to estimate the relative permittivity of composite structures. Conversely, these models can be used to probe the degree of filler dispersion and the matrix-filler compatibility by comparing theoretical and experimental values obtained for ε_r. The following equations are used to calculate the relative permittivity of HDPE-CLSP composites (Sebastian *et al.*, 2010).

$$\frac{\varepsilon_{eff}-\varepsilon_m}{\varepsilon_{eff}+2\varepsilon_m} = v_f \frac{\varepsilon_f-\varepsilon_m}{\varepsilon_f+2\varepsilon_m} \qquad \text{(Maxwell-Garnett Equation)} \quad (5.2)$$

$$\log \varepsilon_{eff} = (1-V_f)\log \varepsilon_m + V_f \log \varepsilon_f \qquad \text{(Lichtenecker Equation)} \quad (5.3)$$

$$\varepsilon_{eff} = \frac{\varepsilon_m(1-v_f)+\varepsilon_f v_f\left[\frac{3\varepsilon_m}{\varepsilon_f+2\varepsilon_m}\right]\left[1+\frac{3v_f(\varepsilon_f-\varepsilon_m)}{(\varepsilon_f+2\varepsilon_m)}\right]}{(1-v_f)+\ v_f\left[\frac{3\varepsilon_m}{\varepsilon_f+2\varepsilon_m}\right]\left[1+\frac{3v_f(\varepsilon_f-\varepsilon_m)}{(\varepsilon_f+2\varepsilon_m)}\right]} \qquad \text{(Jayasundere- Smith Equation)} \quad (5.4)$$

$$\varepsilon_{eff} = \varepsilon_m \left[1 + \frac{v_f (\varepsilon_f - \varepsilon_m)}{\varepsilon_m + n(1 - v_f)(\varepsilon_f - \varepsilon_m)} \right] \qquad \text{(Effective Medium Theory)} \quad (5.5)$$

where ε_{eff}, ε_f and ε_m are the relative permittivity of the composite, filler and matrix respectively. V_f is the volume fraction of the filler and n is a shape factor determined empirically. Figure 5.4 shows a comparison of theoretical and experimental values of relative permittivity. The values of relative permittivity obtained using Maxwell-Garnett, Lichtenecker and Jayasundere-Smith equations show considerable deviation from the experimentally observed values (Fig. 5.4) especially at higher filler loading. The Maxwell-Garnett mixing rule has been derived for a composite system in which the electromagnetic interaction between filler particles is weak (Mallet *et al.*, 2005). Hence this model is valid only at low filler concentration. Lichtenecker model assumes the composite as a system of randomly oriented spheroids uniformly distributed in the matrix (Goncharenko *et al.*, 2000). In the present study, the observed misfit between the theoretical values of ε_r calculated using Lichtenecker equation and the experimental values may be due to the violation of basic assumptions. Jayasundere- Smith equation has been derived by assuming the filler particles as spheres with equal radius dispersed in the continuous matrix (Jayasundere *et al.*, 1993). Moreover, the relative permittivity of the filler has been assumed to be very large compared to that of the matrix. Deviation from these criteria may be the reason for the difference in ε_r obtained experimentally and using Jayasundere- Smith equation. The values of relative permittivity obtained using Effective Medium Theory (EMT) for n = 0.2 are found to be matching with the experimental data (Fig. 5.4). In EMT model the composites has been considered as an effective medium with random unit cell (RUC), comprising a core of filler and shell of matrix, embedded in it (Rao *et al.*, 2000). EMT model imposes no restriction on the shape of filler particles to be used and the calculation of ε_r accounts for shape of filler particles through the factor n.

The temperature dependence of ε_r is a characteristic of major concern for practical applications. Figure 5.5 depicts the variation of ε_r at 1 MHz with the operating temperature for HDPE-CLSP composites. The composites show a decrease in ε_r as the temperature increases. It is also noteworthy that the variation in

ε_r decreases with filler loading from ~ 8% for 0.1 V_f CLSP to ~ 5% for 0.4 V_f. In polymers, ε_r may decrease with temperature due to the increase in specific volume (Rao *et al.*, 2000). Earlier, such an observation has been made in HDPE (Ahmed *et al.*, 2008). Hence, in HDPE presence of filler particles may further reduce the temperature variation of ε_r by hindering the expansion of polymer matrix.

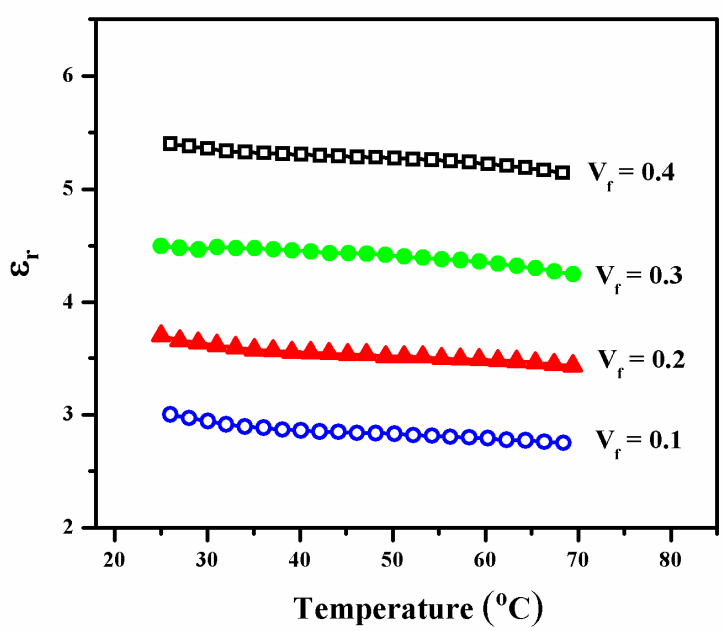

Figure 5.5 Temperature variation of ε_r at 1 MHz

Figure 5.6 shows the variation of linear coefficient of thermal expansion (CTE) with filler volume fraction. From Fig. 5.6 it is clear that the CTE decreases almost linearly from 207 ppm/^{o}C to 117 ppm/^{o}C as the filler loading increases from 0.1 to 0.4 V_f. The CTE of HDPE matrix (250 ppm/^{o}C) (Thomas *et al.*, 2009) is much higher than that of CLSP filler (5 ppm/^{o}C) (Chapter 3). Such a difference in CTE of matrix and filler will produce thermal stress in the composite while heating. The CTE of the matrix will be effectively lowered if the interfaces between matrix and filler are capable of transmitting the stress developed (Holliday *et al.*, 1973; Raghava, 1988). In HDPE-CLSP composites, the linear decrease in CTE with filler V_f indicates that the matrix-filler adhesion is good enough to withstand the thermal stress.

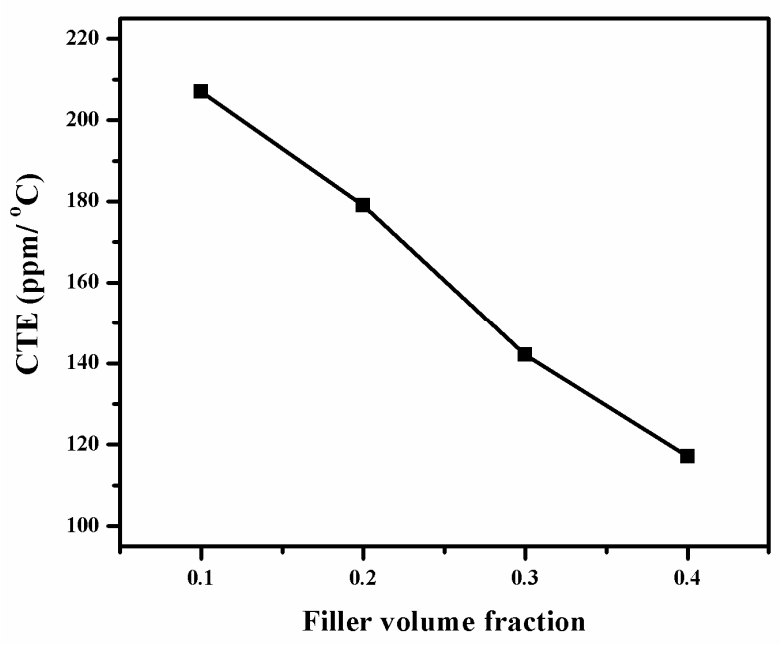

Figure 5.6 Variation of linear coefficient of thermal expansion (CTE) with filler loading

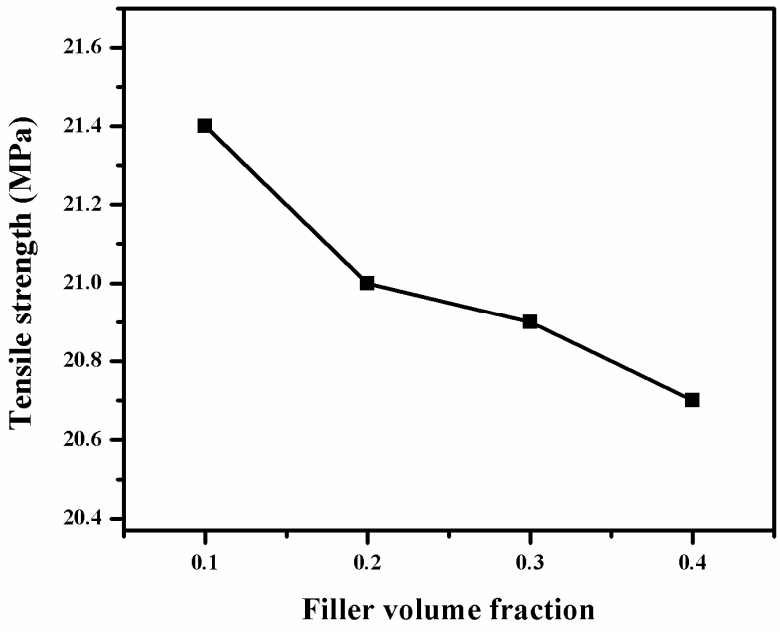

Figure 5.7 Tensile strength as a function of filler concentration

The variation of tensile strength of the composites with filler loading is shown in Fig. 5.7. Tensile strength decreases from 21.4 MPa to 20.7 MPa as the filler concentration increases from 0.1 to 0.4 V_f. The mechanical strength of HDPE

is mainly due to its semi-crystalline structure. In HDPE matrix composites, the presence of filler particles modifies the crystallinity and hence the mechanical strength (Rusu *et al.*, 2001). Moreover, the increase in porosity with filler loading may also bring about a decrease in tensile strength (Murali *et al.*, 2009).

Table 5.2 Comparison of properties of HDPE-CLSP composites with commercial products

Material	Supplier	Property				
		Density (gcm^{-3})	ε_r	tan δ ($\times10^{-3}$)	Moisture absorption (wt%)	CTE (ppm/°C)
RT/duroid 5870	Rogers corporation	2.2	2.3	1.2	0.02	173
RT/duroid 6002	Rogers corporation	2.1	2.9	1.2	0.02	24
HDPE+0.1 V_f CLSP	(Present work)	1.3	2.9	0.9	0.03	207
25FR	Arlon	1.8	3.6	3.5	0.09	59
HDPE+0.2 V_f CLSP	(Present work)	1.7	3.6	2.3	0.03	179
FR4	P+M Services	1.8	4.7	14	0.10	11
HDPE+0.4 V_f CLSP	(Present work)	2.4	5.1	2.3	0.04	117

A comparison of properties of HDPE-CLSP composites with some commercially available polymer based substrates having similar values of ε_r is given in Table 5.2.

5.3 Mechanically flexible butyl rubber-$Ca_4La_6(SiO_4)_4(PO_4)_2O_2$ composite dielectrics for microwave substrate applications

Flexible electronics has been emerged as an alternative for applications where the conventional electronics is not competent to fulfill the requirements (Park *et al.*, 2008). Nowadays, conventional electronic circuits are being largely replaced with flexible modules. The advances in materials and technologies accelerate this transformation. Flexible electronic circuit comprises a flexible dielectric substrate upon which various electronic components are assembled. Such electronic modules can be easily integrated to surfaces of any shape unlike the conventional circuit boards (De Geyter *et al.*, 2008). In addition to being readily bendable, the flexible substrate must also be stretchable to some extent in order to deploy it comfortably over surfaces of irregular geometries (Kim *et al.*, 2008). The other requisite properties for a flexible microwave substrate are low ε_r, low tan δ, temperature stability of dielectric properties, low coefficient of thermal expansion and good

thermal conductivity. The elastomer-ceramic composites can meet all these requirements to a considerable extent.

The microwave dielectric properties of some mechanically flexible composites have been reported earlier. Hakim et al. studied the microwave dielectric properties of butyl rubber loaded with the fillers like talc, $CaCO_3$, barites, dolomite, kaolin and precipitated silica (Hakim *et al.*, 1988). They prepared these composites with rather low filler loading (≤ 50 wt.%) and the maximum ε_r obtained is 2.9 at 10 GHz. Koulouridis et al. investigated the effect of various fillers on the microwave dielectric properties of flexible Polydimethylsiloxane (PDMS) with filler loading varying from 0-0.3 V_f (Koulouridis *et al.*, 2006). PDMS-$BaTiO_3$ composites showed relatively large ε_r (up to 20) and tan δ (1×10^{-2}-4×10^{-2}) at 1 GHz. On the other hand, PDMS loaded with Mg-Ca-Ti-O (of Trans-Tech Inc.) and Bi-Ba-Nd-Titanate (of Ferro Corporation) has comparatively low ε_r (< 8.5) and tan δ (< 1×10^{-2}) (Koulouridis *et al.*, 2006). Polyolefin-$SrTiO_3$ composites have been reported to be suitable for flexible wave guide applications (Xiang *et al.*, 2007). The composites have moderately good dielectric properties with a maximum ε_r of 10.5 and tan $\delta \leq 8.5\times10^{-3}$ at 5 GHz. Butyl rubber-$SrTiO_3$ composites with ε_r varying from 3.5 to 13.2 and tan δ from 2.2×10^{-3} to 2.8×10^{-3} (at 5 GHz) form another class of dielectrics suitable for flexible substrate as well as wave guide applications (Thomas *et al.*, 2011). Similarly, butyl rubber-$Sr_2Ce_2Ti_5O_{15}$ composites have got good microwave dielectric properties (ε_r = 3.5 – 11.9 and tan δ = 1.2×10^{-3} – 1.8×10^{-3}) suitable for practical applications (Janardhanan *et al.*, 2012). Recently, Chameswary et al. reported the microwave dielectric properties of butyl rubber-$Ba_{0.7}Sr_{0.3}TiO_3$ composites suitable for flexible wave guide application (Chameswary *et al.*, 2012). The composite with maximum filler loading of 0.39 V_f $Ba_{0.7}Sr_{0.3}TiO_3$ has ε_r = 13.1 and tan $\delta = 9\times10^{-3}$.

The present work discusses the development of mechanically flexible butyl rubber (BR) matrix composites containing $Ca_4La_6(SiO_4)_4(PO_4)_2O_2$ (CLSP filler). Butyl rubber is a synthetic elastomer. It is a copolymer of isobutylene (C_3H_8) with isoprene (C_5H_8) (Blow, 1971). Butyl rubber shows low permeability to water and good weathering resistance (Barron, 1949). Through the process of vulcanization

(i.e. the formation of cross links between the polymer chains), dimensional stability and elasticity of butyl rubber can be improved (Barron, 1949). Butyl rubber vulcanized by the conventional way using sulfur shows good microwave dielectric properties (ε_r = 2.4 and tan $\delta = 1.7\times10^{-3}$) (Thomas *et al.*, 2011).

5.3.1 Experimental

BR-CLSP composites with different volume fractions of CLSP filler were prepared by sigma mixing in a kneading machine followed by hot pressing at 200 ^oC for 90 minutes. Various additives for the vulcanization of butyl rubber were also added while mixing. In rubber compounding, it is conventional to use parts per hundred parts of rubber (phr) to quantify the ingredients used for vulcanization. Hence, the additives used other than ceramic filler and their amounts in phr are given in Table 5.3 (Barron, 1949; Janardhanan *et al.*, 2012). The properties of BR-CLSP composites were characterized using various experimental techniques discusses in section 5.2.2 and Chapter 2. In order to study the effect of repeated bending on the microwave dielectric properties of BR-CLSP composites the samples were bent manually in such a way that every part of the sample had undergone 180^o bending. The bending cycle was repeated for 150 times and the microwave dielectric properties were measured after every 25 cycles.

Table 5.3 Additives used for butyl rubber vulcanization

Additive	**Quantity (phr)**
Stearic acid	3
Zinc oxide	5
Tetramethylthiuram disulphide (TMTD)	1
Sulfur	0.5

5.3.2 Results and discussion

Figure 5.8 shows the stress-strain curves obtained from tensile tests for BR-CLSP composites containing 0.2 and 0.4 V_f of CLSP filler. Both the composites do not break up to an elongation of 1000%. The BR+0.2 V_f CLSP composite remains almost elastic up to an elongation of ~ 50% and this limit is reduced to ~ 20% at 0.4

V_f of filler loading (Fig. 5.8). BR-CLSP composites retain the required flexibility even at higher filler loading.

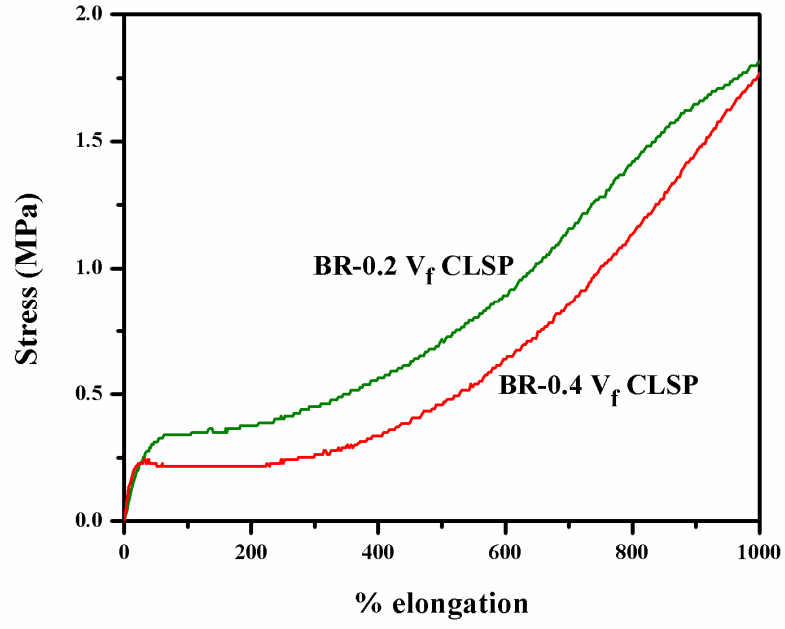

Figure 5.8 Stress-strain curves for BR-CLSP composites

The cross-sectional SEM images of the composites containing 0.2 V_f and 0.4 V_f CLSP are shown in Fig. 5.9 (a) and (b) respectively. From Fig. 5.9 it is obvious that the tendency for filler agglomeration increases at higher filler loading. The inter-particle distance decreases with the increase in filler volume fraction resulting in increased connectivity between the filler particles. The filler connectivity is important as it has significant effect on the electrical, mechanical and thermal properties of composites (McLachlan *et al.*, 1990). The microstructures also reveal some porosity within the composites (Fig. 5.9).

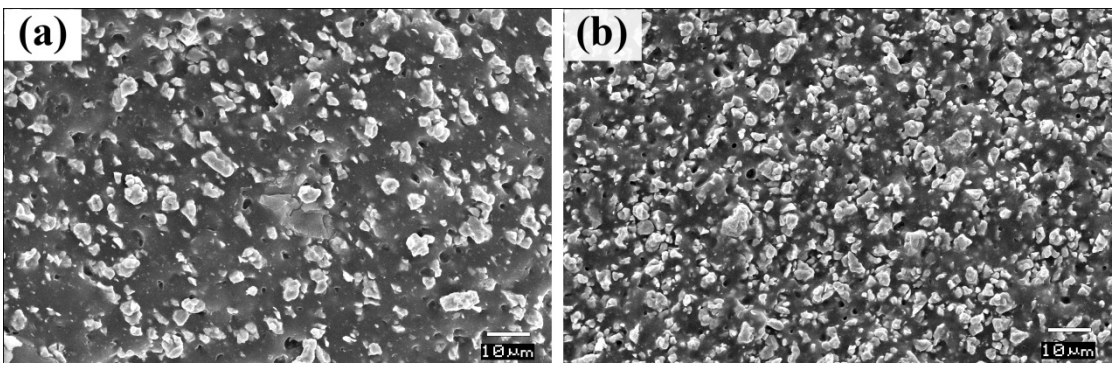

Figure 5.9 SEM images of cross-sections of (a) BR-0.2 V_f CLSP and (b) BR-0.4V_f CLSP composites

The water absorption characteristics and dielectric properties at 1 MHz of BR-CLSP composites are compiled in Table 5.4. The wt.% of water absorption varies from 0.03 to 0.04% and the values are within the limit required for practical applications (Rajesh *et al.*, 2009). The value of ε_r increases gradually with filler loading to a maximum of 5.3 for 0.4 V_f of filler loading due to the large ε_r of CLSP filler compared to the BR matrix. The decrease in distance between filler particles as the filler loading increases and the subsequent increase in dipole-dipole interaction may also be favorable for the increase of ε_r (Dang *et al.*, 2008). The dielectric loss of the composite also increases slowly with filler loading (Table 5.4).

Table 5.4 Water absorption and dielectric properties at 1 MHz of BR-CLSP composite

V_f of filler	Water absorption (wt.%)	At 1 MHz	
		ε_r	tan δ
0.1	0.03	3.0	1.0×10^{-3}
0.2	0.03	3.7	1.3×10^{-3}
0.3	0.03	4.5	1.4×10^{-3}
0.4	0.04	5.3	1.6×10^{-3}

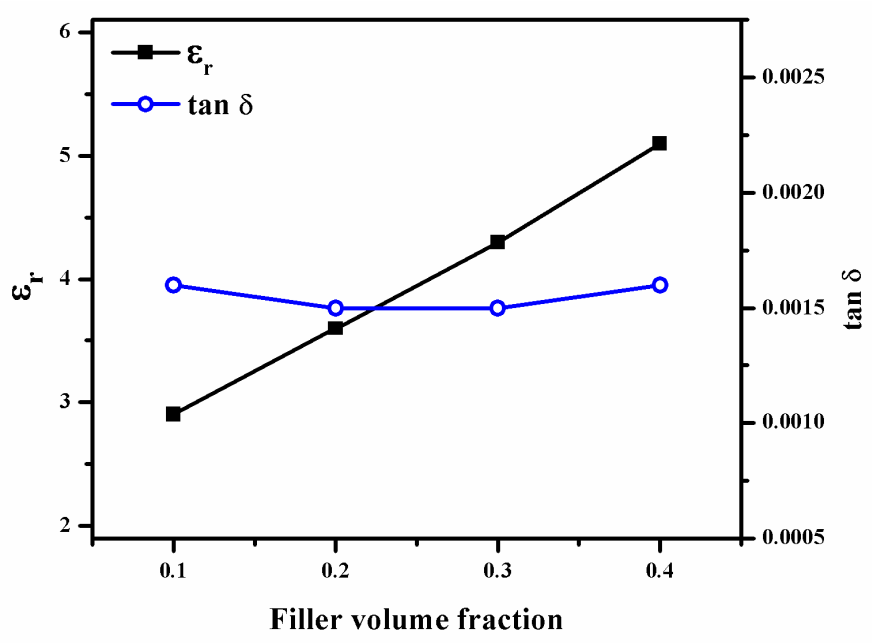

Figure 5.10 Variation of ε_r and tan δ at 5 GHz with filler loading

Figure 5.10 shows the variation of ε_r and tan δ at 5 GHz of the composites with filler volume fraction. ε_r increases linearly from 2.9 at 0.1 V_f to 5.1 at 0.4 V_f of filler. However, tan δ remains almost constant over the entire range of compositions studied. The BR-CLSP composite with maximum filler loading of 0.4 V_f shows an ε_r of 5.1 and tan δ of 1.6×10^{-3}. The dielectric loss of BR+0.4 V_f CLSP composite is small compared to the previously reported flexible composites with similar filler loading (Xiang *et al.*, 2007; Thomas *et al.*, 2011; Chameswary *et al.*, 2012; Janardhanan *et al.*, 2012).

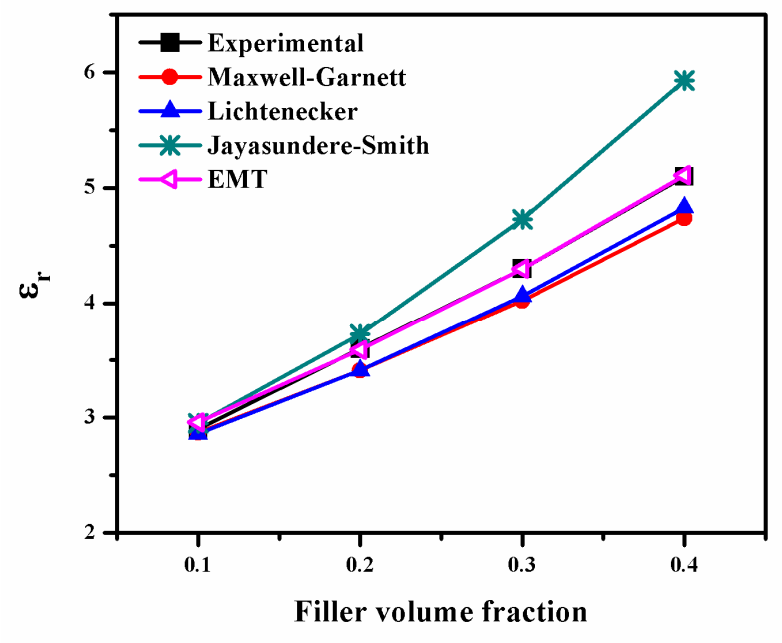

Figure 5.11 Theoretical and experimental values of ε_r as a function of filler volume fraction

The variation of theoretically calculated (using equations (5.2), (5.3), (5.4) and (5.5)) and experimentally measured values of ε_r with filler loading is shown in Fig. 5.11. From Fig. 5.11 it is evident that Maxwell-Garnett, Lichtenecker and Jayasundere-Smith equations are not suitable for modeling the ε_r of BR-CLSP composites similar to that observed in PE-CLSP composites. The values of ε_r calculated for BR-CLSP composites using EMT model with n = 0.24 shows good fit with the experimental data (Fig. 5.11). The morphology factor n is believed to be dependent only on the ceramic filler used (Rao *et al.*, 2000). Nevertheless, the value of n obtained for BR-CLSP composites is slightly different from that obtained for

PE-CLSP composites (n = 0.2) although the filler used (CLSP) is same. Earlier, Teirikangas et al. reported that n factor of EMT model is not independent of the polymer used in their study on polymer-ceramic composites prepared by loading $Ba_{0.55}Sr_{0.45}Ti_{1.01}O_3$ in cyclic olefin polymer, polyphenylene sulfide and epoxy matrices (Teirikangas *et al.*, 2009). They observed a variation of n from ~ 0.1 to ~ 0.25 when the polymer matrix is changed for the same filler and hence concluded that the modeling using EMT should be considered as individual cases for each pair of matrix and filler used.

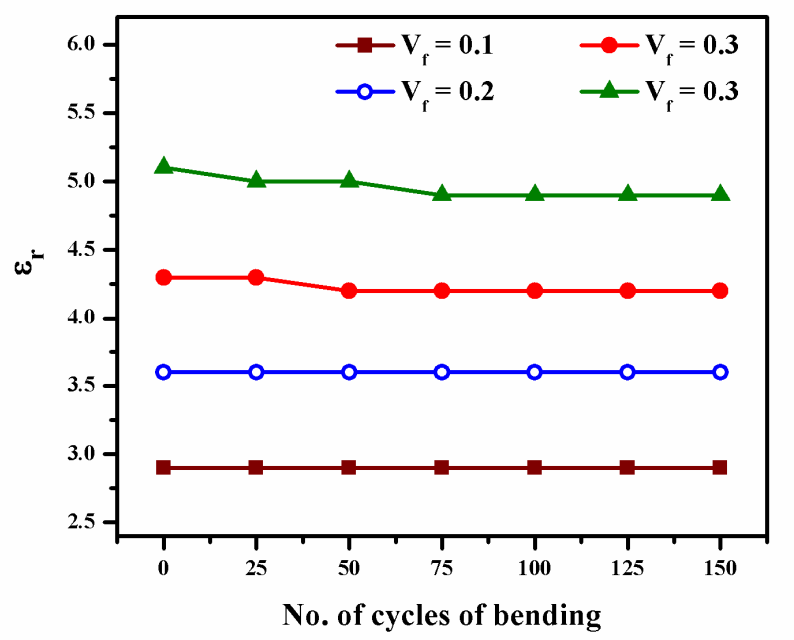

Figure 5.12 Effect of repeated bending on relative permittivity at 5 GHz

Figure 5.12 represents ε_r at 5 GHz of the composites as a function of repeated bending. ε_r remains constant up to 150 cycles of bending for the composites containing 0.1 and 0.2 V_f of filler. For the composites with 0.3 and 0.4 V_f filler loading ε_r initially shows a small decrease and then becomes constant (Fig. 5.12). In the composites containing higher volume fractions of filler, a small amount of butyl rubber will remain trapped within the filler agglomerates losing its identity as matrix (Ward *et al.*, 2003). The repeated bending may release the matrix bound within the agglomerates resulting in a small decrease of effective filler volume fraction (Ward *et al.*, 2003). This may be the reason for the initial decrease in ε_r of highly loaded

composites upon bending (Thomas *et al.*, 2011). The variation of tan δ at 5 GHz of BR-CLSP composites after repeated bending is shown in Fig. 5.13. Tan δ of the composites varies randomly after each 25 cycles of bending. It is also noteworthy that the change in tan δ after bending is very small for all the composites (Fig. 5.13).

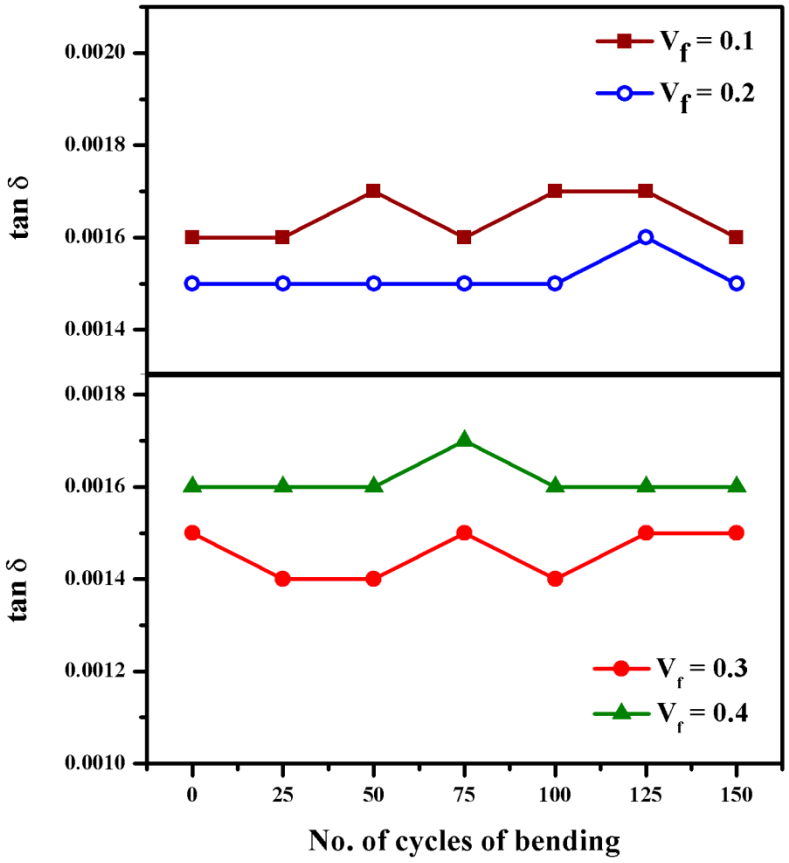

Figure 5.13 Effect of repeated bending on dielectric loss at 5 GHz

The temperature variation of ε_r at 1 MHz for the composites is shown in Fig. 5.14. ε_r decreases slightly with the increase in operating temperature for all the composites. The increase in specific volume of the matrix and the thermal expansion mismatch between matrix and filler may cause to decrease ε_r with the increase in temperature (Rao *et al.*, 2000; Hadik *et al.*, 2009). The composite containing 0.1 V_f CLSP shows ~ 10% decrease of ε_r with the increase in temperature in the temperature range 25-70 ^oC which reduces to ~ 5% at 0.4 V_f filler loading.

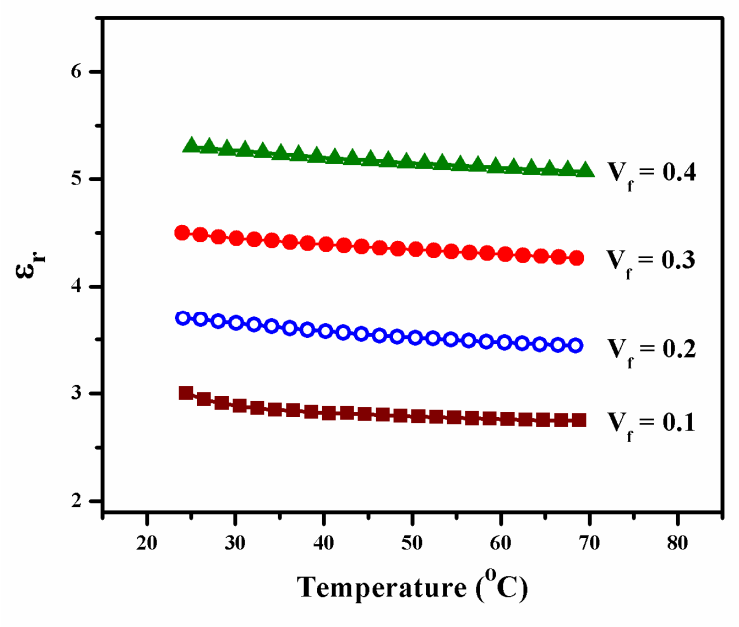

Figure 5.14 Temperature dependence of ε_r at 1 MHz

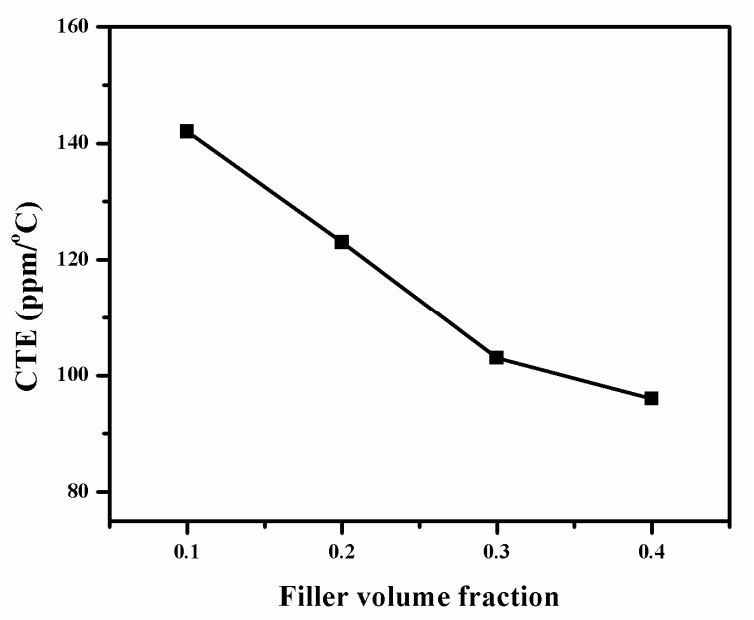

Figure 5.15 CTE of BR-CLSP composites as a function of filler volume fraction

Figure 5.15 depicts the variation of CTE of the composites with filler volume fraction. The CTE decreases from 142 ppm/^{o}C to 96 ppm/^{o}C as the filler loading increases from 0.1 to 0.4 V_f. The observed decrease in CTE is primarily due to the small CTE of CLSP filler (5 ppm/^{o}C) compared to that of BR matrix (191 ppm/^{o}C) (Thomas *et al.*, 2011). In addition, the filler particles present in the composite will

restrict thermal expansion of polymer chains (Goyal *et al.*, 2007) thereby reducing the CTE of matrix itself.

Table 5.5 Comparison of BR-CLSP composites with commercial flexible substrates

Material	Supplier	Property			
		ε_r	tan δ ($\times 10^{-3}$)	Moisture absorption (wt%)	CTE (ppm/^oC)
*fast*Film	Taconic	2.7	1.2	0.03	112
Ultralam 3000	Rogers corporation	2.9	2.5	0.04	150
BR+0.1 V_f CLSP	(present work)	2.9	1.6	0.03	142
Pyralux AX	Dupont	3.4	3.0	0.80	25
R/flex 1000	Rogers corporation	3.6	70	2.4	-
BR+0.2 V_f CLSP	(present work)	3.6	1.5	0.03	123

Table 5.5 compares the properties of mechanically flexible composites developed in the present study with that of commercial flexible substrates having similar values of ε_r.

5.4 Conclusions

HDPE matrix composites filled with $Ca_4La_6(SiO_4)_4(PO_4)_2O_2$ have been developed for microwave substrate applications. The composites show good densification, low water absorption and good microwave dielectric properties. The composite with highest filler concentration of 0.4 V_f has $\varepsilon_r = 5.1$ and tan $\delta = 2.3\times10^{-3}$ at 5 GHz. The fitting of various theoretical models for ε_r with the experimental data is also investigated and only EMT model is found to be suitable. Considerable decrease in CTE occurs for the composites with filler loading and the composite containing 0.4 V_f filler has the minimum CTE of 117 ppm/^oC. The tensile strength of the composite also decreases slightly and reaches 20.7 MPa at 0.4 V_f of filler.

Mechanically flexible composites with butyl rubber as matrix and $Ca_4La_6(SiO_4)_4(PO_4)_2O_2$ as filler have been prepared. Tensile tests establish the flexibility of composites. The relative permittivity at 5 GHz of the composites increases with filler loading without much variation in dielectric loss. Butyl rubber

loaded with the maximum of 0.4 V_f of CLSP has ε_r = 5.1 and tan δ =1.6×10^{-3}. The values of ε_r calculated using EMT model show good fit with the experimental data. The composites show no considerable variation in microwave dielectric properties after repeated bending. The relative permittivity of the composites is observed to decrease slightly with temperature. CTE of the composites is reduced with filler loading reaching the minimum value of 96 ppm/^oC at 0.4 V_f of filler.

Chapter 6

Conclusions and scope for future work

This chapter concludes the thesis by summarizing the results obtained. The chapter also discusses the possible extensions of the work that may be pursed in future.

6.1 Conclusion of the Ph. D. thesis

The rapid growth of wireless communication systems prompted the search for new high performance dielectric materials suitable for microwave applications. Microwave dielectrics have brought about revolutionary changes in wireless communication. Dielectric ceramics and composites with low relative permittivity and loss can function as substrates in microwave modules. The need for a low ε_r value is to maximize the signal propagation speed and to minimize the cross coupling effect with conductors. Similarly low loss is necessary to maintain the signal integrity. Silicates and aluminates have been reported to be promising materials for microwave substrate applications due to their low relative permittivity. Extensive work has been reported on low loss silicates and aluminates for microwave applications. The phosphates also possess low ε_r. However, not much work has been reported on the microwave dielectric properties of phosphates.

The present thesis investigates the microwave dielectric properties of phosphate based dielectric materials. The synthesis and characterization of some phosphate ceramics and ceramic filled polymer matrix composites for various applications such as microwave substrate, LTCC and mechanically flexible substrate have been addressed. The whole work has been divided into three parts as follows:

Part 1: Synthesis and characterization of rare earth bearing apatites for microwave applications

Part 2: Development of phosphate based low loss, glass free dielectric ceramics and tapes for LTCC applications

Part 3: Fabrication of polymer-ceramic composites including mechanically flexible composites for substrate applications

6.1.1 Part 1: Synthesis and characterization of rare earth apatites

Rare earth apatites with general formula $Ca_{2+x}RE_{8-x}(SiO_4)_{6-x}(PO_4)_xO_2$ [RE = La, Pr, Nd, Sm, Eu, Gd, Tb] (x = 0, 2, 4 and 6) have been prepared through solid state reaction. The ceramics have hexagonal crystal structure. Most of the compositions with RE = La, Pr and Nd show good densification ≥ 96%. $Ca_2Tb_8(SiO_4)_6O_2$ ceramic has got the relatively poor densification of 92.8%. The

ceramics have low linear coefficient of thermal expansion (CTE) (2-7 ppm/^{o}C). SEM images of the compositions with RE = La, Pr, Sm and Tb reveal an increase of average grain size with increasing value of x. The relative permittivity of the ceramics varies from 9.2 to 14.8. The value of ε_r has been calculated theoretically using Clausius-Mosotti equation and the values are compared with the experimentally measured values. The composition $Ca_2La_8(SiO_4)_6O_2$ shows the highest $Q_u \times f$ of 33100 GHz and $Ca_4Gd_6(SiO_4)_4(PO_4)_2O_2$ has the lowest $Q_u \times f$ of 5700 GHz. The ceramics have τ_f varying from -42 to + 5 ppm/^{o}C. Most of the ceramics show a non linear variation of both $Q_u \times f$ and τ_f with the value of x. $Ca_4La_6(SiO_4)_4(PO_4)_2O_2$ ceramic has got balanced microwave dielectric properties (ε_r = 13.8, $Q_u \times f$ = 27900 GHz and τ_f = -11 ppm/^{o}C).

Table 6.1 Properties of some useful rare earth apatites

Composition	**Relative density (%)**	**ε_r**	**$Q_u \times f$ (GHz)**	**τ_f (ppm/^{o}C)**	**CTE (ppm/^{o}C)**
$Ca_4La_6(SiO_4)_4(PO_4)_2O_2$	98.7	13.8	27900	-11	5
$Ca_4Tb_6(SiO_4)_4(PO_4)_2O_2$	94.7	12.0	19000	-10	4
$Ca_4La_4Pr_2(SiO_4)_4(PO_4)_2O_2$	97.9	13.8	26000	-7	4
$Ca_4La_2Pr_4(SiO_4)_4(PO_4)_2O_2$	97.2	13.8	21800	-5	4
$Ca_4La_6(GeO_4)_4(PO_4)_2O_2$	98.2	15.2	20400	-11	4

The effect of various isovalent substitutions on the microwave dielectric properties of $Ca_4La_6(SiO_4)_4(PO_4)_2O_2$ ceramic has also been studied. The investigation involves the gradual replacement of Ca^{2+} with Sr^{2+}, La^{3+} with Pr^{3+}, $(SiO_4)^{4-}$ with $(GeO_4)^{4-}$ and $(PO_4)^{3-}$ with $(VO_4)^{3-}$. The substitutions produce solid solutions having hexagonal structure. The ceramics show densification varying from ~95 to ~99%. The substitution of Sr^{2+} for Ca^{2+} decreases ε_r from 13.8 to 12.7. ε_r remains more or less same on Pr^{3+} substitution. $(GeO_4)^{4-}$ and $(VO_4)^{3-}$ substitutions increase ε_r. $Q_u \times f$ decreases for all the substitutions studied with the variation being large for Sr^{2+} substitution and small for $(VO_4)^{3-}$ substitution. The τ_f of $Ca_4La_6(SiO_4)_4(PO_4)_2O_2$ ceramic increases in the negative direction with Sr^{2+} and $(VO_4)^{3-}$ substitutions. No considerable change occurs for τ_f on $(GeO_4)^{4-}$ substitution. The value τ_f increases gradually from -11 to +2 ppm/^{o}C with Pr^{3+} substitution. Only

the partial substitution of Pr^{3+} for La^{3+} in $Ca_4La_6(SiO_4)_4(PO_4)_2O_2$ improves the τ_f without much affecting ε_r and $Q_u \times f$. Some of the useful dielectric ceramics developed in Part 1of the work and their microwave dielectric properties are given in Table 6.1.

6.1.2 Part 2: Phosphates for LTCC applications

Microwave dielectric ceramics in the series $LiMg_{(1-x)}Zn_xPO_4$ have been developed for LTCC applications. The ceramics can be sintered at a temperature ≤ 950 ^oC without any additives like glass. The compositions up to x = 0.2 have orthorhombic structure and start transforming to monoclinic structure at x = 0.3. CTE of the ceramics decreases gradually from 11 to 5 ppm/^oC as the value of x increases. The ε_r of the ceramics is observed to be dependent on the dielectric polarizability of ions present and crystal structure. $Q_u \times f$ of the ceramics varies non-linearly between 79100 GHz and 99700 GHz depending on porosity and phase purity. The ceramics show τ_f varying from -55 to -80 ppm/^oC. The large negative τ_f of $LiMgPO_4$ and $LiMg_{0.9}Zn_{0.1}PO_4$ cermics has been tuned nearly to zero through TiO_2 addition. For $LiMgPO_4$, addition of 0.12 volume fraction (V_f) of TiO_2 reduces the τ_f from -55 ppm/^oC to +1 ppm/^oC. $LiMg_{0.9}Zn_{0.1}PO_4$ + 0.12 V_f TiO_2 sintered at 950 ^oC shows the best microwave dielectric properties: ε_r = 10.1, $Q_u \times f$ = 52900 GHz and τ_f = -5 ppm/^oC. The newly developed composites are found to be compatible with the common electrode material (Ag) in LTCC modules. The microwave dielectric properties of some of the compositions developed in the present study are superior to several commercially available dielectric materials for LTCC applications. The major results of the investigation on the microwave dielectric properties of $LiMg_{(1-x)}Zn_xPO_4$ ceramics and composites are summarized in Table 6.2.

$LiMgPO_4$ ceramic has been cast into thin tapes (thickness = 70 μm) using doctor blade technique. The amount of dispersant (fish oil) required to prepared well dispersed, stable tape casting slurry of $LiMgPO_4$ has been optimized by viscosity measurements and sedimentation analysis. The final tape casting slurry with typical shear thinning behavior has been prepared using xylene-ethanol mixture as solvent

vehicle, polyvinyl butyral as binder and butyl benzyl phthalate and polyethylene glycol as plasticizers. The green tape has a tensile strength of 0.22 MPa, average surface roughness of 0.25 μm, relative density of 56% and ε_r = 3.2, tan δ = 0.0688 at 5 GHz. The relative density and microwave dielectric properties of $LiMgPO_4$ tape is improved after sintering at 950 ^oC. The sintered tape shows good densification (97.4%) and microwave dielectric properties (ε_r =6.4 and tan δ =0.0002 at 5 GHz). $LiMgPO_4$ ceramic shows a thermal conductivity of 7.1 $Wm^{-1}K^{-1}$ at room temperature. The fired properties of $LiMgPO_4$ tape are found to be comparable with commercial LTCC tapes.

Table 6.2 Properties of some selected phosphate based materials for LTCC applications

Composition	**Sintering temperature (^oC)**	**Relative density (%)**	**ε_r**	**$Q_u \times f$ (GHz)**	**τ_f (ppm/^oC)**
$LiMgPO_4$	950	95.0	6.6	79100	-55
$LiMg_{0.9}Zn_{0.1}PO_4$	925	94.9	6.7	99700	-62
$LiMg_{0.8}Zn_{0.2}PO_4$	900	93.9	6.7	93900	-66
$LiMgPO_4$+0.12 V_f TiO_2	950	95.0	10.0	26900	+1
$LiMg_{0.9}Zn_{0.1}PO_4$ + 0.12 V_f TiO_2	950	95.5	10.1	52900	-5

6.1.3 Part 3: Polymer-ceramic composites for microwave substrate applications

Polymer-ceramic composites with high density polyethylene (HDPE) and flexible butyl rubber (BR) as matrices have been developed. $Ca_4La_6(SiO_4)_4(PO_4)_2O_2$ (CLSP) ceramic with good microwave dielectric properties has been selected as filler. The maximum filler loading achieved is 0.4 V_f for both the composites. The microstructure of the composites has been analyzed to study the extent of filler dispersion. The filler particles show a tendency for agglomeration at higher loading. The composites show very low water absorption ≤ 0.04 wt%. BR-CLSP composites show required flexibility and stretchability even at higher filler loading. For HDPE-CLSP composites ε_r at 5 GHz increases from 2.9 to 5.1 and tan δ increases from 1.1×10^{-3} to 2.3×10^{-3} as the filler volume fraction increases from 0.1 to 0.4. Similarly for BR-CLSP composites ε_r increase from 2.9 to 5.1 and tan δ varies in between 1.5×10^{-3} and 1.6×10^{-3}. The values of ε_r for the composites have been calculated

using various theoretical models and compared with the experimentally observed values at 5 GHz. For both the composites only the EMT model has been observed to be suitable for modeling the relative permittivity. The ε_r of the composites shows small temperature dependence. The CTE of the composites decreases considerably with the increase in filler volume fraction. The minimum value of CTE obtained is 117 ppm/^oC for HDPE-CLSP composites and 96 ppm/^oC for BR-CLSP composites at the maximum filler loading of 0.4 V_f. The effect of repeated bending on the microwave dielectric properties of BR-CLSP flexible composites has also been studied. The composites show only marginal variation in microwave dielectric properties after bending. The properties of the composites developed in the present study are comparable to that of similar commercial polymer based substrates. The properties of some of the selected composites developed as a part of this work are given in Table 6.3.

Table 6.3 Properties of newly developed polymer-ceramic composites

Material	**ε_r**	**tan δ ($\times 10^{-3}$)**	**Moisture absorption (wt%)**	**CTE (ppm/^oC)**
HDPE+0.2 V_f CLSP	3.6	2.3	0.03	179
HDPE+0.4 V_f CLSP	5.1	2.3	0.04	117
BR+0.2 V_f CLSP	3.6	1.5	0.03	123
BR+0.4 V_f CLSP	5.1	1.6	0.04	96

6.2 Scope for future work

A detailed structural investigation of $Ca_{2+x}RE_{8-x}(SiO_4)_{6-x}(PO_4)_xO_2$ ceramics may be done to understand the observed non linear variation in microwave dielectric properties. The fabrication of microwave circuits using the $LiMgPO_4$ LTCC tape in order to study and overcome the challenges in practical applications is another interesting topic to be pursued. LTCC tapes of $LiMgPO_4$ + 0.12 V_f TiO_2 composites with typical microwave dielectric properties may be developed and utilized in future microwave modules. The development of Cu clad laminates of the new polymer-ceramic composites is of significant technological importance. Such laminates,

especially those with mechanical flexibility have great significance in future microwave devices.

List of publications

1. **Dhanesh Thomas** and Mailadil T. Sebastian, "Temperature-compensated $LiMgPO_4$: A new glass-free low-temperature co-fired ceramic," *J. Am. Ceram. Soc.*, **93** [11] 3828–3831 (2010).

2. **Dhanesh Thomas**, Chameswary Janardhanan and Mailadil T.Sebastian, "Mechanically flexible butyl rubber–$SrTiO_3$ composite dielectrics for microwave applications," *Int. J. Appl. Ceram. Technol.*, **8** [5] 1099–1107 (2011).

3. **Dhanesh Thomas** and Mailadil T. Sebastian, "Microwave dielectric properties of $Ca_{2+x}La_{8-x}(SiO_4)_{6-x}(PO_4)_xO_2$ solid solution," *J. Am. Ceram. Soc.*, **94** [8] 2276–2278 (2011).

4. Chameswary Janardhanan, **Dhanesh Thomas**, Ganesanpotti Subodh, Soumya Harshan, Jacob Philip and Mailadil T. Sebastian, "Microwave dielectric properties of flexible butyl rubber–strontium cerium titanate composites," *J. Appl. Polym. Sci.***124**, 3426–3433 (2012).

5. **Dhanesh Thomas**, K. T. Rethika and M. T. Sebastian, "Microwave dielectric properties of $BaNb_{(2-x)}Ta_xP_2O_{11}$ (x= 0, 0.5, 1, 1.5 and 2) ceramics," *J. Mater. Sci: Mater. Electron.* **23**, 1268–1271(2012).

6. **Dhanesh Thomas** and Mailadil T. Sebastian "Effect of Zn^{2+} substitution on the microwave dielectric properties of $LiMgPO_4$ and the development of a new temperature stable glass free LTCC," *J. Eur. Ceram. Soc.* **32**, 2359–2364 (2012).

7. **Dhanesh Thomas,** Abhilash P. and Mailadil T. Sebastian "Casting and characterization of $LiMgPO_4$ glass free LTCC tape for microwave applications," *J. Eur. Ceram. Soc.* **33**, 87-93 (2013)

8. **Dhanesh Thomas,** Abhilash P. and Mailadil T. Sebastian "Effect of isovalent substitutions on the microwave dielectric properties of $Ca_4La_6(SiO_4)_4(PO_4)_2O_2$ apatite," *J. Alloys Compd.* **546**, 72–76 (2013).

9. **Dhanesh Thomas** and Mailadil T. Sebastian "HDPE matrix composites filled with $Ca_4La_6(SiO_4)_4(PO_4)_2O_2$ for microwave applications" (communicated).

Conference proceedings

1. **Dhanesh Thomas** and M. T. Sebastian, "A new phosphate based dielectric ceramic for substrate applications," *72nd annual session of The Indian Ceramic Society*, January, 2009, Jaipur.
2. **Dhanesh Thomas**, J. Chameswary and M. T. Sebastian, "Dielectric properties of Butyl Rubber-$SrTiO_3$ flexible composite," *IEEE Applied Electromagnetics Conference (AEMC)*, December, 2009, Kolkatta.
3. K M Manu, **Dhanesh Thomas**, Matjaz Valant, Anna-Karin Axelsson and M T Sebastian, "Preparation and characterisation of PVDF -$BiFeO_3$ -Silver three phase composites," *International Conference on Advanced Functional Materials (ICAFM)*, December, 2009, Trivandrum.
4. **Dhanesh Thomas** and M. T. Sebastian, "Microwave dielectric properties of a new series of phosphates," *XVI National Seminar on Ferroelectrics and Dielectrics (NSFD-XVI)*, December, 2010, Bilaspur (C.G).
5. **Dhanesh Thomas**, K. P. Sreelakshmi, K. M. Manu and M. T. Sebastian, "Polystyrene-silver composites for embedded capacitor applications," *IEEE Applied Electromagnetics Conference (AEMC)*, December, 2011, Kolkatta.
6. Abhilash P., **Dhanesh Thomas** and M. T. Sebastian, "Microwave dielectric properties of green tape for LTCC applications," *IEEE Applied Electromagnetics Conference (AEMC)*, December, 2011, Kolkatta.
7. **Dhanesh Thomas**, P. Abhilash and M. T. Sebastian, "Novel glass free ceramic for LTCC applications," *IMAPS/ACerS 8th International Conference and Exhibition on Ceramic Interconnect and Ceramic Microsystems Technologies (CICMT 2012)*, April, 2012, Germany.

References

Ahmed, H. M. and Aziz, S. A. B. "Dielectric properties of commercial non-polar polymers," *J. Zankoy Sulaimani Part A* **11**: 1-8 (2008).

Alford, N. M. and Penn, S. J. "Sintered alumina with low dielectric loss," *J. Appl. Phys.* **80**(10): 5895-5898 (1996).

Alford, N. M., Wang, X., Penn, S. J., Poole, M. and Jones, A. *Br. Ceram. Trans* **99**: 212 (2000).

Alford, N. M., Breeze, J., Wang, X., Penn, S. J., Dalla, S., Webb, S. J., Ljepojevic, N. and Aupi, X. "Dielectric loss of oxide single crystals and polycrystalline analogues from 10 to 320 K," *J. Eur. Ceram. Soc.* **21**(15): 2605-2611 (2001).

Alm, B., Knitter, R. and Haußelt, J. "Development of a ceramic micro heat exchanger – design, construction, and testing," *Chem. Eng. Technol.* **28**(12): 1554-1560 (2005).

Amagai, M. "Mechanical reliability in electronic packaging," *Microelectron. Reliab.* **42**(4–5): 607-627 (2002).

Anjana, P. S. "Investigations on ceria based dielectric ceramic materials for wireless communication," Ph. D Thesis in Physics, Cochin University of Science and Technology, Cochin (2008).

Anjana, P. S., Deepu, V., Uma, S., Mohanan, P., Philip, J. and Sebastian, M. T. "Dielectric, thermal, and mechanical properties of CeO_2-filled HDPE composites for microwave substrate applications," *J. Polym. Sci. B: Polym. Phys.* **48**(9): 998-1008 (2010).

Anjana, P. S., Uma, S., Philip, J. and Sebastian, M. T. "Thermal properties of low loss PTFE-CeO_2 dielectric ceramic composites for microwave substrate applications," *J. Appl. Polym. Sci.* **118**(2): 751-758 (2010).

Arai, Y. *Chemistry of powder production*, Chapman and Hall, London (1996).

Ardanova, L. I., Get'man, E. I., Loboda, S. N., Prisedsky, V. V., Tkachenko, T. V., Marchenko, V. I., Antonovich, V. P., Chivireva, N. A., Chebishev, K. A. and Lyashenko, A. S. "Isomorphous substitutions of rare earth elements for calcium in synthetic hydroxyapatites," *Inorg. Chem.* **49**(22): 10687-10693 (2010).

Azdouz, M., Manoun, B., Essehli, R., Azrour, M., Bih, L., Benmokhtar, S., Hou, A. A. and Lazor, P. "Crystal chemistry, rietveld refinements and Raman spectroscopy studies of the new solid solution series: $Ba_{3-x}Sr_x(VO_4)_2$ ($0 \leq x \leq 3$)," *J. Alloys Compd.* **498**(1): 42-51 (2010).

Baklouti, S., Bouaziz, J., Chartier, T. and Baumard, J. F. "Binder burnout and evolution of the mechanical strength of dry-pressed ceramics containing poly(vinyl alcohol)," *J. Eur. Ceram. Soc.* **21**(8): 1087-1092 (2001).

Barnwell, P. and O'Neill, M. P. "Enabling ceramic circuit technologies for wireless microelectronics packaging," *Proceedings of wireless communications conference* (1997).

Barron, H. *Modern synthetic rubbers*, Chapman & Hall Ltd., London (1949).

Barsoum, M. W. *Fundamentals of ceramics*, Institute of Physics Publishing, Bristol (2003).

Bhattacharya, S. K. and Tummala, R. R. "Integral passives for next generation of electronic packaging: Application of epoxy/ceramic nanocomposites as integral capacitors," *Microelectron. J.* **32**(1): 11-19 (2001).

Bian, J. I., Kim, D. W. and Hong, K. S. "Microwave dielectric properties of $A_2P_2O_7$ (A = Ca, Sr, Ba; Mg, Zn, Mn)," *Jpn. J. Appl. Phys., Part 1* **43**(6A): 3521-3525 (2004).

Bian, J. J., Kim, D. W. and Hong, K. S. "Glass-free LTCC microwave dielectric ceramics," *Mater. Res. Bull.* **40**(12): 2120-2129 (2005).

Bian, J. J. and Wang, L. "Glass-free LTCC microwave ceramic-$(La_{0.5}Na_{0.5})_{1-x}(Li_{0.5}Nd_{0.5})_xWO_4$," *J. Am. Ceram. Soc.* **94**(10): 3188-3191 (2011).

Bian, J. J. and Wu, J. Y. "Designing of glass-free LTCC microwave ceramic-$Ca_{1-x}(Li_{0.5}Nd_{0.5})_xWO_4$ by crystal chemistry," *J. Am. Ceram. Soc.* **95**(1): 318-323 (2012).

Bitterlich, B., Lutz, C. and Roosen, A. "Rheological characterization of water-based slurries for the tape casting process," *Ceram. Int.* **28**(6): 675-683 (2002).

Blasse, G. "Influence of local charge compensation on site occupation and luminescence of apatites," *J. Solid State Chem.* **14**(2): 181-184 (1975).

Blow, C. M. *Rubber technology and manufacture,* Newnes-Butterworths, London (1971).

Boyer, L., Piriou, B., Carpena, J. and Lacout, J. L. "Study of sites occupation and chemical environment of Eu^{3+} in phosphate-silicates oxyapatites by luminescence," *J. Alloys Compd.* **311**(2): 143-152 (2000).

Breeze, J. D., Perkins, J. M., McComb, D. W. and Alford, N. M. "Do grain boundaries affect microwave dielectric loss in oxides?," *J. Am. Ceram. Soc.* **92**(3): 671-674 (2009).

Buchanan, R. C. *Ceramic Materials for Electronics,* Marcel Dekker, USA (2004).

Bur, A. J. "Dielectric properties of polymers at microwave frequencies: A review," *Polymer* **26**(7): 963-977 (1985).

Cahn, R. W., Haasen, P. and Kramer, E. J. *Materials science and technology, Volume 2A: Characterization of materials, part I,* VCH Publishers, New York (1992).

Calvert, P. D., Tormey, E. S. and Pober, R. L. "Fish oil and triglycerides as dispersants for alumina," *Am. Ceram. Soc. Bull.* **65**: 669-672 (1986).

Castanet, L., Bousquet, M. and Mertens, D. "Simulation of the performance of a Ka-band vsat video conferencing system with uplink power control and data rate reduction to mitigate atmospheric propagation effects," *Int. J. Satell. Commun.* **20**(4): 231-249 (2002).

Chameswary, J. and Sebastian, M. T. "Butyl rubber–$Ba_{0.7}Sr_{0.3}TiO_3$ composites for flexible microwave electronic applications," *Ceram. Int.* (Article in press) (2012).

Chartier, A., Meis, C. and Gale, J. D. "Computational study of cs immobilization in the apatites $Ca_{10}(PO_4)_6F_2$, $Ca_4La_6(SiO_4)_6F_2$ and $Ca_2La_8(SiO_4)_6O_2$," *Phys. Rev. B* **64**(8): 085110 (2001).

Chen, L. F., Ong, C. K., Neo, C. P., Varadan, V. V. and Varadan, V. K. *Microwave electronics: Measurement and materials characterization,* John Wiley & Sons, England (2004).

Chiang, Y. M., Birnie, D. P. and Kingery, W. D. *Physical ceramics: Principles for ceramic science and engineering,* John Wiley and Sons, Inc., New York (1997).

Cho, I. S., Kim, J. R., Kim, D. W. and Hong, K. "Phase transformation and microwave dielectric properties of $BiPO_4$ ceramics," *J. Electroceram.* **16**(4): 379-383 (2006).

Cho, I. S., Choi, G. K., An, J. S., Kim, J. R. and Hong, K. S. "Sintering, microstructure and microwave dielectric properties of rare earth orthophosphates, $RePO_4$ (Re = La, Ce, Nd, Sm, Tb, Dy, Y, Yb)," *Mater. Res. Bull.* **44**(1): 173-178 (2009).

Cho, W. W., Kakimoto, K. I. and Ohsato, H. "Microwave dielectric properties and low-temperature sintering of $MgTiO_3$–$SrTiO_3$ ceramics with B_2O_3 or CuO," *Mater. Sci. Eng. B* **121**(1–2): 48-53 (2005).

Chou, C. F., Changrani, R., Roberts, P., Sadler, D., Burdon, J., Zenhausern, F., Lin, S., Mulholland, A., Swami, N. and Terbrueggen, R. "A miniaturized cyclic PCR device-modeling and experiments," *Microelectron. Eng.* **61-62**: 921-925 (2002).

Chung, D. D. L. "Polymer-matrix composites for microelectronics," *Polym. Polym. Compos.* **8**(4): 219-229 (2000).

Cohn, S. B. and Kelly, K. C. "Microwave measurement of high dielectric constant materials," *IEEE Trans. Microwave Theory Tech.* **14**(9): 406-410 (1966).

Conklin, G. E. "Reduction of dielectric loss in polyethylene," *J. Appl. Phys.* **35**(11): 3228-3235 (1964).

Courtney, W. E. "Analysis and evaluation of a method of measuring the complex permittivity and permeability of microwave insulators," *IEEE Trans. Microw. Theory Technol.* **18**(8): 476-485 (1970).

Cullity, B. D. *Elements of X-ray diffraction*, Addison-Wesley Publishing Company, Inc., Massachusetts (1978).

Curtis, A. J. "Dielectric loss in ``nonpolar'' polymers," *J. Chem. Phys.* **36**(12): 3500-3501 (1962).

Dang, Z. M., Yu, Y. F., Xu, H. P. and Bai, J. "Study on microstructure and dielectric property of the $BaTiO_3$/epoxy resin composites," *Comp. Sci. Technol.* **68**: 171–177 (2008).

De Geyter, N., Morent, R., Axisa, F., De Smet, N., Gengembre, L., De Leersnijder, E., Leys, C., Vanfleteren, J., Rymarczyk-Machal, M., Schacht, E. and Payen,

E. "Medium and atmospheric pressure plasma treatment for improvement of adhesion of PDMS used for flexible and stretchable electronics." *Portable Information Devices, 7th IEEE Conference on Polymers and Adhesives in Microelectronics and Photonics*: 1-3 (2008).

Dias, C. J. and Das-Gupta, D. K. "Inorganic ceramic/polymer ferroelectric composite electrets," *IEEE Trans. Dielectr. Electr. Insul.* **3**(5): 706-734 (1996).

Dong, M., Yue, Z., Zhuang, H., Meng, S. and Li, L. "Microstructure and microwave dielectric properties of TiO_2-doped Zn_2SiO_4 ceramics synthesized through the sol–gel process," *J. Am. Ceram. Soc.* **91**(12): 3981-3985 (2008).

Douglas, T. B., McCoskey, R. E. and Ginnings, D. C. "Thermal properties of aluminum oxide from 0° to 1200 °K," *J. Res. Nat. Bur. Stand.* **57**: 67-82 (1956).

Durif, A. "The development of cyclophosphate crystal chemistry," *Solid State Sci.* **7**(6): 760-766 (2005).

Felsche, J. "Rare earth silicates with the apatite structure," *J. Solid State Chem.* **5**(2): 266-275 (1972).

Field, R. F. "The formation of ionized water films on dielectrics under conditions of high humidity," *J. Appl. Phys.* **17**(5): 318-325 (1946).

Frohlics, H. *Theory of dielectrics*, Clarendon Press, Oxford (1950).

Geffroy, P. M., Chartier, T. and Silvain, J. F. "Innovative approach to metal matrix composites film by tape casting process," *Adv. Eng. Mater.* **9**: 547-553 (2007).

Gemant, A. "The role of solid friction in synthetic dielectrics," *J. Appl. Phys.* **9**(11): 730-734 (1938).

George, S. and Sebastian, M. T. "Microwave dielectric properties of novel temperature stable high Q $Li_2Mg_{1-x}Zn_xTi_3O_8$ and $Li_2A_{1-x}Ca_xTi_3O_8$ (A = Mg, Zn) ceramics," *J. Eur. Ceram. Soc.* **30**(12): 2585-2592 (2010).

George, S., Anjana, P. S., Sebastian, M. T., Krupka, J., Uma, S. and Philip, J. "Dielectric, mechanical, and thermal properties of low-permittivity polymer–ceramic composites for microelectronic applications," *Int. J. Appl. Ceram. Technol.* **7**(4): 461-474 (2010).

George, S., Deepu, V. N., Mohanan, P. and Sebastian, M. T. "Influence of $Ca[(Li_{1/3}Nb_{2/3})_{0.8}Ti_{0.2}]O_{3-\delta}$ filler on the microwave dielectric properties of polyethylene and polystyrene for microelectronic applications," *Polym. Eng. Sci.* **50**(3): 570-576 (2010).

Goldsmith, A. *Wireless communications*, Cambridge University Press, New York (2005).

Golonka, L. J., Roguszczak, H., Zawada, T., Radojewski, J., Grabowska, I., Chudy, M., Dybko, A., Brzozka, Z. and Stadnik, D. "LTCC based microfluidic system with optical detection," *Sens. Actuators, B* **111**: 396-402 (2005).

Golonka, L. J. "Technology and applications of low temperature cofired ceramic (LTCC) based sensors and microsystems," *Bull. Pol. Ac.: Tech.* **54**(2): 221-231 (2006).

Goncharenko, A. V., Lozovski, V. Z. and Venger, E. F. "Lichtenecker's equation: Applicability and limitations," *Opt. Commun.* **174**(1–4): 19-32 (2000).

Gongora-Rubio, M. R., Espinoza-Vallejos, P., Sola-Laguna, L. and Santiago-Aviles, J. J. "Overview of low temperature co-fired ceramics tape technology for meso-system technology (MSST)," *Sens. Actuators, A* **89**(3): 222-241 (2001).

Goyal, R. K., Tiwari, A. N., Mulik, U. P. and Negi, Y. S. "Novel high performance Al_2O_3/poly(ether ether ketone) nanocomposites for electronics applications," *Comp. Sci. Technol.* **67**(9): 1802-1812 (2007).

Guo, Y. P., Ohsato, H. and Kakimoto, K. I. "Characterization and dielectric behavior of willemite and TiO_2-doped willemite ceramics at millimeter-wave frequency," *J. Eur. Ceram. Soc.* **26**(10-11): 1827-1830 (2006).

Gupta, T. K. "Instability of cylindrical voids in alumina," *J. Am. Ceram. Soc.* **61**: 191-195 (1978).

Gurevich, V. L. and Tagantsev, A. K. "Intrinsic dielectric loss in crystals," *Adv. Phys.* **40**(6): 719-767 (1991).

Gwaily, S. E., Nasr, G. M., Badawy, M. M. and Hassan, H. H. "Thermal properties of ceramic-loaded conductive butyl rubber composites," *Polym. Deg. Stab.* **47**(3): 391-395 (1995).

Hadik, N., Outzourhit, A., Elmansouri, A., Abouelaoualim, A., Oueriagli, A. and Ameziane, E. L. "Dielectric behavior of ceramic (BST)/epoxy thick films," *Act. Passive Electron. Compon.* **2009**: 437130 (2009).

Hakim, I. K., Bishai, A. M. and Saad, A. L. "Dielectric properties of butyl rubber mixtures at 10^6−10^{10} Hz," *J. Appl. Polym. Sci.* **35**(4): 1123-1125 (1988).

Hakki, B. W. and Coleman, P. D. "A dielectric resonator method of measuring inductive capacitance in the millimeter range," *IRE Trans. Microwave Theory Tech.* **8**: 402-410 (1960).

Hammond, C. *The basics of crystallography and diffraction*, Oxford University Press, New York (2009).

Hasselman, D. P. H., Syed, R. and Tien, T. Y. "The thermal diffusivity and conductivity of transformation-toughened solid solutions of alumina and chromia," *J. Mater. Sci.* **20**(7): 2549-2556 (1985).

Hayden, H. W., Moffatt, W. G. and Wulff, J. *The structure and properties of materials, Volume III: Mechanical behavior*, Wiley Eastern Ltd. (1984).

Hench, L. L. and West, J. K. *Principles of electronic ceramics*, John Wiley and Sons, Singapore (1990).

Hench, L. L. "Bioceramics: From concept to clinic," *J. Am. Ceram. Soc.* **74**(7): 1487-1510 (1991).

Herbert, J. M. *Ceramic dielectrics and capacitors*, Gordon and Breach Science Publishers, Pennsylvania (1985).

Holliday, L. and Robinson, D. "Review: The thermal expansion of composites based on polymers," *J. Mater. Sci.* **8**(3): 301- 311 (1973).

Honkamo, J., Jantunen, H., Subodh, G., Sebastian, M. T. and Mohanan, P. "Tape casting and dielectric properties of $Zn_2Te_3O_8$-based ceramics with an ultra-low sintering temperature," *Int. J. Appl. Ceram. Technol.* **6**(4): 531-536 (2009).

Howatt, G. N., Breckenridge, R. G. and Brownlow, J. M. "Fabrication of thin ceramic sheets for capacitors," *J. Am. Ceram. Soc.* **30**(8): 237-242 (1947).

Hughes, J. M., Cameron, M. and Crowley, K. D. "Ordering of divalent cations in the apatite structure; crystal structure refinements of natural Mn- and Sr-bearing apatite," *Am. Mineral.* **76**(11-12): 1857-1862 (1991) (a).

Hughes, J. M., Cameron, M. and Mariano, A. N. "Rare-earth-element ordering and structural variations in natural rare-earth-bearing apatites," *Am. Mineral.* **76**(7-8): 1165-1173 (1991) (b).

Imanaka, Y. *Multilayered low temperature cofired ceramics (LTCC) technology*, Springer, Japan (2005).

Janardhanan, C., Thomas, D., Subodh, G., Harshan, S., Philip, J. and Sebastian, M. T. "Microwave dielectric properties of flexible butyl rubber–strontium cerium titanate composites," *J. Appl. Polym. Sci.* **124**(4): 3426-3433 (2012).

Jantunen, H., Rautioaho, R., Uusimaki, A. and Leppävuori, S. "Preparing low-loss low-temperature cofired ceramic material without glass addition," *J. Am. Ceram. Soc.* **83**(11): 2855-2857 (2000).

Jantunen, H., Hu, T., Uusimäki, A. and Leppävuori, S. "Tape casting of ferroelectric, dielectric, piezoelectric and ferromagnetic materials," *J. Eur. Ceram. Soc.* **24**(6): 1077-1081 (2004).

Jayasundere, N. and Smith, B. V. "Dielectric-constant for binary piezoelectric 0-3 composites," *J. Appl. Phys.* **73**(5): 2462-2466 (1993).

Johnson, D. W. "Sol-gel processing of ceramics and glass,"*Am. Ceram. Soc. Bull.* **64**(12): 1597-1602 (1985).

Joseph, T. and Sebastian, M. T. "Microwave dielectric properties of $(Sr_{1-x}A_x)_2(Zn_{1-x}B_x)Si_2O_7$ ceramics (A = Ca, Ba and B = Co, Mg, Mn, Ni)," *J. Am. Ceram. Soc.* **93**(1): 147-154 (2010).

Joseph, T. and Sebastian, M. T. "Microwave dielectric properties of alkaline earth orthosilicates M_2SiO_4 (M = Ba, Sr, Ca)," *Mater. Lett.* **65**(5): 891-893 (2011).

Joseph, T., Sebastian, M. T., Jantunen, H., Jacob, M. and Sreemoolanadhan, H. "Tape casting and dielectric properties of $Sr_2ZnSi_2O_7$-based ceramic–glass composite for low temperature co-fired ceramics applications," *Int. J. Appl. Ceram. Technol.* **8**(4): 854-864 (2011).

Joseph, T., Uma, S., Philip, J. and Sebastian, M. T. "Dielectric, thermal and mechanical properties of $Sr_2ZnSi_2O_7$ based polymer/ceramic composites," *J. Mater. Sci.: Mater. Electron.* **23**(6): 1243-1254 (2012).

Kajfez, D. and Guillon, P. *Dielectric resonators*, Noble Publishing Corporation, Atlanta, USA (1998).

Kemethmueller, S., Hagymasi, M., Stiegelschmitt, A. and Roosen, A. "Viscous flow as the driving force for the densification of low-temperature co-fired ceramics," *J. Am. Ceram. Soc.* **90**(1): 64-70 (2007).

Kendrick, E., Islam, M. S. and Slater, P. R. "Developing apatites for solid oxide fuel cells: Insight into structural, transport and doping properties," *J. Mater. Chem.* **17**(30): 3104-3111 (2007).

Khawaja, B. A. and Cryan, M. J. "Characterization of multimode fibers for use in millimeter wave radio-over-fiber systems," *Microwave Opt. Technol. Lett.* **50**(8): 2005-2007 (2008).

Khichar, R. and Upadhyay, S. S. "Wireless sensor networks and their applications in geomatics: Case study on developments in developing countries," *Appl. Geomat.* **2**(2): 43-48 (2010).

Khoong, L. E., Tan, Y. M. and Lam, Y. C. "Carbon burnout and densification of self-constrained LTCC for fabrication of embedded structures in a multi-layer platform," *J. Eur. Ceram. Soc.* **29**: 457–463 (2009).

Kim, D. H. and Rogers, J. A. "Stretchable electronics: Materials strategies and devices," *Adv. Mater.* **20**(24): 4887-4892 (2008).

Kim, J. Y. "Parallel concatenated convolutional coding for a local multipoint distribution service system," *IEEE Trans. Consum. Electron.* **46**(1): 154-160 (2000).

Kinemuchi, Y., Tsugoshi, T. and Watari, K. "Binder burnout from layers of alumina ceramics under centrifugal force," *J. Am. Ceram. Soc.* **89**: 805-809 (2006).

Kingery, W. D. and Berg, M. "Study of the initial stages of sintering solids by viscous flow, evaporation-condensation, and self-diffusion," *J. Appl. Phys.* **26**: 1205 (1955).

Kingery, W. D. *Introduction to ceramics*, John Wiley and Sons, New York (1960).

Knickerbocker, S. H., Kumar, A. H. and Herron, L. W. "Cordierite glass-ceramics for multilayer ceramic packaging," *Am. Ceram. Soc. Bull.* **72**(1): 90-95 (1993).

Kobayashi, Y. and Tanaka, S. "Resonant modes of a dielectric rod resonator short-circuited at both ends by parallel conducting plates," *IEEE Trans. Microwave Theory Tech.* **28**(10): 1077-1085 (1980).

Koulouridis, S., Kiziltas, G., Zhou, Y. J., Hansford, D. J. and Volakis, J. L. "Polymer-ceramic composites for microwave applications: Fabrication and performance assessment," *IEEE Trans. Microwave Theory Tech.* **54**(12): 4202-4208 (2006).

Krupka, J., Geyer, R. G., Jarvis, J. B. and J., C. "Measurements of the complex permittivity of microwave circuit board substrates using split dielectric resonator and reentrant cavity techniques," *Seventh International Conference on Dielectric Materials, Measurements and Applications. Conf. Publ. No. 430, Bath, UK*: 21-24 (1996).

Krupka, J., Derzakowski, K. D., Riddle, B. and Jarvis, J. B. "A dielectric resonator for measurements of complex permittivity of low loss dielectric materials as a function of temperature," *Meas. Sci. Technol.* **9**: 1751-1756 (1998).

Krupka, J., Gregonry, A. P., Kochard, O. C., Clarke, R. N., Riddle, B. and Jarvis, J. B. "Uncertainty of complex permittivity measurements by split-post dielectric resonator technique," *J. Eur. Ceram. Soc.* **21**: 2673- 2676 (2001).

Krupka, J. "Frequency domain complex permittivity measurements at microwave frequencies," *Meas. Sci. Technol.* **17**(6): R55 (2006).

Kwon, D. K., Lanagan, M. T. and Shrout, T. R. "Microwave dielectric properties and low-temperature cofiring of $BaTe_4O_9$ with aluminum metal electrode," *J. Am. Ceram. Soc.* **88**(12): 3419-3422 (2005).

Kwon, D. K., Lanagan, M. T. and Shrout, T. R. "Microwave dielectric properties of $BaO–TeO_2$ binary compounds," *Mater. Lett.* **61**(8–9): 1827-1831 (2007).

Lal, R., Gokhale, N. M., Krishnan, R. and Ramakrishnan, P. "Effect of sintering parameters on the microstructure and properties of strontium modified PZT ceramics prepared using spray-dried powders," *J. Mater. Sci.* **24**(8): 2911-2916 (1989).

Lampman, S. R., Woods, M. S. and Zorc, T. B. *Ceramics and glasses*, ASM International, Ohio (1991).

Lee, J. H., Yonathan, P., Yoon, D. H., Kim, W. J. and Park, J. Y. "Dispersion stability and its effect on tape casting of solvent-based SiC slurries," *J. Ceram. Process. Res.* **10**: 301-307 (2009).

Leu, L. C., Thomas, S., Sebastian, M. T., Zdzieszynski, S., Misture, S. and Ubic, R. "Crystal structure of apatite type rare-earth silicate $(Sr_2RE_2)(RE_6)(SiO_4)_6O_2$ (RE = La, Pr, Tb, Tm, and Y)," *J. Am. Ceram. Soc.* **94**(8): 2625-2632 (2011).

Li, J. and Ananthasuresh, G. K. "Three-dimensional low-temperature co-fired ceramic shells for miniature systems applications," *J. Micromech. Microeng.* **12**(3): 198-203 (2002).

Li, S., Zhang, Q., Yang, H. and Zou, D. "Fabrication and characterization of $Li_{1+x-y}Nb_{1-x-3y}Ti_{x+4y}O_3$ substrates using aqueous tape casting process," *Ceram. Int.* **35**(1): 421-426 (2009).

Li, Y., Bian, J. and Yuan, L. "A new glass-free low-temperature fired microwave ceramic," *J. Mater. Sci.* **44**(1): 328-330 (2009).

Liang, M. H., Wu, S. Y., Hu, C. T. and Lin, I. N. "Enhancing the sinterability of $Ba(Mg_{1/3}Ta_{2/3})O_3$ dielectrics by using chemically-derived powders," *Mater. Chem. Phys.* **79**(2-3): 276-281 (2003).

Lin, Y., Yang, H., Zhu, J. and Wang, F. "Magnetic and dielectric properties of YIG/HDPE composites for high-frequency application," *Optoelectron. Adv. Mater.* **4**(4): 509-511 (2010).

Lorenzen, D. and Hennig, P. "Highly thermally conductive substrates with adjustable cte for diode laser bar packaging," *Proc. Spie 4945, MEMS/MOEMS: Advances in photonic communications, sensing, metrology, packaging and assembly*. **4945:** 174-185 (2002).

Luftl, S., Balluch, B., Smetana, W. and Seidler, S. "Kinetic study of the polymeric binder burnout in green low temperature co-fired ceramic tapes," *J. Therm. Anal. Calorim.* **103**: 157–162 (2011).

Maexa, K., Baklanov, M. R., Shamiryan, D., Iacopi, F., Brongersma, S. H. and Yanovitskaya, Z. S. "Low dielectric constant materials for microelectronics," *J. Appl. Phys.* **93**(11): 8793-8841 (2003).

Mallet, P., Guérin, C. A. and Sentenac, A. "Maxwell-garnett mixing rule in the presence of multiple scattering: Derivation and accuracy," *Phys. Rev. B* **72**(1): 014205 (2005).

McLachlan, D. S., Blaszkiewicz, M. and Newnham, R. E. "Electrical resistivity of composites," *J. Am. Ceram. Soc.* **73**(8): 2187-2203 (1990).

Mistler, R. E. and Twiname, E. R. *Tape casting: Theory and practice*, The American Ceramic Society, Ohio, USA (2000).

Molla, J., Gonzalez, M., Vila, R. and Ibarra, A. "Effect of humidity on microwave dielectric losses of porous alumina," *J. Appl. Phys.* **85**(3): 1727-1730 (1999).

Monma, H. "Catalytic behavior of calcium phosphates for decompositions of 2-propanol and ethanol," *J. Catal.* **75**: 200-203 (1982).

Moreno, R. "The role of slip additives in tape casting technology: Part II – binders and plasticizers," *Am. Ceram. Soc. Bull.* **71**: 1647-1657 (1992).

Mukherjee, A., Maiti, B., Das Sharma, A., Basu, R. N. and Maiti, H. S. "Correlation between slurry rheology, green density and sintered density of tape cast yttria stabilised zirconia," *Ceram. Int.* **27**(7): 731-739 (2001).

Murali, K. P., Rajesh, S., Prakash, O., Kulkarni, A. R. and Ratheesh, R. "Preparation and properties of silica filled ptfe flexible laminates for microwave circuit applications," *Composites: Part A* **40**(8): 1179-1185 (2009).

Murray, G., White, C. V. and Weise, W. *Introduction to engineering materials*, C R C Press, Taylor & Francis Group, Boca Raton, FL (2008).

Newnham, R. E., Skinner, D. P. and Cross, L. E. "Connectivity and piezoelectric-pyroelectric composites," *Mater. Res. Bull.* **13**(5): 525-536 (1978).

Newnham, R. E., Bowen, L. J., Klicker, K. A. and Cross, L. E. "Composite piezoelectric transducers," *Mater. Des.* **2**(2): 93-106 (1980).

Newnham, R. E. "Composite electroceramics," *Annu. Rev. Mater. Sci.* **16**(1): 47-68 (1986).

Norton, F. H. *Fine ceramics: Technology and applications*, McGraw-Hill, Inc., New York (1970).

Onoda, G. Y. and Hench, L. L. *Ceramic processing before firing*, Wiley Interscience, New York (1973).

Palmqvist, L., Lyckfeldt, O., Carlström, E., Davoust, P., Kauppi, A. and Holmberg, K. "Dispersion mechanisms in aqueous alumina suspensions at high solids loadings," *Colloid. Surface. A: Physicochem. Eng. Aspects* **274**(1–3): 100-109 (2006).

Park, I., Ko, S. H., Pan, H., Grigoropoulos, C. P., Pisano, A. P., Fréchet, J. M. J., Lee, E. S. and Jeong, J. H. "Nanoscale patterning and electronics on flexible

substrate by direct nanoimprinting of metallic nanoparticles," *Adv. Mater.* **20**(3): 489-496 (2008).

Park, J. H., Kim, B. K., Park, J. G. and Kim, Y. "Effect of microstructure on the microwave properties in dielectric ceramics," *J. Eur. Ceram. Soc.* **21**(15): 2669-2672 (2001).

Parker, W. J., Jenkins, R. J., Butler, C. P. and Abbott, G. L. "Flash method of determining thermal diffusivity, heat capacity, and thermal conductivity," *J. Appl. Phys.* **32**(9): 1679-1684 (1961).

Pasero, M., Kampf, A. R., Ferraris, C., Pekov, I. V., Rakovan, J. and White, T. J. "Nomenclature of the apatite supergroup minerals," *Eur. J. Mineral.* **22**: 163–179 (2010).

Penn, S. J., Alford, N. M., Templeton, A., Wang, X. R., Xu, M. S., Reece, M. and Schrapel, K. "Effect of porosity and grain size on the microwave dielectric properties of sintered alumina," *J. Am. Ceram. Soc.* **80**(7): 1885-1888 (1997).

Pennisi, L. *The firing process, engineered materials hand book, ceramics and glasses*. ASM International, The material information society, Ohio (1991).

Peterson, K. A., Patel, K. D., Ho, C. K., Rohde, S. B., Nordquist, C. D., Walker, C. A., Wroblewski, B. D. and Okandan, M. "Novel microsystem applications with new techniques in low-temperature co-fired ceramics," *Int. J. Appl. Ceram. Technol.* **2**(5): 345-363 (2005).

Pillai, S. O. *Solid state physics*, New age international publishers, New Delhi (2001).

Piwonski, M. A. and Roosen, A. "Low pressure lamination of ceramic green tapes by gluing at room temperature," *J. Eur. Ceram. Soc.* **19**: 263-270 (1999).

Pozar, D. M. *Microwave engineering*, John Wiley and Sons, Singapore (2008).

Raghava, R. S. "Thermal expansion of organic and inorganic matrix composites: A review of theoretical and experimental studies," *Polym. Compos.* **9**(1): 1-11 (1988).

Rahaman, M. N. *Ceramic processing and sintering*, Marcel Dekker, New York (1999).

Rajesh, S., Nisa, V. S., Murali, K. P. and Ratheesh, R. "Microwave dielectric properties of PTFE/rutile nanocomposites," *J. Alloys Compd.* **477**(1-2): 677-682 (2009).

Rao, V., Ashokan, P. V. and Shridhar, M. H. "Studies of dielectric relaxation and a.c. conductivity in cellulose acetate hydrogen phthalate–poly(methyl methacrylate) blends," *Mater. Sci. Eng. A* **281**(1–2): 213-220 (2000).

Rao, Y., Qu, J., Marinis, T. and Wong, C. P. "A precise numerical prediction of effective dielectric constant for polymer-ceramic composite based on effective-medium theory," *IEEE Trans. Compon. Packag. Technol.* **23**(4): 680-683 (2000).

Rashchi, F. and Finch, J. A. "Polyphosphates: A review their chemistry and application with particular reference to mineral processing," *Miner. Eng.* **13**(10-11): 1019-1035 (2000).

Reimer, L. *Scanning electron microscopy, physics of image formation and microanalysis*, Springer, Berlin (1985).

Richerson, D. W. *Modern ceramic engineering: Properties, processing, and use in design*, Taylor and Francis Group, CRC press, London (2006).

Rimdusit, S. and Ishida, H. "Development of new class of electronic packaging materials based on ternary systems of benzoxazine, epoxy, and phenolic resins," *Polymer* **41**(22): 7941-7949 (2000).

Rose, H. E. and Sullivan, R. M. E. *A treatise on the internal mechanics of ball, tube and rod mills*, Chemical Publishing, Boston (1958).

Rosenberg, H. M. *The solid state: An introduction to the physics of crystals for students of physics, materials science, and engineering*, Oxford University Press, New York (1988).

Rusu, M., Sofian, N. and Rusu, D. "Mechanical and thermal properties of zinc powder filled high density polyethylene composites," *Polym. Test.* **20**(4): 409-417 (2001).

Saito, S. *Fine ceramics*, Elsevier, London (1985).

Salam, L. A., Matthews, R. D. and Robertson, H. "Optimisation of thermoelectric green tape characteristics made by the tape casting method," *Mater. Chem. Phys.* **62**: 263-272 (2000).

Sanoj, M. A., Reshmi, C. P. and Varma, M. R. "Finite size effect on the sinterability and dielectric properties of $ZnNb_2O_6$–ZBS glass composites," *J. Am. Ceram. Soc.* **92**(11): 2648-2653 (2009).

Schroeder, L. W. and Mathew, M. "Cation ordering in $Ca_2La_8(SiO_4)_6O_2$," *J. Solid State Chem.* **26**(4): 383-387 (1978).

Schwartz, B. "Microelectronic packaging: II," *Am. Ceram. Soc. Bull.* **63**(4): 577-581 (1984).

Schwartz, M., *Mobile wireless communications*, Cambridge University Press, New York (2005).

Sebastian, M. T. *Dielectric materials for wireless communication*, Elseiver Publishers, Oxford (2008).

Sebastian, M. T. and Jantunen, H. "Low loss dielectric materials for LTCC applications: A review," *Inter. Mater. Rev.* **53**(2): 57-90 (2008).

Sebastian, M. T. and Jantunen, H. "Polymer-ceramic composites of 0-3 connectivity for circuits in electronics: A review," *Int. J. Appl. Ceram. Technol.* **7**(4): 415-434 (2010).

Serret, A., Cabañas, M. V. and Vallet-Regí, M. "Stabilization of calcium oxyapatites with lanthanum(III)-created anionic vacancies," *Chem. Mater.* **12**(12): 3836-3841 (2000).

Shannon, R. D. "Revised effective ionic radii and systematic study of interatomic distances in halides and chalcogenides," *Acta Crystallogr.* **A32**: 751-757 (1976).

Shannon, R. D. and Rossman, G. R. "Dielectric constants of silicate garnets and the oxide additivity rule," *Am. Mineral.* **77**: 94-100 (1992).

Shannon, R. D. "Dielectric polarizabilities of ions in oxides and fluorides," *J. Appl. Phys.* **73**(1): 348-366 (1993).

Shimada, Y., Utsumi, K., Suzuki, M., Takamizawa, H., Nitta, M. and Watari, T. "Low firing temperature multilayer glass-ceramic substrate," *IEEE Trans. Compon., Hybrids, Manuf. Technol.* **6**(4): 382-388 (1983).

Shimada, Y., Kobayashi, Y., Kata, K., Kurano, M. and Takamizawa, H. "Large scale multilayer glass-ceramic substrate for supercomputer," *IEEE Trans. Compon., Hybrids, Manuf. Technol.* **13**(4): 751-758 (1990).

Siegel, A. C., Phillips, S. T., Dickey, M. D., Lu, N., Suo, Z. and Whitesides, G. M. "Foldable printed circuit boards on paper substrates," *Adv. Funct. Mater.* **20**(1): 28-35 (2010).

Sisodia, M. L. and Gupta, V. L. *Microwaves: Introduction to circuits, devices and antennas*, New Age International (P) Ltd, New Delhi (2001).

Sneed, M. C. and Brasted, R. C. *Comprehensive inorganic chemistry*, D. Van Nostrand, Inc., New York (1956).

Snitzer, E. "Cylindrical dielectric waveguide modes," *J. Opt. Soc. Am.* **51**(5): 491-498 (1961).

Steeman, P. A. M., Maurer, F. H. J. and van Es, M. A. "Dielectric monitoring of water absorption in glass-bead-filled high-density polyethylene," *Polymer* **32**(3): 523-530 (1991).

Strohm, K. M., Bloecher, H. L., Schneider, R. and Wenger, J. "Development of future short range radar technology." *European Radar Conference, EURAD 2005*: 165-168 (2005).

Subodh, G. and Sebastian, M. T. "Glass-free $Zn_2Te_3O_8$ microwave ceramic for ltcc applications," *J. Am. Ceram. Soc.* **90**(7): 2266-2268 (2007).

Subodh, G., Deepu, V., Mohanan, P. and Sebastian, M. T. "Dielectric response of high permittivity polymer ceramic composite with low loss tangent," *Appl. Phys. Lett.* **95**(6): 062903-062903 (2009).

Surendran, K. P., Santha, N., Mohanan, P. and Sebastian, M. T. "Temperature stable low loss ceramic dielectrics in $(1-x)ZnAl_2O_4$-$xTiO_2$ system for microwave substrate applications," *Eur. Phys. J. B* **41**(3): 301-306 (2004).

Surendran, K. P., Bijumon, P. V., Mohanan, P. and Sebastian, M. T. "$(1-x)MgAl_2O_4$-$xTiO_2$ dielectrics for microwave and millimeter wave applications," *Appl. Phys. A Mater. Sci. Proc.* **81**(4): 823-826 (2005).

Teirikangas, M., Juuti, J., Hu, T. and Jantunen, H. "Extrinsic influences of the polymer matrix on electrical properties of high frequency composites," *Ferroelectrics* **387**(1): 70-76 (2009).

Templeton, A., Wang, X. R., Penn, S. J., Webb, S. J., Cohen, L. F. and Alford, N. M. "Microwave dielectric loss of titanium oxide," *J. Am. Ceram. Soc.* **83**(1): 95-100 (2000).

Thirumal, M., Jain, P. and Ganguli, A. K. "Molten salt synthesis of complex perovskite-related dielectric oxides," *Mater. Chem. Phys.* **70**(1): 7-11 (2001).

Thomas, D., Janardhanan, C. and Sebastian, M. T. "Mechanically flexible butyl rubber–$SrTiO_3$ composite dielectrics for microwave applications," *Int. J. Appl. Ceram. Technol.* **8**(5): 1099–1107 (2011).

Thomas, D., Rethika, K. T. and Sebastian, M. T. "Microwave dielectric properties of $BaNb_{(2-x)}Ta_xP_2O_{11}$ (x = 0, 0.5, 1, 1.5 and 2) ceramics," *J. Mater. Sci.: Mater. Electron.* **23**(6): 1268-1271 (2012).

Thomas, S. and Sebastian, M. T. "Microwave dielectric properties of $SrRE_4Si_3O_{13}$ (RE = La, Pr, Nd, Sm, Eu, Gd, Tb, Dy, Er, Tm, Yb, and Y) ceramics," *J. Am. Ceram. Soc.* **92**(12): 2975-2981 (2009).

Thomas, S., Deepu, V., Uma, S., Mohanan, P., Philip, J. and Sebastian, M. T. "Preparation, characterization and properties of $Sm_2Si_2O_7$ loaded polymer composites for microelectronic applications," *Mater. Sci. Eng. B* **163**(2): 67-75 (2009).

Tinga, W. R., Voss, W. A. G. and Blossey, D. F. "Generalized approach to multiphase dielectric mixture theory," *J. Appl. Phys.* **44**(9): 3897-3902 (1973).

Todd, M. G. and Shi, F. G. "Molecular basis of the interphase dielectric properties of microelectronic and optoelectronic packaging materials," *IEEE Trans. Compon. Packag. Technol.* **26**(3): 667-672 (2003).

Tolchard, J. R., Sansom, J. E. H., Islam, M. S. and Slater, P. R. "Structural studies of apatite-type oxide ion conductors doped with cobalt," *Dalton Trans.* **7**: 1273-1280 (2005).

Tsunooka, T., Androu, M., Higashida, Y., Sugiura, H. and Ohsato, H. "Effects of TiO_2 on sinterability and dielectric properties of high-Q forsterite ceramics," *J. Eur. Ceram. Soc.* **23**(14): 2573-2578 (2003).

Tummala, R. R. "Ceramic and glass-ceramic packaging in the 1990s," *J. Am. Ceram. Soc.* **74**(5): 895-908 (1991).

Tummala, R., Kosec, M., Jones, W. K. and Belavic, D. *Electronic packaging for high reliability; low cost electronics*, Kluwer Academic Publishers, Dordrecht, The Netherlands (1999).

Udovic, M., Valant, M. and Suvorov, D. "Dielectric characterisation of ceramics from the TiO_2-TeO_2 system," *J. Eur. Ceram. Soc.* **21**(10-11): 1735-1738 (2001).

Udovic, M., Valant, M. and Suvorov, D. "Phase formation and dielectric characterization of the Bi_2O_3–TeO_2 system prepared in an oxygen atmosphere," *J. Am. Ceram. Soc.* **87**(4): 591-597 (2004).

Valant, M. and Suvorov, D. "Chemical compatibility between silver electrodes and low-firing binary-oxide compounds: Conceptual study," *J. Am. Ceram. Soc.* **83**(11): 2721–2729 (2000).

Valant, M. and Suvorov, D. "Processing and dielectric properties of sillenite compounds $Bi_{12}MO_{20-\delta}$ (M = Si, Ge, Ti, Pb, Mn, $B_{1/2}P_{1/2}$)," *J. Am. Ceram. Soc.* **84**(12): 2900-2904 (2001).

Valant, M. and Suvorov, D. "Glass-free low-temperature cofired ceramics: Calcium germanates, silicates and tellurates," *J. Eur. Ceram. Soc.* **24**(6): 1715-1719 (2004).

Vidya, S., Solomon, S. and Thomas, J. K. "Synthesis, sintering and optical properties of $CaMoO_4$: A promising scheelite LTCC and photoluminescent material," *Phys. Status Solidi A* **209**(6): 1067-1074 (2012).

Vineis, C., Davies, P. K., Negas, T. and Bell, S. "Microwave dielectric properties of hexagonal perovskites," *Mater. Res. Bull.* **31**(5): 431-437 (1996).

Vozdecky, P., Roosen, A., Ma, Q., Tietz, F. and Buchkremer, H. P. "Properties of tape-cast Y-substituted strontium titanate for planar anode substrates in SOFC applications," *J. Mater. Sci.* **46**: 3493-3499 (2011).

Wanmaker, W. L., ter Vrugt, J. W. and Verlijsdonk, J. G. "Luminescence of alkaline earth yttrium and lanthanum phosphate-silicates with apatite structure," *J. Solid State Chem.* **3**(3): 452-457 (1971).

Ward, A. A. M., Stoll, B., von Soden, W., Herminghaus, S. and Mansour, A. A. "Effect of cyclic deformations on the dynamic-mechanical properties of silica-filled butyl rubber," *Macromol. Mater. Eng.* **288**(12): 971-979 (2003).

Waseda, Y., Matsubara, E. and Shinoda, K. *X-ray diffraction crystallography*, Springer, Berlin (2011).

Watanabe, H., Yamada, N. and Okaji, M. "Linear thermal expansion coefficient of silicon from 293 to 1000 K," *Int. J. Thermophys.* **25**(1): 221-236 (2004).

Waye, B. E. *Introduction to technical ceramics*, Maclaren and Sons Ltd., London (1967).

Wazer, J. R. V. *Phosphorus and its compounds, Volume I: Chemistry*, Interscience Publishers, Inc., New York (1958).

Wersing, W. "Microwave ceramics for resonators and filters," *Curr. Opin. Solid State Mater. Sci.* **1**(5): 715-731 (1996).

West, A. R. *Solid-state chemistry and its applications*, John Wiley, Chichester (1984).

Wolff, I. "From antennas to microwave systems - LTCC as an integration technology for space applications," *3rd European Conference on Antennas and Propagation, 2009: EuCAP 2009*: 3-8 (2009).

Xiang, F., Wang, H. and Yao, X. "Preparation and dielectric properties of bismuth-based dielectric/PTFE microwave composites," *J. Eur. Ceram. Soc.* **26**(10-11): 1999-2002 (2006).

Xiang, F., Wang, H. and Yao, X. "Dielectric properties of $SrTiO_3$/POE flexible composites for microwave applications," *J. Eur. Ceram. Soc.* **27**(8-9): 3093-3097 (2007).

Xu, J. W., Moon, K. S., Tison, C. and Wong, C. P. "A novel aluminum-filled composite dielectric for embedded passive applications," *IEEE Trans. Adv. Packag.* **29**(2): 295-306 (2006).

Yao, N. and Wang, Z. L. *Handbook of microscopy for nanotechnology*, Kluwer Academic Publishers, Boston (2005).

Yokoi, A., Ogawa, H., Kan, A. and Nakamura, Y. "Relationship between crystal structure and microwave dielectric properties of melilite-type ceramic," *J. Eur. Ceram. Soc.* **27**(8–9): 2989-2993 (2007).

Zeng, Y. P. and Jiang, D. L. "Fabrication and properties of tape-cast laminated and functionally gradient alumina–titanium carbide materials," *J. Am. Ceram. Soc.* **83**: 2999-3003 (2000).

Zheng, C. W., Wu, S. Y., Chen, X. M. and Song, K. X. "Modification of $MgAl_2O_4$ microwave dielectric ceramics by Zn substitution," *J. Am. Ceram. Soc.* **90**(5): 1483-1486 (2007).

Zhou, D., Wang, H., Pang, L. X., Yao, X. and Wu, X. G. "Microwave dielectric characterization of a Li_3NbO_4 ceramic and its chemical compatibility with silver," *J. Am. Ceram. Soc.* **91**(12): 4115-4117 (2008).

Zhou, D., Wang, H., Pang, L. X., Randall, C. A. and Yao, X. "Bi_2O_3–MoO_3 binary system: An alternative ultralow sintering temperature microwave dielectric," *J. Am. Ceram. Soc.* **92**(10): 2242-2246 (2009).

Zhou, D., Randall, C. A., Wang, H., Pang, L. X. and Yao, X. "Ultra-low firing high-K scheelite structures based on $[(Li_{0.5}Bi_{0.5})_xBi_{1-x}][MO_xV_{1-x}]O_4$ microwave dielectric ceramics," *J. Am. Ceram. Soc.* **93**(8): 2147-2150 (2010).

Zhou, H., Wang, H., Zhang, M., Li, K. and Yang, H. "Synthesis and microwave dielectric properties of $Ba_4Ti_3P_2O_{15}$ ceramics," *Mater. Chem. Phys.* **119**(1–2): 4-6 (2010).

Zhou, W. Y., Qi, S. H., Zhao, H. Z. and Liu, N.-L. "Thermally conductive silicone rubber reinforced with boron nitride particle," *Polym. Comp.* **28**(1): 23-28 (2007).